University of East Anglia

Studies of iron- sulfur cluster containing regulators of the Rrf2 family

PhD thesis
School of Chemistry
May 2017

María Teresa Pellicer Martínez

Declaration

I declare that the work contained in this thesis, submitted by me for the degree of PhD, is my own original work, except where due reference is made to other authors, and has not been previously submitted by me for a degree at this or any other university.

<div align="right">

María Teresa Pellicer Martínez

May 2017

</div>

Acknowledgements

I would firstly like to express my appreciation to my supervisor, Prof. Nick Le Brun, for trusting me since the first interview and for the unending advice and direction he has given me throughout my studies at the University of East Anglia.

I must express thanks to Dr. Jason Crack, for giving me the skills required working with iron- sulfur proteins, as well as always being approachable when I had queries and doubts. Thanks for your patience with me, I will be eternally grateful.

I must give special mention to Dr. Myles Cheesman for his advices and helping me with the CD experiments. Many thanks to Prof. Andy Johnston and Dr. Jonathan Todd for the guidance and effort they put into helping me with my studies with RirA, to Prof. Julea Butt for helping me with the electrochemistry, to Dr. Erin Dodd for her advice, support and for being a good friend, to Dr. Justin Bradley for his technical assistance and advice, to Dr. Dimitri A. Svistunenko for helping me with the EPR measurements, to Dr. Nicholas Watmough for use of the stopped-flow instrument, to Prof Saeed Kamali, for teaching me how Mössbauer works and for welcoming me when I went to his university, and to Prof. Michael K. Johnson for his guidance in Resonance Raman and for welcoming me in his university.

Also thanks to the UEA Science faculty for funding my PhD studentship, without which nothing at all would have been achievable.

(Spanish) Me gustaría agradecer en especial el apoyo incondicional que mi familia me ha ofrecido durante todo este tiempo. A mi madre y a mi padre, por haber estado cada noche al otro lado de la pantalla para preocuparse por mí. A mis hermanos, porque aunque no lo parezca siempre han estado ahí y a mis sobrinos, porque lo son todo para mí.

A Crisa y Carla por haber sido mis más fieles confidentes y haberme brindado todo su apoyo.

A mi queridísimo amigo Marc, por haber estado a mi lado tanto en lo bueno como en lo malo, por haberme hecho la estancia en Norwich mucho más llevadera y por quererme tal y como soy.

A Patricia, por haberme sacado siempre una sonrisa.

A Tamara y Teresa por haberme hecho pasar tan buenos momentos juntas, que no son pocos.

Y por último, a ti, por haberte sentido siempre tan cerca a pesar de la distancia y por haberme apoyado en todo momento. ¡Fuiste, eres y siempre serás mi más bonita casualidad!

¡Gracias a todos los que habéis estado a mi lado en esta etapa tan difícil
pero a la vez tan especial!

Thank you to all those who have helped me through this difficult
but at the same time, very special period!

Abstract

Members of the Rrf2 superfamily of transcription factors are widespread in bacteria but their biological functions are largely unknown. The aim of the work described in this thesis was to uncover the distinct iron-sulfur cluster properties and biological functions of two uncharacterised members of the Rrf2 family.

RirA (Rhizobial iron regularor A) is a global iron regulator in *Rhizobium* and many related α-proteobacteria. Spectroscopic and ESI-MS data for cluster-reconstituted RirA indicated that the protein binds a [4Fe-4S] cluster cofactor. [4Fe-4S] RirA binds DNA, consistent with its function as a repressor of expression of genes involved in iron uptake. Under low iron conditions, [4Fe-4S] RirA undergoes cluster conversion resulting in a [2Fe-2S] form, which binds DNA with lower affinity. If low iron conditions persist, the [2Fe-2S] cluster is lost, resulting in a cluster-free (apo) form. This does not bind DNA and can no longer function as a repressor and so the iron-uptake machinery of the cell is activated. The data are consistent with RirA functioning as a sensor of iron via both iron-sulfur cluster availability and the fragility of its cluster. The significant sensitivity of RirA to O_2 suggests that even when iron is sufficient, the protein is susceptible to cluster conversion/loss; the interplay between iron and O_2 might be important *in vivo*.

A new member of the Rrf2 superfamily from *Streptomyces*, RsrR (Redox sensitive response Regulator), was also characterised. RsrR is isolated containing a [2Fe-2S] cluster than undergoes facile redox cycling. This modulates its DNA-binding behaviour: it binds RsrR-regulated promoter DNA tightly only in its oxidised state. Spectroscopic analyses revealed that the cluster has properties characteristic of His-coordinated [2Fe-2S] clusters and His12 was identified through site-directed mutagenesis as a likely cluster ligand. Substitution of Glu8 also significantly affected the cluster properties suggesting it might also be a cluster ligand.

Contents

Table of Contents

List of Figures

List of Tables

Abbreviations

Abs, A	Absorbance
BNF	Biological nitrogen fixation
BSA	Bovine serum albumin
CD	Circular dichroism
Da (kDa)	Dalton (kilodalton)
DNA	Deoxyribonucleic acid
DNIC	Dinitrosyl iron complex
DTT	Dithiothreitol
ε	Extinction coefficient (M^{-1} cm^{-1})
e−	Electron
EDTA	Ethylenediaminetetraacetic acid
EPR	Electron paramagnetic resonance
ESI-MS	Electrospray Ionization Mass Spectrometry
FAM	6-Carboxyfluorescein
Fe-S	Iron- Sulfur
FNR	Fumarate and nitrate reductase
HEPES	4-(2-hydroxyethyl)-1-piperazineethanesulfonic acid
HiPIP	High potential iron sulphur protein
IPTG	Isopropyl-β-D-galactoside
IRO	Iron responsive operator
IRP	Iron regulatory protein
ISC	Iron sulphur cluster
IscR	Iron-sulfur cluster Regulator
L (μL, mL)	Litre (microlitre, millilitre)
LB	Luria-Bertani broth
m (nm, μm, mm, cm)	Metre (nanometre, micrometre, millimetre, centimetre)
M (nM, μM, mM)	Mole (nanomole, micromole, millimole)

Mw	Molecular weight
MWCO	Molecular weight cut-off
NHE	Standard hydrogen electrode
NsrR	Nitric oxide sensitive response Regulator
OD	Optical density
PAGE	Polyacrylamide gel electrophoresis
PMSF	Phenylmethanesulfonylfluoride
RBS	Roussin's Black Salt
RirA	Rhizobial iron regulator A
RNA	Ribonucleic acid
rpm	Revolutions per minute
RRE	Roussin's red ester
RsrR	Redox sensitive response Regulator
S^{2-}	Sulfide
SDS	Sodium dodecyl sulphate
SUF	Sulphur mobilization
T (mT)	Tesla (millitesla)
TEMED	N,N,N',N'-tetra-methyl-ethylenediamine
Tris	Tris(hydroxymethyl)aminomethane
UV	Ultraviolet
V (mV)	Volt (millivolt)
Ve	Elution volume
v/v	Volume-volume
V0	Void volume
w/v	Weight-volume

Chapter 1. Introduction.

1.1. Background.

Many proteins have a non-protein component called a cofactor. When the protein contains the cofactor it is called a holo-protein; if the cofactor is removed, it is referred to as an apo-protein. Proteins have acquired a wide variety of cofactors that provide them with functions they would not otherwise be able to perform [1]. These low-molecular-mass compounds bind covalently or non-covalently to well-defined sites and may be divided into three groups: organic, metal-organic compounds and inorganic cofactors. In the case of organic cofactors, there are various nucleotides (such as flavin mononucleotide and flavin adenine dinucleotide), vitamins (biotin, pantothenate and folate), etc. Some examples of metal–organic compounds are haem and the molybdopterin cofactor. Common inorganic cofactors include various metal ions such as Mg^{2+}, Zn^{2+}, Mn^{2+}, $Cu^{2+/1+}$, $Fe^{3+/2+}$, etc. One of the most important groups of inorganic cofactors are iron-sulfur (Fe-S) clusters [2]. These prosthetic groups are amongst the most ancient in nature. The atmosphere on earth during the first billion years was anaerobic, but with plentiful supplies of soluble iron and sulfur. Ancient organisms utilised these to make Fe-S clusters as protein co-factors. Among other functions, these co-factors could transfer electrons and bind oxyanions and nitrogenous species [3]. As the earth's atmosphere became oxygenated, fragile and reactive Fe-S clusters were susceptible to degradation, and some were replaced through the process of evolution with other cofactors e.g. Zn^{2+}, but many were retained because of their essential reactivity.

In the early 1960s, ferredoxins were the first proteins that contain Fe-S clusters to be discovered. This was achieved by purifying proteins and applying the new technique of electron paramagnetic resonance (EPR) spectroscopy, which was able to detect characteristic signals from paramagnetic cluster forms [4]. Some of the first Fe–S proteins to be discovered include plant and bacterial ferredoxins and respiratory complexes I–III of

bacteria and mitochondria [2]. It was originally thought that these cofactors could assemble spontaneously on proteins. However, genetic, biochemical and cell-biological studies in the 1990s provided ample evidence that the maturation of Fe-S clusters in living cells is a catalysed process that requires a complex biosynthetic machinery [2, 5, 6]. Nowadays, in excess of 120 distinct types of enzymes and proteins are known to contain Fe-S clusters [7].

1.2.   Structures and properties of biological Fe-S clusters.

There is no single canonical primary amino acid sequence that defines an Fe-S cluster-binding motif within polypeptides. In fact, variations in the spacing, environment and type of Fe-S cluster ligands found in different Fe-S proteins is a significant contributor to the wide range of the electronic and chemical properties of their associated Fe-S clusters [8]. Despite the extraordinary biological versatility of Fe-S proteins, the composition of Fe-S metal sites is relatively simple, with the iron coordination tetrahedral throughout [9]. The structure and function of the Fe-S cluster proteins are intimately related. This section will outline the basic structures available to this important cofactor, and examples of how the structure relates to the function will follow in section 1.3.

The [2Fe-2S] rhomb can be considered as the basic building block for assembly on the basis of both structural and electronic considerations. It is composed of two iron ions bridged by two sulfide (S^{2-}) ions and coordinated by four cysteinyl ligands as in [2Fe-2S]-ferredoxins, by two cysteines and two histidines as in Rieske proteins and other coordination environments are possible, see Figure 1.1.

Figure 1.1. Structure of the [2Fe-2S] cluster.

2

Cubane [4Fe-4S] clusters can be visualized as two [2Fe-2S] rhombs fused together and lying perpendicular to one another. They can also be viewed as consisting of two interpenetrating tetrahedra of iron (as Fe^{3+} or Fe^{2+}) and S^{2-} ions, forming a cube that is linked to the protein framework by four amino acid residues at the vertices of a tetrahedron (Figure 1.2).
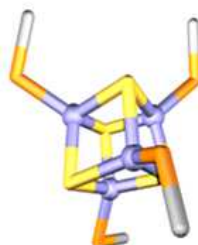
Figure 1.2. Structure of the [4Fe-4S] cluster.

[3Fe-4S] clusters, derived from [4Fe-4S] clusters by removal of one iron atom from one of the cube vertices, are found in biology in a variety of enzymes/protein including ferredoxins and respiratory enzymes. They are also formed transiently during cluster interconversion reactions [5, 10].

Fe-S clusters are typically coordinated by cysteine residues, although, in more complex Fe-S clusters different ligands (His, Asp, Arg, Ser, etc.) have been found [7]. Some Fe-S clusters proteins contain metal ions in addition to iron [2]. For example, the nitrogenase MoFe protein is a heterodimeric protein found in diazotrophs that functions to reduce or fix atmospheric N_2 into ammonia. The Fe protein contains one [4Fe-4S] cluster and shuttles electrons to the MoFe protein where N_2 reduction occurs. The MoFe protein contains two unique [Fe-S] clusters: the P cluster ([8Fe-7S]) and the FeMo cofactor ([7Fe-Mo-9S-homocitrate-C]). This protein provides an example of an Fe-S protein that contains more than one type of Fe-S cluster [2, 11].

In addition, there are enzymes in which a [4Fe-4S] cluster is bridged directly via a cysteine ligand to another metallic center, such as in the iron-only hydrogenase, in which the cofactor is [4Fe4S]-SCys-Fe_2(dtn)[3]$_2$(CN)$_2$, (dtn = di(thiomethyl)amine) [7].

1.3. Functions of biological Fe-S clusters.

Due to the chemical versatility of iron and sulfur, Fe–S clusters have developed different functions in a variety of important physiological processes, mainly as electron transport proteins, but also as catalytic centers for substrate binding/activation, Fe-S storage and as sensors or regulators [12, 13]. In many cases the precise role of the Fe-S cluster is still unclear, and it is possible that in some proteins the Fe-S cluster simply plays a structural role.

1.3.1. Iron-Sulfur Cluster Function – Electron Transfer.

The first Fe-S proteins with a known function were ferredoxins, which are involved in several processes of life, including photosynthesis, respiration and nitrogen fixation. The clusters have the ability to delocalise electron density over iron atoms, and the presence of at least two redox states, readily accessible under normal biological conditions for most types of Fe–S clusters, makes them ideally suited for their purpose as electron transfer agents [14]. [2Fe-2S] clusters are found in chloroplast ferredoxins acting as electron donors to enzymes such as nitrite reductase and glutamate synthase, and in many animal tissues, acting as electron donors to cytochrome P450 [15]. [3Fe-4S] and [4Fe-4S] cluster ferredoxins were found in *Streptomyces griseolus* and *Desulfovibrio gigas*, respectively [16]. Bacterial ferredoxins may also contain two [4Fe-4S] or [3Fe-4S] clusters or a [4Fe-4S] [3Fe-4S] cluster combination, and act primarily as low potential electron transfer proteins. The majority of the ferredoxins, which operate in the 2+/1+ redox couple, are able to exchange electrons at a low potential (from –250 to –650 mV versus NHE) [17, 18]. In the case of the high potential Fe-S proteins (HiPIP), they are able to exchange electrons at potentials from +50 to +450 mV because they operate via a different redox couple, 3+/2+. HiPIPs contain a typical cubic [4Fe-4S] cluster and are

found in purple photosynthetic bacteria and are likely a photosynthetic electron carrier between the cytochrome bc_1 complex and reaction centres [5, 14, 16].

Rieske iron–sulfur proteins play a vital role in the linkage between electron transfer and proton pumping through the electron transport chain of mitochondria and in photosynthesis. In the "Rieske" proteins containing the cluster $[2Fe-2S(S.Cys)_2(N.His)_2]$, ionization of a co- ordinated imidazole group may be coupled to oxidation-reduction. By binding Cys ligands from different subunits, iron sulfur clusters affect dimer formation, as in the Fe protein of nitrogenase and cluster Fx of Photosystem I [11, 13]. Although in the majority of clusters only one electron is transferred, the [8Fe-7S] cluster in nitrogenase has the ability to act as an electron carrier for two electrons [14].

1.3.2. Iron Sulfur Cluster Function – Catalytic and Structural functions.

Fe–S clusters can also have a catalytic role, for example aconitase [19], in which a non-protein- coordinated iron at one edge of a [4Fe–4S] cluster serves as a Lewis acid to assist H_2O abstraction from citrate which is converted to isocitrate [2, 11]. Further, by straddling protein structural elements, Fe–S clusters are able to stabilize structures that are required for specific functions. That appears to be the case with endonuclease III of *E. coli*, where a specific DNA binding site is stabilized, and in MutY [12, 13]. In a related function, clusters have been shown to protect proteins from the attack of intracellular proteases, for example, an amidotransferase of *Bacillus subtilis* needs a [4Fe-4S] cluster in order to be protected from proteases [20]. Fe-S clusters may also serve a storage function for iron and possibly sulfide [5, 13, 21].

1.3.3. Iron Sulfur Cluster Function – Gene Regulation.

There are now several well-characterized examples of Fe-S clusters involved in transcriptional or translational regulation of gene expression in bacteria and in eukaryotes.

Each senses a different type of environmental stimulus and uses a distinct sensing mechanism involving cluster assembly, conversion, or redox chemistry.

1.3.3.1. Fumarate and nitrate reduction (FNR) regulator; the master aerobic/anaerobic switch.

Fumarate and nitrate reduction (FNR) regulatory proteins are dioxygen sensing bacterial transcription factors that control the switch between aerobic and anaerobic metabolism. FNR is a member of the cAMP receptor protein (CRP)-FNR superfamily of homodimeric transcriptional regulators. The best characterized FNR protein is that from *E. coli*, considered to be the paradigm system, although there are clearly variations in properties and sensory units between FNR proteins. The *E. coli* protein becomes activated under anaerobic conditions by insertion of an O_2-labile $[4Fe-4S]^{2+}$ cluster into the N-terminal sensory domain by the Isc iron–sulfur cluster [22] biosynthetic machinery. This causes conformational changes that diminish inter-subunit electrostatic repulsion, resulting in the dimerization of the 30 kDa monomer. This enables the C-terminal DNA-binding domain to recognize specific binding sites within FNR-controlled promoters [23]. In response to elevated O_2 levels, the $[4Fe-4S]^{2+}$ cluster undergoes a rapid conversion to a $[2Fe-2S]^{2+}$ cluster, resulting in a dimer-to-monomer transition and loss of site-specific DNA binding [5, 24]. The cluster conversion mechanism consists in a two-step reaction involving a $[3Fe-4S]^{1+}$ intermediate and sequential release of Fe(II) and Fe(III) ions. Since the initial $[4Fe-4S]^{2+}$ cluster contained two Fe(II) and two Fe(III) ions, the reaction with O_2 is proposed to result in oxidation to a superoxidized state, $[4Fe-4S]^{3+}$, that is unstable and immediately ejects an Fe(II) ion, forming a $[3Fe-4S]^{1+}$ species [25]. Once formed, the $[3Fe-4S]^{1+}$ cluster is only transiently stable, ejecting one Fe(III) ion and two sulfide ions (S^{2-}) to generate the product $[2Fe-2S]^{2+}$ (Figure 1.3). The $[2Fe-2S]^{2+}$ cluster of FNR is also not very stable in the presence of O_2 and slowly degrades to form cluster-free (apo-)

protein. In this way, *E. coli* FNR regulates > 300 genes, most of which are associated with anaerobic metabolism [23, 26].
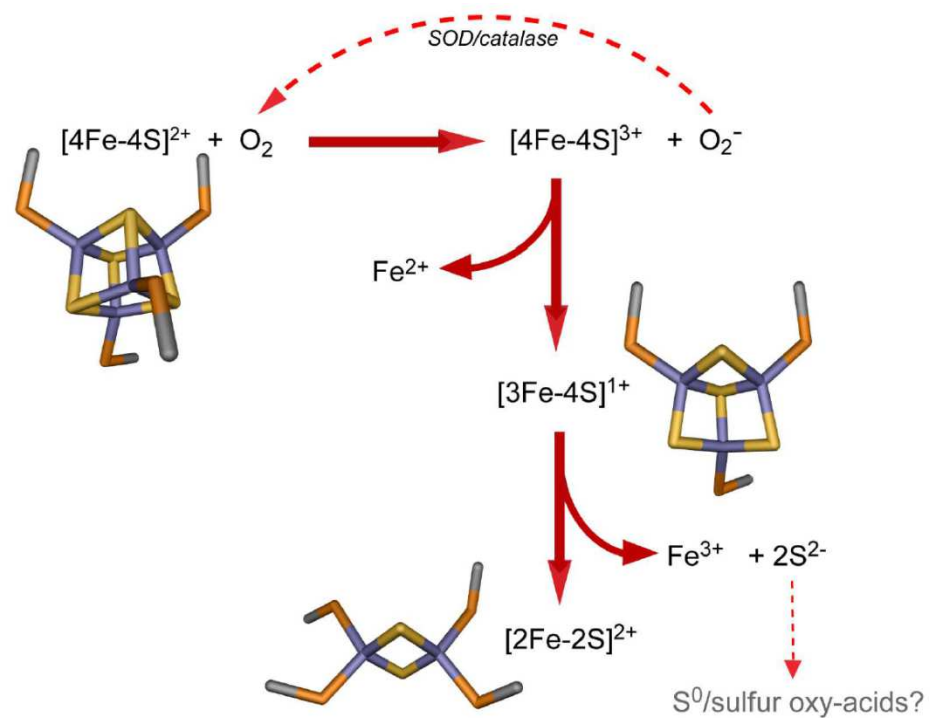
Figure 1.3. Mechanism of the reaction of [4Fe-4S]$^{2+}$ FNR with O$_2$ [23]**.**

Recently, the structure of *Aliivibrio fischeri* [4Fe-4S] FNR, a close homologue of *E. coli* FNR, was solved with the cluster bound [27]. This provides a structural framework in which to interpret the wealth of *in vivo* and biochemical data available for the *E. coli* FNR protein.

Anaerobic exposure of *E. coli* cells to physiologically relevant concentrations of NO led to up-regulation of multiple FNR-repressed genes and down-regulation of FNR-activated genes, suggesting that NO inactivates FNR [28]. Among those genes up-regulated due to FNR inactivation in the presence of NO is *hmp*, encoding a flavohemoglobin that constitutes a principal NO detoxification pathway in *E. coli* and a wide range of other bacteria. It also plays an important role in the establishment of infection by pathogens. Reaction of [4Fe-4S] FNR with NO *in vitro* was shown to

generate iron nitrosyl species associated with FNR, which bound DNA with reduced affinity [28].

Different techniques have been used to characterize the interconversion between $[4Fe-4S]^{2+}$ and $[2Fe-2S]^{2+}$ clusters in FNR. These include Mössbauer spectroscopy [29], resonance Raman, UV-visible absorption/CD spectroscopies, mass spectrometry and electron paramagnetic resonance [23, 30, 31].

1.3.3.2.   IscR: regulator of Fe-S biogenesis.

IscR is widely conserved in bacteria and is part of the large Rrf2 family of transcription factors. It is a global regulator that directly or indirectly controls expression of ~40 genes in *E. coli*. The 17 kDa *E. coli* protein consists of a winged helix-turn-helix (HTH) DNA binding domain in the N-terminal region and a motif with three cysteines and one histidine (Cys92, Cys98, Cys104, His107) required for coordination of a [2Fe-2S] cluster in the C-terminal region [32]. Anaerobically purified IscR showed an EPR signal with g values at 1.99, 1.94, and 1.88, typical for a [2Fe-2S] cluster in the reduced, 1+ state. When the sample was oxidized in air, the signal was lost and the colour of the protein changed from red to brown, indicative of $[2Fe-2S]^{1+}$ cluster oxidation to the 2+ oxidation state. After reduction the signal at g = 1.99, 1.94, 1.88 was again observed with no significant loss in intensity, demonstrating that the cluster undergoes reversible oxidation reduction [33]. IscR acts as a sensor of cellular Fe-S levels and a global transcription regulator for Fe-S biogenesis under both 'normal' and stressful conditions. Analysis of IscR regulated genes revealed that IscR recognizes two different DNA binding motifs (referred to as type 1 and 2). Only [2Fe-2S]-IscR binds to type 1 sites, whereas both [2Fe-2S]-IscR and apo-IscR bind to type 2 sites with similarly high affinity, indicating that the Fe-S cluster is not required for interaction with type 2 sites. [2Fe-2S]-IscR represses the expression of the *isc* operon that encodes the housekeeping Isc iron–sulfur biogenesis system in *E. coli*. When insufficient clusters are being synthesized, apo-IscR becomes the

dominant form, and this no longer binds the *isc* operator sequence, thus up-regulating the cluster biogenesis pathway (see Figure 1.4). The apo-form activates the transcription of the *suf* operon. The balance between apo- and holo-IscR is predicted to be influenced by growth conditions such as oxidative and nitrosative [11] stresses or iron limitation [6, 21, 34, 35].

X-ray structures of apo-IscR from *E. coli* and *Thermincola potens* have been reported, together with *E. coli* apo-IscR in complex with DNA containing a type 2 site. These structures reveal important information about the nature of the protein-DNA interaction, but a full understanding of the regulatory mechanism is currently hindered by the lack of structural information for the Fe-S cluster bound form [36].
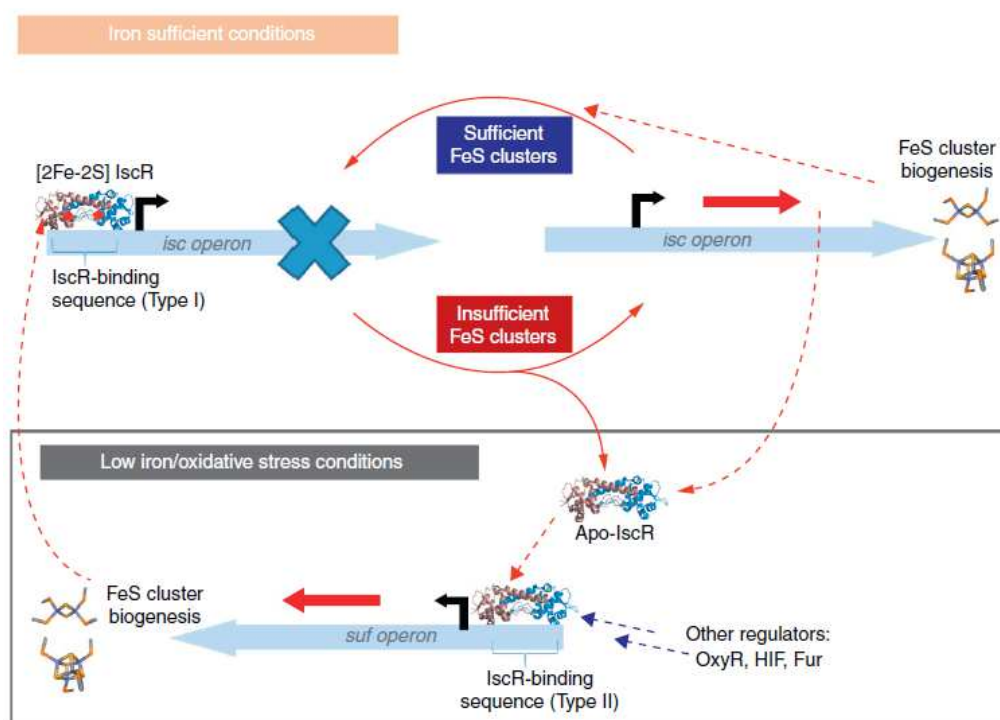
Figure 1.4. Diagram of IscR regulation [34].

1.3.3.3. NsrR: sensor of nitrosative stress.

NsrR is another member of the Rrf2 family and it is dedicated to the detection of NO stress and the protection against reactive nitrogen species. NsrR in *Bacillus subtilis* bears significant homology (30% identity and 48% similarity) to IscR in *E. coli*. Notably,

among the residues conserved between these proteins are the three cysteine residues that coordinate the Fe-S cluster in IscR, although the number of residues separating the first Cys from the CX_5C motif varies in IscR and NsrR orthologues [37]. In *Streptomyces coelicolor,* anaerobically purified NsrR binds a $[4Fe-4S]^{2+}$ cluster and is a homodimer irrespective of the presence of cluster. The [4Fe-4S] form reacts slowly with O_2, consistent with the fact that *S. coelicolor* is an obligate aerobe. However, *in vitro* the protein has been shown to undergo an O_2-mediated conversion from the [4Fe-4S] to a [2Fe-2S] form, a process that is dependent on the presence of a coordinating, non- physiological low molecular weight thiol [38]. In most of the organisms investigated to date, NsrR is a global regulator, controlling a complex network of genes, only some of which are directly related to NO detoxification. In the soil bacterium *S. coelicolor*, however, NsrR has a more specialized function, regulating only the *nsrR* gene itself and two *hmp* genes (*hmpA1* and *hmpA2*) (24) encoding NO detoxifying flavohaemoglobins that converts NO to NO_3^- under aerobic conditions (and N_2O under anaerobic conditions) [38, 39].

The reaction of [4Fe-4S] NsrR with NO affects DNA binding differently depending on the gene promoter. Binding to the *hmpA2* promoter was abolished at 2 NO per cluster, although for the *hmpA1* and *nsrR* promoters, 4 and 8 NO molecules, respectively, were required to abolish DNA binding [39]. Spectroscopic evidence indicates that this is achieved through the formation of iron- nitrosyl complexes: mainly Roussin's red ester (RRE) -type and Roussin's Black Salt (RBS) -type complexes, a small (~16%) proportion of mononuclear iron dinitrosyl iron complex (DNIC), and possibly others [39]. The precise relationship between iron- nitrosyl species and DNA-binding is not yet understood. In addition to nitrosylated forms of NsrR, apo-NsrR also does not bind DNA [38]. Interestingly, in *Bacillus subtilis*, the protein was also shown to bind at another type of DNA sequence, and this was not dependent on the cluster, suggesting that in some organisms at least, apo-NsrR may also play a role in regulation [40].

1.4. Iron-sensing regulators.

With the exception of the family *Lactobacillaceae*, iron is an essential micronutrient for all bacteria. In anaerobic conditions Fe^{2+} is soluble at physiological pH and cells obtain iron without much difficulty from the external medium. In aerobic environments, however, this element is not easily available to microorganisms because the ion (Fe^{2+}), upon exposure to oxygen, is oxidized to Fe^{3+} and forms insoluble hydroxides at neutral pH, making the available metal very scarce. In this case it is necessary for bacteria to actively sequester iron from the extracellular medium. For this purpose, all aerobic bacteria produce and secrete low-molecular-weight compounds termed siderophores (sideros phoros, greek for 'iron carriers'), which chelate Fe^{3+} with high affinity and specificity. Subsequently, the cell recovers the ferrisiderophore complexes through specific outer membrane receptors [41]. As well as inorganic iron in ferric form, other types of iron sources are available to bacteria including inorganic iron in ferrous form, heme as a protein constituent or as a free molecule and proteins such as ferritin or transferrin [42]. However, an excess of iron is toxic because ferrous iron can catalyse the conversion of hydrogen peroxide and superoxide to the hydroxyl radical, known as the Haber-Weiss reaction (Equation 1), via Fenton chemistry.

$$H_2O_2 + O_2^{\cdot-} \rightarrow O_2 + HO^{\cdot} + HO^{-} \qquad \text{Equation 1}$$

This reaction is catalysed by metal ions, particularly by ferrous ions *in vivo*. Hydrogen peroxide can oxidise Fe^{2+} ions in the Fenton reaction [43] shown in Equation 2. The Fe^{3+} can then be re-reduced by the superoxide ion (Equation 3) or another cellular reductant.

$$Fe^{2+} + H_2O_2 \rightarrow Fe^{3+} + HO^{\cdot} + HO^{-} \qquad \text{Equation 2}$$
$$Fe^{3+} + O_2^{\cdot-} \rightarrow Fe^{2+} + O_2 \qquad \text{Equation 3}$$

The net result is the Haber-Weiss reaction. Superoxide and hydrogen peroxide are both present in cells that respire aerobically. Therefore any free iron species could lead to

the production of hydroxyl radicals, which is the most reactive species known in biology and can damage cellular components, including lipids membranes, nucleic acids and proteins leading, eventually, to cell death [44, 45]. Therefore, iron uptake has to be regulated in cells to maintain the intracellular concentration of iron within a certain range, to ensure sufficient supply of this essential nutrient while preventing toxic accumulation [46, 47].

In many Gram-negative bacteria, regulation of the cellular iron concentration is carried out by the ferric uptake regulator (Fur). In *E. coli*, where it was first described, the Fur protein is 17 kDa in size and is dimeric in both apo and Fe^{2+} bound forms. The crystal structure revealed two domains: the C-terminal domain is involved in dimerisation and the N-terminal domain is involved in DNA recognition and binding [48]. The working model for the Fur protein of *E. coli* proposes that, when bound by ferrous iron (Fe^{2+}), Fur acquires a conformation in which it is able to bind the target operator DNA, called the Fur box, within the promoter of the regulated gene to repress transcription. However, when iron is limited in the cell, the equilibrium is displaced to release Fe^{2+}, the RNA polymerase accesses cognate promoters, and the genes for the biosynthesis of siderophores and other iron-related functions are expressed. The Fe-bound siderophores are subsequently transported into the cell to satisfy its Fe^{2+} requirement [46, 49].

The physiological role of DtxR (diphtheria toxin repressor protein) is similar to that of Fur. They have structural and mechanistic similarities, however, the two proteins share little if any amino acid sequence homology. DtxR is the prototype of a family of metal-dependent regulatory proteins that have been identified in numerous bacteria, including both Gram-positive and Gram-negative species [50, 51]. The Gram-positive bacterium *Corynebacterium diphtheriae* is the causative agent of the severe respiratory disease diptheria. It colonizes the upper respiratory tract of the human host, where it secretes the potent diphtheria toxin [52]. Expression of diphtheria toxin (DT) is regulated by iron availability, with maximum production occurring in low-iron conditions. The *tox*

gene, the structural gene for DT, is regulated in an iron-dependent manner by DtxR. It is not only involved in the regulation of expression of DT but also responsible for regulating the synthesis and export of siderophores, the siderophore-dependent uptake of iron, and the synthesis of specific systems for the utilization of iron from heme, hemin and hemoglobin [50, 51, 53].

In some branches of the α-proteobacteria, iron responsive regulation differs substantially from the canonical Fur-Fe^{2+}/ DtxR-Fe^{2+} regulatory models. In these bacteria, Fur is present but it is usually relegated to less central roles in iron regulation or, in some cases, functions to regulate the cellular response to manganese rather than iron levels. In this case, it is more appropriately termed Mur (manganese uptake regulator) [54]. In place of Fur, many of the α-proteobacteria use the iron regulator Irr. Irr is a member of the Fur superfamily of metalloregulators, but its properties are quite distinct from those of Fur. It appears to be the only member described thus far that is functional (for DNA-binding) only in the absence of the regulatory metal cofactor, which is heme rather than non-heme iron. Furthermore, it contains only a single cysteine residue rather than multiple cysteines found in the other Fur proteins [55, 56]. Irr functions under iron limitation and acts as both a positive and negative regulator of gene expression, modulating a number of genes related to iron metabolism [47]. Irr in *Bradyrhizobium japonicum* binds heme by forming a complex with the heme biosynthetic enzyme ferrochelatase, thus responding to the status of heme at the site of synthesis. The Irr-heme complex is extremely unstable and is rapidly degraded via an unknown mechanism that involves the redox activity of heme and oxidation of the protein. Because iron levels directly influence heme levels, in iron-replete conditions, Irr is not available to repress or activate its target genes. Reactive oxygen species (ROS) [57] seem to promote the heme dependent degradation of Irr. In *Rhizobium leguminosarum*, Irr also senses heme but responds to it in a different way. The Irr-heme complex does not degrade but heme binding decreases the affinity of the protein for DNA

[58]. Although the regulatory input information for Irr is the status of heme biosynthesis, it is clear that Irr is a global regulator of iron homeostasis and metabolism [59].

Rhizobia and closely related α- proteobacteria contain a second global regulator of iron, named RirA (*r*hizobial *i*ron *r*egulator *A*) [26, 60]. *In silico* analyses of genome sequences indicate that Irr occurs in all members of the Rhizobiales and the Rhodobacterales and that RirA is found in all but one branch of these two lineages, the exception being the clade that includes *B. japonicum* [61]. RirA repressed >80 transcriptional units in *Rhizobium*, *Sinorhizobium* and *Mesorhizobium*, in iron-replete media. It is also found in the human pathogen *Bartonella*, the animal pathogen *Brucella*, and the phytopathogen *Agrobacterium*. RirA was initially discovered in *Rhizobium leguminosarum* and is a member of the Rrf2 family of putative transcriptional regulators, which also contains IscR and NsrR (see above).

A major focus of this thesis is RirA from *Rhizobium leguminosarum.* Amongst the soil bacteria Rhizobium is the only group that has a beneficial effect on the growth of legumes. They can live in the soil or in nodules formed on the roots of legumes. In root nodules, they form a symbiotic association with the legume, obtaining nutrients from the plant and producing ammonium in a process called biological nitrogen fixation (BNF), which is very demanding for iron due to the intracellular abundance of iron–sulfur proteins [14, 62].

A single monomer of RirA has a molecular mass of 17441 Da, is composed of 160 amino acid residues and has no detectable sequence similarity to Fur or to DtxR, indicating that RirA represents a novel class of Fe-responsive regulator for maintaining iron homeostasis [34]. RirA contains three essential cysteine residues in its amino acid sequence as shown in Figure 1.5. These three cysteines, at positions 92, 101 and 107, are conserved in 70% of the Rrf2 family of proteins and it is thought that these cysteines function as ligands for an iron-sulfur cluster, just as they do in NsrR and IscR.

```
MRLTKQTNYA VRMLMYCAAN DGHLSRIPEI AKAYGVSELF
LFKILQPLNK AGLVETVRGR NGGVRLGKPA ADISLFDVVR
VTEDSFAMAE CFEDDGEVEC PLVDSCGLNS ALRKALNAFF
AVLSEYSIDD LVKARPQINF LLGITGEPAY RKPAIVAPAA
```

Figure 1.5. Sequence of RirA from *R. leguminosarum*. Yellow highlights denote the three essential cysteine residues.

As mentioned above, RirA acts as a repressor of many iron-responsive genes under iron-replete conditions. The DNA recognition sites for RirA are significantly different from the well-documented Fur boxes to which Fur binds. The promoter regions of RirA-repressed genes have a conserved sequence, the IRO box, which is a cis-acting regulatory sequence with the consensus sequence TGA-N_9-TCA [56]. In low iron conditions RirA fails to bind to its cognate IRO boxes and transcription can occur. However, in high iron conditions, RirA is proposed to bind an Fe-S cluster (about which nothing is known), in turn causing it to bind to the IRO boxes and repress expression of the downstream genes. In many cases, the genes which feature an IRO box in their promoter region have clear links with iron, being predicted or demonstrated to be involved in the uptake of the metal or in its intracellular metabolism or storage. The RirA regulon includes genes for the synthesis (*vbs*) and uptake (*fhu*) of the siderophore vicibactin, genes involved in heme uptake (*hmu* and *tonB*), genes encoding hemin-binding proteins (*hbp*), genes that probably participate in the transport of Fe^{3+} (*sfu*), genes for the synthesis of Fe-S clusters (*suf*), *rirA* itself, etc. [14, 61, 63].

1.5.   Redox-sensing regulators.

Living organisms have evolved diverse antioxidant systems to protect themselves against the harmful effects of reactive oxygen species, such as superoxide and hydrogen peroxide (H_2O_2), which are inevitably generated as by-products during aerobic respiration [64]. Reactive oxygen species can damage DNA, lipid membranes, and proteins and have been implicated in numerous degenerative diseases [65]. These antioxidant defence

systems have been best characterized in *E. coli*, in which the OxyR and SoxR transcription factors activate antioxidant genes in response to H_2O_2, and to redox active molecules, respectively.

OxyR, a LysR-type transcriptional regulator, responds to elevated H_2O_2, concentrations [64] by rapidly inducing the expression of *oxyS* (a small, nontranslated regulatory RNA), *katG* (hydrogen peroxidase I), *gorA* (glutathione reductase), and other genes that function in protecting the cell against oxidative stress [65]. Purified OxyR is directly sensitive to oxidation. Only the oxidized form of OxyR can activate transcription *in vitro*, and footprinting experiments indicate that oxidized and reduced OxyR have different conformations [66]. Oxidation of OxyR leads to the formation of an intramolecular disulfide bond between cysteine residues 199 and 208. OxyR is reduced by enzymatic reduction of this disulfide bond [65, 66].

SoxR is a member of the MerR family of transcriptional activators. It forms a homodimer containing a pair of [2Fe-2S] clusters anchored to four cysteine residues in the C-terminal region of the polypeptide. The [2Fe-2S] cluster is essential for the activity of SoxR. The SoxR protein of *E. coli* senses oxidative stress via oxidation of the $[2Fe-2S]^+$ cluster to a $[2Fe2S]^{2+}$ form, which activates transcription of *soxS*, which itself encodes a transcriptional regulator responsible for activating the transcription of numerous genes encoding enzymes involved in the response to oxidative stress caused by superoxide and other redox active molecules [5]. In some species, SoxS is not present and so SoxR functions alone in regulating the response to redox-active compounds [67]. Nitric oxide also activates SoxR by direct nitrosylation of the [2Fe-2S] cluster but it is unclear how this activates transcription of the *soxS* gene [68]. Apo-SoxR and reduced SoxR can bind to DNA with an affinity similar to that of oxidized SoxR, but only oxidized SoxR is able to activate the transcription of the *soxS* gene. Therefore, SoxR senses oxidative stress using the redox states of the [2Fe-2S] cluster and regulates the transcription of the *soxS* gene by structural changes between the oxidized and reduced forms, see Figure 1.6 [69].
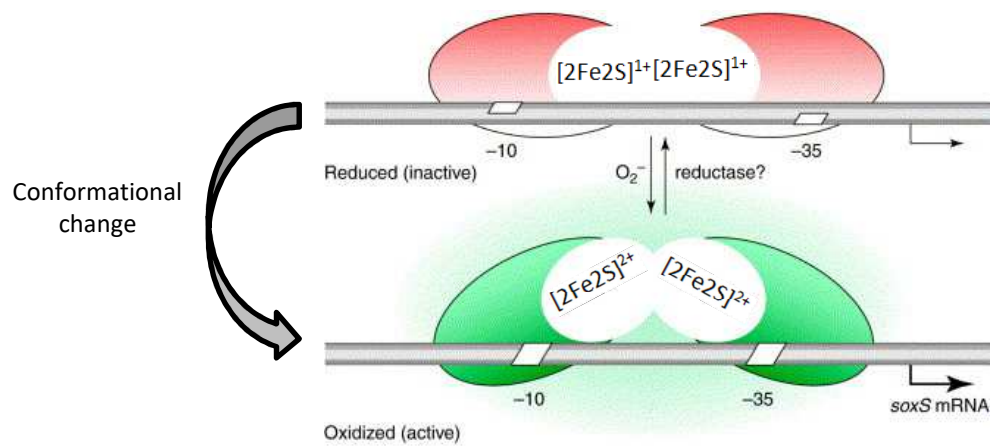
Figure 1.6. Oxidation of [2Fe-2S]$^{1+}$ cluster causes a conformational change now enabling *E. coli* SoxR to act as a transcriptional activator [69].

Recently, RsrR (<u>R</u>edox <u>s</u>ensitive <u>r</u>esponse <u>R</u>egulator), a new member of the Rrf2 family has been discovered in *Streptomyces venezuelae*, which was originally mis-annotated as an NsrR homologue in the *S. venezuelae* genome. ChIP-seq analysis revealed that rather than regulating the nitrosative stress response like *Streptomyces coelicolor* NsrR, RsrR binds to a conserved motif located in the promoter regions of a different, much larger set of genes with a diverse range of functions, including a number of regulators, genes required for glutamine synthesis, NADH/NAD(P)H metabolism, as well as general DNA/RNA and amino acid/protein turn over [70]. Figure 1.7 shows the sequence of RsrR from *S. venezuelae* including the three essential cysteine residues that function as ligands for an iron- sulphur cluster in NsrR and IscR.

```
MKLSGGVEWA  LHCCVVLTAA  SRPVPAARLA  ELHDVSPSYL
AKQMQALSRA  GLVRSVQGKT  GGYVLTRPAV  EITLLDVVQA
VDGPDPAFVC  TEIRQRGPLA  TPPEKCTKAC  PIARAMGAAE
AAWRASLAAT  TIADLVATVD  DESGPDALPG  VGAWLIEGLG
```

Figure 1.7. Sequence of RsrR from *S. venezuelae*. Yellow highlights denote the three essential cysteine residues.

1.6. Aims of the project.

The overall aims of the project were to obtain detailed mechanistic understanding of the sensing mechanisms that are employed by Fe-S cluster binding members of the Rrf2 family of transcriptional regulators. These include the bacterial proteins *R. leguminosarum* RirA and *S. venezuelae* RsrR. Although it is believed that these proteins contain an Fe-S cluster, because they are a members of the same family (Rrf2 family) as NsrR and IscR and, like them, they contain three conserved cysteine residues, details of their Fe-S cluster binding properties are unknown. Thus, an aim of the project was to uncover which type of Fe-S cluster RirA and RsrR bind. In the case of RirA, the next aim was to elucidate the mechanism by which iron is sensed and therefore how regulation is achieved. For example, RirA might sense iron directly, or via the cellular level of Fe-S clusters. For RsrR, the subsequent aim was to determine what it senses and how it functions.

1.7. References.

1. Stevens, J.M., et al., *Covalent cofactor attachment to proteins: cytochrome c biogenesis.* Biochem Soc Trans, 2005. **33**(Pt 4): p. 792-5.
2. Lill, R., *Function and biogenesis of iron–sulphur proteins.* Nature, 2009. **460**(7257): p. 831-838.
3. Cowan, J.A., *Iron Sulfur Cluster Biosynthesis*, in *Bioinorganic Chemistry*. 2009, American Chemical Society. p. 3-16.
4. Cutsail, G.E., 3rd, J. Telser, and B.M. Hoffman, *Advanced paramagnetic resonance spectroscopies of iron-sulfur proteins: Electron nuclear double resonance (ENDOR) and electron spin echo envelope modulation (ESEEM).* Biochim Biophys Acta, 2015. **1853**(6): p. 1370-94.
5. Johnson, D.C., et al., *Structure, function, and formation of biological iron-sulfur clusters.* Annu Rev Biochem, 2005. **74**: p. 247-81.
6. Vinella, D., et al., *In vivo [Fe-S] cluster acquisition by IscR and NsrR, two stress regulators in Escherichia coli.* Mol Microbiol, 2013. **87**(3): p. 493-508.
7. Kalyvas, C. and U.o. Michigan, *Synthesis of Metal/iron/sulfur Clusters Relevant to Biological Systems and Minerals.* 2008: University of Michigan.
8. Frazzon, J. and D.R. Dean, *Formation of iron-sulfur clusters in bacteria: an emerging field in bioinorganic chemistry.* Curr Opin Chem Biol, 2003. **7**(2): p. 166-73.
9. Kiley, P.J. and H. Beinert, *The role of Fe-S proteins in sensing and regulation in bacteria.* Curr Opin Microbiol, 2003. **6**(2): p. 181-5.
10. Peters, J.W., et al., *Redox-dependent structural changes in the nitrogenase P-cluster.* Biochemistry, 1997. **36**(6): p. 1181-7.
11. Noodleman, L., et al., *Insights into properties and energetics of iron-sulfur proteins from simple clusters to nitrogenase.* Curr Opin Chem Biol, 2002. **6**(2): p. 259-73.
12. Broderick, J.B., *Iron–Sulfur Clusters in Enzyme Catalysis.* Elsevier Academic Press, 2003. **8**: p. 739–757.

13. Beinert, H., R.H. Holm, and E. Munck, *Iron-sulfur clusters: nature's modular, multipurpose structures.* Science, 1997. **277**(5326): p. 653-9.

14. Holmes, J.D., *Magneto-optical Studies of RirA and Cytochrome cd1.* Ph.D. thesis, University of East Anglia, Norwich, 2012.

15. Ortiz de Montellano, P.R., *Cytochrome P450-activated prodrugs.* Future Med Chem, 2013. **5**(2): p. 213-28.

16. Brzoska, K., S. Meczynska, and M. Kruszewski, *Iron-sulfur cluster proteins: electron transfer and beyond.* Acta Biochim Pol, 2006. **53**(4): p. 685-91.

17. Agapakis, C.M. and P.A. Silver, *Modular electron transfer circuits for synthetic biology: insulation of an engineered biohydrogen pathway.* Bioeng Bugs, 2010. **1**(6): p. 413-8.

18. Sticht, H. and P. Rosch, *The structure of iron-sulfur proteins.* Prog Biophys Mol Biol, 1998. **70**(2): p. 95-136.

19. Pilon, M., et al., *Biogenesis of iron-sulfur cluster proteins in plastids.* Genet Eng (N Y), 2006. **27**: p. 101-17.

20. Jang, S., *The metabolism of iron-sulfur clusters during hydrogen peroxide stress en Escherichia coli.* Ph.D. thesis, University of Illinois at Urbana-Champaign, 2010.

21. Romsang, A., et al., *The iron-sulphur cluster biosynthesis regulator IscR contributes to iron homeostasis and resistance to oxidants in Pseudomonas aeruginosa.* PLoS One, 2014. **9**(1): p. e86763.

22. Fleischhacker, A.S., et al., *Characterization of the [2Fe-2S] cluster of Escherichia coli transcription factor IscR.* Biochemistry, 2012. **51**(22): p. 4453-62.

23. Crack, J.C., et al., *Bacterial iron-sulfur regulatory proteins as biological sensor-switches.* Antioxid Redox Signal, 2012. **17**(9): p. 1215-31.

24. Melville, S.B. and R.P. Gunsalus, *Isolation of an oxygen-sensitive FNR protein of Escherichia coli: interaction at activator and repressor sites of FNR-controlled genes.* Proc Natl Acad Sci U S A, 1996. **93**(3): p. 1226-31.

25. Crack, J.C., et al., *Signal perception by FNR: the role of the iron-sulfur cluster.* Biochem Soc Trans, 2008. **36**(Pt 6): p. 1144-8.

26. Crack, J.C., et al., *Iron-sulfur clusters as biological sensors: the chemistry of reactions with molecular oxygen and nitric oxide.* Acc Chem Res, 2014. **47**(10): p. 3196-205.

27. Volbeda, A., et al., *The crystal structure of the global anaerobic transcriptional regulator FNR explains its extremely fine-tuned monomer-dimer equilibrium.* Sci Adv, 2015. **1**(11): p. e1501086.

28. Crack, J.C., et al., *Mechanism of [4Fe-4S](Cys)4 cluster nitrosylation is conserved among NO-responsive regulators.* J Biol Chem, 2013. **288**(16): p. 11492-502.

29. Kiley, P.J. and H. Beinert, *Oxygen sensing by the global regulator, FNR: the role of the iron-sulfur cluster.* FEMS Microbiol Rev, 1998. **22**(5): p. 341-52.

30. Zhang, B., et al., *Reversible cycling between cysteine persulfide-ligated [2Fe-2S] and cysteine-ligated [4Fe-4S] clusters in the FNR regulatory protein.* Proc Natl Acad Sci U S A, 2012. **109**(39): p. 15734-9.

31. Crack, J.C., et al., *Influence of association state and DNA binding on the O(2)-reactivity of [4Fe-4S] fumarate and nitrate reduction (FNR) regulator.* Biochem J, 2014. **463**(1): p. 83-92.

32. Lim, J.G. and S.H. Choi, *IscR is a global regulator essential for pathogenesis of Vibrio vulnificus and induced by host cells.* Infect Immun, 2014. **82**(2): p. 569-78.

33. Schwartz, C.J., et al., *IscR, an Fe-S cluster-containing transcription factor, represses expression of Escherichia coli genes encoding Fe-S cluster assembly proteins.* Proc Natl Acad Sci U S A, 2001. **98**(26): p. 14895-900.

34. Crack, J.C., et al., *Iron-sulfur cluster sensor-regulators.* Curr Opin Chem Biol, 2012. **16**(1-2): p. 35-44.

35. Rajagopalan, S., et al., *Studies of IscR reveal a unique mechanism for metal-dependent regulation of DNA binding specificity.* Nat Struct Mol Biol, 2013. **20**(6): p. 740-7.

36. Santos, J.A., et al., *The unique regulation of iron-sulfur cluster biogenesis in a Gram-positive bacterium.* Proc Natl Acad Sci U S A, 2014. **111**(22): p. E2251-60.

37. Yukl, E.T., et al., *Transcription Factor NsrR from Bacillus subtilis Senses Nitric Oxide with a 4Fe-4S Cluster (dagger).* Biochemistry, 2008. **47**(49): p. 13084-92.

38. Crack, J.C., et al., *NsrR from Streptomyces coelicolor is a nitric oxide-sensing [4Fe-4S] cluster protein with a specialized regulatory function.* J Biol Chem, 2015. **290**(20): p. 12689-704.

39. Crack, J.C., et al., *Differentiated, Promoter-specific Response of [4Fe-4S] NsrR DNA Binding to Reaction with Nitric Oxide.* J Biol Chem, 2016. **291**(16): p. 8663-72.

40. Kommineni, S., et al., *Global transcriptional control by NsrR in Bacillus subtilis.* J Bacteriol, 2012. **194**(7): p. 1679-88.

41. Chu, B.C., et al., *Siderophore uptake in bacteria and the battle for iron with the host; a bird's eye view.* Biometals, 2010. **23**(4): p. 601-11.

42. Caza, M. and J.W. Kronstad, *Shared and distinct mechanisms of iron acquisition by bacterial and fungal pathogens of humans.* Front Cell Infect Microbiol, 2013. **3**: p. 80.

43. Neyens, E. and J. Baeyens, *A review of classic Fenton's peroxidation as an advanced oxidation technique.* J Hazard Mater, 2003. **98**(1-3): p. 33-50.

44. Gutteridge, J.M. and B. Halliwell, *Free radicals and antioxidants in the year 2000. A historical look to the future.* Ann N Y Acad Sci, 2000. **899**: p. 136-47.

45. Stohs, S.J. and D. Bagchi, *Oxidative mechanisms in the toxicity of metal ions.* Free Radic Biol Med, 1995. **18**(2): p. 321-36.

46. Escolar, L., J. Perez-Martin, and V. de Lorenzo, *Opening the iron box: transcriptional metalloregulation by the Fur protein.* J Bacteriol, 1999. **181**(20): p. 6223-9.

47. Hibbing, M.E. and C. Fuqua, *Antiparallel and interlinked control of cellular iron levels by the Irr and RirA regulators of Agrobacterium tumefaciens.* J Bacteriol, 2011. **193**(14): p. 3461-72.

48. Pohl, E., et al., *Architecture of a protein central to iron homeostasis: crystal structure and spectroscopic analysis of the ferric uptake regulator.* Mol Microbiol, 2003. **47**(4): p. 903-15.

49. Friedman, Y.E. and M.R. O'Brian, *The ferric uptake regulator (Fur) protein from Bradyrhizobium japonicum is an iron-responsive transcriptional repressor in vitro.* J Biol Chem, 2004. **279**(31): p. 32100-5.

50. Schmitt, M.P., *Analysis of a DtxR-like metalloregulatory protein, MntR, from Corynebacterium diphtheriae that controls expression of an ABC metal transporter by an Mn(2+)-dependent mechanism.* J Bacteriol, 2002. **184**(24): p. 6882-92.

51. De Zoysa, A., A. Efstratiou, and P.M. Hawkey, *Molecular characterization of diphtheria toxin repressor (dtxR) genes present in nontoxigenic Corynebacterium diphtheriae strains isolated in the United Kingdom.* J Clin Microbiol, 2005. **43**(1): p. 223-8.

52. Schmidt, C.L., et al., *Purification and characterization of the Rieske iron-sulfur protein from the thermoacidophilic crenarchaeon Sulfolobus acidocaldarius.* FEBS Lett, 1995. **359**(2-3): p. 239-43.

53. Brune, I., et al., *The DtxR protein acting as dual transcriptional regulator directs a global regulatory network involved in iron metabolism of Corynebacterium glutamicum.* BMC Genomics, 2006. **7**: p. 21.

54. Peuser, V., B. Remes, and G. Klug, *Role of the Irr protein in the regulation of iron metabolism in Rhodobacter sphaeroides.* PLoS One, 2012. **7**(8): p. e42231.

55. Small, S.K., et al., *Positive control of ferric siderophore receptor gene expression by the Irr protein in Bradyrhizobium japonicum.* J Bacteriol, 2009. **191**(5): p. 1361-8.

56. Yeoman, K.H., et al., *Evidence that the Rhizobium regulatory protein RirA binds to cis-acting iron-responsive operators (IROs) at promoters of some Fe-regulated genes.* Microbiology, 2004. **150**(Pt 12): p. 4065-74.

57. Small, S.K., S. Puri, and M.R. O'Brian, *Heme-dependent metalloregulation by the iron response regulator (Irr) protein in Rhizobium and other Alpha-proteobacteria.* Biometals, 2009. **22**(1): p. 89-97.

58. Singleton, C., et al., *Heme-responsive DNA binding by the global iron regulator Irr from Rhizobium leguminosarum.* J Biol Chem, 2010. **285**(21): p. 16023-31.

59. Sangwan, I., S.K. Small, and M.R. O'Brian, *The Bradyrhizobium japonicum Irr protein is a transcriptional repressor with high-affinity DNA-binding activity.* J Bacteriol, 2008. **190**(15): p. 5172-7.

60. Dupuy, J., et al., *Crystal structure of human iron regulatory protein 1 as cytosolic aconitase.* Structure, 2006. **14**(1): p. 129-39.

61.   Diaz-Mireles, E., et al., *The Fur-like protein Mur of Rhizobium leguminosarum is a Mn(2+)-responsive transcriptional regulator.* Microbiology, 2004. **150**(Pt 5): p. 1447-56.

62.   Johnston, A.W., et al., *Living without Fur: the subtlety and complexity of iron-responsive gene regulation in the symbiotic bacterium Rhizobium and other alpha-proteobacteria.* Biometals, 2007. **20**(3-4): p. 501-11.

63.   Ngok-Ngam, P., et al., *Roles of Agrobacterium tumefaciens RirA in iron regulation, oxidative stress response, and virulence.* J Bacteriol, 2009. **191**(7): p. 2083-90.

64.   Teramoto, H., M. Inui, and H. Yukawa, *OxyR acts as a transcriptional repressor of hydrogen peroxide-inducible antioxidant genes in Corynebacterium glutamicum R.* Febs j, 2013. **280**(14): p. 3298-312.

65.   Zheng, M., F. Aslund, and G. Storz, *Activation of the OxyR transcription factor by reversible disulfide bond formation.* Science, 1998. **279**(5357): p. 1718-21.

66.   Aslund, F., et al., *Regulation of the OxyR transcription factor by hydrogen peroxide and the cellular thiol-disulfide status.* Proc Natl Acad Sci U S A, 1999. **96**(11): p. 6161-5.

67.   Wu, J. and B. Weiss, *Two divergently transcribed genes, soxR and soxS, control a superoxide response regulon of Escherichia coli.* J Bacteriol, 1991. **173**(9): p. 2864-71.

68.   Ding, H., E. Hidalgo, and B. Demple, *The redox state of the [2Fe-2S] clusters in SoxR protein regulates its activity as a transcription factor.* J Biol Chem, 1996. **271**(52): p. 33173-5.

69.   Pomposiello, P.J. and B. Demple, *Redox-operated genetic switches: the SoxR and OxyR transcription factors.* Trends Biotechnol, 2001. **19**(3): p. 109-14.

70.   Munnoch, J.T., et al., *Characterization of a putative NsrR homologue in Streptomyces venezuelae reveals a new member of the Rrf2 superfamily.* Sci Rep, 2016. **6**: p. 31597.

Chapter 2. Materials and methods.

2.1. Overexpression of RirA and RsrR and variants.

5 L Luria- Bertani media [1] was inoculated with freshly transformed *E. coli* BL21 λDE3 containing a pET11a vector with the *rirA* gene from *R. leguminosarum* (pRirA) or a pGS-21a vector containing the *S. venezuelae* rsrR gene (pRsrR-His), synthesised them by GenScript, for production of non-tagged RirA and C-terminally $(His)_6$-tagged RsrR, respectively. 100 µg/mL ampicillin and 20 µM ammonium ferric citrate were added and the cultures were grown at 37 °C, 200 rpm until $OD_{600 \, nm}$ was 0.6-0.9. To facilitate *in vivo* iron-sulfur cluster formation, the flasks were placed on ice for 18 min, then induced with 7.5 µM and 100 µM IPTG for RirA and RsrR, respectively, and incubated at 30 ºC and 105 rpm. After 50 min, the cultures were supplemented with 200 µM ammonium ferric citrate and 25 µM L-methionine and incubated for a further 3.5 hr at 30 ºC. The cells were harvested by centrifugation at 10000 × g (Beckman JLA9.1000 rotor) for 15 min at 4 ºC. For Mössbauer studies, [57]Fe (Goss Scientific) labelled RsrR was produced *in vivo* as described previously [2].

All work from this point was done inside an anaerobic cabinet unless otherwise stated. The cells were resuspended in 70 mL of buffer A (see 2.2 section) and placed in a 100 mL beaker and 30 mg/mL of lysozyme and 30 mg/mL of phenylmethanesulfonyl fluoride (PMSF) were added. The cell suspension was sonicated twice, each time for 8 min 20 sec (0.2 sec bursts, 50% power), in an aerobic microbiological cabinet. The cell lysate was centrifuged at 40000 × g for 45 min at 4 ºC (Beckman Coulter Allega™ 64R Centrifuge). The pellet was discarded and the supernatant was used for further purification steps.

2.2.   Chromatographic Purification.

2.2.1.   Chromatographic Purification of RirA.

HiTrap Heparin column: The supernatant (70 mL) was applied to a HiTrap Heparin (2 x 5 mL; GE Healthcare) column on an ÄKTA Prime system at 1 mL/min. The column was washed with buffer A (25 mM HEPES, 2.5 mM CaCl$_2$, 50 mM NaCl, pH 7.5) until A$_{280 \text{ nm}}$ <0.1. Bound proteins were eluted using a 100 mL linear gradient from 0 to 100% (v/v) buffer B (25 mM HEPES, 2.5 mM CaCl$_2$, 50 mM NaCl, 750 mM KCl, pH 7.5).

Fractions (1 mL) with the highest absorbance at 280 nm were analyzed by SDS-PAGE. The straw brown appearance of those fractions indicated the presence of a cluster. The fractions containing RirA at high concentration and purity were pooled and frozen in an anaerobic freezer for further experiments. The fractions obtained after the Heparin column will be referred to 'as isolated' RirA protein.

Gel filtration column: 2 mL of the as isolated RirA was applied to a Sephacryl S-100 HR column (120 mL; GE Healthcare) equilibrated with buffer A on an ÄKTA Prime system. Proteins were eluted at 1 mL/min over one column volume with buffer C (25 mM HEPES, 2.5 mM CaCl$_2$, 50 mM NaCl, 333 mM KCl, pH 7.5). Fractions (1 mL) with the highest absorbance at 280 nm were analyzed by SDS-PAGE. The lack of the straw brown colour from fractions indicated the absence of a cluster. Those with the highest concentration and purity of RirA were pooled and frozen in an anaerobic freezer for further experiments.

Table 2.1. Summary of the buffers used in the chromatographic purification of RirA.

Buffer A	25 mM HEPES, 2.5 mM CaCl$_2$, 50 mM NaCl, pH 7.5
Buffer B	25 mM HEPES, 2.5 mM CaCl$_2$, 50 mM NaCl, 750 mM KCl, pH 7.5
Buffer C	25 mM HEPES, 2.5 mM CaCl$_2$, 50 mM NaCl, 333 mM KCl, pH 7.5

2.2.2. Chromatographic Purification of RrsR and variants.

HiTrap IMAC column: The supernatant (70 mL) was applied to a HiTrap IMAC HP (1 x 5 mL; GE Healthcare) column using an ÄKTA Prime system at 1 mL/min. The column was washed with buffer D (50 mM TRIS, 50 mM NaCl, 5% (v/v) glycerol, pH 8) until $A_{280\ nm}$ <0.1. Bound proteins were eluted using a 100 mL linear gradient from 0 to 100% buffer E (50 mM TRIS, 100 mM $CaCl_2$, 200 mM L- histidine, 5% (v/v) glycerol, pH 8). A HiTrap Heparin (1 x 1 mL; GE Healthcare) column equilibrated in buffer D was used to remove the L- histidine, using buffer F (50 mM TRIS, 2 M NaCl, 5% (v/v) glycerol, pH 8) to elute the protein. Fractions (1 mL) containing RsrR-His (highest absorbance at 280 nm and pink/purple in colour) were pooled and stored in an anaerobic freezer until needed.

Gel filtration column: 2 mL of the as isolated RsrR was applied to a Sephacryl S-100 HR column (120 mL; GE Healthcare) equilibrated with buffer (buffer F was used for the holo RsrR and buffer G (50 mM Tris, 2 M NaCl, 5% (v/v) glycerol, 2 mM DTT, pH 8.0) for the apo-RsrR) on an ÄKTA Prime system. Proteins were eluted at 1 mL/min over one column volume with the respective buffer. Fractions (1 mL) with the highest absorbance at 280 nm were analyzed by SDS-PAGE. Those with the highest concentration and purity of RsrR were pooled and frozen in an anaerobic freezer for further experiments.

Table 2.2. Summary of the buffers used in the chromatographic purification of RsrR.

Buffer D	50 mM TRIS, 50 mM NaCl, 5% (v/v) glycerol, pH 8
Buffer E	50 mM TRIS, 100 mM $CaCl_2$, 200 mM L- histidine, 5% (v/v) glycerol, pH 8
Buffer F	50 mM TRIS, 2 M NaCl, 5% (v/v) glycerol, pH 8
Buffer G	50 mM Tris, 2 M NaCl, 5% (v/v) glycerol, 2 mM DTT, pH 8.0

2.3. Protein Determination Assays.

A calibration curve was prepared with bovine serum albumin (BSA). 0 µL, 20 µL, 40 µL, 60 µL, 80 µL, 100 µL of a 1 mg/mL stock solution of BSA were added to plastic test tubes. Those stock solutions were diluted with buffer A to a final volume of 100 µL giving a range of concentrations from 0 to 1.0 mg/mL BSA. As well as these standards, different volumes of protein with unknown concentration were transferred to the test tubes and also diluted to a final volume of 100 µL. A working strength Bio-Rad dye (Coomassie brilliant blue G-250) was prepared by diluting one part Bio-Rad dye-reagent concentrate with four parts distilled water. 5 mL of this solution were added in each tube and vortexed briefly to mix. In the presence of protein the dye-reagent changes colour from red-brown to blue. Absorbance of the samples was measured using a Helios spectrophotometer at 595 nm and 1 cm pathlength cuvettes. Because absorbance increases over time with this assay, the absorbance of each sample was measured three times to take an average. A standard curve was drawn from which the concentrations of protein were calculated [3].

2.4. Iron assays.

A calibration curve was prepared with Spectrosol standard iron solution (stock concentration 17.87 ± 0.09 mM Fe^{3+}, BDH) in the range of 0-200 µM iron. Appropriate dilutions of the protein with unknown concentration were made. All samples were diluted with distilled water to give a final volume of 100 µL. 100 µL of 21.7% (v/v) HNO_3 was added to each sample and standard and incubated at 95 ºC for 30 min. The samples and standards were cooled for 2 min and then centrifugated at 9000 x g for 1 min. Each sample was then treated with 0.6 mL of 7.5% (w/v) ammonium acetate, 0.1 mL of 12.5% (w/v) ascorbic acid and 0.1 mL of 10 mM Ferene (3-(2-Pyridyl)-5,6-di(2-furyl)-1,2,4-triazine-5′,5″-disulfonic acid disodium salt). The samples were mixed and incubated at room temperature for 30 min. The concentration of the iron was calculated from measurements

of absorbance at 593 nm. Assay mixtures produced a dark blue colour in the presence of iron. A standard curve was plotted and the iron concentrations of the unknown samples were calculated [3].

2.5. Reconstitution of RirA.

In some cases, the cluster content of as isolated samples of RirA was enhanced by *in vitro* reconstitution. For this, ~5 mL of the as isolated sample (~1 mM) was placed in a reconstitution vessel and 50 µL of 270 mM DTT was added. The following were then added: an appropriate aliquot of 105 mM L-cysteine and 270 mM DTT so that the total concentrations were 1 mM; an appropriate volume of 20 mM ammonium iron(II) sulfate solution to provide 10 mol Fe^{2+} per RirA monomer; and, a volume of buffer A equivalent to the starting volume of the protein sample. The reconstitution reaction was initiated by introducing 10 µL of NifS (225 nM final concentration), a cysteine desulfurase (purified by J.Crack, School of Chemistry, University of East Anglia, Norwich [4]) and incubated at 37 ℃. A yellow-brown colour started to develop as the reaction proceeded. Once the reaction was deemed to be complete (when there were no further changes in colour as observed by eye, usually after 30 mins), the reconstitution mixture was purified through removal of excess iron and sulfur using a 1 mL HiTrap Heparin HP column. The reconstituted protein was eluted with buffer B and transferred to an anaerobic fridge for storage at 4 ℃ for further experiments. The fractions obtained after reconstitution will be referred to as the 'reconstituted' sample.

2.6. Preparation of apo- protein.

Apo-RsrR -His and apo-RirA were prepared from as isolated holoprotein by aerobic incubation with 1mM EDTA overnight.

2.7. Electrophoretic mobility shift assay (EMSA).

2.7.1. Electrophoretic mobility shift assay (EMSA) with RirA.

A DNA fragment (581 bp) carrying the *fhuA* promoter region (pRL120322) was PCR-amplified using *R. leguminosarum* genomic DNA with 5' 6-carboxyfluorescein (FAM)-modified primers (Eurofins). It was supplied by Dr J. Todd (School of Biological Sciences, University of East Anglia, Norwich, UK) for use in electrophoretic mobility shift assay (EMSA) experiments. This gene is under the regulatory control of RirA *in vivo*. The PCR products were extracted and purified using a QIAquick gel extraction kit (Qiagen) according to the manufacturer's instructions. Probes were quantitated using a nanodrop ND2000c. The molecular weights of the double stranded FAM labelled probes were calculated using OligoCalc [5]. The sequence of DNA used and its respective binding region is shown in Figure 2.1 [6].

5'-<u>CGCAGCCATCGAGGGGGCCCC</u>AGCTGGTCCCGCGGGCTGCCAGGACATCGGCATCTATG
ACCGGACGATCCGGGCTTACCGAGCGACAGGTCTCTTCCCGTAATTGCCGGCGACTCTAATG
GGAGTGGCAGTTGCTCAAGTGAGGGCGATGGTCTTTTGCGCAAGTCCGCCGGCCGACCTAT
CCGGCGAGCCACTTCAGCGGCATCTGCAGTCGAAATACCCCTCCTACTCAGTCAGGTGATAC
TCTGGCGCGGGCGTGGTTCAAAATCAGCAGCAAATACGGGATCGTCGGGTCCATCCCCGTC
AAGACCGGCAGGTTGGCCATCGTCTCGGTGCGCGCTTGGTCTCGCGCGCGGCAGAACTGCC
TCTGTTTGGCAGCCCCACAGAACGTTACGAGGCCTCGATTCTACGTGCAACCTGTTCGGGAG
TGTTGAAGGCGTGGATTTATCGATTTAAAGG<mark>TGACTAAAATAATCATC</mark>TTATGTTGACAAGGCC
AATTTCGCTCCATAGGTTCCGCCCGCATCCGTGGCGTAGGGACCAAACA**ATG**GCACGTGTTT
TTTTGAAT<u>GTTTCTAATAATGTATCGCG</u>-3'

Figure 2.1. Sequence of DNA carrying the *fhuA* promoter. The nucleotides underlined were used as primers to amplify a 581 bp PCR fragment from *Rhizobium leguminosarum* strain J251 genomic DNA, which contains the *fhuA* gene promoter. The *fhuA* start codon is in bold and the IRO (Iron- responsive operator) sequence is highlighted in grey [7].

EMSA (also known as bandshift) reactions were carried out on ice in binding buffer (10 mM Tris, 60 mM KCl, pH 7.52) in 0.5 mL safe-lock tubes. 1 µL of DNA was titrated with varying aliquots of RirA. H_2O was added to give a final volume of 20 µL. After 2 min, 2 µL of loading dye (50% glycerol (v/v), 0.3% (w/v) bromophenol blue, 50 mM Tris, 300 mM KCl, pH 7.52) was added and the reaction mixtures were separated immediately on a 7.5% (v/v) polyacrylamide gel [8] in TBE running buffer (89 mM Tris,

89 mM boric acid, 2 mM EDTA), using a Mini Protean III system (Bio-Rad). Polyacrylamide gels were run at 30 mA for 30 min (pre-run at 30 mA for 2 min prior to use). Gels were visualized (excitation, 488 nm; emission, 530 nm) on a molecular imager FX Pro (Bio-Rad).

2.7.2. Electrophoretic mobility shift assay (EMSA) with RsrR.

DNA fragments carrying the intergenic region between *sven1847* and *sven1848* of the *S. venezualae* chromosome were PCR amplified using *S. venezualae* genomic DNA with 5′ 6-FAM modified primers (supplied by John T. Munnoch, School of Biological Sciences, University of East Anglia, Norwich, UK), see Figure 2.2. The PCR products were extracted and purified using a QIAquick gel extraction kit (Qiagen) according to the manufacturer's instructions. Probes were quantitated using a nanodrop ND2000c. The molecular weights of the double stranded FAM labelled probes were calculated using OligoCalc [5].

Bandshift reactions (20 µl) were carried out on ice in 10 mM Tris, 60 mM KCl, pH 7.52. Briefly, 1 µL of DNA was titrated with varying aliquots of RsrR. 2 µL of loading dye (containing 0.01% (w/v) bromophenol blue), was added and the reaction mixtures were immediately separated at 30 mA on a 7.5% (w/v) polyacrylamide gel in 1 x TBE (89 mM Tris,89 mM boric acid, 2 mM EDTA), using a Mini Protean III system (Bio-Rad). Gels were visualized (excitation, 488 nm; emission, 530 nm) on a molecular imager FX Pro (Bio-Rad). Polyacrylamide gels were pre-run at 30 mA prior to use (2 min for the apo and oxidized form and 50 min for the reduced form). For investigations of $[2Fe-2S]^{1+}$ RsrR DNA binding, in order to maintain the cluster in the reduced state, 5 mM of sodium dithionite was added to the isolated protein and the running buffer (de-gassed for 50 min prior to running the gel). Analysis by UV-visible spectroscopy confirmed that the cluster remained reduced under these conditions.

```
5'-CCGGTGTGGCGGTCACCGGTAGTCGTTCACGTCCGGCTTGCCCGTCTCGCCCGCGAGGATGAAGCCCCAG
5'-GCGTCGGGCTGTGAGCCGTCCGCGTCGGTGAAGCCGTACTCCCGGGCGAGCCCGCCGCTGTCGAGCGACC
5'-GGCCGTTCCAGCGGTGGCGGTCCGCGTCGGCGGCGAGGGCCGCCACCGCCCTGCCCACGTACGCCGGGGA
5'-CTCGGCGACCGCGAAGTCGGGGATCTTCGCGACGGCGTCGCGCCAGTTCTCCTCGGTGACGCCGAAGCCT
5'-TCCAGCATCTGCTCGGAGCGGAGCCAGCCGGGGCTGACGCAGACCGCGGTGCCGCCGTACTCCGCGAGTT
5'-CCTTGCCGAGGCCGAACGCCATCCGGATCGGGGCGTTCTTGGCGAGGTCGTAGAAGAGGTTCTCGCGGAA
5'-GCGGGTGCCGTTGTACGCGGAGGTGCCGTCGGTGATCTCGACGACCAGGGCGCCCGGGTGCCGGATGAGC
5'-AGCGGGAGCGCCGTGTGCGAGGTGATGGCGTGGGTCTTCACGCCCAGTTCGAGCATCCGCAGGCCGCCGG
5'-CGAGGTCGTTCTCCCAGGTCTTCTTCCCGAAGGAGAGGAGGTGCTCGCCGCCCCACACGTCGTTCACGAG
5'-GACGTCGAGCCGCCCGTGCTCGCGGTCGATCCGCTCGACCAGCGCCTTCACCTGCTCGACGTCCAGGTGG
5'-TCGGTGGGGACGGCGATGCCTTCGCCGCCGGCGGCCGTCACCAGTTCGGCGGTCTCCTCGATGGTCTCGG
5'-TGGCCCGGCCGACCTCGCTGAGCTTCGCGCGGGTGGTCCGTCCGGTGACGTACACCGTGGCGCCCGCCGC
5'- GCCGAGCTGGACGGCGATGCCCCGTCCGGCGCCCCGGGTGGCCCCGGCGACCAGGCAGATCCGTCCGCGC
```
} SVEN_1847

```
5'-AGGCTGTTCGTGTCCTTCTTCTCCGTCGTCATCGCACCAGCGTGACAGGGAAATCAGACATCTTCTGTC
3'-TCCGACAAGCACAGGAAGAAGAGGCAGCAGTACGCGTGGTCGCACTGTCCCTTTAGTCTGTAGAAGACAG
```

```
5'-TGGTTTCATTTCGGGCTTTCCGGGTGCGTCGCACCCCCCGAACCAGGATGCTGGTCCCGTGATGGACGAG
3'-ACCAAAGTAAAGCCCGAAAGGCCCACGCAGCGTGGGGGGCTTGGTCCTACGACCAGGGCACTACCTGCTC
```

```
5'-ACGGAGTTCTGGGAGATCATCGACGCCAGCCGCGAGGAAGCCGAGGGCGACCCCGAGGAACAGGCCGACC
5'-TGCTCGTGGAGCGGCTGACCCGGCTGGACCCCGACTCCGTGCTCGACTACGCCCGCCATTTCGAGGCCCG
5'-CTACAACCGCGCGTACCTCTGGGATCTGTGGGGCGCGGCGGCCGTGCTGTTCGACGGGGCGGGCGAGGAG
5'-ACCTTCGACTCGTTCCGCTGCTGGCTCATCGGCCAGGGCCGGGAGGTCTACGAGGGCGCGGTGCACGATC
5'-CGGACGCGCTCGCGGAGCTGCTCGGCGACTTCGACGTGGAGATCGACGGGGACGGTGAGGAGATCGGCTT
5'-CGCGGCCGACGAGGCGTACGAGCAGCTGACCGGCGCCGAGACCCCGGACCTGGGCATTCCGATGCCGGGC
5'-GGGGAGCCGCTGGGCGCCCCCTTCGACCTGGACGACGAGAAGGTGCTCGCGGCCCGTTTCCCCCGGCTGT
5'-GGGAGCGGTTCGGGACGGGGTGACGGGGCCGGGG
```
} SVEN_1848

Figure 2.2. Sequence of DNA carrying the intergenic region between *sven1847* **and** *sven1848* **of the** *S. venezualae* **chromosome.** *Sven 1847* in black is located on complementary strand; *Sven 1848* in blue is located on the 5'-3' strand. Start codon is highlighted in green and the stop codon in red. RsrR binding site is highlighted in grey. The nucleotides underlined were used as primers. Coloured arrows indicate direction of gene.

2.8. Techniques.

UV-visible absorbance measurements were performed using a Jasco V500 spectrometer, and CD spectra were measured with a Jasco J810 spectropolarimeter. EPR measurements were made with an X-band Bruker EMX EPR spectrometer equipped with an ESR-900 helium flow cryostat (Oxford Instruments). Spin intensities of paramagnetic samples were estimated by double integration of EPR spectra using a solution of 1 mM Cu(II) and 10 mM EDTA as the standard. EPR experiments were carried out in the laboratory of Dr Dimitri A. Svistunenko, School of Biological Sciences, University of Essex, Colchester, UK.

Mössbauer measurements were performed using a MS4 spectrometer in the constant acceleration mode in transmission geometry (~1 mM in Fe-S cluster ^{57}Fe-labelled). The measurements were performed at 6 K using a Janis cryostat. 50 mCi of ^{57}Co in rhodium held at room temperature was used as the source. All centroid isomer shifts, δ, are given with respect to metallic α–Fe at room temperature. The spectra were least square fitted to extract hyperfine parameters, which are δ, quadrupole splitting (ΔE_Q), Lorentzian linewidth (Γ), $\alpha v\delta$ intensities (I). Experiments were carried out in the laboratory of Dr Saeed Kamali, University of Tennessee Space Institute, Tullahoma, USA.

Resonance Raman spectra were recorded at 22 K using 15 µL frozen droplets of protein (~5 mM in Fe-S cluster) mounted on the cold finger of a Displex Model CSA-202E closed cycle refrigerator (Air Products, Allentown, PA), using a Ramanor U1000 scanning spectrometer (Instruments SA, Edison, NJ) coupled with a Sabre argon-ion laser (Coherent, Santa Clara, CA). The laser power at the sample was 200 mW for 514 nm and 488 nm and 100 mW for 458 nm. Each scan involved photon counting for 1 s at 0.5 cm^{-1} increments with a 7 cm^{-1} spectral resolution and the spectra shown are the sum of ~ 10 scans. The vibrational modes of the frozen buffer solution were subtracted, after normalization of the intensities of the lattice mode of ice at 230 cm^{-1}. Where necessary, an estimated exponentially increasing fluorescence baseline was also subtracted. Experiments were carried out in the laboratory of Prof. Michael Johnson, Department of Chemistry, University of Georgia, Athens, USA.

Mass spectrometry (MS) of folded proteins employs soft ionisation (electrospray ionisation, ESI) together with broad mass detection (time of flight, TOF) to study proteins in their native, folded states at, or close to, physiological pH [11]. In positive ion mode (when the spraying nozzle is kept at positive potential) the charging generally occurs via protonation (sometimes metalation also) [12].

For native ESI-MS analysis, RsrR and variants and RirA were exchanged into 250 mM ammonium acetate, pH 8 and 7.32, respectively, using mini-PD10 (GE Healthcare) desalting columns, diluted with anaerobic buffer B to ~25 μM cluster in a 1 ml gas tight syringe [10] and infused directly using a syringe pump (0.3 mL/hr) into the ESI source of a Bruker micrOTOF-QIII mass spectrometer (Bruker Daltonics, Coventry, UK) operating in the positive ion mode. The ESI-TOF was calibrated using ESI-L Low Concentration Tuning Mix (Agilent Technologies, San Diego, CA). Prior to the introduction of sample, the gas tight syringe [10] and associated PEEK tubing (Upchurch Scientific) were flushed with 5 ml of anaerobic buffer. The oxygen permeability of PEEK tubing is 14 ml per 250 cm^2 (atm/25 °C) over 24 h (Upchurch Scientific). RirA mass spectra (*m*/*z* 500–1750 for monomer; *m*/*z* 1800-3500 for dimer) were recorded with acquisition controlled by Bruker oTOF Control software, with parameters as follows: dry gas flow 4 L/min, nebuliser gas pressure 0.8 Bar, dry gas 180 °C, capillary voltage 2750 V, offset 500 V, ion energy 5 eV, collision RF 180 Vpp, collision cell energy 10 eV. Optimization of experimental conditions for the transmission of dimeric species was achieved by increasing the capillary voltage to 4000 V and the collision RF to 600 Vp. RsrR mass spectra (*m*/*z* 550–2000 for monomer; *m*/*z* 2000-3000 for dimer) were recorded with parameters as follows: dry gas flow 4 L/min, nebuliser gas pressure 0.8 Bar, dry gas 180 °C, capillary voltage 2000 V, offset 500 V, ion energy 5 eV, collision RF 200 Vpp, collision cell energy 10 eV [13].

Processing and analysis of MS experimental data was carried out using Compass Data Analysis version 4.1 (Bruker Daltonik, Bremen, Germany). Neutral mass spectra were generated using the ESI Compass version 1.3 Maximum Entropy deconvolution algorithm over a mass range of 17300– 18000 Da for the monomer and 34600 – 35800 Da for the dimer. For kinetic modelling, in order to clearly resolve overlapping peaks, multiple Gaussian functions were fitted to the experimental data using a least-squares regression function in Origin 8 (Microcal) [13]. Exact masses are reported from peak centroids representing the isotope average neutral mass. For apo-proteins, these are

derived from *m/z* spectra, for which peaks correspond to $[M + nH]^{n+}/n$. For cluster-containing proteins, where the cluster contributes charge, peaks correspond to $[M + FeS^{x+} + (n-x)H]^{n+}/n$, where M is the molecular mass of the protein, FeS is the mass of the iron-sulfur cluster of x+ charge, H is the mass of the proton and n is the total charge. In the expression, the x+ charge of the cluster offsets the number of protons required to achieve the observed charge state (n+) [14]. Predicted masses are given as the isotope average of the neutral protein or protein complex, in which cofactor binding is expected to be charge compensated [11]. For analysis of the time resolved MS intensity data, kinetic schemes were modelled using Dynafit 4 (BioKin Ltd). A series of mechanistic models, starting with simple mechanisms and increasing in complexity, represented by a set of chemical equations, were applied to find the best fit for the cluster degradation process [15].

2.9. References.

1. Singleton, C., et al., *Heme-responsive DNA binding by the global iron regulator Irr from Rhizobium leguminosarum.* J Biol Chem, 2010. **285**(21): p. 16023-31.
2. Crack, J.C., et al., *Techniques for the production, isolation, and analysis of iron-sulfur proteins.* Methods Mol Biol, 2014. **1122**: p. 33-48.
3. Bradford, M.M., *A rapid and sensitive method for the quantitation of microgram quantities of protein utilizing the principle of protein-dye binding.* Anal Biochem, 1976. **72**: p. 248-54.
4. Rajagopalan, S., et al., *Studies of IscR reveal a unique mechanism for metal-dependent regulation of DNA binding specificity.* Nat Struct Mol Biol, 2013. **20**(6): p. 740-7.
5. Kibbe, W.A., *OligoCalc: an online oligonucleotide properties calculator.* Nucleic Acids Res, 2007. **35**(Web Server issue): p. W43-6.
6. Diaz-Mireles, E., et al., *The Fur-like protein Mur of Rhizobium leguminosarum is a Mn(2+)-responsive transcriptional regulator.* Microbiology, 2004. **150**(Pt 5): p. 1447-56.
7. Rodionov, D.A., et al., *Computational reconstruction of iron- and manganese-responsive transcriptional networks in alpha-proteobacteria.* PLoS Comput Biol, 2006. **2**(12): p. e163.
8. Hellman, L.M. and M.G. Fried, *Electrophoretic mobility shift assay (EMSA) for detecting protein-nucleic acid interactions.* Nat Protoc, 2007. **2**(8): p. 1849-61.
9. Crack, J.C., et al., *Differentiated, Promoter-specific Response of [4Fe-4S] NsrR DNA Binding to Reaction with Nitric Oxide.* J Biol Chem, 2016. **291**(16): p. 8663-72.
10. Crack, J.C., et al., *NsrR from Streptomyces coelicolor is a nitric oxide-sensing [4Fe-4S] cluster protein with a specialized regulatory function.* J Biol Chem, 2015. **290**(20): p. 12689-704.
11. Kay, K.L., C.J. Hamilton, and N.E. Le Brun, *Mass spectrometry of B. subtilis CopZ: Cu(i)-binding and interactions with bacillithiol.* Metallomics, 2016. **8**(7): p. 709-19.
12. Banerjee, S. and S. Mazumdar, *Electrospray ionization mass spectrometry: a technique to access the information beyond the molecular weight of the analyte.* Int J Anal Chem, 2012. **2012**: p. 282574.
13. Laganowsky, A., et al., *Mass spectrometry of intact membrane protein complexes.* Nat Protoc, 2013. **8**(4): p. 639-51.

14. Johnson, K.A., et al., *Probing the stoichiometry and oxidation states of metal centers in iron-sulfur proteins using electrospray FTICR mass spectrometry.* Anal Chem, 2000. **72**(7): p. 1410-8.

15. Kuzmic, P., *Program DYNAFIT for the analysis of enzyme kinetic data: application to HIV proteinase.* Anal Biochem, 1996. **237**(2): p. 260-73.

Chapter 3. Characterization of the iron- sulfur cluster of R. leguminosarum RirA.

RirA is a global regulator of iron metabolism in a range of α-proteobacteria. In this chapter, the over-expression/purification of RirA from *Rhizobium leguminosarum* is described, along with biophysical studies of its iron- sulfur cluster. Spectroscopic properties and native ESI-MS of cluster-reconstituted RirA are characteristic of a [4Fe-4S] cluster cofactor, and this form of the protein shows only moderate sensitivity to O_2, resulting in gradual loss of the cluster.

3.1. Alignment of *R. leguminosarum* RirA with NsrR and IscR sequences from different bacteria.

Members of the Rrf2 superfamily of transcription factors are widespread in bacteria but their biological functions are largely unknown. Many have C-terminal cysteine residues that are known, or predicted, to coordinate an Fe-S cluster. The few that have been characterised in detail are NsrR, which senses nitric oxide [1] and IscR which senses the Fe-S cluster status of the cell [2]. These proteins are described in detail in Chapter 1. RirA has previously been predicted as an Fe-S cluster protein on the basis of bioinformatic analysis and alignment with other members of the Rrf2 family that contain an Fe-S cluster, see Figure 3.1.
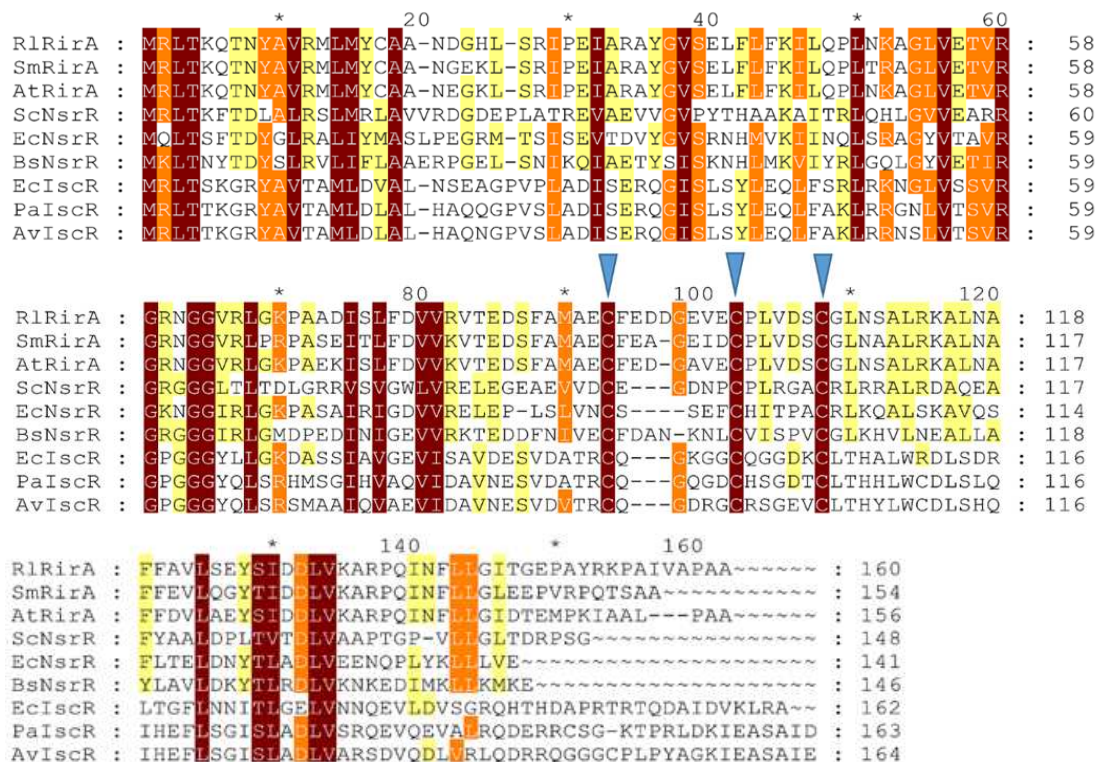
Figure 3.1. Alignment of *R. leguminosarum* RirA with other Rrf2 family regulators. Alignment of *R. leguminosarum* RirA (RlRirA) with RirA sequences from *Sinorhizobium meliloti* (SmRirA) and *Agrobacterium tumefaciens* (AtRirA), NsrR sequences from *Streptomyces coelicolor* (ScNsrR), *E. coli* (EcNsrR) and *Bacillus subtilis* (BsNsrR), and IscR sequences from *E. coli* (EcIscR), *Pseudomonas aeruginosa* (PaIscR) and *Azotobacter vinelandii* (AvIscR). The three conserved cysteine residues predicted to ligate Fe-S clusters in Rrf2 family regulators are indicated by blue arrow heads. The alignment was carried out using Clustal Omega [3] and presented using Genedoc [4].

3.2. RirA as isolated and following reconstitution.

Purification of RirA using a HiTrap Heparin column (see Chapter 2, section 2.2.1) following over-expression in *E. coli* resulted in a straw-brown colored solution. Iron and protein analyses revealed a low ratio of iron to protein (~ 9%) indicating that the majority of the protein was in the apo-form. A small proportion (<5%) of the protein was present as a truncated form (Figure 3.2 inset), which was shown by mass spectrometry to have a mass of 15451 Da, consistent with the loss of 20 C-terminal residues compared to the full length protein (M_w 17441 Da).

Although the growth and the purification were always carried out following the same protocol described in Chapter 2 (section 2.1-2.2), CD measurements showed that samples varied between the preparations (made on different dates). This could be because

E. coli does not efficiently incorporate an Fe-S cluster into *R. leguminosarum* RirA, or that minor variations in the conditions of the purification, for example in the pH of the buffer or conditions of sonication, lead to substantial changes in the small proportion of the protein molecules that contain a cluster.

In order to determine whether an increased cluster incorporation might be achieved through an *in vitro* reconstitution, RirA was treated as described in Chapter 2 (section 2.5). *In vitro* cluster reconstitution of as isolated RirA resulted in a much darker brown solution. As isolated and reconstituted samples of RirA were analyzed by UV-visible absorbance, see Figure 3.2. From the UV-visible absorbance spectrum it is very clear that the quantity of Fe-S cluster in the reconstituted sample is higher than in the isolated sample. Also, it is possible to see that the shape of the spectrum is different in the two samples, in that the maximum peak for the Fe-S cluster appears at a different wavelength. In the case of the as isolated sample, the maximum is at 410 nm while for the reconstituted sample it is at 382 nm, see Figure 3.2. The spectrum of the reconstituted sample has the characteristic of a [4Fe-4S] cluster [5] and the as isolated spectrum is more characteristic of a mixture of both [2Fe-2S] and [4Fe-4S] clusters [5-7]. The extinction coefficient obtained with the absorbance measurements can be used to help determine the type of cluster. The extinction coefficient for the as isolated, determined from iron concentration at 410 nm is 7622 $M^{-1}.cm^{-1}$, which correlates with a [2Fe-2S] cluster, typically have an extinction coefficient of ~8000 $M^{-1}.cm^{-1}$. For the reconstituted sample the maximum was at 382 nm with an extinction coefficient of 11739 $M^{-1}.cm^{-1}$; this is lower than that expected for a [4Fe-4S] cluster (~16000 $M^{-1}.cm^{-1}$) but in this case it is not possible to distinguish if it is a [3Fe-4S] or a [4Fe-4S] with 3 cysteines as ligands. For the reconstituted sample the concentration of [4Fe-4S] cluster and RirA were 457 and 741 µM respectively, indicating ~62% cluster incorporation. In Figure 3.2 it is also possible to see the absorbance peak due to the protein at 280 nm.

Figure 3.2. UV-visible absorbance spectra for the as isolated (black) and reconstituted (red) RirA samples. The protein used for the reconstitution was the as isolated sample. Inset is another representation of the data in which the as isolated data have been multiplied 4.5 times to permit easier comparison of the shape of the absorbance bands due to the Fe-S clusters. Spectra were recorded for RirA, in buffer B (25 mM HEPES, 2.5 mM $CaCl_2$, 50 mM NaCl, 750 mM KCl, pH 7.5), where the concentrations of the protein for the as isolated and reconstituted samples were 1099 µM and 741 µM, respectively. The measurements were obtained using a 1 mm sealed anaerobic cuvette and buffer B for the UV-visible baseline.

Circular dichroism also revealed differences between the as isolated and the reconstituted samples (Figure 3.3). The most notable change was the broad peak that only appeared for the reconstituted sample in the area between 530 and 650 nm. In the ranges between 380-530 nm and 280-380 nm, while the as isolated sample spectrum contained only one broad peak, the reconstituted sample spectrum appeared to have two (Figure 3.3). Therefore from UV-visible and CD experiments, it can be concluded that the as isolated and the reconstituted samples are not the same in terms of the type of cluster they may contain.
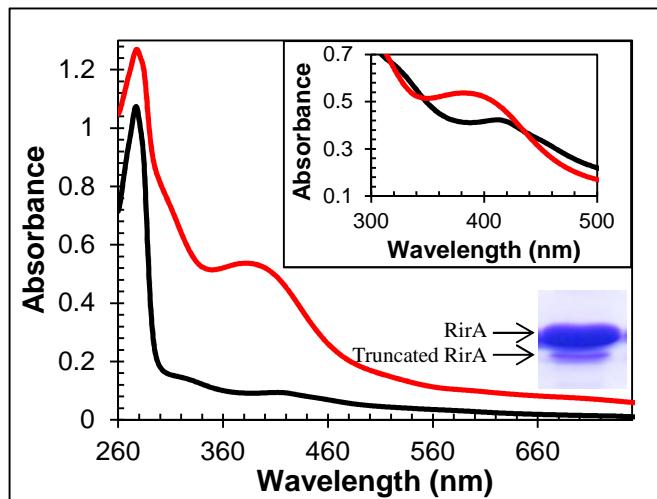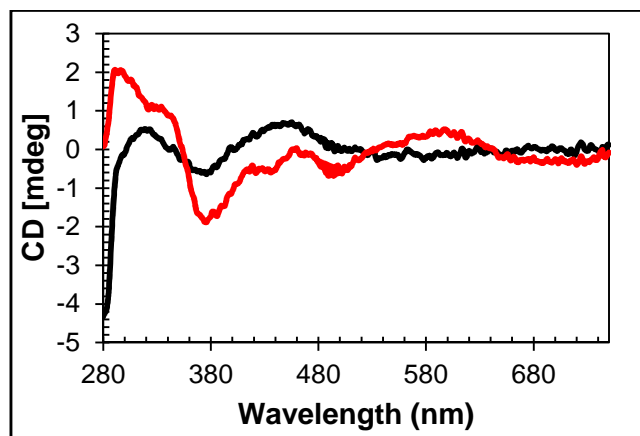
Figure 3.3. Circular dichroism spectra for the as isolated (black) and the reconstituted (red) samples. The protein used for the reconstitution was the as isolated sample. Spectra were recorded for RirA, in buffer B, where the concentrations of the protein for the as isolated and reconstituted samples were 1099 µM and 741 µM, respectively. The measurements were obtained using a 1 mm sealed anaerobic cuvette and buffer B (25 mM HEPES, 2.5 mM $CaCl_2$, 50 mM NaCl, 750 mM KCl, pH 7.5) for the CD baseline correction.

A second step was carried out in the purification of RirA. As shown in Figure 3.4A, fractions collected from the HiTrap Heparin column (as isolated sample) containing the RirA protein had a number of additional bands and three apparent RirA degradation products. Thus, the protein was further purified using a gel filtration column. After gel filtration the protein was essentially pure with only one of the degradation products remaining (at low concentration), see Figure 3.4B. However, the shape of the UV-visible absorbance showed changes. The absorbance band at 410 nm was broadened and the shoulder at ~320 nm became more defined, see Figure 3.5. It is unclear what causes the observed changes, but one possibility is that the cluster generated *in vivo* is not stably coordinated and is partially lost/altered during gel filtration. Further investigation of this is needed.

SDS-PAGE, UV-visible and CD spectra (CD data not shown) reflect the dilution of the sample during the gel filtration process. The concentration of RirA was 1646 µM after the Heparin column and 123 µM after gel filtration. After gel filtration the fractions obtained with the higher absorbance at 280 nm were colourless, reflecting the loss of the cluster.
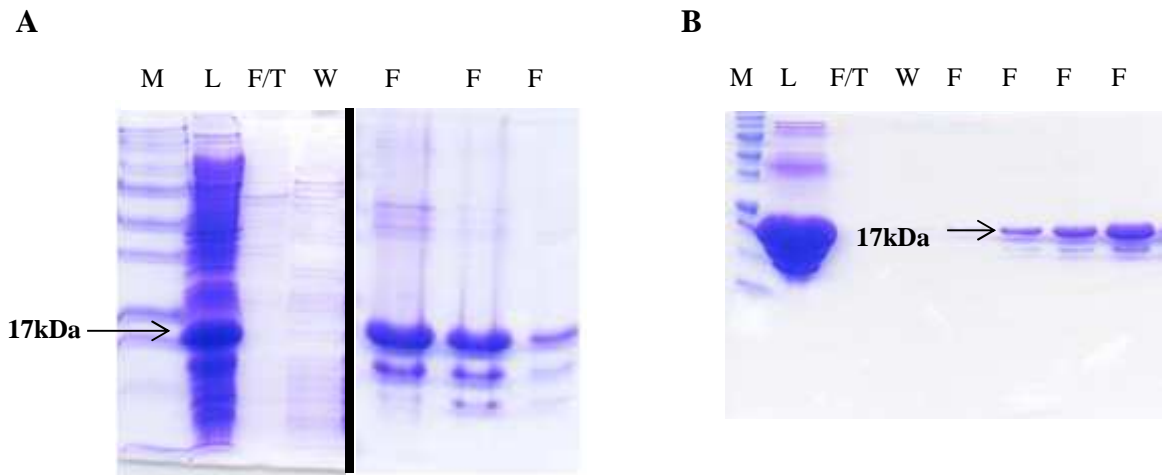
Figure 3.4. 14% SDS-PAGE gel for the fractions obtained after the Heparin column (A) and after gel filtration column (B). Abbreviations: M: marker, L: load (*in vivo* sample), F/T: flow through, W: wash, F: fractions which show the maxima absorbance at 280 nm.
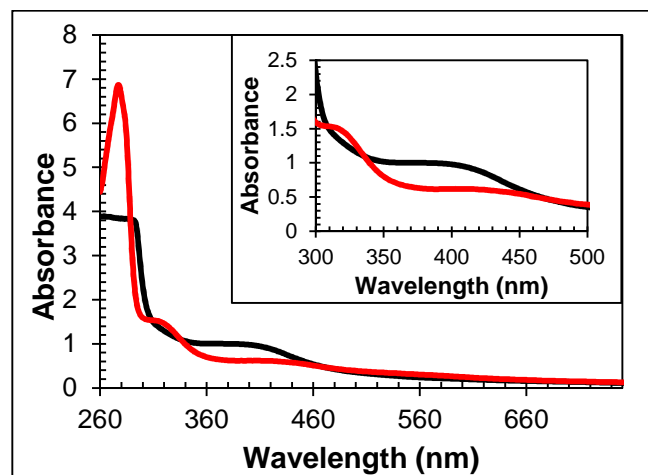
Figure 3.5. UV-visible absorbance spectra for the as isolated sample and the sample obtained after further purification using gel filtration. Spectra were recorded for RirA where the concentration of protein before (black line) and after gel filtration (red line) were 1646 µM and 123 µM, respectively. RirA before was in buffer B (25 mM HEPES, 2.5 mM CaCl$_2$, 50 mM NaCl, 750 mM KCl, pH 7.5) and after gel filtration was in buffer C (25 mM HEPES, 2.5 mM CaCl$_2$, 50 mM NaCl, 333 mM KCl, pH 7.5). The measurements were obtained using a 1 cm sealed anaerobic cuvette and buffer B and C for the UV-visible baseline before and after gel filtration, respectively.

Gel filtration purification was also performed with the reconstituted sample. In this case the UV-vis spectrum did not show any change in shape, see Figure 3.6A. The CD spectra of the two samples did reveal some differences, see the broken line box of Figure 3.6B. In the spectrum for the reconstituted sample two peaks at 428 and 469 nm appear although they are not very well defined. For the sample after gel filtration, there is only a

broad peak between 416 and 483 nm. This could be because the sample after gel filtration

is diluted 24 times compared with the reconstituted sample.
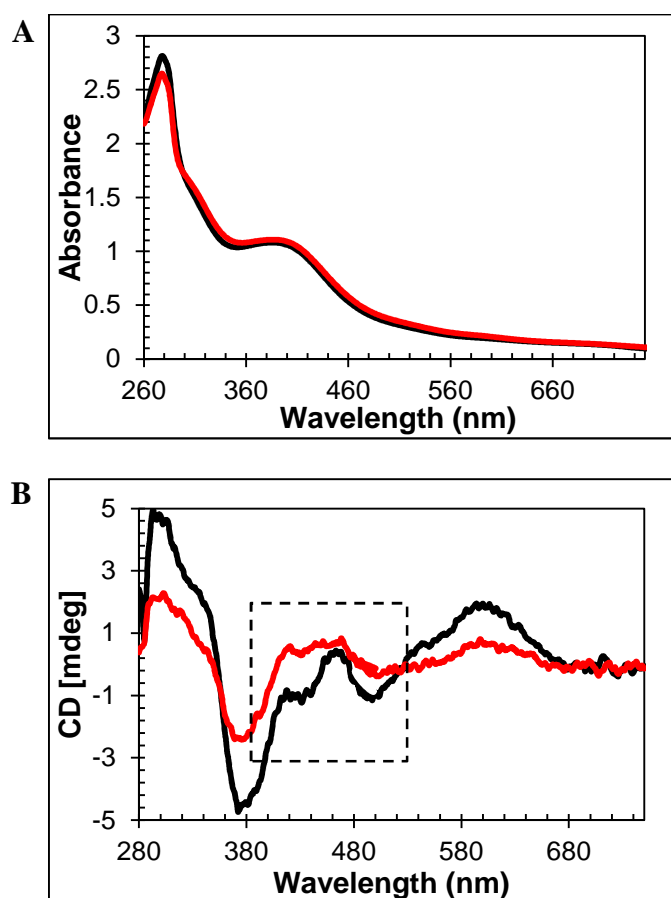
Figure 3.6. UV-visible absorbance (A) and CD (B) spectra for the reconstituted (black line) sample and the sample obtained after gel filtration (red line). In A, the data after gel filtration have been multiplied 2.7 times to permit easier comparison of the shape of the absorbance bands due to the Fe-S clusters. Spectra were recorded for RirA where the concentration before and after gel filtration was 1248 µM and 52 µM, respectively. RirA before was in buffer B (25 mM HEPES, 2.5 mM $CaCl_2$, 50 mM NaCl, 750 mM KCl, pH 7.5) and after gel filtration was in buffer C (25 mM HEPES, 2.5 mM $CaCl_2$, 50 mM NaCl, 333 mM KCl, pH 7.5). The measurements were obtained using a 1 mm sealed anaerobic cuvette for the reconstituted sample and a 1 cm sealed anaerobic cuvette for the sample after gel filtration. Buffer B and CD were used for the UV-visible baseline and CD baseline correction before and after gel filtration, respectively.

Gel filtration was also used to determine the oligomeric state of the protein,

specifically whether RirA is monomeric or multimeric. This is a technique whereby

proteins of known sizes are applied to a gel filtration column under the same conditions.

The proteins elute at differing elution volumes (Ve) according to their size, with larger

molecules passing through the gel more rapidly. From the data obtained, a calibration line

can be plotted (see Figure 3.7). The protein of unknown mass or oligomeric state can then

40

be applied to the column. The elution volume of this protein is then compared with the known standards to determine the molecular weight/oligomeric state [8]. The elution volume for the reconstituted RirA was 56 mL and from the calibration plot, the deduced molecular mass was 37.7 kDa. This indicates that RirA is a dimer, as the mass of a RirA monomer is 17.4 kDa. Furthermore, because the sample of RirA analysed was a mixture of apo- and holo-proteins, it appears that the associated state is not dependent on the status of the cluster.
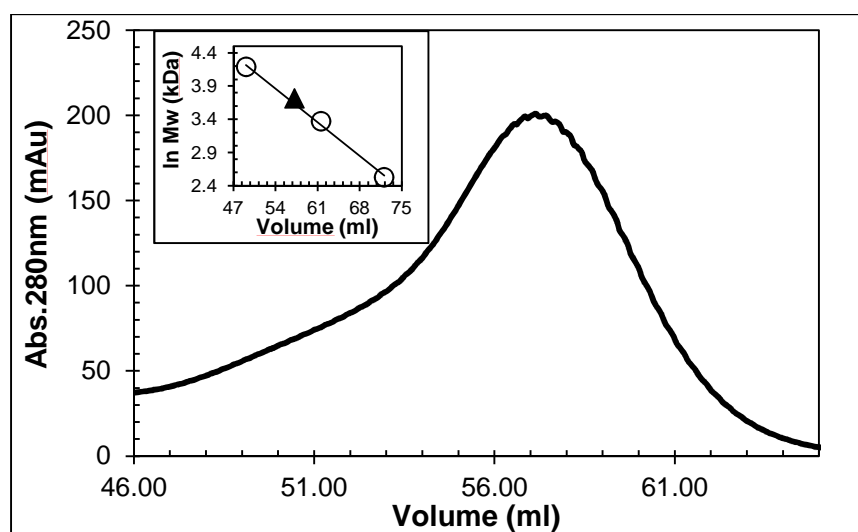
Figure 3.7. Analysis of RirA association state. Analytical gel filtration chromatogram of reconstituted RirA (707 µM in [4Fe-4S] cluster, 57% cluster loaded) in buffer C (25 mM HEPES, 2.5 mM CaCl$_2$, 50 mM NaCl, 333 mM KCl, pH 7.5). *Inset*, calibration curve for the Sephacryl 100HR column. Standard proteins (open circles) were BSA (66 kDa), carbonic anhydrase (29 kDa), and cytochrome *c* (13 kDa). [4Fe-4S]-RirA is shown as a black triangle. mAu, milli-absorbance units.

Unless otherwise stated, the remainder of the work in RirA was performed with the reconstituted samples without gel filtration purification because the concentration of protein and extent of cluster incorporation is higher than for the as isolated sample, and also for the gel filtrated samples. Furthermore the spectroscopic properties of reconstituted RirA were entirely reproducible.

41

3.2.1. EPR studies.

To help clarify if the reconstituted protein contains an [2Fe-2S], [3Fe-4S] or [4Fe-4S] cluster, EPR spectroscopy was used to further investigate the nature of the cluster(s) in reconstituted RirA. The [3Fe-4S] cluster in its +1 state is paramagnetic ($S = \frac{1}{2}$) and it is therefore EPR active, while [4Fe-4S] and [2Fe-2S] forms (in their most common 2+ states) are diamagnetic and therefore EPR silent [9-11].

The spectrum of reconstituted RirA, Figure 3.8, contained a very low intensity signal with g-value of 2.03, which is characteristic of a $S = \frac{1}{2}$ $[3Fe4S]^{1+}$ cluster [12]. Double integration of the signal revealed that this accounts for <1% of the cluster concentration, consistent with the vast majority of the cluster being EPR silent, i.e. as $[4Fe-4S]^{2+}$ as suggested by the UV-visible absorbance data. Addition of sodium dithionite led to essentially complete loss of the [3Fe-4S] signal (Figure 3.8), consistent with reduction to the EPR-silent state, $[3Fe-4S]^{0}$. No evidence for a reduced $[4Fe-4S]^{1+}$ form was observed.

Figure 3.8. EPR study. EPR spectra of [4Fe-4S] RirA (black), and following: addition of 100 μM of sodium dithionite (red) and gel filtration (green). Inset is an expanded view of the signal in the reconstituted sample before and after addition of dithionite. RirA (100 μM [4Fe-4S] RirA; ~55% cluster-loaded) was in buffer B (25 mM HEPES, 2.5 mM CaCl$_2$, 50 mM NaCl, 750 mM KCl, pH 7.5).
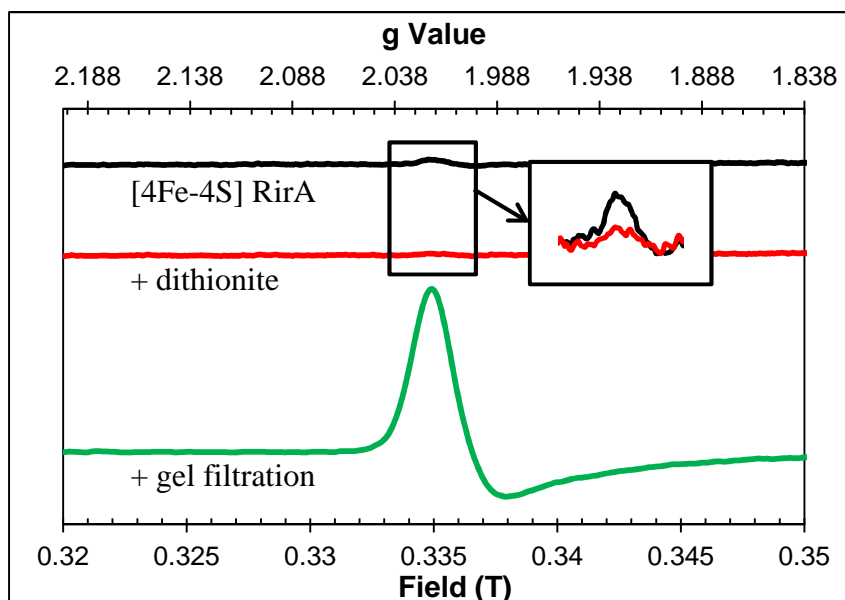
Gel filtration of reconstituted RirA under anaerobic conditions resulted in an increase in the [3Fe-4S]$^{1+}$ signal in the EPR spectrum to ~3% of the total cluster concentration. Since the [3Fe-4S] form arises from loss of iron from the [4Fe-4S] cluster, this suggests that the cluster is susceptible to loss of iron under the conditions of the experiment.

3.2.2. Native ESI-MS of [4Fe-4S] RirA.

Electrospray ionization mass spectrometry (ESI-MS) has been used previously to study Fe-S cluster proteins under non-denaturing conditions under which the cluster remains bound to the protein [13, 14]. Conditions were established for the ionization of cluster-reconstituted RirA under non-denaturing conditions. Reconstituted and as isolated samples were analysed. The *m/z* spectrum for the reconstituted sample could be divided into two distinct regions, corresponding to monomeric RirA (*m/z* 500-1750), and dimeric RirA (*m/z* 1800-3500). Although RirA is a dimer in solution, it is apparent that the protein monomerises to a significant extent during ionisation, as recently observed for another dimeric Fe-S cluster regulator, FNR [15], see Figure 3.9.

The major peak in the deconvoluted mass spectrum of RirA in the monomer region, Figure 3.10A, was at 17792 Da, corresponding to [4Fe-4S] RirA (see Table 3.1). To the lower mass side of the major peak was a collection of smaller peaks corresponding to a range of cluster breakdown species, including [4Fe-3S], [3Fe-4S], [4Fe-2S], [3Fe-3S], [3Fe-2S], [3Fe-S], [2Fe-2S], see Figure 3.10A and Table 3.1. A small peak due to apo-protein was also observed at 17441 Da. The deconvoluted mass spectrum of the dimer region, Figure 3.10B, contains a major peak at 35585 Da corresponding to the RirA dimer containing two [4Fe-4S] clusters. To the higher mass side were a number of less abundant peaks at +32, +64 and +96 Da, corresponding to one, two and three sulfane sulfur adducts, which arise because Cys residues readily pick up additional sulfurs as persulfides [15, 16]. To the lower mass side were smaller peaks due to the RirA dimer containing [3Fe-

4S]/[4Fe-4S], [3Fe-4S]/[3Fe-4S], [3Fe-3S]/[3Fe-4S], and [3Fe-3S]/[3Fe-3S] clusters, with a very low intensity peak due to [2Fe-2S]/[2Fe-2S] RirA. Each of these most likely represents a breakdown product of the [4Fe-4S] cluster form. The observation of a range of cluster breakdown species is consistent with the fragility of the [4Fe-4S] cluster. No apo-RirA was observed in the dimer region.
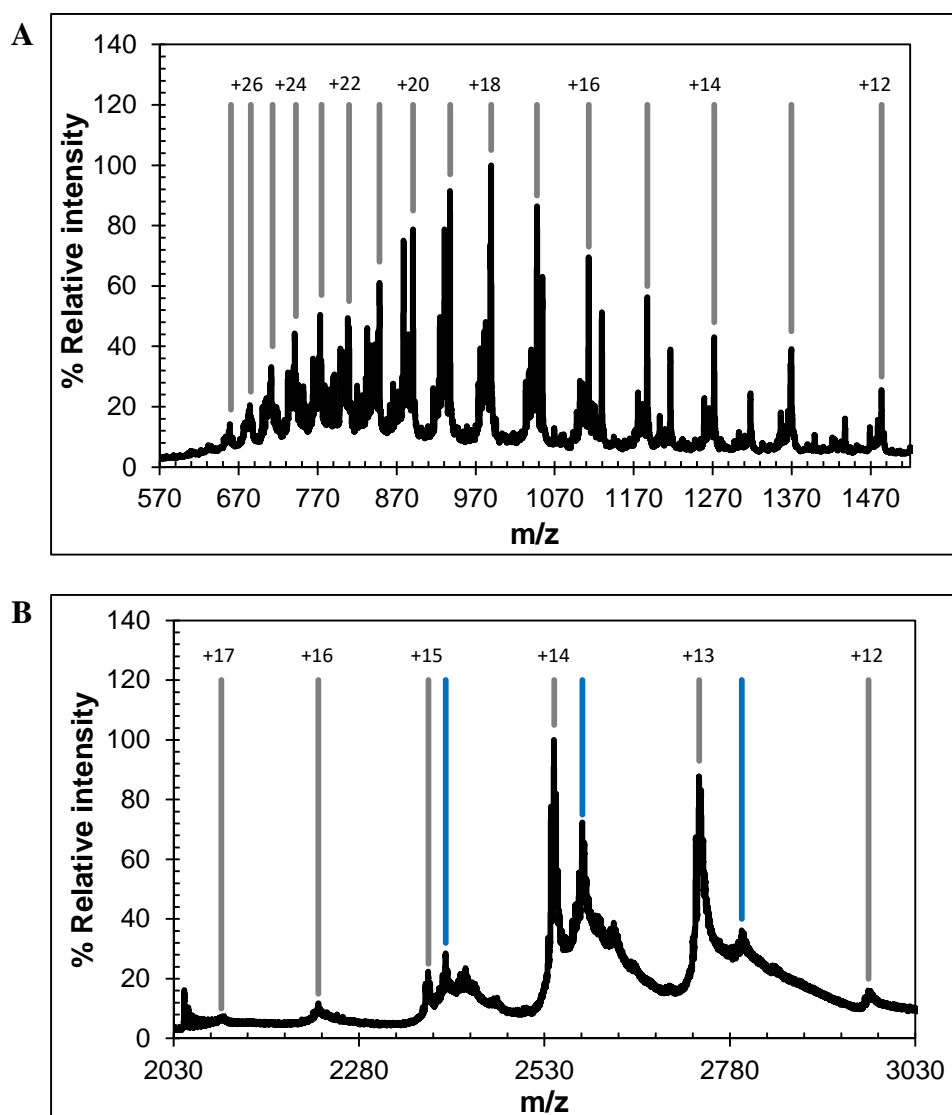
Figure 3.9. ESI-MS *m/z* spectra of reconstituted RirA. (**A**) monomer and (**B**) dimer regions of the *m/z* spectrum are plotted with charge states as indicated. Blue lines indicate the presence of a truncated form of RirA.

Figure 3.10. ESI-MS analysis of reconstituted RirA under native conditions. Positive ion mode ESI-TOF native mass spectra of ~30 µM [4Fe-4S] RirA in 250 mM ammonium acetate pH 7.32. Deconvoluted spectrum in the (**A**) monomer and (**B**) dimer mass regions.

Table 3.1. Predicted and observed masses for apo- and cluster-bound forms of RirA.

RirA species	Predicted mass (Da)[a]	Average observed mass (Da)[b]	ΔMass (Predicted - observed) (Da)
Monomeric			
Apo	17442	17441	+1
[4Fe-4S]$^{2+}$	17792	17792	0
[4Fe-3S]$^{4+}$	17758	17758	0
[3Fe-4S]$^{1+}$	17737	17736	+1
[4Fe-2S]$^{6+}$	17724	17723	+1
[3Fe-3S]$^{3+}$	17703	17703	0
[3Fe-2S]$^{5+}$	17669	17668	+1
[3Fe-S]$^{7+}$	17635	17635	0
[2Fe-2S]$^{2+}$	17616	17615	+1
[2Fe-S]$^{4+}$	17582	17582	0
2Fe^{2+}	17550	17550	0
Dimeric			
Apo	34884	-	-
[4Fe-4S]$^{2+}$/[4Fe-4S]$^{2+}$	35584	35585	-1
[3Fe-4S]$^{1+}$/[4Fe-4S]$^{2+}$	35529	35528	+1
[3Fe-4S]$^{1+}$/[3Fe-4S]$^{1+}$	35474	35475	-1
[3Fe-3S]$^{3+}$/[3Fe-4S]$^{1+}$	35440	35441	-1
[3Fe-3S]$^{3+}$/[3Fe-3S]$^{3+}$	35406	35407	-1
[2Fe-2S]$^{2+}$/[2Fe-2S]$^{2+}$	35232	35232	0

[a]The difference in predicted mass depending on the overall charge on the cluster is due to charge compensation of cluster binding. A lower overall cluster charge would result in more protons remaining bound and consequently a higher mass [17, 18].
[b]The average observed mass is derived from at least three independent experiments, with standard deviation of ± 1 Da.

For the as isolated sample, in the monomer region the only significant peak corresponds to the apo-RirA (17441 Da) (Figure 3.11A). In the dimer region the most abundant peak corresponds to the apo-RirA dimer (34884 Da) but cluster bound forms were observed, corresponding to break- down products of the [4Fe-4S]/[4Fe-4S] form, see Figure 3.11B. These data are consistent with the presence of a broad mixture of [4Fe-4S] and [2Fe-2S] clusters, as well as possible intermediate species.
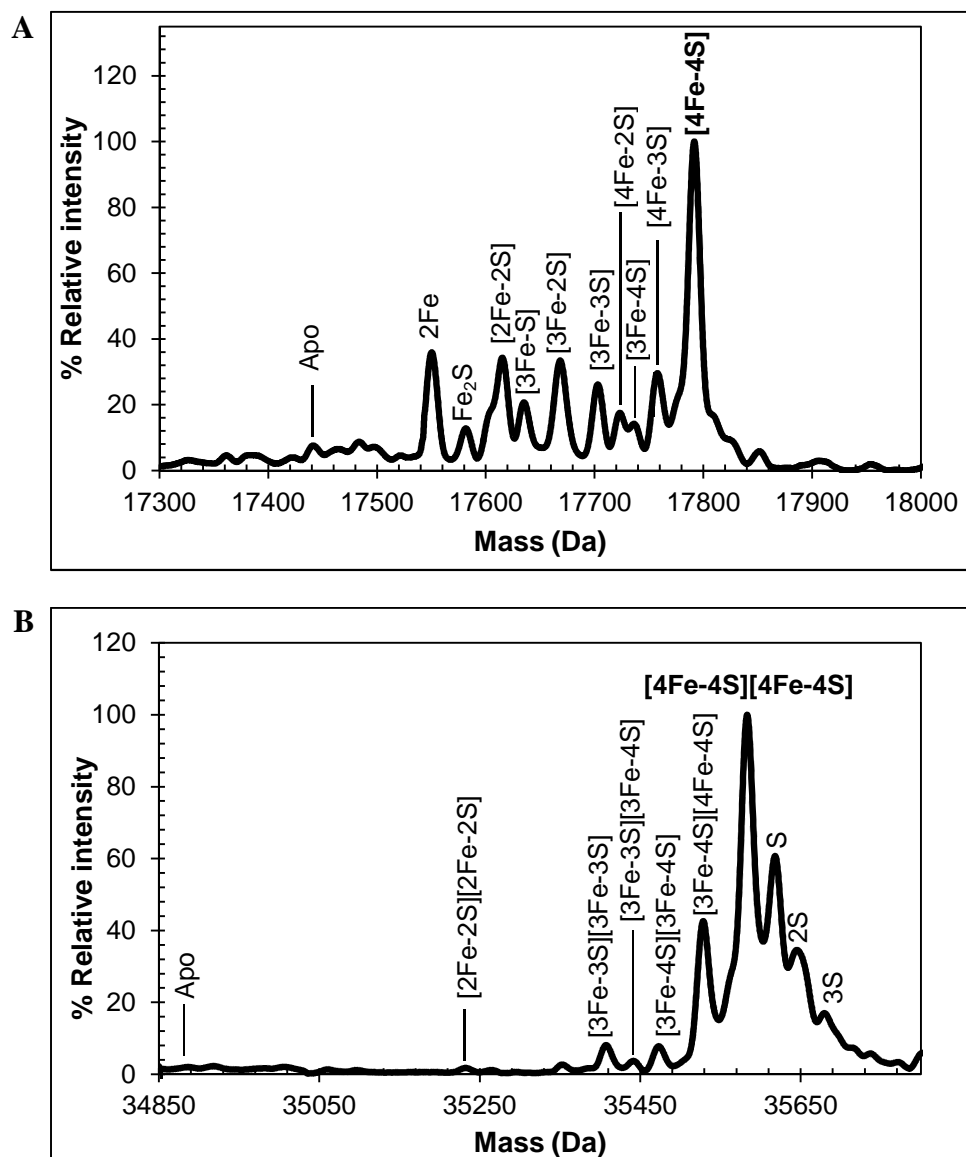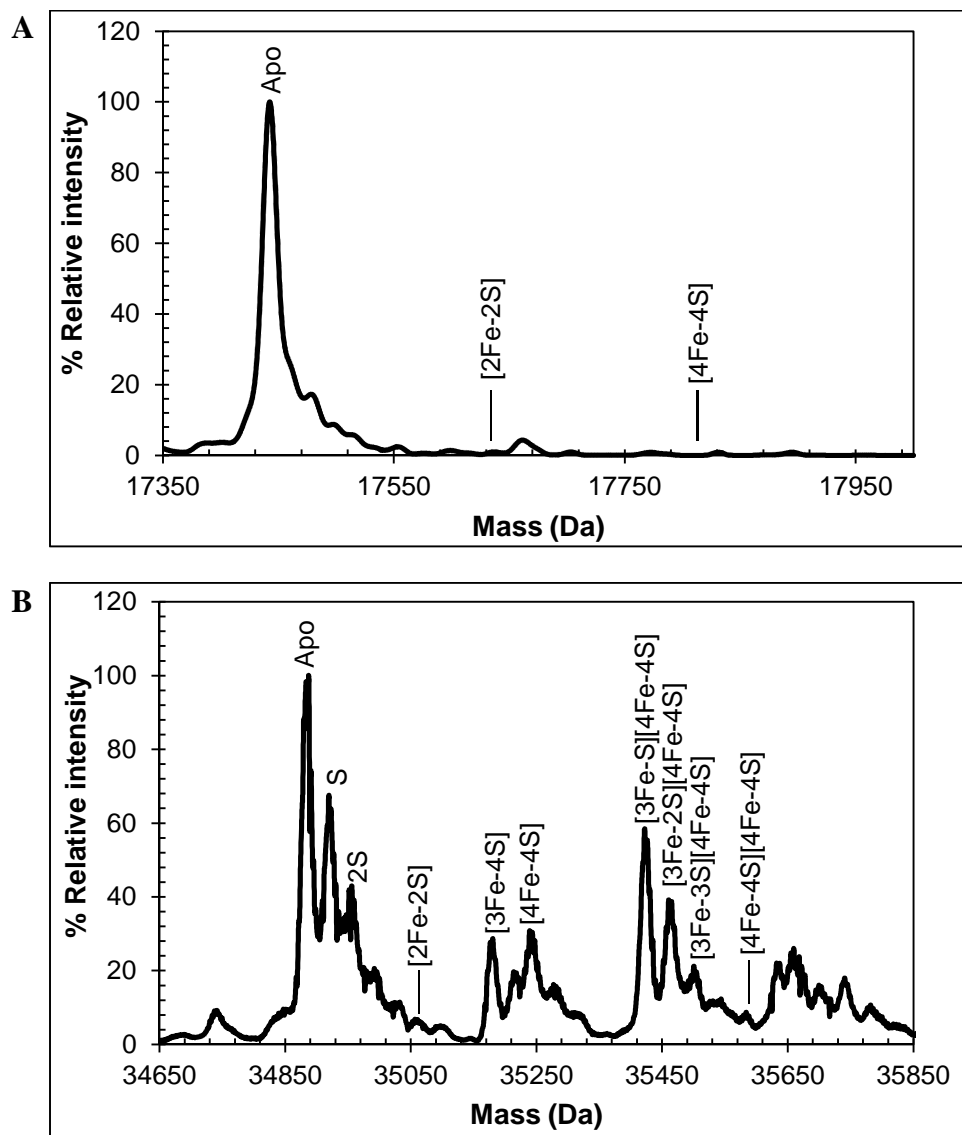
Figure 3.11. ESI-MS analysis of as isolated RirA under native conditions. Positive ion mode ESI-TOF native mass spectra of ~30 µM [4Fe-4S] RirA in 250 mM ammonium acetate pH 7.32. Deconvoluted spectrum in the (**A**) monomer and (**B**) dimer mass regions.

3.3. Stability of [4Fe-4S]-RirA.

3.3.1. Stability of [4Fe-4S]-RirA under anaerobic and aerobic conditions at room temperature.

In order to determine the stability of RirA under anaerobic conditions at room temperature, CD measurements were made over a period of time. As Figure 3.12 shows, the CD spectrum did not change when RirA was left for 7 hours. In fact, [4Fe-4S] RirA could be stored for several weeks at 4 °C under anaerobic conditions without significant

degradation. This experiment demonstrates that the changes observed in further experiments are not due to an inherent instability of RirA.
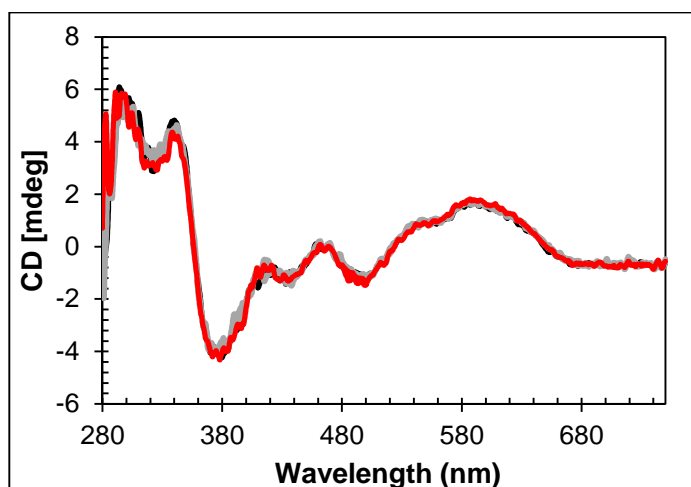
Figure 3.12. CD spectra of [4Fe-4S] RirA under anaerobic conditions as a function of time. CD spectra recorded at 0 min (black) and 7 hr (red). Intervening spectra are in grey. Protein and [4Fe-4S] RirA concentrations were respectively: 2075 µM and 1396 µM. The measurements were obtained in 1 mm sealed anaerobic cuvette, using buffer B (25 mM HEPES, 2.5 mM CaCl$_2$, 50 mM NaCl, 750 mM KCl, pH 7.5) for the CD baseline correction.

To investigate the effects of exposure to aerobic conditions, UV-visible and CD spectra of [4Fe-4S] RirA in the presence of saturating concentrations of O$_2$ were measured. These revealed a red shift of the absorbance band at 383 nm over the first 45 min, followed by gradual loss of absorbance intensity (Figure 3.13A). Changes in the CD spectrum were consistent with this, with an increase in the positive band at 464 nm over the first 45 min, followed by the loss of all bands as the apo-protein was formed (Figure 3.13B).

The observed changes are characteristic of the formation of a [2Fe-2S] cluster prior to complete loss of the cluster. Conversion of [4Fe-4S] RirA to a [2Fe-2S] form could involve formation of a transiently stable [3Fe-4S]$^{1+}$, which can be detected by EPR spectroscopy [19]. Addition of O$_2$ (by exposure to air) or potassium ferricyanide (100 µM final concentration) respectively led to increases in the g = 2.01 EPR signal due to a [3Fe-

4S]$^{1+}$ form to ~11% and ~39% of the original cluster concentration after 30 min (Figure 3.14).
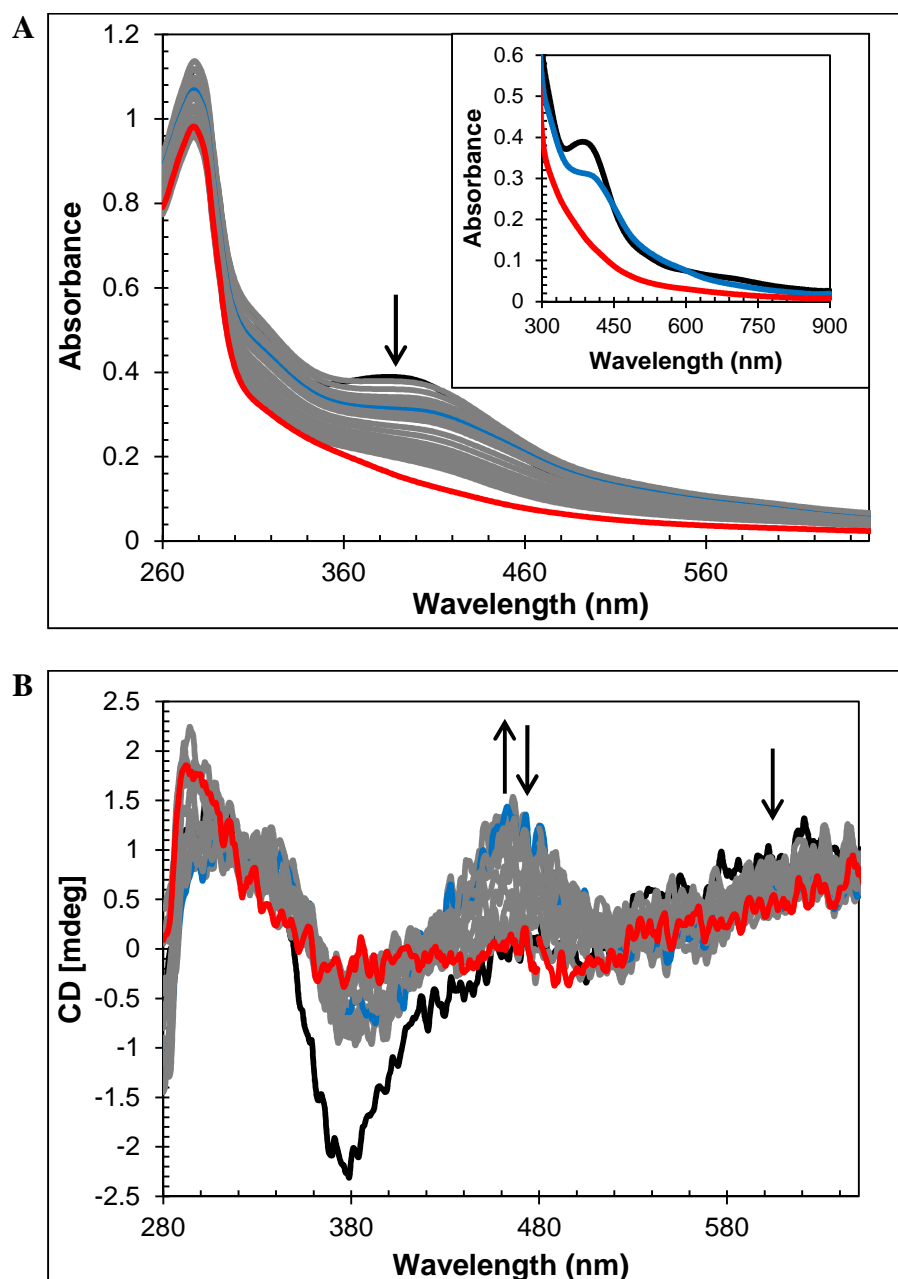
Figure 3.13. O$_2$ sensitivity of [4Fe-4S] RirA. (A) UV-visible absorption spectra and **(B)** CD spectra were recorded over several hours following exposure of [4Fe-4S] RirA (30 µM in cluster in buffer B (25 mM HEPES, 2.5 mM CaCl$_2$, 50 mM NaCl, 750 mM KCl, pH 7.5); ~89% cluster-loaded) to 230 µM O$_2$. Inset in (A) are absorbance spectra recorded at 0 min (black), 44 min (blue) and 24 hr (1440 min, red). In (B), CD spectra recorded at 0 min (black), 44 min (blue) and 5.5 hr (red). Intervening spectra are in grey. The measurements were obtained using a 1 cm cuvette. Buffer B was used for the UV-visible baseline and CD baseline correction.
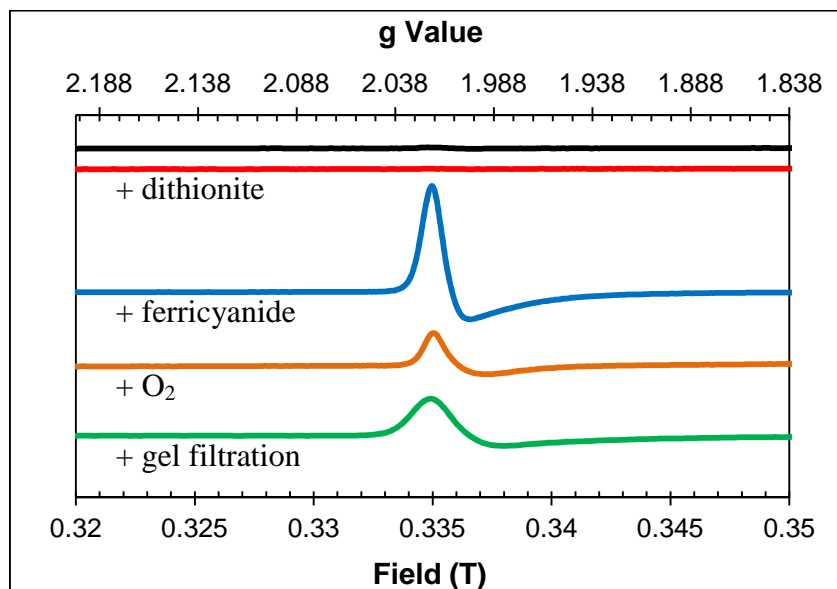
Figure 3.14. EPR study of O₂ sensitivity of [4Fe-4S] RirA. EPR spectra of [4Fe-4S] RirA (black), and following: addition of 100 µM of sodium dithionite (red); addition of 100 µM of potassium ferricyanide (blue); exposure to 230 µM O_2 for 30 min (orange) and gel filtration (green). RirA (100 µM [4Fe-4S] RirA; ~55% cluster-loaded) was in buffer B (25 mM HEPES, 2.5 mM $CaCl_2$, 50 mM NaCl, 750 mM KCl, pH 7.5).

The effects of a range of lower O_2 concentrations were examined by monitoring cluster degradation via absorbance at 383 nm. These traces revealed that the rate of reaction with O_2 increased along with O_2 concentration. Each of the traces could be fitted with a single exponential function, which revealed a rate constant, $k = 0.019 \pm 0.004$ min⁻¹, that was essentially independent of the O_2 concentration, consistent with the rate-limiting step of the reaction not involving O_2, see Figure 3.15.

Compared to other Fe-S regulatory proteins, such as the O_2-sensing regulatory protein FNR [20], the RirA cluster is not very sensitive to molecular oxygen, as expected for an iron sensor from an aerobic organism.
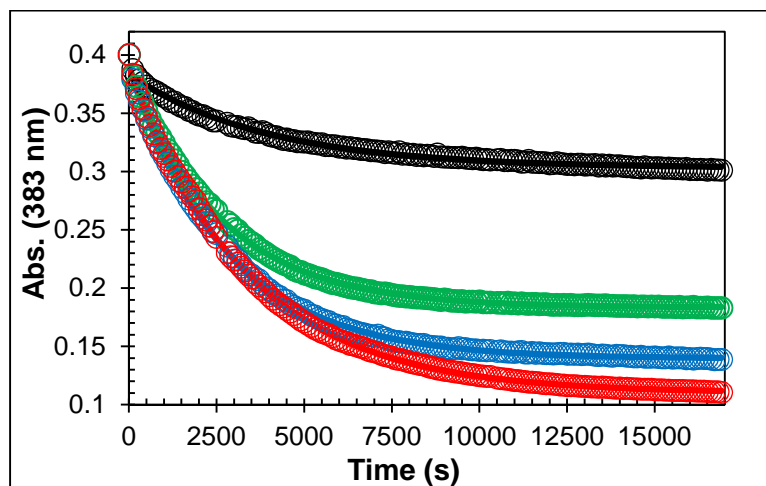
Figure 3.15. Effects of lower O₂ concentrations. Plots of UV-visible absorbance at 383 nm as a function of time following addition of increasing concentrations of O_2 to [4Fe-4S] RirA (30 µM in cluster in buffer B (25 mM HEPES, 2.5 mM $CaCl_2$, 50 mM NaCl, 750 mM KCl, pH 7.5); ~62% cluster-loaded). 58 µM O_2 (black), 115 µM O_2 (green), 172 µM O_2 (blue) and 230 µM O_2 (red). Fits to the data are represented by solid lines.

3.3.2. Stability of [4Fe-4S]-RirA in the presence of L- glutathione.

L-glutathione is present in the cytoplasm of *R. leguminosarum* [21, 22]. An anaerobic titration of RirA was carried out with the additions of L-glutathione made inside the glove box. The concentration range was between 0 and 1.6 mM. With further additions of L-glutathione the solution precipitated. Figure 3.16 shows UV-visible and CD spectra for all the additions. The data clearly demonstrate there is no interaction between L-glutathione and the cluster as there are no changes in the spectrum.
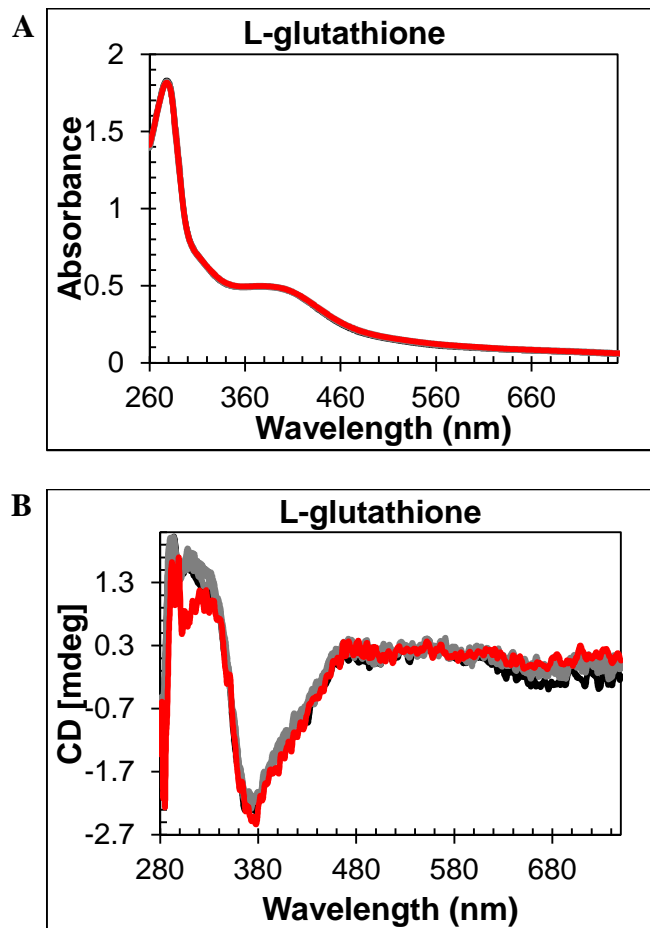
Figure 3.16. UV-visible (A) and CD (B) titration of RirA against L-glutathione under anaerobic conditions. RirA and [4Fe-4S] RirA concentrations were respectively: 226 µM and 139 µM. Starting spectrum is in black (0 mM L-glutathione), end point spectrum (1.6 mM L-glutathione) is in red and intervening spectra are in grey. The measurements were obtained in a 1 cm sealed anaerobic cuvette, using buffer B (25 mM HEPES, 2.5 mM CaCl$_2$, 50 mM NaCl, 750 mM KCl, pH 7.5) as a baseline.

As the UV-visible and CD spectra did not change when the concentration of L-glutathione was 1.60 mM (corresponding with the CD spectrum at 0 min in the Figure 3.17) the solution was exposed to ambient O$_2$. Figure 3.17 revealed gradual loss of the cluster until the apo-RirA form was achieved after 22 hours.
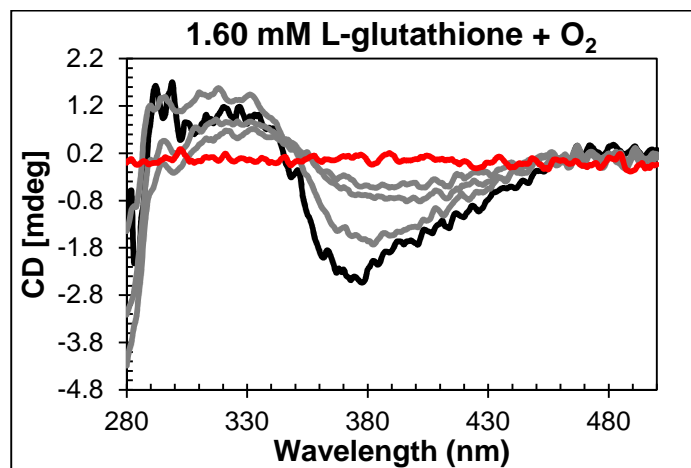
Figure 3.17. Sensitivity of [4Fe-4S] RirA to L-glutathione in presence of O₂. RirA and [4Fe-4S] RirA concentrations were respectively: 226 µM and 139 µM. Starting spectrum is in black (1.6 mM L-glutathione, no O₂), end point spectrum is in red (1.6 mM L-glutathione, after 22hr in the presence of O₂) and intervening spectra are in grey. The measurements were obtained in 1 cm cuvette, using buffer B (25 mM HEPES, 2.5 mM CaCl₂, 50 mM NaCl, 750 mM KCl, pH 7.5) for the CD baseline correction.

3.4. Discussion.

In *R. leguminosarum* and its near relatives, the regulation of many genes involved in iron acquisition is mediated by RirA [23]. Together with the heme-sensing global iron regulator Irr [24], RirA is functionally analogous to the ferric iron uptake regulator, Fur, of *E. coli* and other organisms. RirA is a member of the Rrf2 family of transcriptional regulators, as are NsrR and IscR, which respectively regulate responses to NO stress and iron-sulfur cluster biosynthesis [20]. These proteins have three essential cysteine residues that function as ligands for an iron-sulfur cluster. Although both IscR and NsrR contain iron-sulfur clusters, these are of different types: IscR binds a [2Fe-2S] cluster [25], while NsrR binds a [4Fe-4S] cluster [14]. Thus, while the presence of these Cys residues and the effects of their substitution [26] strongly suggested that RirA also is an iron-sulfur cluster regulator, the type of cluster, if any, was unknown.

Here the over-expression/purification of RirA and biophysical studies of its iron-sulfur cluster and DNA-binding properties are described. The research establishes that iron-sensing and regulation of the RirA regulon occurs in a way that is very different from

that of the well characterised iron sensors Fur and DtxR [27]. Spectroscopic properties and ESI-MS of cluster-reconstituted RirA shown the presence of a [4Fe-4S] cluster cofactor. Size exclusion chromatography showed that RirA apo- and holo- protein are dimeric, and ESI-MS data were consistent with this. This correlates with published work on NsrR and IscR in which it has reported that these proteins are also dimeric in cluster- free and bound forms [28, 29].

The identity of the presumed fourth ligand of the RirA [4Fe-4S] cluster is unknown. In [2Fe-2S] IscR, the fourth ligand is a His residue (His106 *E. coli* IscR numbering) [30], but this residue is not conserved in RirA (Figure 3.1). The crystal structure of [4Fe-4S] ScNsrR reveals the coordination of the cluster by the three invariant Cys (Cys93, Cys99 and Cys105) residues from one monomer and, unexpectedly, Asp8 from the other [31]. In the position 8 of the RirA sequence appears Asn, therefore, there is clearly some variability in the nature of the cluster coordination between members of the Rrf2 super-family, which is likely to be important in determining the type of iron-sulfur cluster that is present in each Rrf2 protein, and how it functions.

Under anaerobic conditions, [4Fe-4S] RirA was found to be stable; RirA samples contained a small component of an EPR-detectable $[3Fe-4S]^{1+}$ cluster, which was also observed by ESI-MS. However, passage of the protein sample down a gel filtration column significantly increased the $[3Fe-4S]^{1+}$ component, indicating that the [4Fe-4S] cluster of RirA is susceptible to loss of iron if there is a means to separate it from the residual cluster.

In the symbiotic bacteroids of leguminous plant root nodules, O_2 levels are kept sufficiently low to prevent damage to the N_2-fixing nitrogenase enzyme, while permitting aerobic respiration [32]. Under these conditions, it is unlikely that RirA would be exposed to very much O_2. However, free-living *R. leguminosarum* (and many other RirA-containing α-proteobacteria) grows aerobically in the soil and will experience varying concentrations of O_2, depending on conditions. Therefore, the sensitivity of [4Fe-4S] RirA

to O_2 was examined. A response to O_2 was observed, with cluster degradation to apo-RirA occurring via a transient [2Fe-2S] form over a period of hours. Interestingly, the observed rate constant was independent of O_2 concentration, indicating that the O_2 reaction is not the rate-limiting step. Thus, Fe^{2+} dissociation from $[4Fe-4S]^{2+}$ is likely to be required in order for the reaction with O_2 to proceed.

3.5.   References.

1.   Crack, J.C., et al., *Bacterial iron-sulfur regulatory proteins as biological sensor-switches.* Antioxid Redox Signal, 2012. **17**(9): p. 1215-31.
2.   Rajagopalan, S., et al., *Studies of IscR reveal a unique mechanism for metal-dependent regulation of DNA binding specificity.* Nat Struct Mol Biol, 2013. **20**(6): p. 740-7.
3.   Sievers, F., et al., *Fast, scalable generation of high-quality protein multiple sequence alignments using Clustal Omega.* Mol Syst Biol, 2011. **7**: p. 539.
4.   Nicholas, K.B., *GeneDoc: analysis and visualization of genetic variation.*
5.   Crack, J., J. Green, and A.J. Thomson, *Mechanism of oxygen sensing by the bacterial transcription factor fumarate-nitrate reduction (FNR).* J Biol Chem, 2004. **279**(10): p. 9278-86.
6.   Tucker, N.P., et al., *There's NO stopping NsrR, a global regulator of the bacterial NO stress response.* Trends Microbiol, 2010. **18**(4): p. 149-56.
7.   Tucker, N.P., et al., *The transcriptional repressor protein NsrR senses nitric oxide directly via a [2Fe-2S] cluster.* PLoS One, 2008. **3**(11): p. e3623.
8.   Holmes, J.D., *Magneto-optical Studies of RirA and Cytochrome cd1.* Ph.D. thesis, University of East Anglia, Norwich, 2012.
9.   Alam, M.S., S.K. Garg, and P. Agrawal, *Molecular function of WhiB4/Rv3681c of Mycobacterium tuberculosis H37Rv: a [4Fe-4S] cluster co-ordinating protein disulphide reductase.* Mol Microbiol, 2007. **63**(5): p. 1414-31.
10.   Helmut Beinert, M.C.K.a.C.D.S., *Aconitase as Iron−Sulfur Protein, Enzyme, and Iron-Regulatory Protein.* Chem. Rev. , 1996. **96**: p. 2335–2373.
11.   Chen, D., F.J. Ruzicka, and P.A. Frey, *A novel lysine 2,3-aminomutase encoded by the yodO gene of bacillus subtilis: characterization and the observation of organic radical intermediates.* Biochem J, 2000. **348 Pt 3**: p. 539-49.
12.   Sanakis, Y., et al., *Evidence for antisymmetric exchange in cuboidal [3Fe-4S](+) clusters.* Journal of the American Chemical Society, 2000. **122**(48): p. 11855-11863.
13.   Munnoch, J.T., et al., *Characterization of a putative NsrR homologue in Streptomyces venezuelae reveals a new member of the Rrf2 superfamily.* Sci Rep, 2016. **6**: p. 31597.
14.   Crack, J.C., et al., *NsrR from Streptomyces coelicolor is a nitric oxide-sensing [4Fe-4S] cluster protein with a specialized regulatory function.* J Biol Chem, 2015. **290**(20): p. 12689-704.
15.   Crack, J.C., A.J. Thomson, and N.E. Le Brun, *Mass spectrometric identification of intermediates in the O2-driven [4Fe-4S] to [2Fe-2S] cluster conversion in FNR.* Proc Natl Acad Sci U S A, 2017. **114**(16): p. E3215-e3223.
16.   Zhang, B., et al., *Reversible cycling between cysteine persulfide-ligated [2Fe-2S] and cysteine-ligated [4Fe-4S] clusters in the FNR regulatory protein.* Proc Natl Acad Sci U S A, 2012. **109**(39): p. 15734-9.
17.   Johnson, K.A., et al., *Probing the stoichiometry and oxidation states of metal centers in iron-sulfur proteins using electrospray FTICR mass spectrometry.* Anal Chem, 2000. **72**(7): p. 1410-8.
18.   Kay, K.L., C.J. Hamilton, and N.E. Le Brun, *Mass spectrometry of B. subtilis CopZ: Cu(i)-binding and interactions with bacillithiol.* Metallomics, 2016. **8**(7): p. 709-19.

19. Crack, J.C., et al., *Superoxide-mediated amplification of the oxygen-induced switch from [4Fe-4S] to [2Fe-2S] clusters in the transcriptional regulator FNR.* Proceedings of the National Academy of Sciences of the United States of America, 2007. **104**(7): p. 2092-2097.

20. Crack, J.C., et al., *Iron-sulfur cluster sensor-regulators.* Curr Opin Chem Biol, 2012. **16**(1-2): p. 35-44.

21. Hassan, S. and U. Mathesius, *The role of flavonoids in root-rhizosphere signalling: opportunities and challenges for improving plant-microbe interactions.* J Exp Bot, 2012. **63**(9): p. 3429-44.

22. Riccillo, P.M., et al., *Glutathione is involved in environmental stress responses in Rhizobium tropici, including acid tolerance.* J Bacteriol, 2000. **182**(6): p. 1748-53.

23. Todd, J.D., et al., *RirA, an iron-responsive regulator in the symbiotic bacterium Rhizobium leguminosarum.* Microbiology, 2002. **148**(Pt 12): p. 4059-71.

24. Singleton, C., et al., *Heme-responsive DNA binding by the global iron regulator Irr from Rhizobium leguminosarum.* J Biol Chem, 2010. **285**(21): p. 16023-31.

25. Schwartz, C.J., et al., *IscR, an Fe-S cluster-containing transcription factor, represses expression of Escherichia coli genes encoding Fe-S cluster assembly proteins.* Proceedings of the National Academy of Sciences of the United States of America, 2001. **98**(26): p. 14895-14900.

26. Bhubhanil, S., et al., *Cysteine desulphurase-encoding gene sufS2 is required for the repressor function of RirA and oxidative resistance in Agrobacterium tumefaciens.* Microbiology, 2014. **160**(Pt 1): p. 79-90.

27. Johnston, A.W., et al., *Living without Fur: the subtlety and complexity of iron-responsive gene regulation in the symbiotic bacterium Rhizobium and other alpha-proteobacteria.* Biometals, 2007. **20**(3-4): p. 501-11.

28. Yukl, E.T., et al., *Transcription Factor NsrR from Bacillus subtilis Senses Nitric Oxide with a 4Fe-4S Cluster (dagger).* Biochemistry, 2008. **47**(49): p. 13084-92.

29. Santos, J.A., et al., *The unique regulation of iron-sulfur cluster biogenesis in a Gram-positive bacterium.* Proc Natl Acad Sci U S A, 2014. **111**(22): p. E2251-60.

30. Fleischhacker, A.S., et al., *Characterization of the [2Fe-2S] cluster of Escherichia coli transcription factor IscR.* Biochemistry, 2012. **51**(22): p. 4453-62.

31. Volbeda, A., et al., *Crystal structures of the NO sensor NsrR reveal how its iron-sulfur cluster modulates DNA binding.* Nat Commun, 2017. **8**: p. 15052.

32. Downie, J.A., *Legume haemoglobins: symbiotic nitrogen fixation needs bloody nodules.* Curr Biol, 2005. **15**(6): p. R196-8.

Chapter 4. Studies of iron- dependent cluster conversion in *R. leguminosarum* RirA.

The mechanism by which RirA senses iron and therefore how regulation is achieved is unknown but must involve the Fe-S cluster. Two potential mechanisms can be considered. In the first, RirA senses iron indirectly through the availability of Fe-S clusters. In the second, RirA senses iron directly through a cluster conversion process involving loss of iron. In this chapter, the response of [4Fe-4S] RirA to low iron conditions generated by a range of iron chelators is reported, along with the DNA-binding properties of different forms of RirA.

4.1. Response of [4Fe-4S] RirA to low iron conditions.

4.1.1. Ferrozine.

The effect of the strong iron chelator Ferrozine (see Figure 4.1) on [4Fe-4S] RirA was investigated.
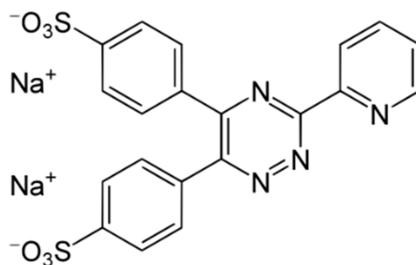
Figure 4.1. Structure of Ferrozine disodium salt.

UV-visible absorbance spectroscopy showed an increase in intensity of a peak at 562 nm upon titration of [4Fe-4S] RirA with Ferrozine, characteristic of the complex [Fe(Ferrozine)$_3$]$^{4-}$ indicating that the chelator binds iron from the cluster. In addition, the spectrum displays 280 nm absorption that results from Ferrozine's aromatic structure, see Figure 4.2A. In the case of CD, the most significant change appeared at 454 nm; the intensity of this peak increased with the addition of Ferrozine and also shifted to the red. After the addition of 2.32 mM Ferrozine the maximum appeared at 464 nm. Another

change occurred at 588 nm; in this case the intensity of the peak decreased with the additions of Ferrozine, and became blue shifted to a wavelength of 568 nm. The intense free Ferrozine absorbance at 280 nm obscures the signals at wavelengths below 380 nm. These changes can be observed in Figure 4.2B.
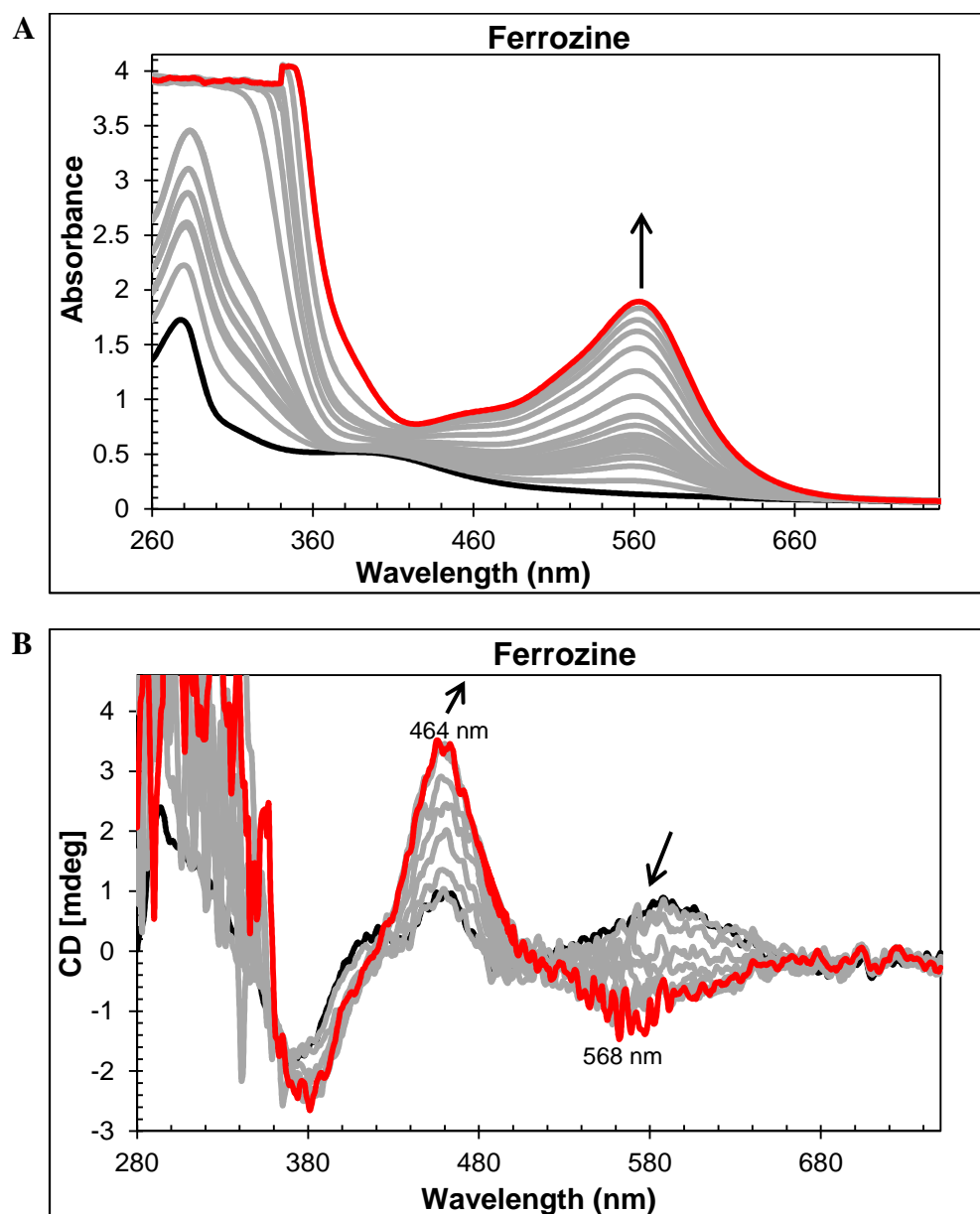
Figure 4.2. Response of [4Fe-4S] RirA to low iron conditions generated by Ferrozine. (A) UV-visible absorbance and **(B)** CD spectra of [4Fe-4S] RirA (54 µM in cluster in buffer B (25 mM HEPES, 2.5 mM CaCl$_2$, 50 mM NaCl, 750 mM KCl, pH 7.5); ~42% cluster-loaded) following addition of increasing concentrations of the iron chelator Ferrozine (up to 2.3 mM) under anaerobic conditions. Starting and end-point spectra are in black and red, respectively. Intervening spectra are in grey. The measurements were obtained using a 1 cm sealed anaerobic cuvette, with buffer B as a baseline. In (A), the changes are mostly due to the formation of the Fe(II)(Ferrozine)$_3$ complex.

In Figure 4.3, it is possible to observe that when a further addition was made (total concentration of Ferrozine = 3.20 mM), there were no further significant changes in the spectrum and the reaction was apparently complete.
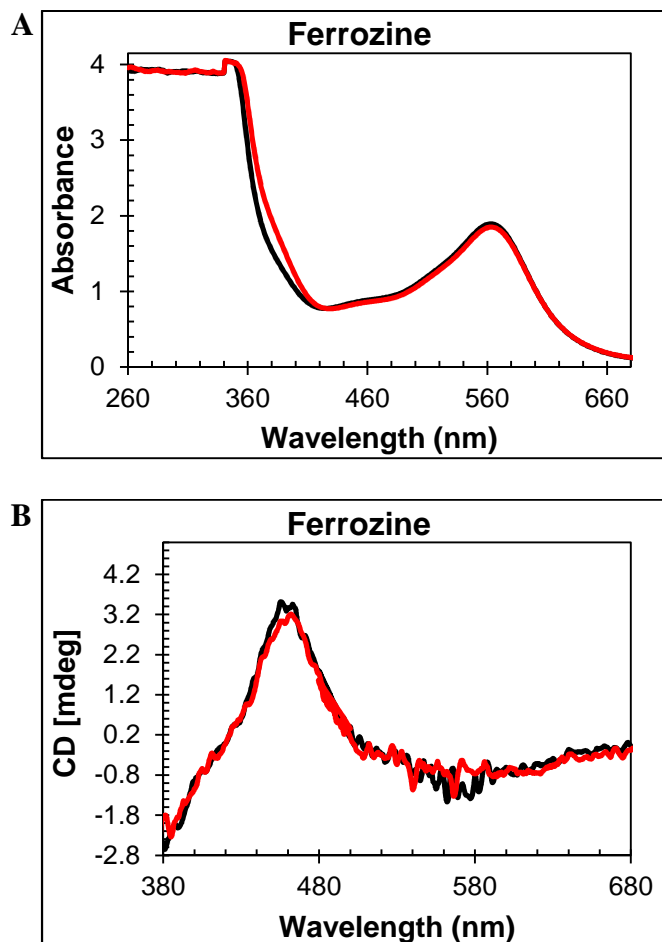
Figure 4.3. UV-visible absorbance (A) and CD (B) spectra for RirA in presence of Ferrozine at 2.32 mM (black line) and 3.2 mM (red line). RirA and [4Fe-4S] RirA concentrations were 131 µM and 54 µM, respectively. The measurements were obtained using a 1 cm sealed anaerobic cuvette, with buffer B (25 mM HEPES, 2.5 mM CaCl$_2$, 50 mM NaCl, 750 mM KCl, pH 7.5) as a baseline.

When the sample containing 3.20 mM Ferrozine was exposed to ambient oxygen, the UV-visible absorbance peak at 562 nm increased over time, see Figure 4.4A. For the CD, the peak at 464 nm was eventually lost and a negative peak at 551 nm appeared after 15 hours. This could be an artefact due to the high absorbance at this wavelength, see Figure 4.4B.
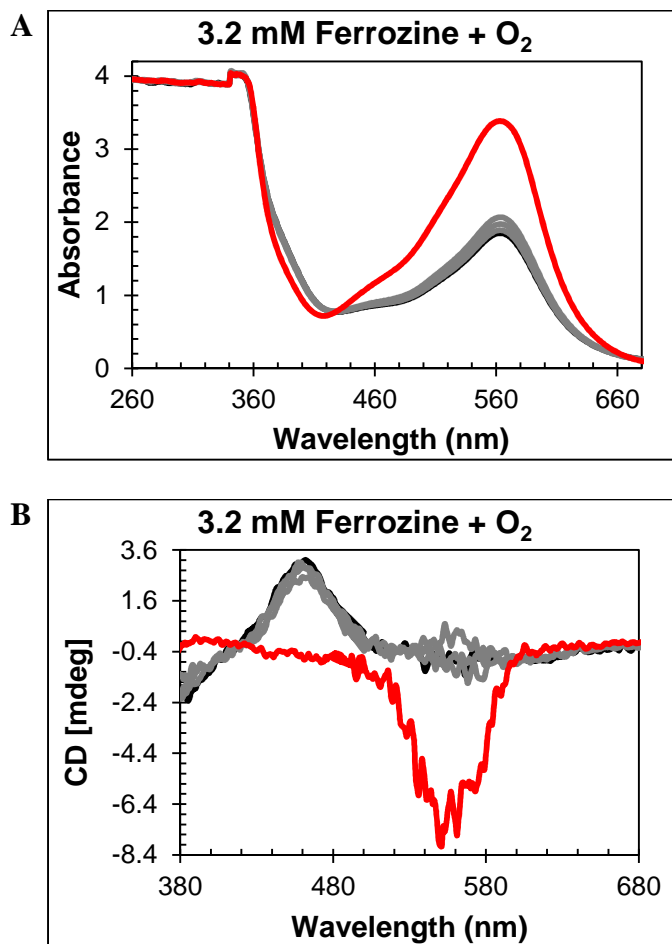
Figure 4.4. Time dependence of the UV-visible absorbance (A) and CD (B) spectra of RirA in the presence of 3.2 mM of Ferrozine under aerobic conditions. RirA and [4Fe-4S] RirA concentrations were respectively: 131 µM and 54 µM. Starting spectrum is in black (3.2 mM Ferrozine, no O_2), end point spectrum is in red (3.2 mM Ferrozine, after 15 hr in the presence of O_2) and intervening spectra are in grey. The measurements were obtained using a 1 cm cuvette, with buffer B (25 mM HEPES, 2.5 mM $CaCl_2$, 50 mM NaCl, 750 mM KCl, pH 7.5) as a baseline.

4.1.2. EDTA.

Another iron chelator was used to simulate low iron conditions. Ethylenediaminetetraacetic acid (EDTA) is a commonly used metal iron chelator. It forms a stable complex with both Fe^{2+} and Fe^{3+}, but has a higher affinity for Fe^{3+} (log K ~ 14.3 vs ~ 25.1) [1]. Titration of [4Fe-4S] RirA with EDTA under anaerobic conditions resulted in similar changes to those observed with Ferrozine but, crucially, without the interference of the absorbance at 280 and 562 nm due to the ligand/iron-ligand complex. The UV-visible absorbance spectrum after the addition of 8.23 mM of EDTA is characteristic of a [2Fe-2S], see Figure 4.5A. With further additions of EDTA the protein precipitated. In the

CD spectrum, the most significant change was the evolution of a band at 464 nm, see Figure 4.5B. In addition, the negative feature at 380 nm was red shifted while the band at ~600 nm changed sign and red shifted to ~610 nm. The CD data for EDTA and Ferrozine are very similar indicating that similar changes take place with both chelators.
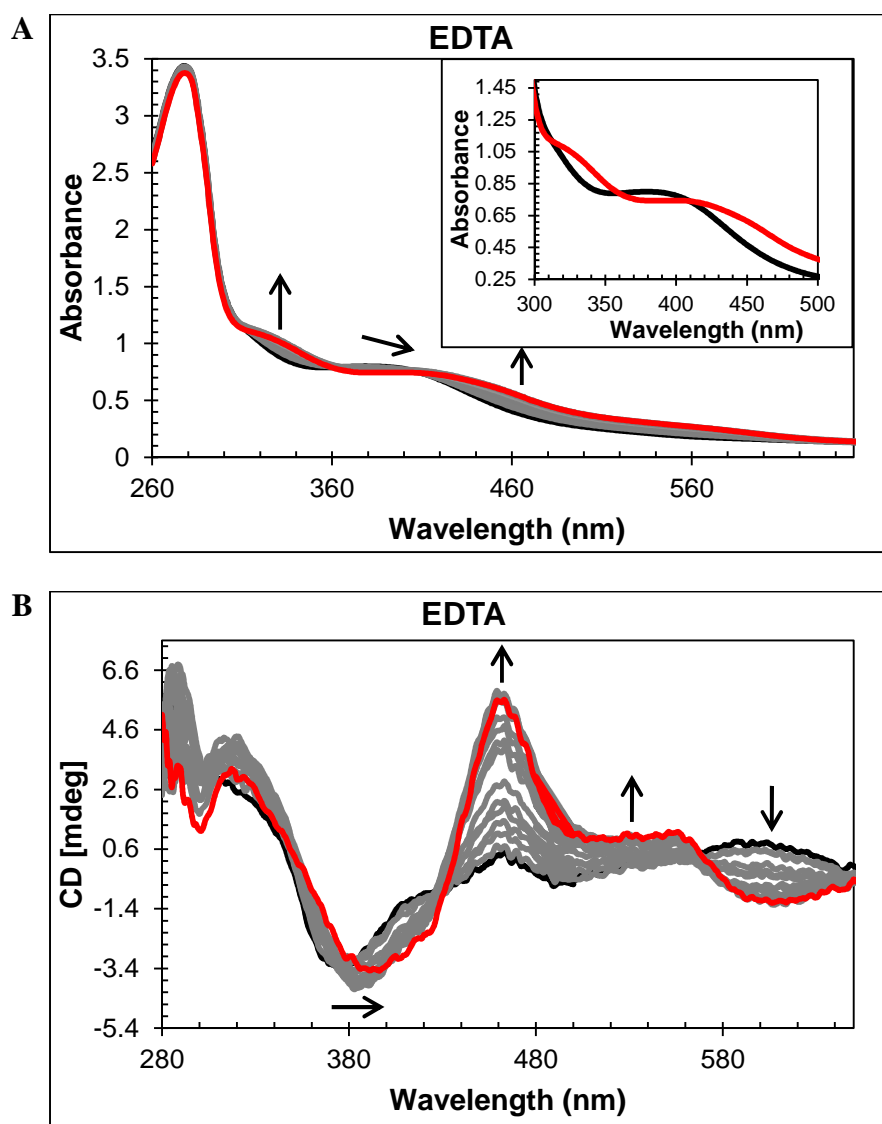
Figure 4.5. Response of [4Fe-4S] RirA to low iron conditions following the additions of EDTA. (**A**) UV-visible absorbance spectra and (**B**) CD spectra of [4Fe-4S] RirA (77 µM in cluster in buffer B (25 mM HEPES, 2.5 mM CaCl$_2$, 50 mM NaCl, 750 mM KCl, pH 7.5); ~50% cluster-loaded) following addition of increasing concentrations of EDTA (up to 8.2 mM) under anaerobic conditions. Starting and end-point spectra are in black and red, respectively. Intervening spectra are in grey. Inset in (A) are absorbance spectra in the absence of EDTA (black) and with 8.2 mM EDTA (red). The measurements were obtained using a 1 cm sealed anaerobic cuvette, with buffer B as a baseline.

The changes observed in the UV-visible and CD spectra demonstrate that the addition of EDTA leads to a conversion of the Fe-S cluster. Absorbance changes indicate that the new cluster is a [2Fe-2S] form.

To ilustrate the changes in the CD spectrum during the titration with EDTA, CD absorbance intensity at 464 and 603 nm was plotted versus the concentration of EDTA, see Figure 4.6. These are the peaks that showed the greatest shifts in intensity. The peak at 464 nm increased in intensity until a concentration of 3.7 mM of EDTA was reached; after this concentration the intensity remained stable. The peak at 603 nm decreased moderately in intensity until a concentration of 3.5 mM of EDTA, and then remained stable.
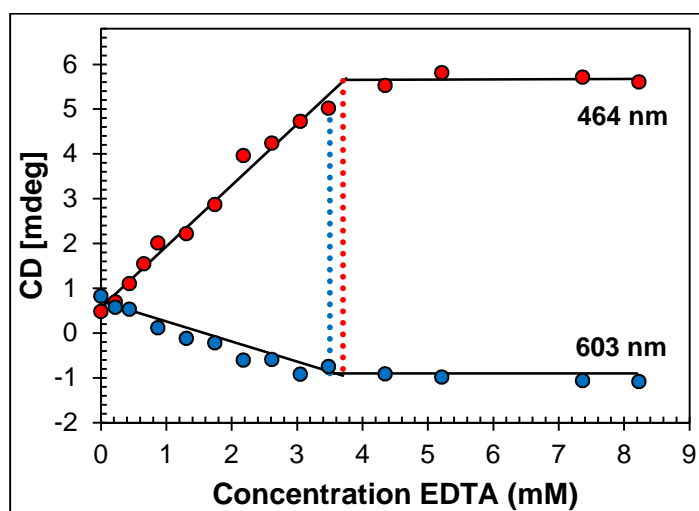
Figure 4.6. CD absorbance of the peaks at 464 and 603 nm versus the concentration of EDTA. The peak at 464 nm increased in intensity until a concentration of 3.7 mM of EDTA was reached (red dot line). The peak at 603 nm decreased in intensity until a concentration of 3.5 mM of EDTA (blue dot line).

After the last addition of EDTA (final concentration 8.23 mM of EDTA) the solution was left for 22 hours and was centrifuged to remove precipitated protein before re-recording UV-visible and CD spectra. These show that, after 22 hours, apo-RirA was the principal form of the protein (Figure 4.7).
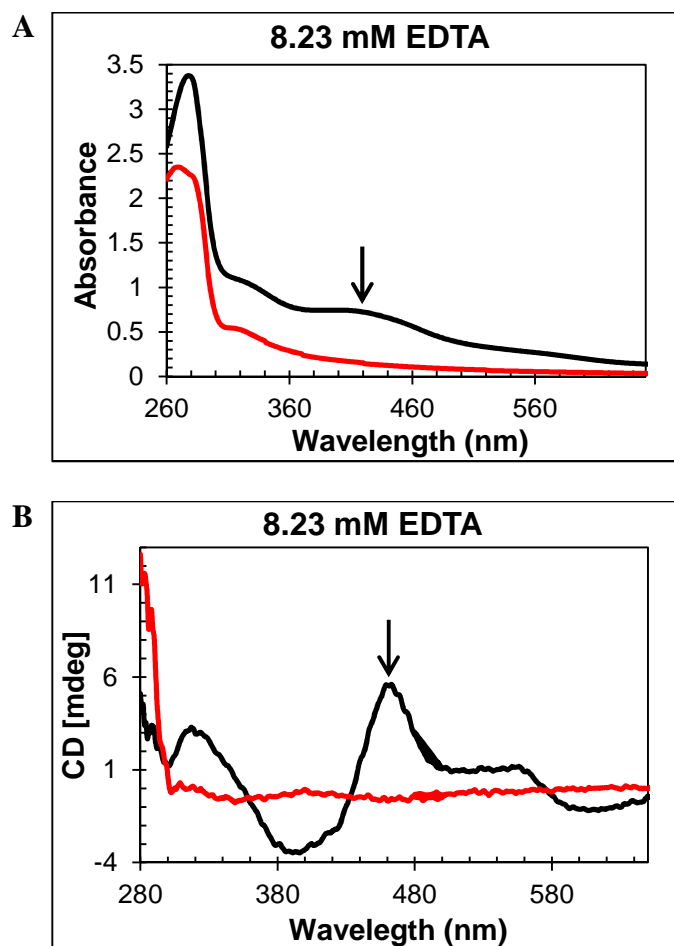
Figure 4.7. UV-vis (A) and CD (B) spectra for RirA after 22hr in 8.23 mM of EDTA. 8.23 mM of EDTA (black line) and after 22 hr (red line). RirA and [4Fe-4S] RirA concentrations were respectively: 154 µM and 77 µM. The measurements were obtained using a 1 cm sealed anaerobic cuvette, with buffer B (25 mM HEPES, 2.5 mM CaCl$_2$, 50 mM NaCl, 750 mM KCl, pH 7.5) as a baseline.

The same experiment was performed under aerobic conditions. In this case the UV-visible spectra show the degradation of the cluster up to an EDTA concentration of 4.73 mM, at which point apo-RirA was the major product, with a small amount of [2Fe-2S] cluster remaining (Figure 4.8A). In the equivalent CD experiment, the peak at 464 nm was observed to increase, maximizing at 1.30 mM EDTA (blue spectrum) but then was subsequently lost as further additions of EDTA were made, consistent with the formation and loss of the [2Fe-2S] form, see Figure 4.8B.
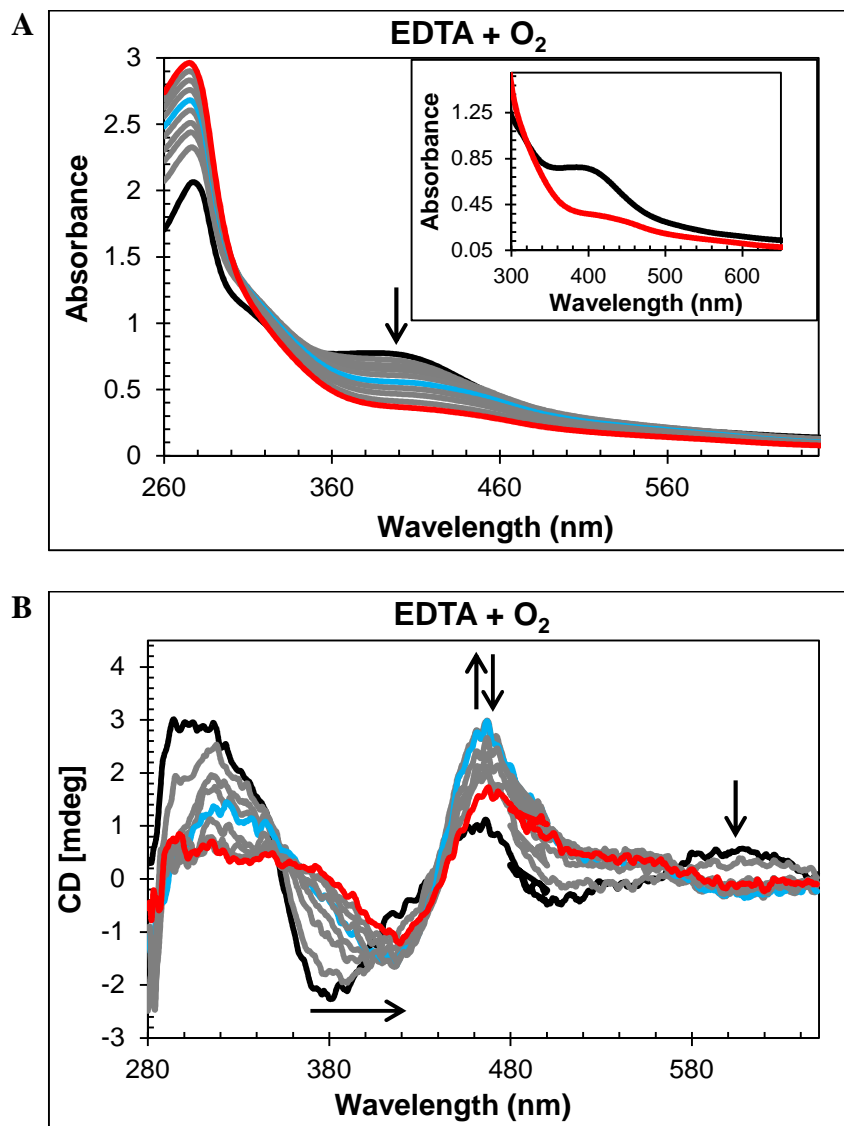
Figure 4.8. UV-visible (A) and CD (B) titration of RirA with EDTA under aerobic conditions. RirA and [4Fe-4S] RirA concentrations were 62 µM and 49 µM, respectively. Starting spectrum is in black (0 mM EDTA), end point spectrum is in red (4.73 mM EDTA), blue spectrum is 1.3 mM EDTA and intervening spectra are in grey. The measurements were obtained using a 1 cm cuvette, with buffer B (25 mM HEPES, 2.5 mM $CaCl_2$, 50 mM NaCl, 750 mM KCl, pH 7.5) as a baseline.

To illustrate the difference between the experiment under anaerobic and aerobic conditions, the CD absorbance at 464 nm versus the concentration of EDTA were plotted for both. Under anaerobic conditions the product of the conversion reaction was stable and only started to precipitate at higher concentration of EDTA. Under aerobic conditions the product formed under anaerobic conditions was not stable and was observed to form at a lower concentration of EDTA. After further additions of EDTA (>0.86 mM), a mixture of both the product and apo-RirA form was formed, see Figure 4.9.
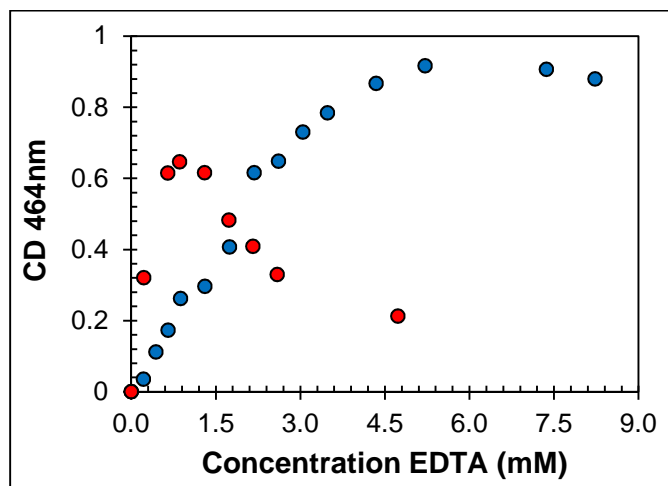
Figure 4.9. CD absorbance at 464 nm versus the concentration of EDTA. EDTA titration under anaerobic (blue circle) and aerobic (red circle) conditions. Data from Figure 4.5 and Figure 4.8.

As the UV-visible absorbance of RirA after the anaerobic addition of an iron-chelator has the characteristics of a [2Fe-2S] cluster [2, 3], it is proposed that the product was the [2Fe-2S] form of RirA and, therefore, that the iron- chelators promote the conversion from [4Fe-4S] cluster to [2Fe-2S] cluster.

4.1.2.1.   Native ESI-MS of [2Fe-2S] RirA.

To further establish the nature of the cluster conversion process that RirA undergoes under low iron conditions, native ESI-MS was employed. The *m/z* and deconvoluted spectra of [4Fe-4S] RirA in ammonium acetate buffer were presented in Chapter 3 (section 3.2.2). Treatment of [4Fe-4S] RirA with EDTA and subsequent removal of the chelator generated the same converted form of RirA as that described above see Figure 4.12. The *m/z* spectrum again revealed the presence of monomeric and dimeric forms of RirA (Figure 4.10).
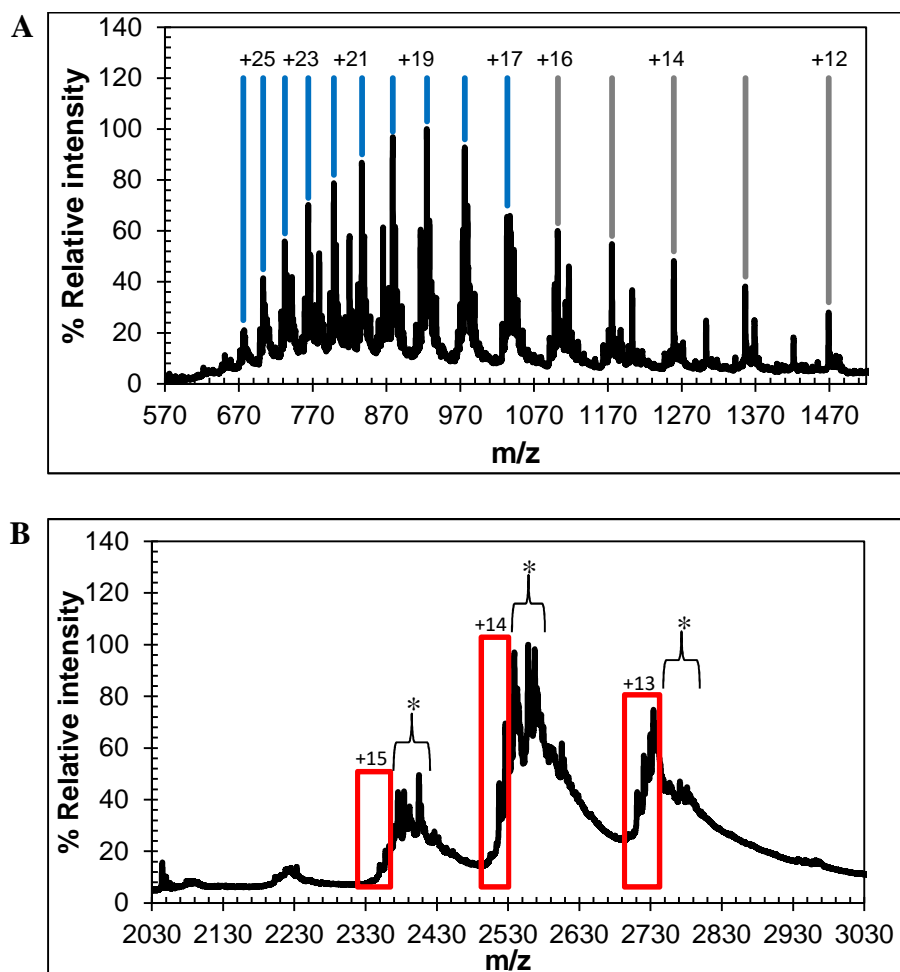
Figure 4.10. ESI-MS *m/z* spectra of [4Fe-4S] RirA (~21 µM in cluster) in 250 mM ammonium acetate pH 7.35 following exposure to 1 mM EDTA for 2.5 hr and removal of EDTA by gel filtration. (**A**) monomer and (**B**) dimer regions of the *m/z* spectrum are plotted with charge states as indicated. In A, grey and blue lines indicate the [2Fe-2S] and 2Fe adduct forms of RirA, respectively. In B, charge states due to cluster bound forms of dimeric RirA are indicated (red boxes). Peaks indicated by asterisks are due to overlapping charge states of a truncated form of RirA.

The deconvoluted mass spectrum in the monomer region (Figure 4.11A) featured two main peaks, corresponding to RirA containing a [2Fe-2S] cluster and to RirA containing two irons (see Chapter 3, Table 3.1), which most likely represents a breakdown product of the [2Fe-2S] cluster. As expected from the earlier spectrophotometric observations, the peak due to [4Fe-4S] RirA is of much lower intensity. Other [4Fe-4S] cluster breakdown species, corresponding to [4Fe-3S], [3Fe-4S], [3Fe-3S] and [3Fe-2S] clusters, were also observed, along with [2Fe-S] and apo-RirA (Figure 4.11A), but all of these were at low abundance relative to the [2Fe-2S] form.
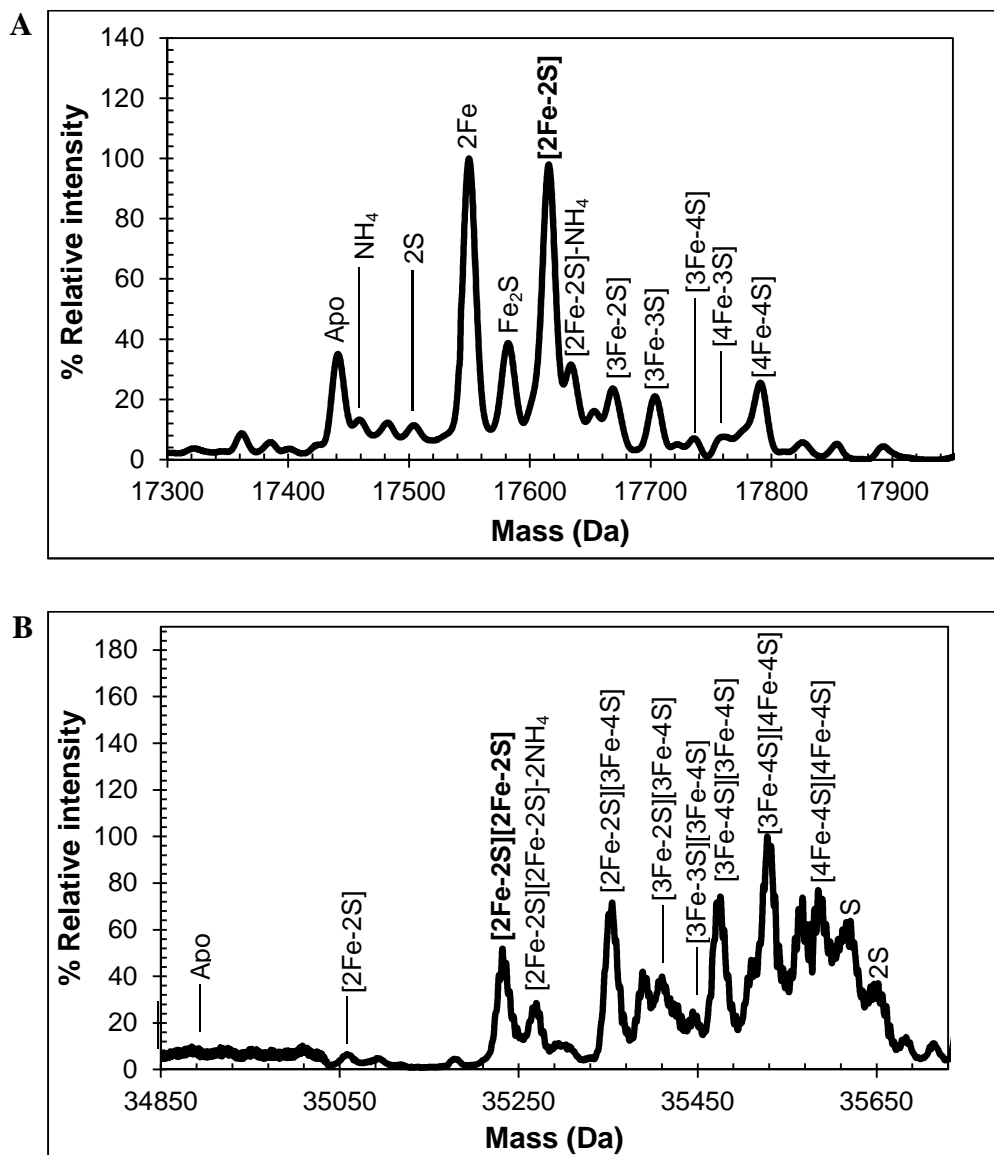
Figure 4.11. ESI-MS analysis of RirA following low iron-mediated cluster conversion. Positive ion mode ESI-TOF native mass spectra of ~~21 µM [4Fe-4S] RirA in 250 mM ammonium acetate pH 7.35 following treatment with 1 mM EDTA for 2.5 hr and removal of EDTA by gel filtration. Deconvoluted spectrum in the monomer (**A**) and dimer (**B**) mass regions.

In the dimer region, the signal to noise was relatively poor but peaks were still clearly present (Figure 4.11B). A significant peak due to the RirA dimer containing two [2Fe-2S] clusters was observed, along with a low intensity peak due to [4Fe-4S]/[4Fe-4S] RirA (see Chapter 3, Table 3.1). Various cluster breakdown forms were also present, including [3Fe-4S]/[4Fe-4S], [3Fe-4S]/[3Fe-4S], [3Fe-3S]/[3Fe-4S], [3Fe-2S]/[3Fe-4S] and [2Fe-2S]/[3Fe-4S] RirA, consistent with conversion of [4Fe-4S] into [2Fe-2S] clusters. Again, the dimer region contained fewer breakdown products (between [2Fe-2S]

and apo-RirA). For example, there was no evidence of RirA containing two irons (observed in the monomer region), consistent with the cluster being more stable within the dimer form of RirA during the MS experiment.

4.1.2.2. Kinetic studies of cluster conversion.

The rate of cluster conversion under anaerobic conditions upon addition of 1 or 4 mM EDTA was investigated by UV-visible absorbance and CD spectroscopies, Figure 4.12 and Figure 4.13. The same changes that occurred in the thermodynamic titration experiments were observed, indicating cluster conversion. Fitting of absorbance data at 382 nm and CD data at 380 nm (Figure 4.12C and Figure 4.13C) gave a rate constant of ~0.002 min^{-1} and ~0.007 min^{-1}, respectively, for 1 and 4 mM EDTA. Removal of EDTA by passage of the sample down a gel filtration column did not affect the shape of the absorbance or CD spectra, consistent with a stable [2Fe-2S] product of cluster conversion (e.g. Figure 4.12A). Prolonged (overnight) exposure of [2Fe-2S] RirA to EDTA led to significant loss of the cluster such that apo-RirA was the principal form of the protein (Figure 4.13A-B).

Figure 4.12. Time dependence of RirA [4Fe-4S] to [2Fe-2S] conversion promoted by 1 mM EDTA under anaerobic conditions. (**A**) UV-visible absorption and (**B**) CD spectra were recorded over several hours following exposure of [4Fe-4S] RirA (28 µM in cluster in buffer B (25 mM HEPES, 2.5 mM CaCl$_2$, 50 mM NaCl, 750 mM KCl, pH 7.5); ~51% cluster-loaded) to 1 mM EDTA under anaerobic conditions. Starting spectrum is in black, end point (620 min) spectrum is in red and intervening spectra are in grey. In (A) the spectrum of the protein following passage down a gel filtration column equilibrated in buffer B is shown in blue. **C1** is a plot of A$_{382\ nm}$ as a function of time; the solid line represents a fit to the data ($k = (1.79 \pm 0.45) \times 10^{-3}$ min^{-1}). **C2** is a plot of CD$_{464\ nm}$ as a function of time; the solid line represents a fit to the data ($k = (2.84 \pm 0.59) \times 10^{-3}$ min^{-1}). The measurements were obtained using a 1 cm sealed anaerobic cuvette, with buffer B as a baseline.
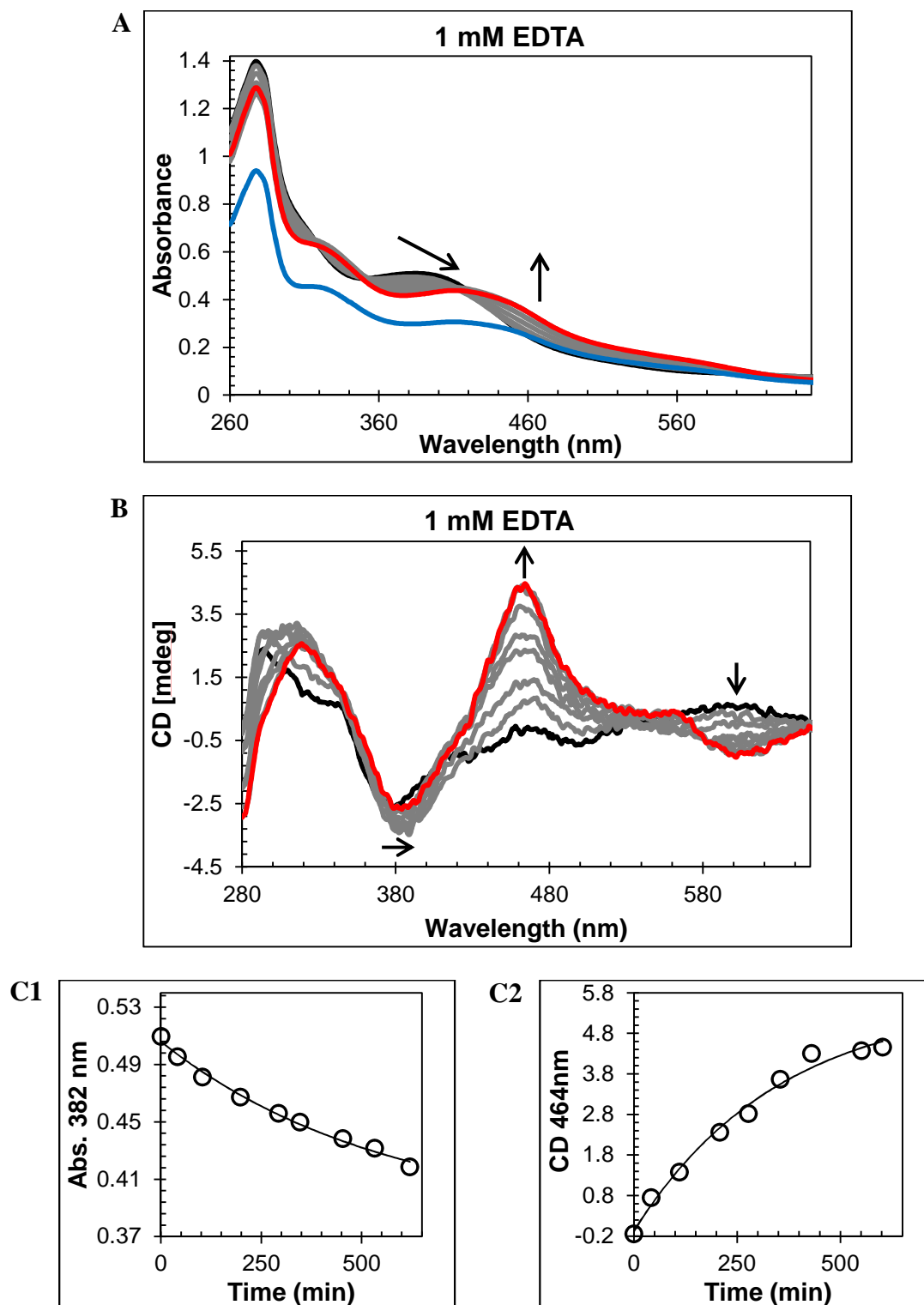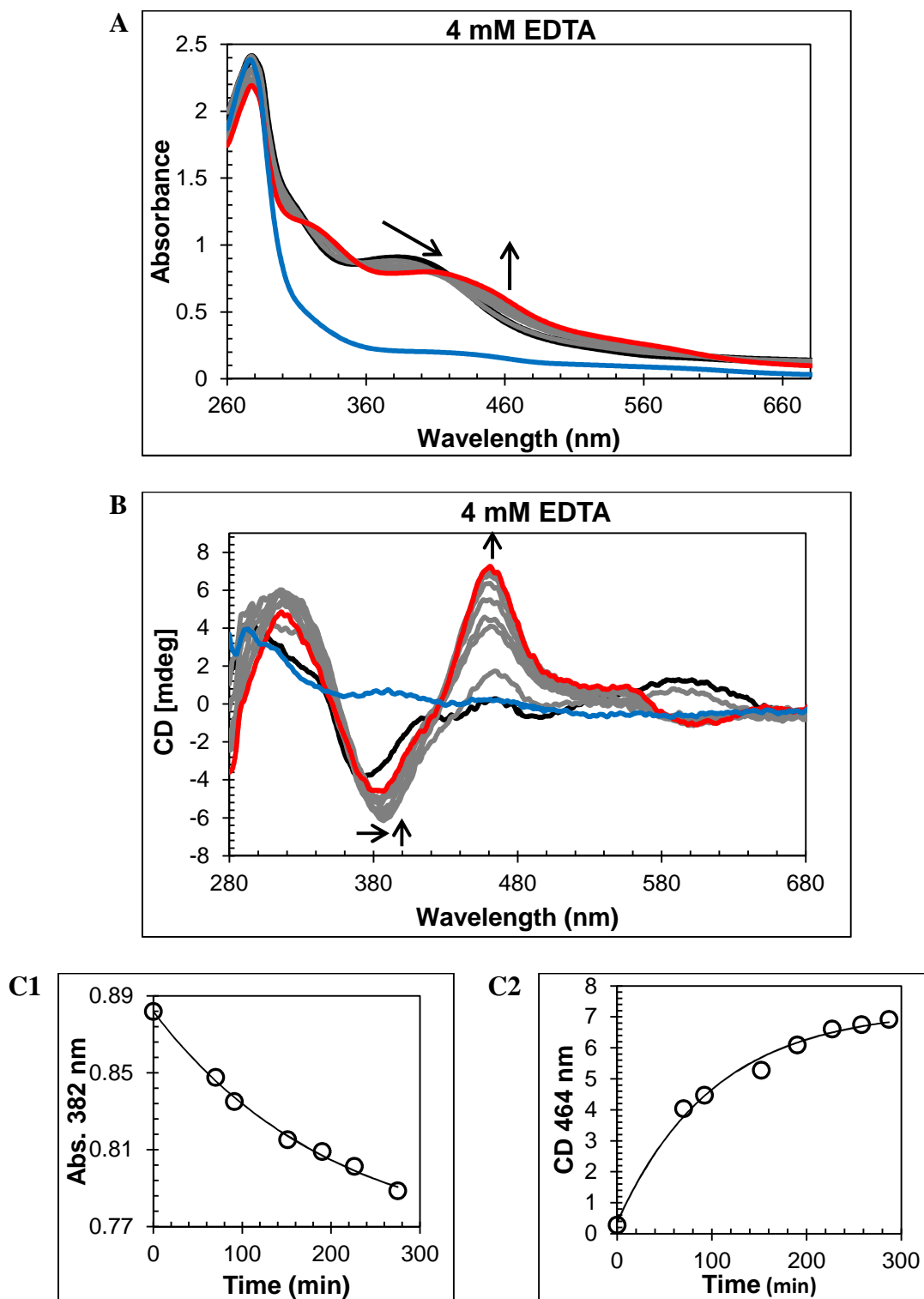
Figure 4.13. Time dependence of RirA [4Fe-4S] to [2Fe-2S] conversion promoted by 4 mM EDTA under anaerobic conditions. (A) UV-visible absorption and **(B)** CD spectra were recorded over several hours following exposure of [4Fe-4S] RirA (77 μM in cluster in buffer B (25 mM HEPES, 2.5 mM CaCl$_2$, 50 mM NaCl, 750 mM KCl, pH 7.5); ~80% cluster-loaded) to 4 mM EDTA under anaerobic conditions. Starting spectrum is in black, red spectrum (290 min) is the formation of the [2Fe-2S] cluster, intervening spectra are in grey and blue spectrum is the formation of the apo-RirA (23 hr). **C1** is a plot of A$_{382\,nm}$ as a function of time; the solid line represents a fit of the data ($k = (4.96 \pm 0.80) \times 10^{-3}$ min^{-1}). **C2** is a plot of CD$_{464\,nm}$ as a function of time; the solid line represents a fit to the data ($k = (9.76 \pm 0.37) \times 10^{-3}$ min^{-1}). The measurements were obtained using a 1 cm sealed anaerobic cuvette, buffer B as a baseline.
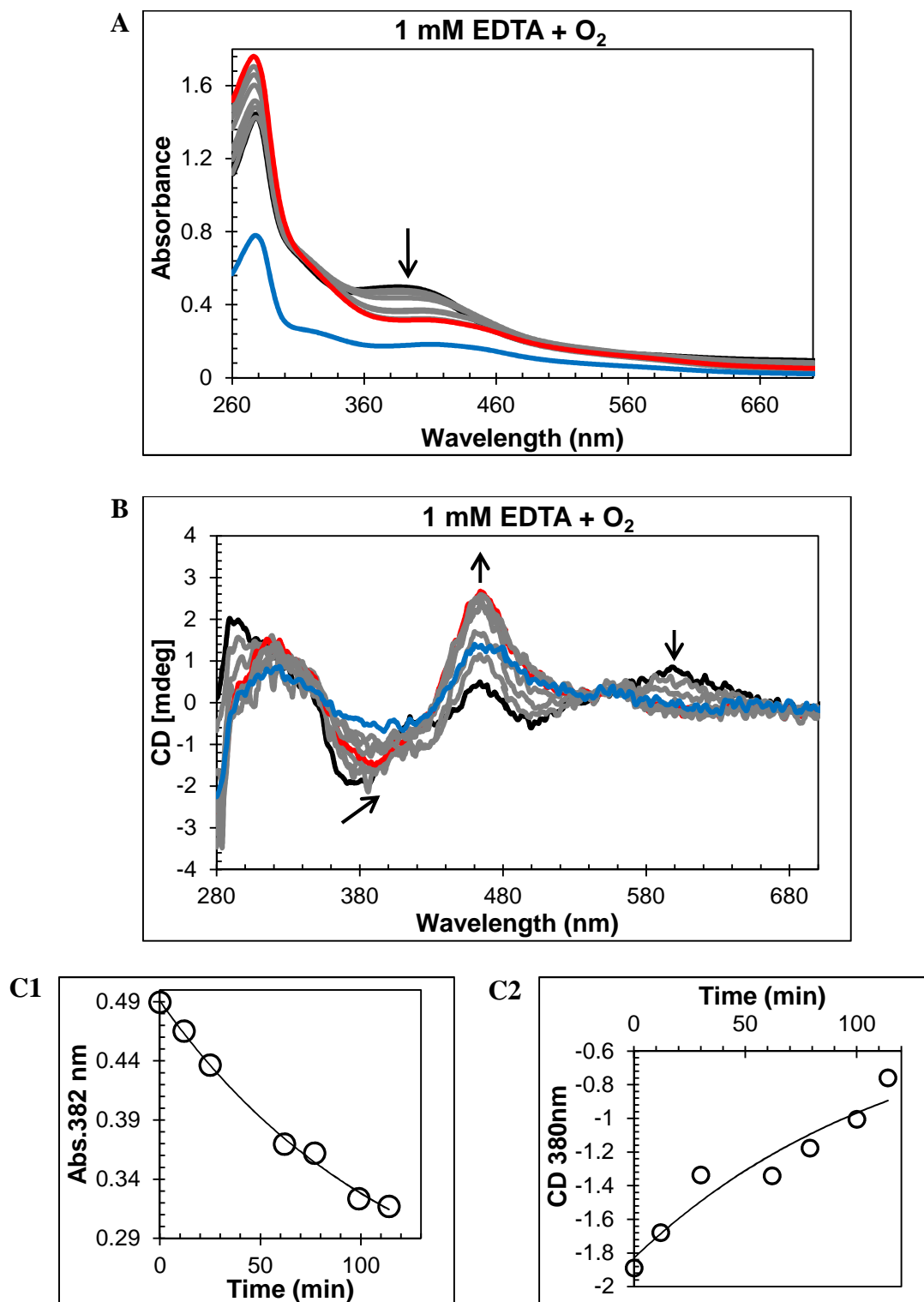
Figure 4.14. Time dependence of RirA [4Fe-4S] to [2Fe-2S] conversion promoted by iron chelators under aerobic conditions. (**A**) UV-visible absorption and (**B**) CD spectra were recorded over several hours following exposure of [4Fe-4S] RirA (28 µM in cluster in buffer B (25 mM HEPES, 2.5 mM CaCl$_2$, 50 mM NaCl, 750 mM KCl, pH 7.5); ~51% cluster-loaded) to 1 mM EDTA under aerobic conditions. Starting spectrum is in black, end point spectrum is in red (120 min) and intervening spectra are in grey. Spectra of the protein following passage down a gel filtration column equilibrated in buffer B are shown in blue. **C1** is a plot of A$_{382\ nm}$ as a function of time; the solid line represents a fit to the data ($k = (8.45 \pm 0.19) \times 10^{-3}$ min^{-1}). **C2** is a plot of CD$_{380\ nm}$ as a function of time; the solid line represents a fit to the data ($k = (8.29 \pm 0.81) \times 10^{-3}$ min^{-1}). The measurements were obtained using a 1 cm cuvette, with buffer B as a baseline.

71

The combined effects of low iron and saturating levels of O_2 on [4Fe-4S] RirA were investigated. Addition of 1 mM EDTA to [4Fe-4S] RirA under aerobic conditions resulted in a similar reaction to that under anaerobic conditions (Figure 4.14), but cluster breakdown occurred significantly more rapidly. Both absorbance and CD revealed the transient formation of the [2Fe-2S] form, which decayed further to form apo-RirA as the final product. Fitting of absorbance data at 382 nm and CD data at 380 nm gave a rate constant of ~0.008 min^{-1} (Figure 4.14C), ~4-fold higher than that for the same reaction under anaerobic conditions.

4.1.3. Chelex 100.

In the above experiments, EDTA and Ferrozine were in the same solution as RirA and therefore could potentially interact directly with RirA to promote cluster conversion in a non-physiological reaction. To investigate cluster conversion in the absence of direct interaction with a chelator, an experiment was performed in which a solid chelating resin (Chelex 100) was separated from the protein by a semi-permeable membrane. Under anaerobic conditions, absorbance (Figure 4.15A) and CD (Figure 4.15B) intensity due to the cluster was lost gradually over several hours, but with formation of only small amounts of [2Fe-2S], showing that under these conditions apo-RirA was formed without significant stabilization of [2Fe-2S] RirA. Absorbance decay at 382 nm and CD decay at 380 nm were fitted with a single exponential, giving a rate constant of ~0.002 min^{-1} (Figure 4.15C), similar to that observed in the presence of 1 mM EDTA.
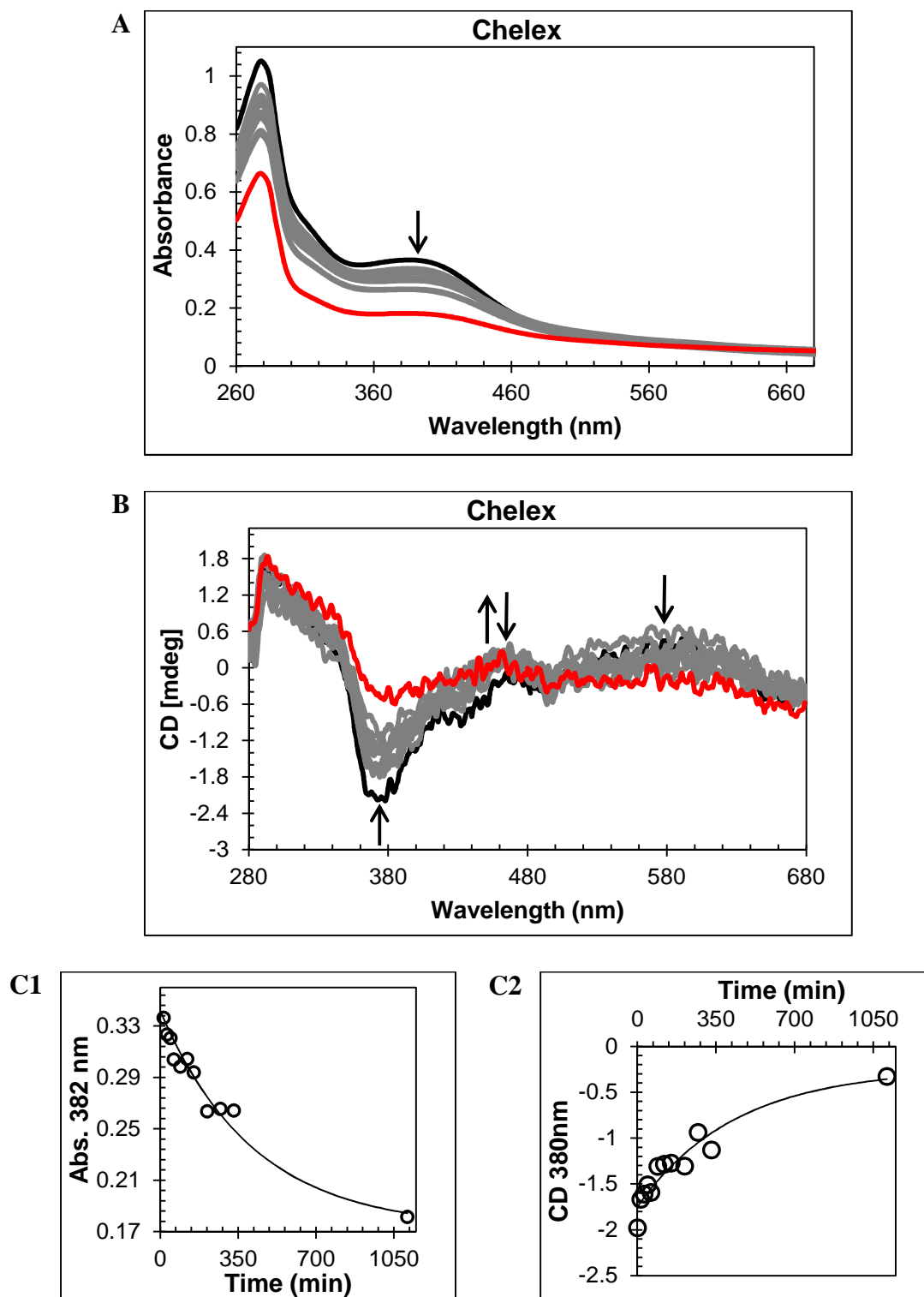
Figure 4.15. Response of [4Fe-4S] RirA to low iron conditions promoted by Chelex 100. (A) UV-visible absorbance spectra and **(B)** CD spectra of [4Fe-4S] RirA (30 µM in cluster in buffer B (25 mM HEPES, 2.5 mM CaCl$_2$, 50 mM NaCl, 750 mM KCl, pH 7.5); ~89% cluster-loaded) using Chelex-100 as an iron chelator, separated from the protein by dialysis membrane. Starting spectrum is in black, end point spectrum is in red (19 hr) and intervening spectra are in grey. **C1** is a plot of A$_{382\ nm}$ as a function of time; the solid line represents a fit of the data ($k = (2.39 \pm 0.59) \times 10^{-3}$ min^{-1}). **C2** is a plot of CD$_{380\ nm}$ as a function of time; the solid line represents a fit of the data ($k = (2.31 \pm 0.73) \times 10^{-3}$ min^{-1}). The measurements were obtained using a 1 cm sealed anaerobic cuvette, with buffer B as a baseline.

73
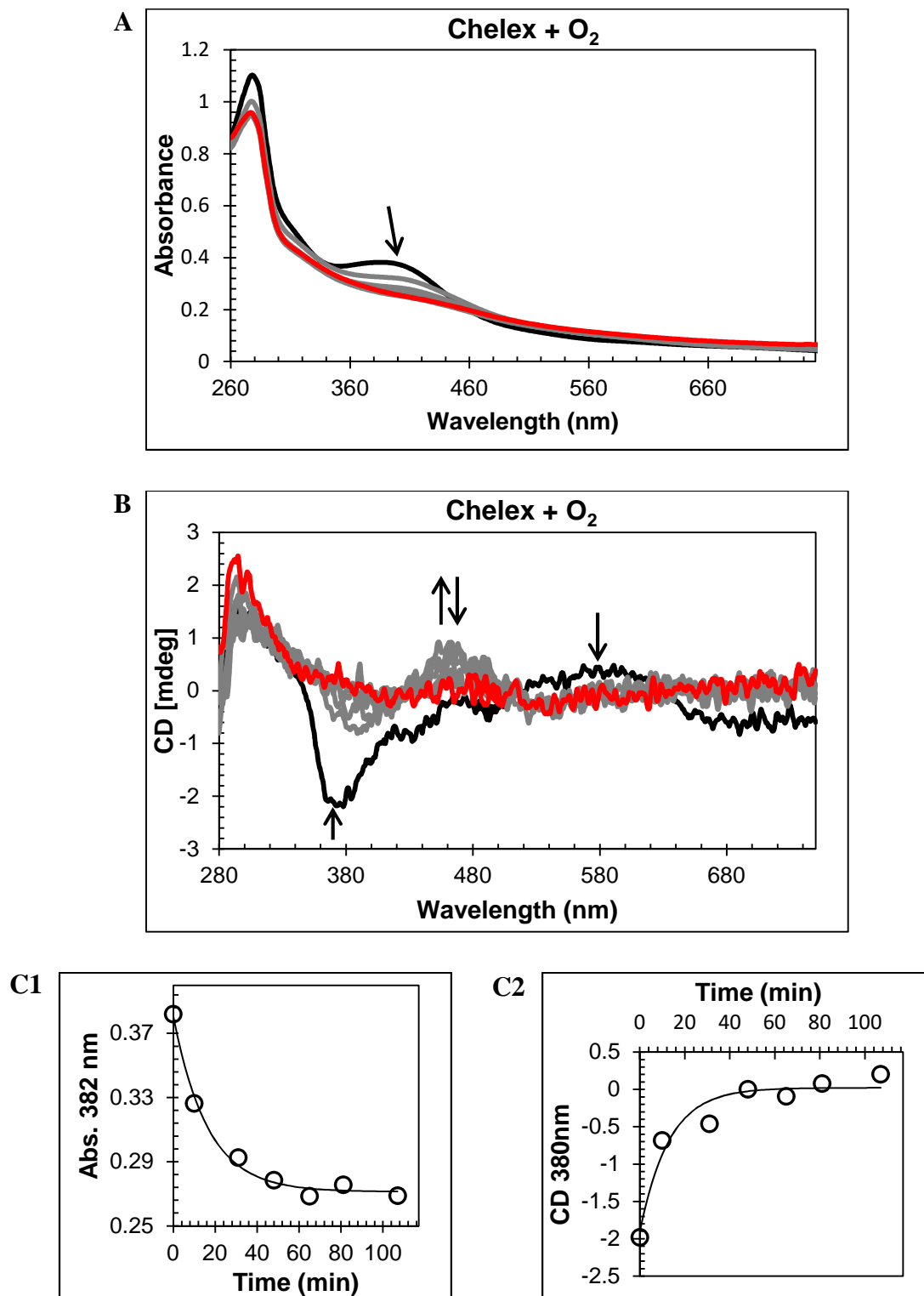
Figure 4.16. Time dependence of RirA [4Fe-4S] to [2Fe-2S] conversion promoted by Chelex 100 under aerobic conditions. (**A**) UV-visible absorbance spectra and (**B**) CD spectra of [4Fe-4S] RirA (30 µM in cluster in buffer B (25 mM HEPES, 2.5 mM CaCl$_2$, 50 mM NaCl, 750 mM KCl, pH 7.5); ~89% cluster-loaded) using Chelex-100 as an iron chelator under aerobic conditions, separated from the protein by dialysis membrane. Starting spectrum is in black, end point spectrum is in red (110 min) and intervening spectra are in grey. **C1** is a plot of A$_{382 nm}$ as a function of time; the solid line represents a fit of the data ($k = 0.061 \pm 0.008$ min^{-1}). **C2** is a plot of CD$_{380 nm}$ as a function of time; the solid line represents a fit of the data ($k = 0.078 \pm 0.016$ min^{-1}). The measurements were obtained using a 1 cm cuvette, with buffer B as a baseline.

Under the low iron conditions generated by Chelex 100 resin, the presence of O_2 also increased the rate of reaction, with a rate constant (~0.07 min^{-1}) (Figure 4.16C), ~35-fold higher than under anaerobic conditions. Both absorbance and CD data (Figure 4.16A-B) were consistent with the transient formation of a [2Fe-2S] form before decay to the apo-protein. Why the effect of O_2 is greater in the case of Chelex 100 compared to EDTA is not clear.

4.1.4. Protein chelators of iron.

BFR (1.4 µM) and apo-transferrin (64 µM) were used as iron-chelators following the same protocol as that used for Chelex 100 experiments, where the chelating species is too large to cross the semi-permeable membrane and so cannot interact directly with the RirA cluster. The rationale was that Fe^{2+}-(bacterioferritin) and Fe^{3+}-(transferrin) binding proteins would chelate iron but would not be able to interact directly with iron bound to RirA. Data similar to that observed for Chelex 100 were obtained (see Figure 4.17 and Figure 4.20), in that the [4Fe-4S] cluster decayed, resulting in apo-RirA, but with evidence of a transiently stable [2Fe-2S] intermediate form. Fitting of the absorbance and CD decay data for RirA in the presence of BFR under anaerobic conditions gave a rate constant (~0.004 min^{-1}) similar to that observed for the small molecule chelators, (Figure 4.17C). In the presence of O_2, the rate constant increased approx. six-fold (to ~0.024 min^{-1}), see Figure 4.18C. For RirA in the presence of transferrin, fitting of the absorbance and CD data gave a rate constant (~0.045 min^{-1}) significantly higher than observed for other chelators (Figure 4.19C), and this did not increase substantially (~0.049 min^{-1}) in the presence of O_2, (Figure 4.20C).
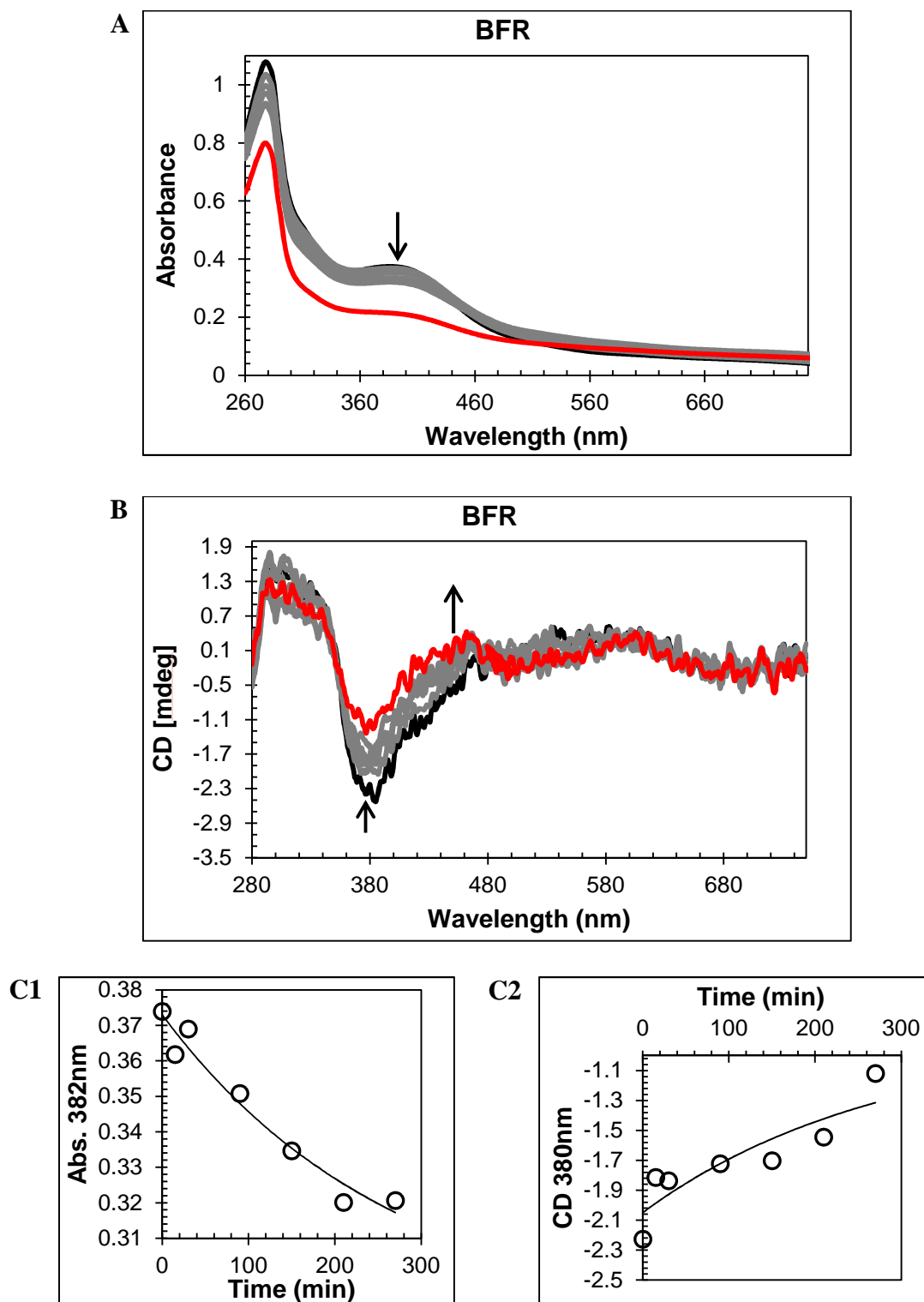
Figure 4.17. Time dependence of RirA [4Fe-4S] to [2Fe-2S] conversion promoted by BFR.
(**A**) UV-visible absorption spectra and (**B**) CD spectra were recorded over time following exposure of [4Fe-4S] RirA (30 µM in cluster in buffer B (25 mM HEPES, 2.5 mM $CaCl_2$, 50 mM NaCl, 750 mM KCl, pH 7.5); ~89% cluster-loaded) to 1.4 µM BFR under anaerobic conditions. Starting spectrum is in black, end point spectrum is in red (UV-vis: 1230 min; CD: 270 min) and intervening spectra are in grey. **C1** is a plot of $A_{382\,nm}$ as a function of time; the solid line represents a fit of the data ($k = (3.85 \pm 0.36) \times 10^{-3}$ min^{-1}). **C2** is a plot of $CD_{380\,nm}$ as a function of time; the solid line represents a fit of the data ($k = (3.62 \pm 0.7) \times 10^{-3}$ min^{-1}). The measurements were obtained using a 1 cm sealed anaerobic cuvette, with buffer B as a baseline.

Figure 4.18. Time dependence of RirA [4Fe-4S] to [2Fe-2S] conversion promoted by BFR under aerobic conditions. (**A**) UV-visible absorption spectra and (**B**) CD spectra were recorded over time following exposure of [4Fe-4S] RirA (30 µM in cluster in buffer B (25 mM HEPES, 2.5 mM CaCl$_2$, 50 mM NaCl, 750 mM KCl, pH 7.5); ~89% cluster-loaded) to 1.4 µM BFR under aerobic conditions. Starting spectrum is in black, end point spectrum is in red (UV-vis: 1192 min; CD: 232 min) and intervening spectra are in grey. **C1** is a plot of A$_{382\ nm}$ as a function of time; the solid line represents a fit of the data ($k = 0.023 \pm 0.006$ min^{-1}). **C2** is a plot of CD$_{380\ nm}$ as a function of time; the solid line represents a fit of the data ($k = 0.024 \pm 0.006$ min^{-1}). The measurements were obtained using a 1 cm cuvette, with buffer B as a baseline.
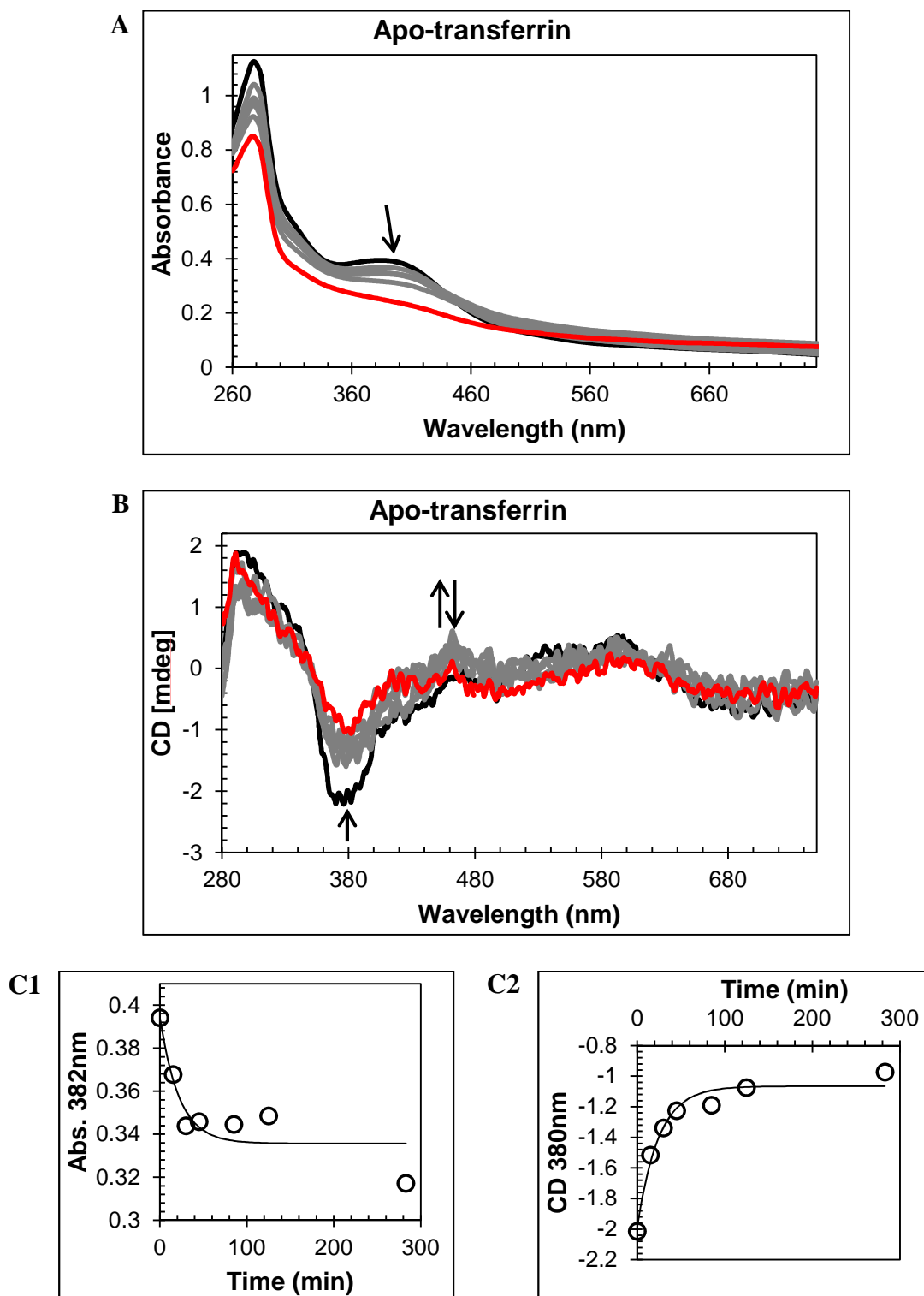
Figure 4.19. Time dependence of RirA [4Fe-4S] to [2Fe-2S] conversion promoted by apo-transferrin. (**A**) UV-visible absorption spectra and (**B**) CD spectra were recorded over time following exposure of [4Fe-4S] RirA (30 µM in cluster in buffer B (25 mM HEPES, 2.5 mM CaCl$_2$, 50 mM NaCl, 750 mM KCl, pH 7.5); ~89% cluster-loaded) to 64 µM apo-transferrin under anaerobic conditions. Starting spectrum is in black, end point spectrum is in red (UV-vis: 1243 min; CD: 283 min) and intervening spectra are in grey. **C1** is a plot of A$_{382\,nm}$ as a function of time; the solid line represents a fit of the data ($k = 0.045 \pm 0.014$ min^{-1}). **C2** is a plot of CD$_{380\,nm}$ as a function of time; the solid line represents a fit of the data ($k = 0.041 \pm 0.008$ min^{-1}). The measurements were obtained using a 1 cm sealed anaerobic cuvette, with buffer B as a baseline.
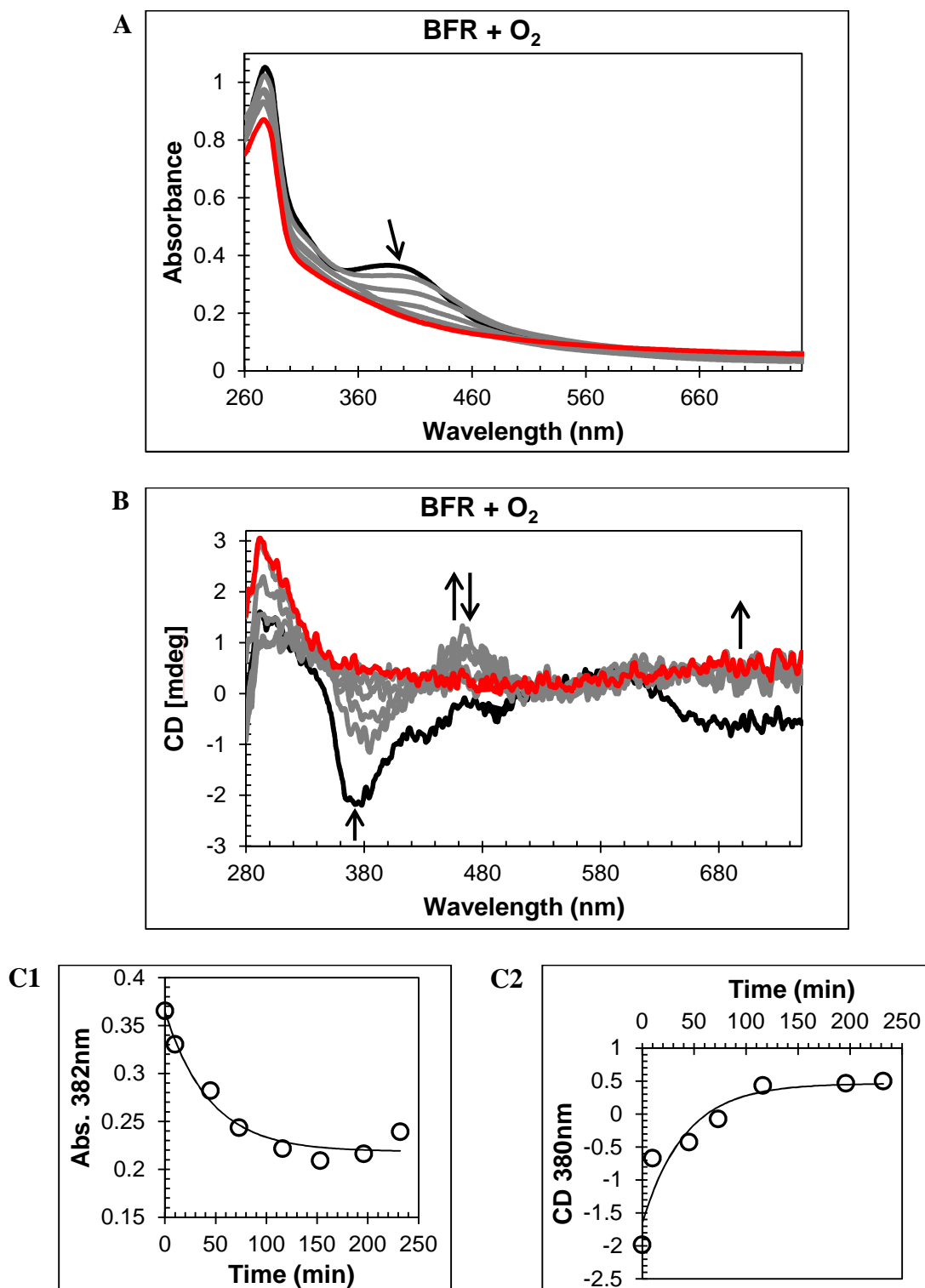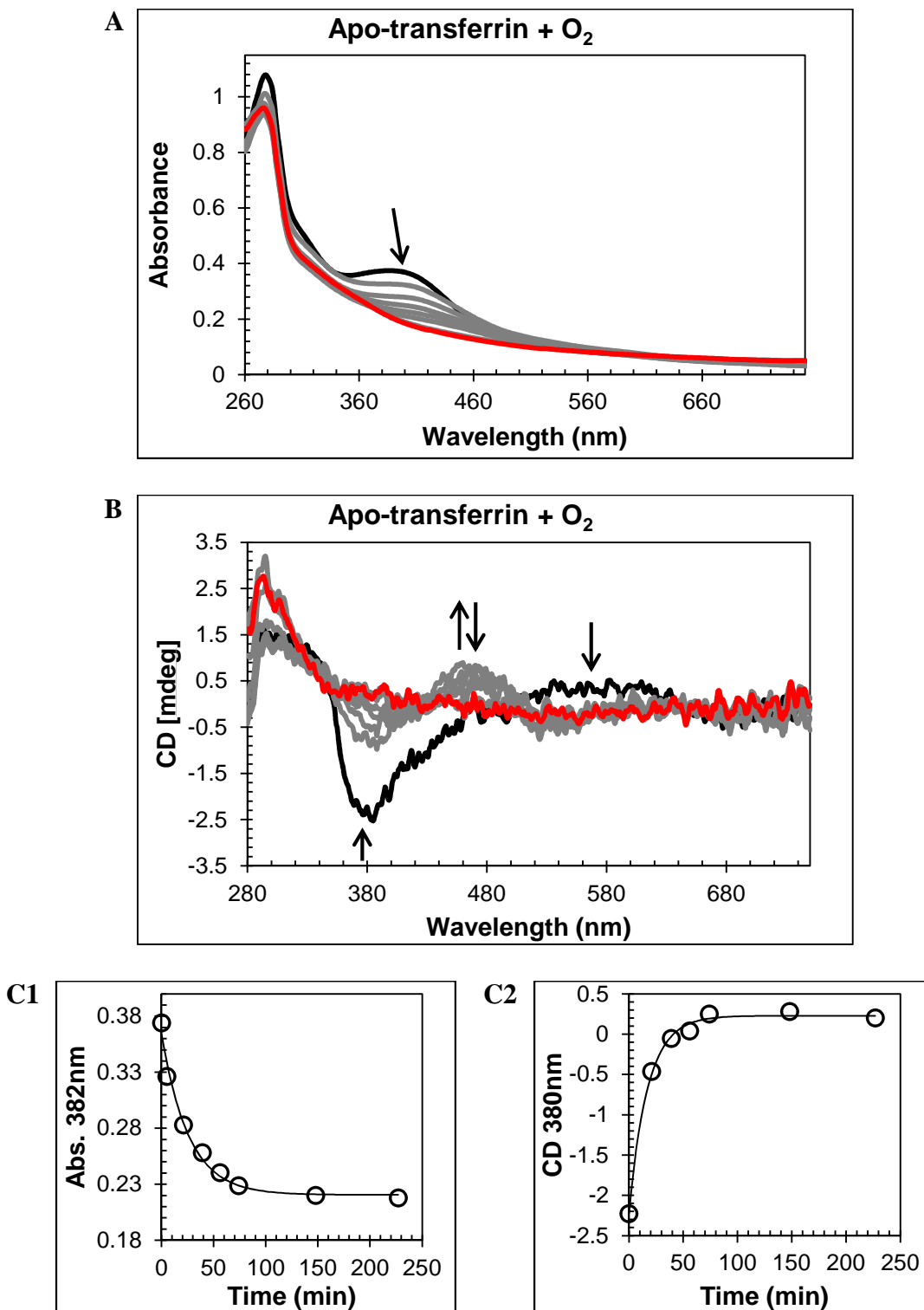
Figure 4.20. Time dependence of RirA [4Fe-4S] to [2Fe-2S] conversion promoted by apo-transferrin under aerobic conditions. (**A**) UV-visible absorption spectra and (**B**) CD spectra were recorded over time following exposure of [4Fe-4S] RirA (30 µM in cluster in buffer B (25 mM HEPES, 2.5 mM CaCl$_2$, 50 mM NaCl, 750 mM KCl, pH 7.5); ~89% cluster-loaded) to 64 µM apo-transferrin under aerobic conditions. Starting spectrum is in black, end point spectrum is in red (227 min) and intervening spectra are in grey. **C1** is a plot of A$_{382 \text{ nm}}$ as a function of time; the solid line represents a fit of the data ($k = 0.039 \pm 0.005$ min^{-1}). **C2** is a plot of CD$_{380 \text{ nm}}$ as a function of time; the solid line represents a fit of the data ($k = 0.058 \pm 0.004$ min^{-1}). The measurements were obtained using a 1 cm cuvette, with buffer B as a baseline.

4.1.5. Sensitivity of [2Fe-2S] RirA to O_2.

The [2Fe-2S] form of RirA generated by exposure of [4Fe-4S] RirA to EDTA followed by removal of the chelator, was exposed to ambient O_2 to determine its stability. UV-visible and CD spectra were obtained over a period of time. The UV-visible spectrum revealed gradual loss of the cluster at 382 nm and the CD signal disappeared over time, see Figure 4.21. The apo form of RirA was achieved without precipitation whereas, as was mentioned before, in the case of the [4Fe-4S] form of RirA the solution precipitated after 2 hr 30 min following exposure to O_2. After 2 hours the loss of the cluster was almost the same for the [2Fe-2S] and [4Fe-4S] forms of RirA, 15 and 20% respectively.
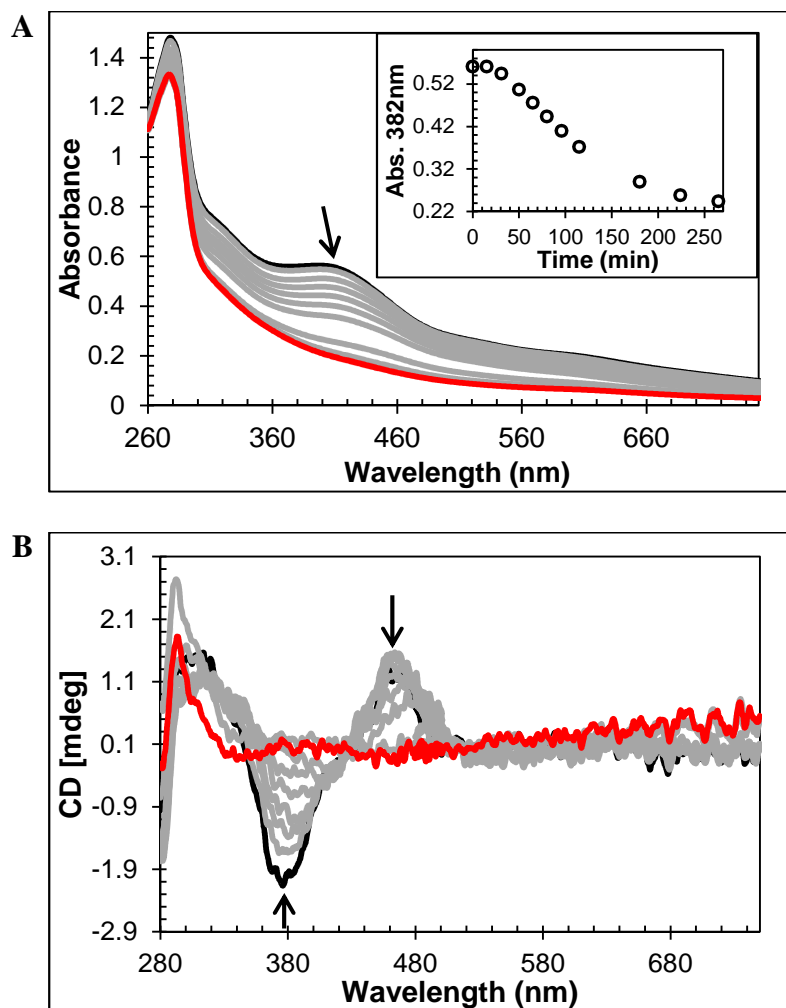
Figure 4.21. Time dependence of [2Fe-2S] RirA under aerobic conditions. (A) UV-visible absorption spectra and **(B)** CD spectra were recorded over time following exposure of [2Fe-2S] RirA (~187 µM in cluster in buffer B (25 mM HEPES, 2.5 mM CaCl$_2$, 50 mM NaCl, 750 mM KCl, pH 7.5); ~89% cluster-loaded) to ~200 µM O_2. Starting spectra are in black, end point spectrum is in red (293 min) and intervening spectra are in grey. Inset in (A) is a plot of A$_{382\ nm}$ as a function of time. The measurements were obtained using a 1 cm cuvette, with buffer B as a baseline.

4.1.6. Cluster stability in NsrR, another [4Fe-4S] Rrf2 regulator.

The apparent sensitivity of the [4Fe-4S] cluster of RirA to low iron conditions raised the question of whether this is a general property of Rrf2 family regulators that bind a [4Fe-4S] cluster. To gain some insight into this, equivalent experiments using Chelex 100 were performed with the [4Fe-4S] cluster form of NsrR (supplied by Dr J. Crack, Centre for Molecular and Structural Biochemistry, School of Chemistry, University of East Anglia, Norwich), another Rrf2 family regulator. In contrast to RirA, no significant cluster loss was observed for NsrR over a 2 hr period (Figure 4.22).
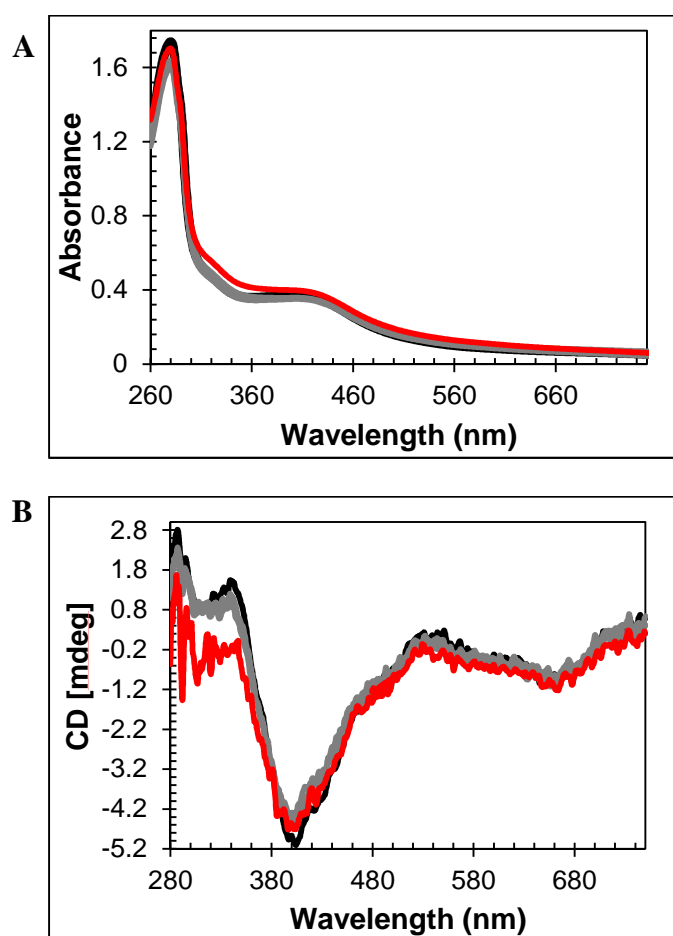
Figure 4.22. Response of [4Fe-4S] NsrR to low iron conditions generated by Chelex 100. (**A**) UV-visible absorbance and (**B**) CD spectra of [4Fe-4S] NsrR (29 µM in cluster in cluster B (25 mM HEPES, 2.5 mM CaCl$_2$, 50 mM NaCl, 750 mM KCl, pH 7.5); ~60% cluster-loaded) following addition of Chelex-100 resin separated by a semi-permeable membrane. Starting and end-point (120 min) spectra are in black and red, respectively. Intervening spectra are in grey. The measurements were obtained using a 1 cm sealed anaerobic cuvette, with buffer B as a baseline.

4.2. Identification of intermediates during cluster conversion using EDTA as iron-chelator by mass spectrometry.

In order to study the mechanism of Fe-sensing by RirA and how the regulation is achieved, [4Fe-4S] RirA in ammonium acetate buffer was combined with 250 µM EDTA at 37°C under anaerobic conditions and continuously infused into the ESI-source of the instrument to simulate low iron conditions in the cell. Figure 4.23 and Figure 4.24 shows the deconvoluted spectra and the 3D plot obtained during the reaction time course over 30 min.
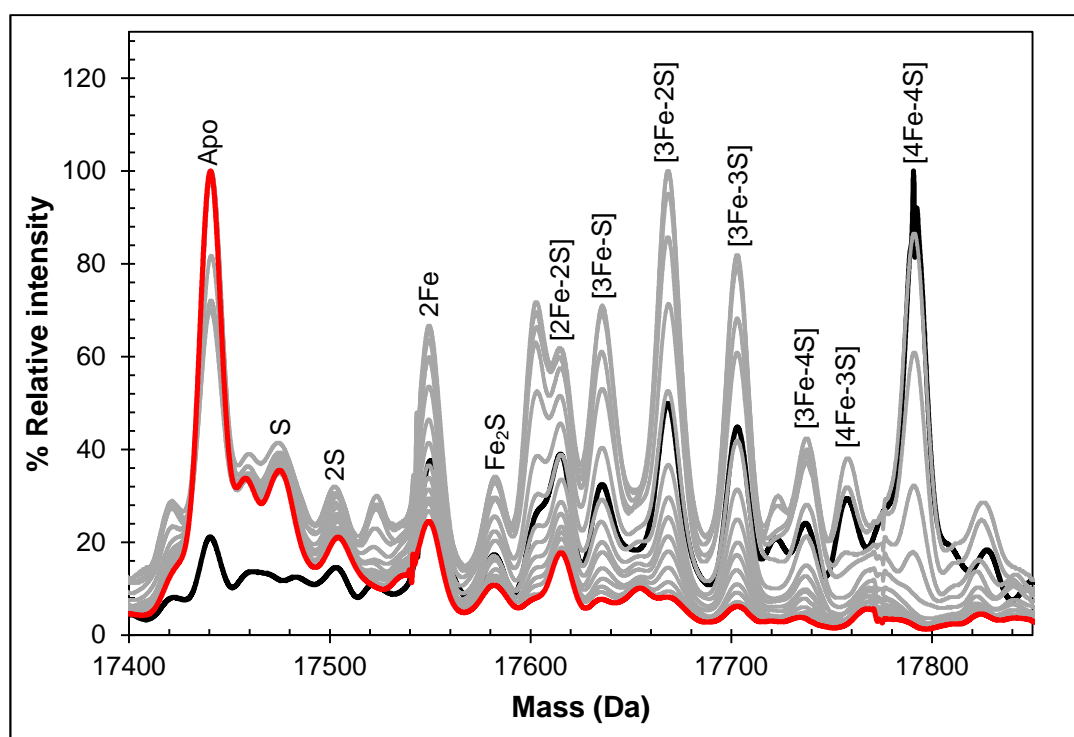
Figure 4.23. Real time native ESI-MS analysis of [4Fe-4S] RirA cluster conversion under low iron conditions generated by exposure to EDTA. Deconvoluted mass spectrum of ~30 µM [4Fe-4S] RirA in 250 mM ammonium acetate pH 7.32 (black line) before and after exposure to 250 µM EDTA at 37°C (30 min exposure, red line). Intervening spectra are in grey. Spectra are representative of multiple repeat experiment.
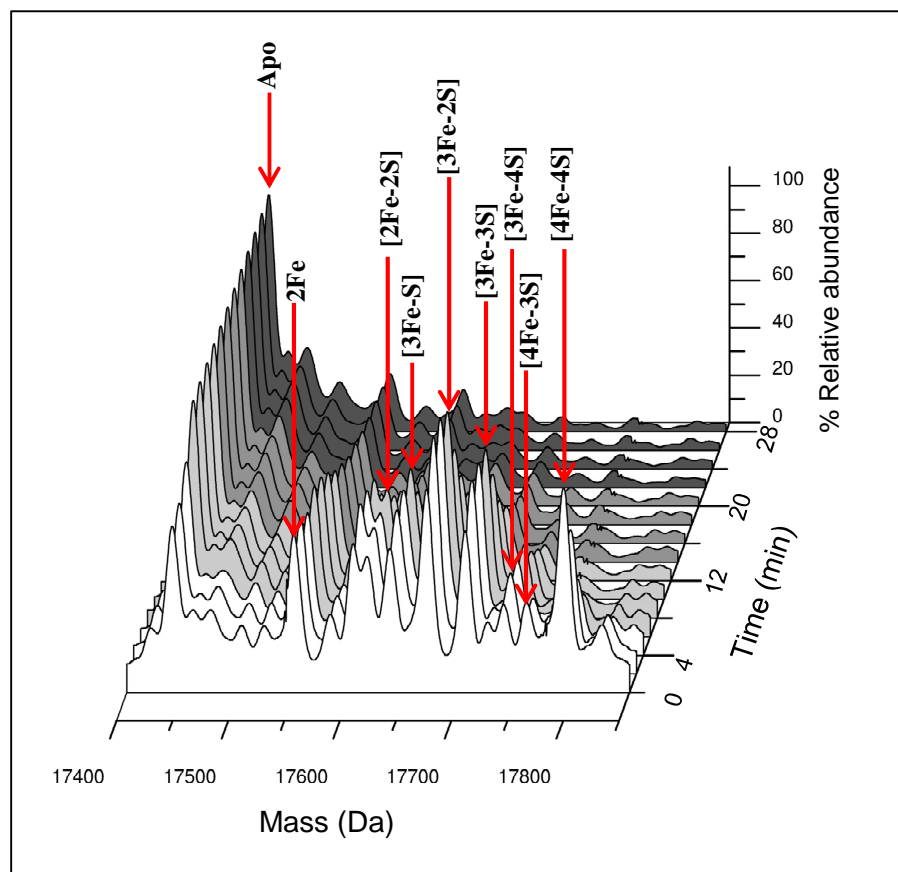
Figure 4.24. 3D plot of real time native ESI-MS analysis of [4Fe-4S] RirA cluster conversion under low iron conditions generated by exposure to EDTA. 3D plot showing the formation and decay of all monomeric RirA species during the EDTA reaction time course. ~30 µM [4Fe-4S] RirA in 250 mM ammonium acetate pH 7.32 for 30 min exposure to 250 µM EDTA at 37°C. Intervening spectra are in grey. Spectra are representative of multiple repeat experiments.

The initial spectrum was very similar to that described for [4Fe-4S] RirA in Chapter 3 (section 3.2.2). Upon exposure to EDTA, the [4Fe-4S] peak decayed away and peaks corresponding to protein bound cluster fragments (17,586 Da – 17,762 Da) increased in intensity, reaching a maximum ~ 4 - 6 min post EDTA exposure before themselves decaying away. These included [4Fe-3S], [3Fe-4S], [3Fe-3S], [3Fe-2S], [3Fe-S] and [2Fe-2S] forms. A peak appeared at 17549 Da which corresponds to RirA containing two irons, with a maximum intensity at 2 min. Peaks were also observed at 17474 Da and 17506 Da, corresponding to one and two sulfur adducts of apo RirA (+32 and +64 Da). The apo peak increased in intensity as a function of time due to the decay of the protein bound clusters, see Figure 4.23 and Figure 4.24. The table with predicted vs observed masses is shown in Chapter 3 (section 3.2.2).

Abundances of the different cluster fragments species in Figure 4.23 and Figure 4.24 were plotted as a function of time, see Figure 4.25. In MS experiments, abundances are reported relative to the most abundant species (arbitrarily set to 100%). For RirA experiments, the most abundant species over most of the time course was the apo form and so the data provide information about the temporal behaviour of all the [Fe-S] forms of RirA. Global analysis of multiple mass spectrometric kinetic data sets led to the reaction scheme shown in Figure 4.26. This scheme was able to model the formation and/or decay of the peak intensities corresponding to [4Fe-4S], [4Fe-3S], [3Fe-4S], [3Fe-3S], [3Fe-2S], [2Fe-2S], and [3Fe-S] RirA species. The kinetic data show that [3Fe-4S] cluster is the first intermediate formed (maximizing at 2 min), followed by [3Fe-3S], [3Fe-2S] and [3Fe-S] forms. It should be emphasized that these intermediates appeared before the formation of the [2Fe-2S] cluster, see Figure 4.25. Table 4.1 shows the observed rate constants required to describe the reaction scheme depicted in Figure 4.26. It is noted that the model suggests that direct conversion of the [4Fe-4S] cluster to the [3Fe-3S] species does not occur. Thus, loss of a single iron or sulfide iron appears to be an obligatory first step in the cluster conversion process with loss of sulfide or iron following. The rate constant describing the loss of an iron to obtain the [3Fe-4S] cluster (k_{obs1} = 0.23 min^{-1}) was much higher than that for the loss of a sulfide, [4Fe-3S] (k_{obs2} = 0.04 min^{-1}), indicating that loss of an initial iron is the favoured route for cluster conversion. Nevertheless, loss of an initial sulfide can also occur, so this represents a first branch point in the mechanism. The temporal nature of [3Fe-3S] RirA, which maximized at ~ 4 min, is consistent with an intermediate in the [4Fe-4S] to [2Fe-2S] cluster conversion pathway. The [3Fe-3S] was formed from [3Fe-4S] and [4Fe-3S] clusters with similar observed rate constants, 0.14 and 0.12 min^{-1}, respectively. The data demonstrate that [2Fe-2S] is formed from [3Fe-3S] (k_{obs6} = 0.18 min^{-1}) and [3Fe-2S] (k_{obs10} = 0.1 min^{-1}) with similar observed rate constants. Breakdown of the [3Fe-S] form, modelled here as resulting in formation of apo-RirA, occurs with a rate constant (k_{obs8} = 0.31 min^{-1}) higher than that for breakdown of [2Fe-2S] (k_{obs9} = 0.19 min^{-1})

again to apo-RirA. It is recognised that this is unlikely to occur directly in a single step, but the data do not provide much data on intermediate species in this process and so further possible steps have not been included in the model. The build-up of [3Fe-S] occurs because the loss of an iron from the [3Fe-2S] cluster is slower than the loss of a sulfide, k = 0.1 min^{-1} and 0.4 min^{-1}, respectively.

Overall the kinetic mass spectrometry data provide a high resolution overview of the cluster conversion process, consistent with the importance of [3Fe-4S], [3Fe-3S] and [3Fe-2S] intermediates.

Table 4.1. Observed rate constants used to fit experimental shown in Figure 4.23 and Figure 4.24 to cluster disassembly model shown in Figure 4.26.

Observed rate constant (min^{-1})		Reaction
k1	0.23	[4Fe-4S] → [3Fe-4S]
k2	0.04	[4Fe-4S] → [4Fe-3S]
k3	0.14	[3Fe-4S] → [3Fe-3S]
k4	0.12	[4Fe-3S] → [3Fe-3S]
k5	0.29	[3Fe-3S] → [3Fe-2S]
k6	0.18	[3Fe-3S] → [2Fe-2S]
k7	0.4	[3Fe-2S] → [3Fe-S]
k8	0.31	[3Fe-S] → Apo
k9	0.19	[2Fe-2S] → Apo
k10	0.1	[3Fe-2S] → [2Fe-2S]
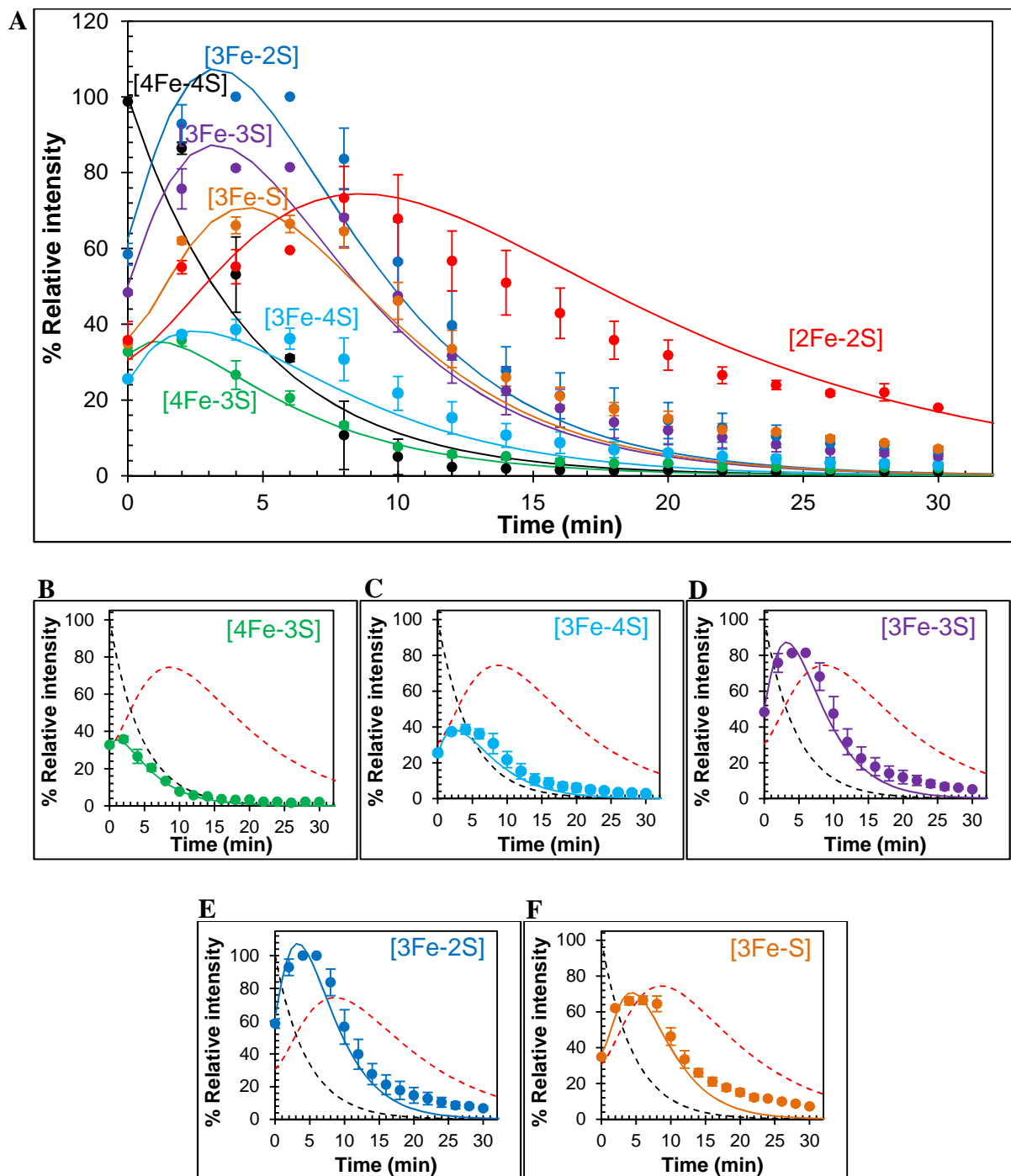
Figure 4.25. Mechanism of [4Fe-4S] cluster conversion. A) Plots of relative abundances of [4Fe-4S] cluster (black), [4Fe-3S] cluster (green), [3Fe-4S] (light blue), [3Fe-3S] (purple), [3Fe-2S] cluster (blue), [3Fe-S] cluster (orange) and [2Fe-2S] cluster (red) species as a function of time following exposure to 250 µM EDTA at 37° C. Global fitting to the experimental data, using the reaction scheme depicted in Figure 4.26, are shown as solid lines. B) – F), plots of relative abundances of the [4Fe-3S] cluster (B), [3Fe-4S] (C), [3Fe-3S] (D), [3Fe-2S] cluster (E), and the [3Fe-S] cluster (F). Global fits to the experimental data are shown as solid lines. Dashed lines show the response of the [4Fe-4S] (black line) and [2Fe-2S] (red line) cluster for easy comparison. Error bars show standard error for average MS dataset (n = 2). The global fitting model was initiated with 100% relative abundance of [4Fe-4S] clusters.
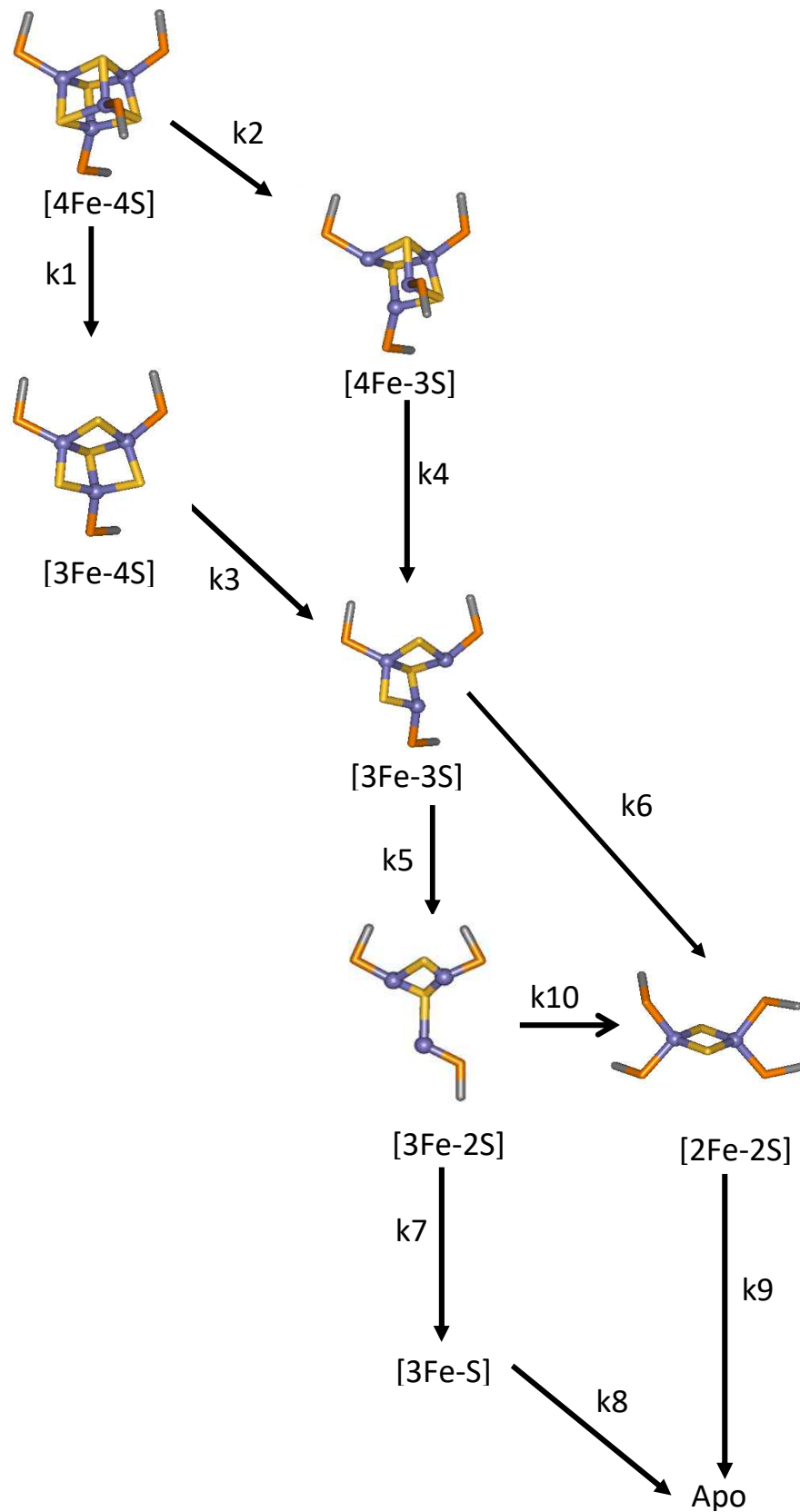
Figure 4.26. Reaction scheme of [4Fe-4S] cluster conversion . Reaction scheme used to simulate the kinetic dependence native-MS data of ~30 µM [4Fe-4S] RirA in 250 mM ammonium acetate pH 7.32 for 30 min exposure to 250 µM EDTA at 37°C.

4.3. [4Fe-4S] RirA, but not apo-RirA, binds RirA-regulated fhuA promoter DNA.

EMSAs were carried out with [4Fe-4S] RirA using the *fhuA* promoter, which harbours an IRO box and is known to be under the control of RirA *in vivo* [4, 5], see Figure 4.27. A titration with increasing concentrations of [4Fe-4S] RirA resulted in increased levels of bound DNA, with essentially full binding observed at a [4Fe-4S] RirA:DNA ratio of 40:1. At higher protein levels, non-specific binding was observed (Figure 4.27A). Importantly, DNA-binding was not observed in an equivalent experiment with apo-RirA (Figure 4.27B). A very small amount of binding was observed at high protein to DNA ratios (> 121:1). The data demonstrate that the [4Fe-4S] form is the active form for DNA-binding. Observations of a [2Fe-2S] form of RirA (above) raised the question of whether such a form would be able to bind DNA. EMSA experiments with the *fhuA* promoter were repeated, Figure 4.27C, using [2Fe-2S] RirA. Although non-specific binding can be seen at higher ratios of protein to DNA, the data clearly show that the [2Fe-2S] form binds DNA. At ratio of 40:1, where the [4Fe-4S] form gave full DNA- binding, only a small proportion of DNA was bound by [2Fe-2S] RirA. Thus, it is concluded that [2Fe-2S] RirA binds DNA significantly more weakly than the [4Fe-4S] form.
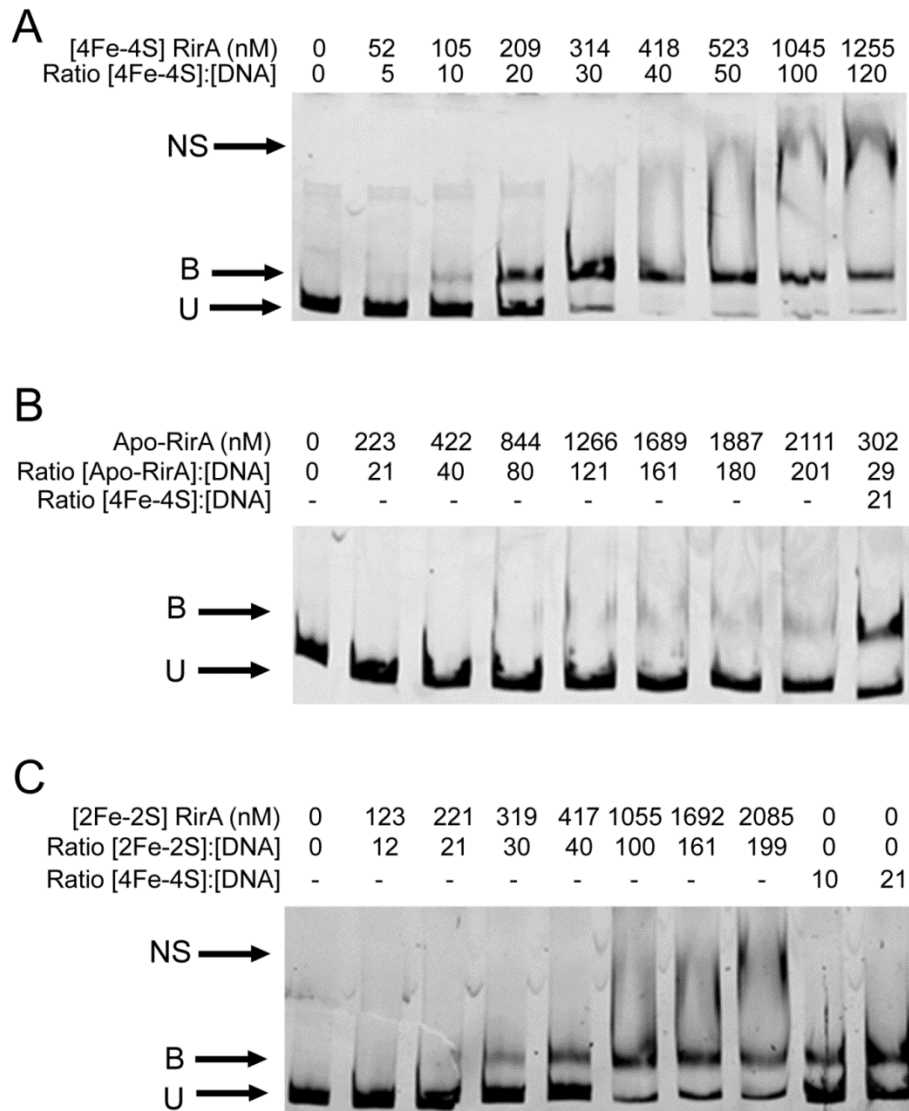
Figure 4.27. Cluster-dependent DNA binding by RirA. EMSAs showing the *fhuA* promoter DNA probe in unbound (U), bound (B), and non-specifically bound (NS) forms by **(A)** [4Fe-4S] RirA, **(B)** apo-RirA and [4Fe-4S] RirA as a control and **(C)** [2Fe-2S] RirA and [4Fe-4S] RirA as a control. Ratios of [4Fe-4S]/[2Fe-2S] RirA and [RirA] to DNA are indicated. The binding buffer contained 10 mM Tris, 60 mM KCl, pH 7.52.

4.4. Discussion.

The simulation of low iron conditions led to the instability of the RirA [4Fe-4S] cluster, resulting in conversion to a [2Fe-2S] form and subsequently to loss of cluster to form apo-RirA. The extent to which the [2Fe-2S] form was stable varied: in the presence of EDTA and Ferrozine, it was readily observed, but with Chelex 100, apo-transferrin, and apo-bacterioferritin it was less stable and was observed only as a transient species prior to

apo- protein formation. Similar experiments with [4Fe-4S] NsrR, which functions through reaction of its cluster with nitric oxide, revealed that its cluster was stable under iron-depleted conditions. This suggests that cluster fragility/conversion is a physiologically important characteristic of [4Fe-4S] RirA and is not a general trait of [4Fe-4S]-containing Rrf2 regulators. The [4Fe-4S] form of RirA, which is likely present in the *Rhizobial* cell under iron replete conditions, binds RirA regulated promoter DNA tightly, consistent with its function as a repressor of expression of genes involved in iron uptake. The [2Fe-2S] form of RirA could be stabilized under anaerobic conditions following removal of chelator. In EMSA experiments it was apparent that the [2Fe-2S] form binds DNA significantly weaker than the [4Fe-4S] form. However, it cannot ruled out that the observed binding could have resulted from a small amount of residual [4Fe-4S] cluster. Under prolonged low iron conditions, the [2Fe-2S] cluster was unstable, resulting in a cluster-free form, which does not bind DNA. In this form, RirA can no longer function as a repressor and the iron-uptake machinery of the cell is fully activated.

The three states ([4Fe-4S], [2Fe-2S] and apo) of RirA may represent three distinct physiological responses within the cell, which are accessed through the lability of iron in the cluster and which have different outcomes in terms of expression of RirA-controlled genes, see Figure 4.28. Further investigation will be needed, including with additional promoters, to determine whether the [2Fe-2S] form of RirA is physiologically relevant. Although there is no information on the cluster configuration of RirA in *R. leguminosarum* itself, anaerobically purified RirA generated from heterologous expression in aerobically grown *E. coli* contained a mixture of both [2Fe-2S] and [4Fe-4S] clusters, see Chapter 3 (section 3.2). This supports a mechanism in which cluster transformation occurs in the cell.
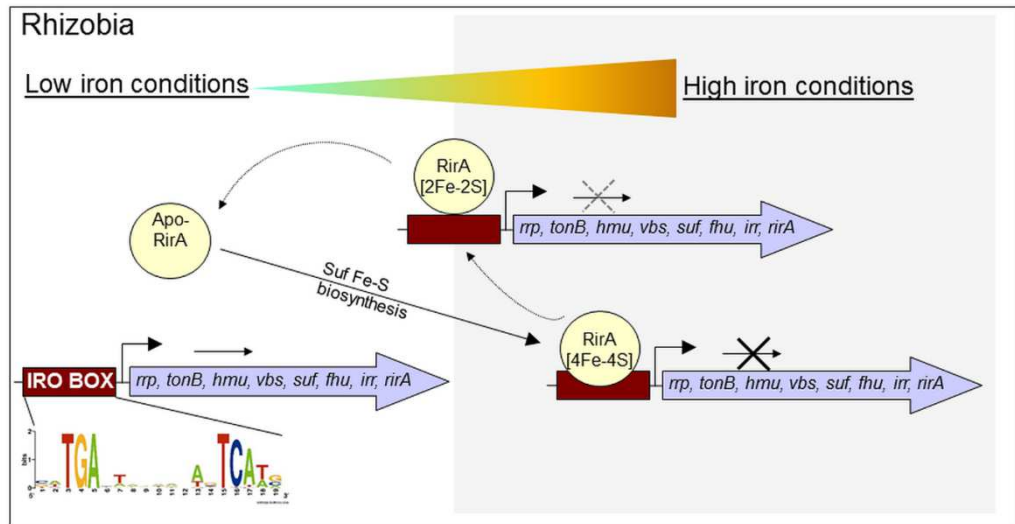
Figure 4.28. RirA mediated regulation of iron-responsive genes in *Rhizobium*. Under iron sufficient conditions, RirA accommodates a [4Fe-4S] cluster (via the Suf system) and binds to the IRO motif (sequence shown) present in the promoter regions of RirA-regulated genes, repressing their transcription. In low iron medium, the [4Fe-4S] cluster of RirA is unstable to conversion/degradation, yielding apo-RirA via a [2Fe-2S] form. Apo-RirA does not bind the IRO motif and so these genes are no longer repressed by RirA. [2Fe-2S] RirA retains some ability to (weakly) bind the IRO motif, resulting in a partial alleviation of repression under conditions of mild iron deficiency. O_2/oxidative stress destabilizes the RirA cluster, leading to increased turnover of [4Fe-4S] RirA even under iron-replete conditions.

The conversion of the [4Fe-4S] RirA cluster to apo under low iron conditions (generated by presence of chelator) was in general much more rapid in the presence of O_2. Thus, it appears that iron insufficiency and the presence of O_2 lead to an enhanced rate of cluster conversion/degradation and the interplay between these conditions will control the rate of cluster reaction. It has been noted that specific, as yet unidentified, cellular factors might also be involved in, and influence the rate of, cluster degradation.

The behaviour of RirA allows comparison with other iron-sulfur cluster-containing regulators. For example FNR controls expression of genes in response to O_2 through reaction with its [4Fe-4S] cluster cofactor. This promotes conversion to a [2Fe-2S] cluster form that can no longer bind DNA [6, 7]. FNR is the master switch for the transition between anaerobic and aerobic metabolism. There are clear similarities in terms of the cluster conversion reactions of FNR and RirA. In the case of RirA, the reaction is mediated by the synergistic influences of low iron and O_2. FNR does not respond to Fe^{2+}/

Fe^{3+} chelators in the absence of O_2, but their presence was found to enhance the rate of [2Fe-2S] formation [8].

ESI-MS experiments and global analysis of chelator-mediated cluster degradation using an approach that was developed to study the FNR cluster conversion reaction [9] showed that the first step of the reaction from the [4Fe-4S] to apo- RirA is the loss of Fe^{2+} from the $[4Fe-4S]^{2+}$ cluster to form a [3Fe-4S] cluster intermediate, step 1. A similar step was also observed in O_2-mediated [4Fe-4S] cluster degradation in FNR [9, 10] , where cluster degradation is initiated by O_2-mediated oxidation. In the case of RirA under anaerobic conditions, there is no oxidant, so the resulting cluster is likely to be $[3Fe-4S]^0$.

In RirA, the [4Fe-4S] cluster can also lose a sulfide ion as the first step of degradation, but the formation of the [4Fe-3S] cluster (presumably with +4 charge) is slower than the formation of the [3Fe-4S] intermediate (0.04 min^{-1} and 0.23 min^{-1}, respectively). It is noted that the [4Fe-3S] form was not observed in FNR disassembly [9].

The [3Fe-3S] cluster was the next intermediate observed. This results from the loss of one sulfide ion from the [3Fe-4S] cluster (step 2) (or the loss of a Fe^{2+} from the [4Fe-3S] form). This novel cluster intermediate was also recently observed during FNR cluster degradation [9]. An inorganic model $[3Fe-3S]^{3+}$ cluster was recently described for the first time, in which all iron and sulfide ions lie in the same molecular plane forming a hexagonal arrangement [11]. The oxidation state of the [3Fe-3S] cluster in RirA is unclear. Loss of sulfide from the $[3Fe-4S]^0$ intermediate would be expected to generate a $[3Fe-3S]^{2+}$ form. The mass spectrometry data is not sufficiently high resolution to determine the overall oxidation state on the cluster intermediates, though the data are consistent with both 2+ and 3+ states, see Chapter 3 (section 3.2.2).

The [3Fe-3S] intermediate undergoes loss of Fe^{2+} and sulfide to [2Fe-2S] and just loss of sulfide to [3Fe-2S], representing a second branch point of the mechanism. The conversion from the [3Fe-3S] to [2Fe-2S] is also observed in the reaction of FNR with O_2 (step 3).

The [3Fe-2S] cluster form is not observed during FNR disassembly [9]. Further loss of sulphide from [3Fe-2S] RirA results in an unusual [3Fe-S] form.

The last part of the conversion is the formation of apo-RirA from either [2Fe-2S] or [3Fe-S] forms. This is the part of degradation reaction about which the mass spectrometry provides the least information. In part, this is because the formation of the apo-protein could not be followed due to the fact that it is the most abundant specie for nearly the entire experiment.

The conversion of [4Fe-4S] RirA to apo-RirA involves steps that are similar to those detected in the reaction of FNR with O_2 although the branches of the reaction mechanism are different and the oxidation states of the intermediate species are likely to be different. Recent ESI-MS studies of the FNR O_2 reaction revealed the cluster conversion reaction in great detail, identifying a novel [3Fe-3S] cluster as an intermediate [9]. In FNR, cluster sulfide is readily oxidized leading to the formation of a persulfide-coordinated [2Fe-2S] cluster, which can undergo conversion back to the [4Fe-4S] form upon addition of reductant and Fe^{2+} [12]. It is noteworthy that no evidence for a persulfide-coordinated [2Fe-2S] cluster in RirA was found, and only small amounts of persulfide adducts of apo-RirA were observed. Thus, it appears that sulfur is not stored on RirA and so repair of the [2Fe-2S] form back to the [4Fe-4S] form would be very unlikely without additional sulfide.

The properties of RirA described here are also clearly related to those of the Rrf2 superfamily member IscR [13], which in *E. coli* controls the expression of approx. 40 genes, including the *isc* and *suf* iron-sulfur cluster biosynthesis operons [14, 15]. Unusually, IscR binds to two types of promoters (type 1 and 2); binding to type 1 is dependent on the presence of a [2Fe-2S] cluster, whereas binding to type 2 promoters is independent of the cluster (apo-IscR binds as tightly as [2Fe-2S] IscR) [14, 15]. Under conditions where there is sufficient iron-sulfur cluster supply, [2Fe-2S] IscR binds type 1 promoters and represses Isc iron-sulfur cluster biogenesis. When iron-sulfur cluster supply

is insufficient, apo-IscR is formed and cluster biosynthesis is de-repressed. Iron-sulfur cluster demand varies and is higher under aerobic conditions than anaerobic, particularly under oxidative stress, where turnover of iron-sulfur clusters in the cell is higher. Under these conditions, apo-IscR is the predominant form and this is able to bind type 2 promoters to inhibit expression of anaerobic iron-sulfur cluster containing respiratory proteins and activate Suf iron-sulfur cluster biosynthesis. Thus, there is a complex interplay between iron-sulfur cluster demand and turnover due to O_2/oxidative stress [14-17]. It has noted that the Rrf2 family NO-responsive regulator NsrR from *Bacillus subtilis* has also been shown to recognize two types of promoter sites, only one of which is cluster-dependent [18].

While there is no evidence for more than one type of DNA-binding site, our *in vitro* data on RirA indicate some similarities to IscR. The significant sensitivity of RirA to O_2 suggests that even when iron is sufficient, the protein is susceptible to cluster conversion/loss [16]. It has been noted that the Suf iron-sulfur cluster biosynthetic machinery of *R. leguminosarum* is under RirA regulation (and is also regulated by Irr) [5, 19]. Under iron sufficiency, iron-sulfur cluster biosynthesis is still required for multiple processes in the cell. The continuous breakdown of [4Fe-4S] RirA by O_2 might be important for the cell to maintain iron-sulfur cluster biosynthesis. Because iron-sulfur cluster biosynthesis is also required for RirA-mediated repression, this provides a mechanism to ensure the cellular demand for iron-sulfur clusters is met. The data are consistent with RirA functioning as a sensor of iron via iron-sulfur cluster availability (see Figure 4.28), rather than as a direct sensor of Fe^{2+} through, for example, a $[4Fe-4S]^{2+} \leftrightarrow [3Fe-4S]^{0}$ equilibrium dependent on Fe^{2+} ion availability, or through repair of [2Fe-2S] RirA back to [4Fe-4S] RirA.

4.5. References.

1. Owda, A.K., M.G. Alam, and S.V. Shah, *Environmental lead exposure and chronic renal disease.* N Engl J Med, 2003. **348**(18): p. 1810-2; author reply 1810-2.
2. Vinella, D., et al., *In vivo [Fe-S] cluster acquisition by IscR and NsrR, two stress regulators in Escherichia coli.* Mol Microbiol, 2013. **87**(3): p. 493-508.
3. Tucker, N.P., et al., *The transcriptional repressor protein NsrR senses nitric oxide directly via a [2Fe-2S] cluster.* PLoS One, 2008. **3**(11): p. e3623.
4. Todd, J.D., et al., *RirA, an iron-responsive regulator in the symbiotic bacterium Rhizobium leguminosarum.* Microbiology-Sgm, 2002. **148**: p. 4059-4071.
5. Todd, J.D., G. Sawers, and A.W.B. Johnston, *Proteomic analysis reveals the wide-ranging effects of the novel, iron-responsive regulator RirA in Rhizobium leguminosarum bv. viciae.* Molecular Genetics and Genomics, 2005. **273**(2): p. 197-206.
6. Johnson, D.C., et al., *Structure, function, and formation of biological iron-sulfur clusters.* Annu Rev Biochem, 2005. **74**: p. 247-81.
7. Melville, S.B. and R.P. Gunsalus, *Isolation of an oxygen-sensitive FNR protein of Escherichia coli: interaction at activator and repressor sites of FNR-controlled genes.* Proc Natl Acad Sci U S A, 1996. **93**(3): p. 1226-31.
8. Crack, J.C., et al., *Influence of the environment on the [4Fe-4S]2+ to [2Fe-2S]2+ cluster switch in the transcriptional regulator FNR.* J Am Chem Soc, 2008. **130**(5): p. 1749-58.
9. Crack, J.C., A.J. Thomson, and N.E. Le Brun, *Mass spectrometric identification of intermediates in the O2-driven [4Fe-4S] to [2Fe-2S] cluster conversion in FNR.* Proc Natl Acad Sci U S A, 2017. **114**(16): p. E3215-e3223.
10. Crack, J.C., et al., *Bacterial iron-sulfur regulatory proteins as biological sensor-switches.* Antioxid Redox Signal, 2012. **17**(9): p. 1215-31.
11. Lee, Y., et al., *A [3Fe-3S](3+) cluster with exclusively mu-sulfide donors.* Chem Commun (Camb), 2016. **52**(6): p. 1174-7.
12. Zhang, B., et al., *Reversible cycling between cysteine persulfide-ligated [2Fe-2S] and cysteine-ligated [4Fe-4S] clusters in the FNR regulatory protein.* Proc Natl Acad Sci U S A, 2012. **109**(39): p. 15734-9.
13. Santos, J.A., P.J. Pereira, and S. Macedo-Ribeiro, *What a difference a cluster makes: The multifaceted roles of IscR in gene regulation and DNA recognition.* Biochim Biophys Acta, 2015. **1854**(9): p. 1101-12.
14. Giel, J.L., et al., *Regulation of iron-sulphur cluster homeostasis through transcriptional control of the Isc pathway by [2Fe-2S]-IscR in Escherichia coli.* Mol Microbiol, 2013. **87**(3): p. 478-92.
15. Giel, J.L., et al., *IscR-dependent gene expression links iron-sulphur cluster assembly to the control of O2-regulated genes in Escherichia coli.* Mol Microbiol, 2006. **60**(4): p. 1058-75.
16. Imlay, J.A., *Iron-sulphur clusters and the problem with oxygen.* Mol Microbiol, 2006. **59**(4): p. 1073-82.
17. Rajagopalan, S., et al., *Studies of IscR reveal a unique mechanism for metal-dependent regulation of DNA binding specificity.* Nat Struct Mol Biol, 2013. **20**(6): p. 740-7.
18. Kommineni, S., et al., *Nitric oxide-sensitive and -insensitive interaction of Bacillus subtilis NsrR with a ResDE-controlled promoter.* Mol Microbiol, 2010. **78**(5): p. 1280-93.
19. Todd, J.D., et al., *The Rhizobium leguminosarum regulator IrrA affects the transcription of a wide range of genes in response to Fe availability.* Molecular Genetics and Genomics, 2006. **275**(6): p. 564-577.

Chapter 5. Characterization of a putative NsrR homologue in *Streptomyces venezuelae*.

Bioinformatic analyses of the genome sequence of Streptomyces venezuelae revealed the presence of a homologue of NsrR called Sven6563. However, in vivo studies revealed that it is not an NsrR, but instead appears to regulate a range of genes in response to redox stress, leading to it being named RsrR. In this chapter, biochemical, spectroscopic and mass spectrometric studies of RsrR are reported that show the protein contains a [2Fe-2S] cluster and that the switch between oxidized and reduced cluster controls its DNA binding activity *in vitro*. Mössbauer and resonance Raman data confirm that RsrR binds a [2Fe-2S] cluster and demonstrate that it is bound by one histidine along with Cys residues. Experiments on site-directed substitution variants of RsrR are consistent with His12 and Glu8 being cluster ligands.

5.1. RsrR contains a redox active [2Fe-2S] cluster.

5.1.1. Absorbance, CD and EPR studies.

RsrR contains three C-terminal cysteine residues which is characteristic of Rrf2 proteins that ligate Fe-S clusters. To investigate the cofactor and DNA binding activity of RsrR, the *rsrR* gene (C-terminally $(His)_6$-tagged RsrR) was over-expressed in *E. coli* and the protein was purified under strictly anaerobic conditions, see Chapter 2 (section 2.2.2). Upon purification, the fractions containing RsrR were pink in colour but rapidly turned brown when exposed to O_2, suggesting the presence of a redox-active cofactor. The UV-visible absorbance spectrum of the as isolated protein, Figure 5.1 (black continuous), revealed broad weak bands in the 300 - 640 nm region. Following exposure to O_2, the spectrum changed significantly, with a more intense absorbance band at 460 nm and a pronounced shoulder feature at 330 nm (Figure 5.1, red). The form of the reduced and oxidized spectra are similar to those previously reported for [2Fe-2S] clusters that are coordinated by three Cys residues and one His [1, 2]. The anaerobic addition of dithionite

to the previously air-exposed sample (at a 1:1 ratio with [2Fe-2S] cluster as determined by iron content) resulted in a spectrum very similar to that of the as isolated protein (Figure 5.1, black dotted), demonstrating that the cofactor undergoes redox cycling.

Because the electronic transitions of iron-sulfur clusters become optically active as a result of the fold of the protein in which they are bound, CD spectra reflect the cluster environment [3]. The near UV-visible CD spectrum of as isolated RsrR (Figure 5.2, black continuous) contained three positive (+) features at 303, 385 and 473 nm and negative features at (-) 343 and 559 nm. When the protein was exposed to ambient O_2 for 30 min, significant changes in the CD spectrum were observed, with features at (+) 290, 365, 500, 600 nm and (-) 320, 450 and 534 nm (Figure 5.2, red). The CD spectra are similar to those reported for Rieske-type [2Fe-2S] clusters [1, 4, 5], which are coordinated by two Cys and two His residues. Anaerobic addition of dithionite (1 equivalent per [2Fe-2S] cluster) resulted in reduction back to the original form (Figure 5.2, black dotted) consistent with the stability of the cofactor to redox cycling.
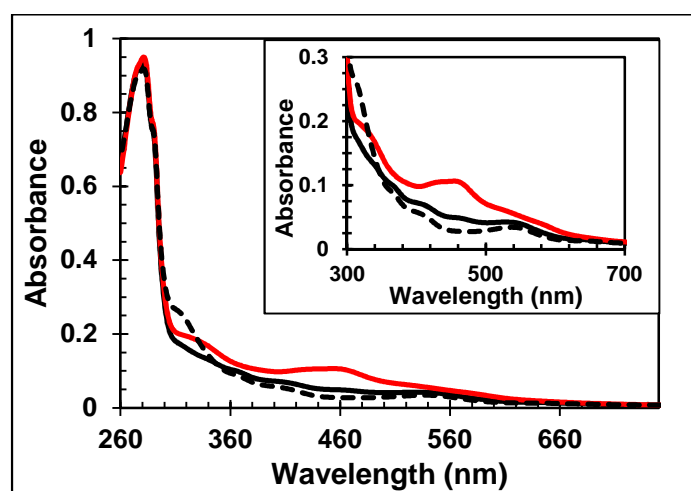
Figure 5.1. UV- visible absorbance characterization of RsrR. UV-visible absorption of 309 μM [2Fe-2S] RsrR (~75% cluster-loaded in buffer F (50 mM TRIS, 2 M NaCl, 5% (v/v) glycerol, pH 8)). As isolated RsrR (black lines), oxidised RsrR (red lines) and reduced RsrR (dashed lines). Initial exposure to ambient O_2 for 30 min was followed by 309 μM sodium dithionite treatment. The measurements were obtained using a 1 mm sealed anaerobic cuvette and buffer F for the UV-visible baseline. Inset is the iron-sulfur cluster absorbance in the 300 – 700 nm region in more detail.
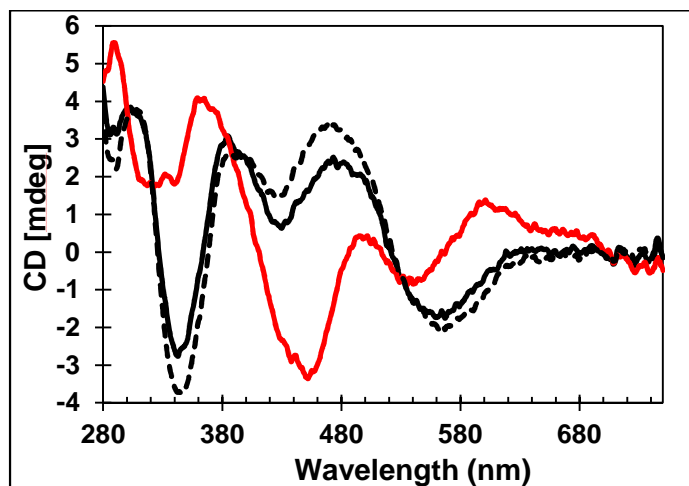
Figure 5.2. CD spectroscopic characterization of RsrR. CD absorption of 309 µM [2Fe-2S] RsrR (~75% cluster-loaded in buffer F (50 mM TRIS, 2 M NaCl, 5% (v/v) glycerol, pH 8)). As isolated RsrR (black lines), oxidised RsrR (red lines) and reduced RsrR (dashed lines). Initial exposure to ambient O_2 for 30 min was followed by 309 µM sodium dithionite treatment. The measurements were obtained using a 1 mm sealed anaerobic cuvette and buffer F for the CD baseline correction.

The absorbance and CD data above indicate that the cofactor is in the reduced state as isolated. [2Fe-2S] clusters in their reduced state are paramagnetic (S = ½) and therefore should give rise to an EPR signal. The EPR spectrum for the as isolated protein contained signals at g = 1.997, 1.919 and 1.867 (Figure 5.3). These g-values and the shape of the spectrum are characteristic of a $[2Fe-2S]^{1+}$ cluster. The addition of excess sodium dithionite to the as isolated protein did not cause any changes in the EPR spectrum (Figure 5.3) indicating that the cluster was fully reduced as isolated. Exposure of the as isolated protein to ambient O_2 resulted in an EPR-silent form, with only a small free radical signal typical for background spectra, consistent with the oxidation of the cluster to the $[2Fe-2S]^{2+}$ form (Figure 5.3), and the same result was obtained upon addition of the oxidant potassium ferricyanide (data not shown).
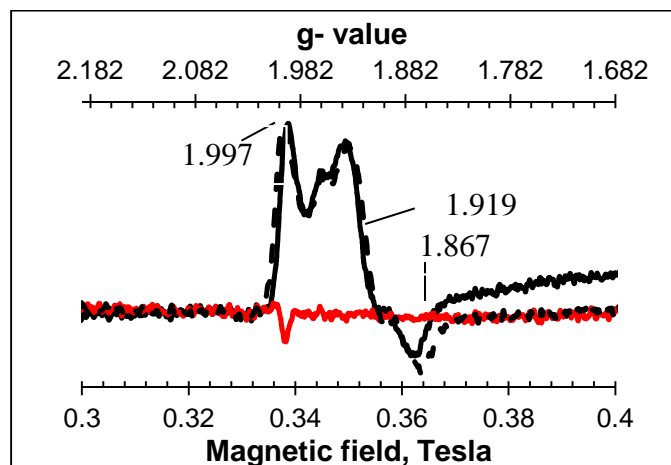
Figure 5.3. EPR spectroscopic characterization of RsrR. EPR spectra of 309 µM [2Fe-2S] RsrR (~75% cluster-loaded in buffer F (50 mM TRIS, 2 M NaCl, 5% (v/v) glycerol, pH 8)). As isolated RsrR (black lines), oxidised RsrR (red lines) and reduced RsrR (dashed lines). As isolated protein was first anaerobically reduced by 309 µM sodium dithionite, then exposed to ambient O_2 for 50 min and followed by 309 µM sodium dithionite treatment.

5.1.2. Mass spectrometry studies.

To further establish the cofactor that RsrR binds, native ESI-MS was employed. Here, a C-terminal His-tagged form of the protein was ionized in a volatile aqueous buffered solution that enabled it to remain folded with its cofactor bound. All Rrf2 proteins studied to date are dimeric, bound and cluster free states [6, 7] and it is expected that RsrR is also a dimer. However, in the ESI-MS experiments, the dimeric form of the protein may not survive ionization, leading to detection of at least some monomer. For MS studies the observation of the monomer is extremely useful because it permits unambiguous determination of cluster- or cluster break down species [8]. The *m/z* spectrum for the reconstituted sample could be divided into two distinct regions, corresponding to monomeric RsrR (*m/z* 550- 2000), and dimeric RsrR (*m/z* 2000- 3000).
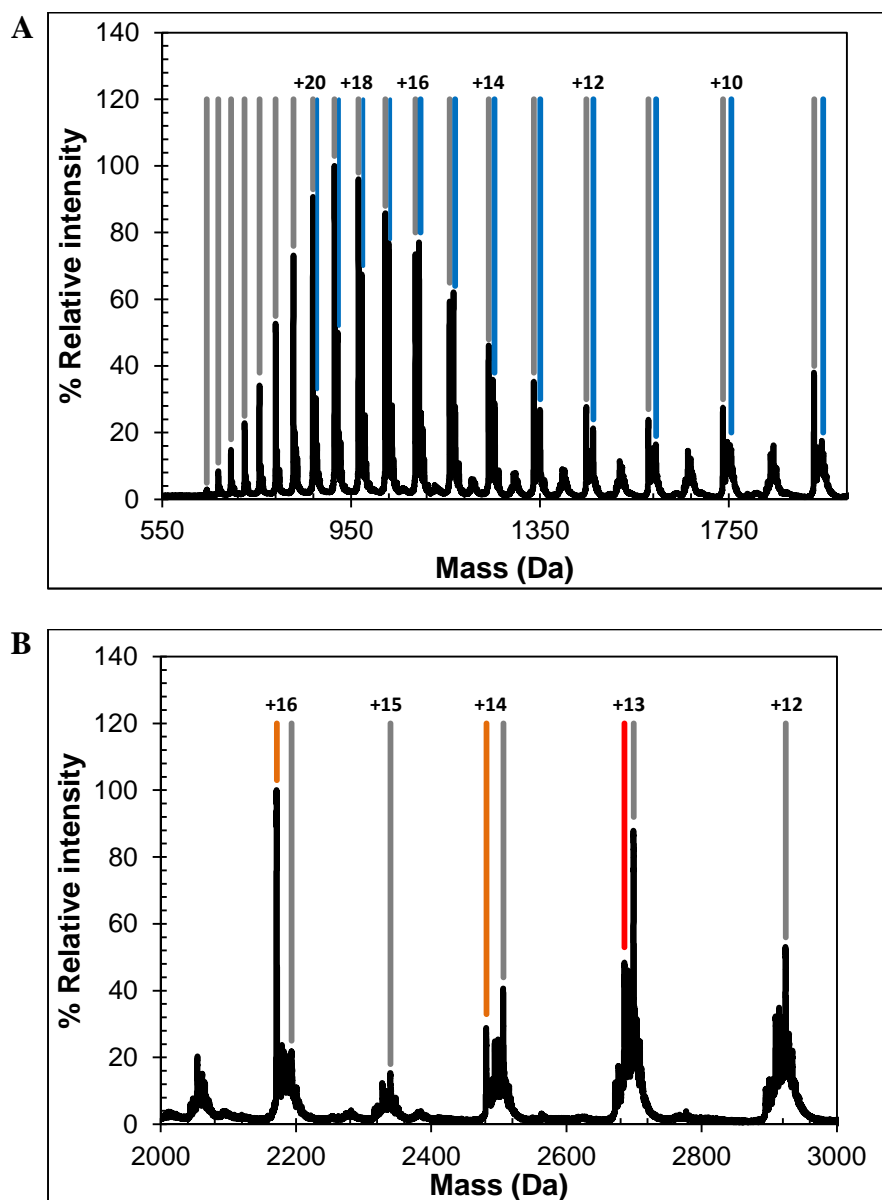
Figure 5.4. ESI-MS *m/z* spectra of native RsrR. (**A**) monomer and (**B**) dimer regions of the *m/z* spectrum are plotted with charge states as indicated. Grey lines indicate the presence of apo-RsrR (monomeric and dimeric RsrR), [2Fe-2S] RsrR (blue lines), [2Fe-2S] (RsrR)$_2$ (red line) and [2Fe-2S][2Fe-2S] (RsrR)$_2$ (orange lines).

The deconvoluted mass spectrum contained several peaks in regions that corresponded to monomer and dimeric forms of the protein. In the monomer region (Figure 5.5A), a peak was observed at 17,363 Da, which corresponds to the apo-protein (predicted mass 17364 Da, see Table 5.1), along with adduct peaks at +23 and +64 Da due to Na$^+$ (commonly observed in native mass spectra) and most likely two additional sulfurs (Cys residues readily pick up additional sulfurs as persulfides [9], respectively). A peak was also observed at +176 Da, corresponding to the protein containing a [2Fe-2S] cluster

(Table 5.1). As for the apo-protein, peaks corresponding to Na$^+$ and sulfur adducts of the cluster species were also observed (Figure 5.5A). A significant peak was also detected at +120 Da which corresponds to a break down product of the [2Fe-2S] cluster (from which one iron is missing, FeS$_2$).
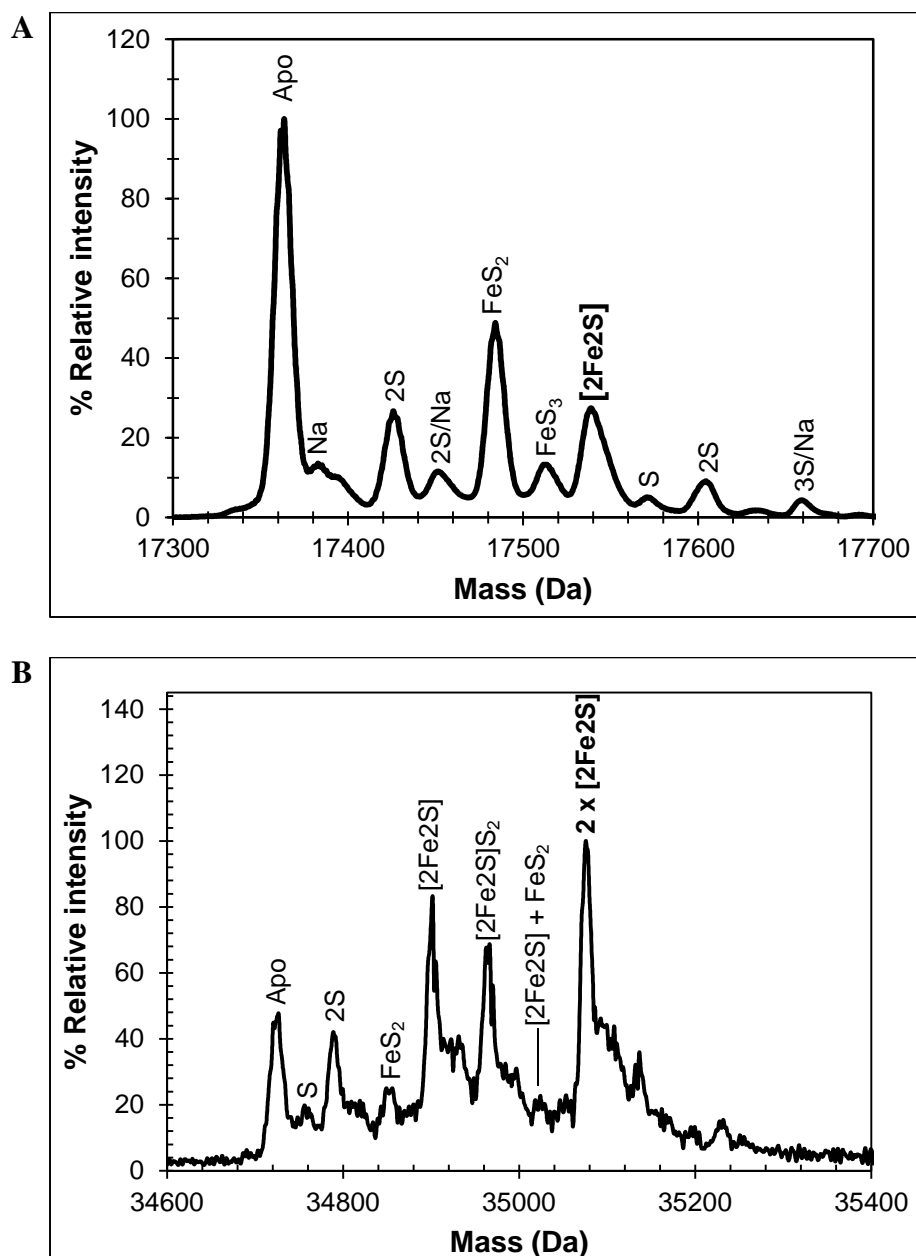

Figure 5.5. Deconvoluted mass spectra of native RsrR. Positive ion mode ESI-TOF native mass spectra of ~21 μM [2Fe-2S] RsrR in 250 mM ammonium acetate pH 8.0, in the RsrR monomer (**A**) and dimer (**B**) regions. Full *m/z* spectra were deconvoluted with Bruker Compass Data analysis with the Maximum Entropy plugin.

In the dimer region, the signal to noise is significantly reduced but peaks are still clearly present (Figure 5.5B). The peak at 34,726 Da corresponds to the apo-RsrR homodimer (predicted mass 34728 Da), and the peak at +352 Da corresponds to the dimer with two [2Fe-2S] clusters. A peak at +176 Da corresponds to the dimer containing one [2Fe-2S] cluster. A range of cluster breakdown products similar to those detected in the monomer region were also observed (Figure 5.5B). Taken together, the ESI-MS data reported here demonstrate that RsrR contains a [2Fe-2S] cluster and are consistent with RsrR being a dimer in solution.

Table 5.1. Predicted and observed masses for apo- and cluster-bound forms of RsrR.

RsrR species	Predicted mass (Da)[a]	Average observed mass (Da)[b]	ΔMass (Predicted - observed) (Da)
Monomeric			
Apo	17364	17364	0
$[2Fe-2S]^{1+}$-S_3Na	17657	17659	-2
$[2Fe-2S]^{1+}$-S_2	17602	17604	-2
$[2Fe-2S]^{1+}$-S	17570	17571	-1
$[2Fe-2S]^{1+}$	**17538**	**17539**	**-1**
$[FeS_3]^{3+}$	17512	17514	-2
$[FeS_2]^{1+}$	17482	17484	-2
2S/Na	17450	17452	-2
2S	17427	17426	+1
Dimeric			
Apo	34728	34725	+3*
$[2Fe-2S]^{1+}$/$[2Fe-2S]^{1+}$	**35076**	**35077**	**-1**
$[2Fe-2S]^{1+}$/$[FeS_2]1^{+}$	35020	35022	-2
$[2Fe-2S]^{1+}$/S_2	34965	34966	-1
$[2Fe-2S]^{1+}$	34901	34901	0
$[FeS_2]^{1+}$	34845	34848	-3
2S	34790	34788	+2*

[a]The difference in predicted mass depending on the overall charge on the cluster is due to charge compensation of cluster binding. A lower overall cluster charge would result in more protons remaining bound and consequently a higher mass [10, 11].
[b]The average observed mass is derived from at least three independent experiments, with standard deviation of ± 1 Da.
*ΔMass could be due to disulfide bonds. One disulfide bond results in -2 Da relative to reduced protein.

Gel filtration was also used to determine the oligomeric state of RsrR in solution. The same experimental set up was used as described for RirA, section 2.2.1. The elution volume for [2Fe-2S]$^{1+}$ RsrR (as isolated) was 59.3 mL and from the calibration plot, the deduced molecular mass was 32.2 kDa. This indicates that the reduced form is a dimer, as the mass of RsrR monomer is 17.4 kDa. Similarly, the elution volume for [2Fe-2S]$^{2+}$ RsrR was 58.7 mL giving a deduced molecular mass of 33.6 kDa. Therefore the oxidized form is also a dimer. Removal of the cluster to generate apo-protein sample also gave rise to a elution band at a mass of 33.2 kDa, along with an elution band at a mass of 128.4 kDa, that most likely arises from some aggregated RsrR (possibly consisting of 3 RsrR dimers), see Figure 5.6. The data presented here clearly indicate that RsrR is a homodimer, irrespective of the presence of the cluster or its oxidation state.
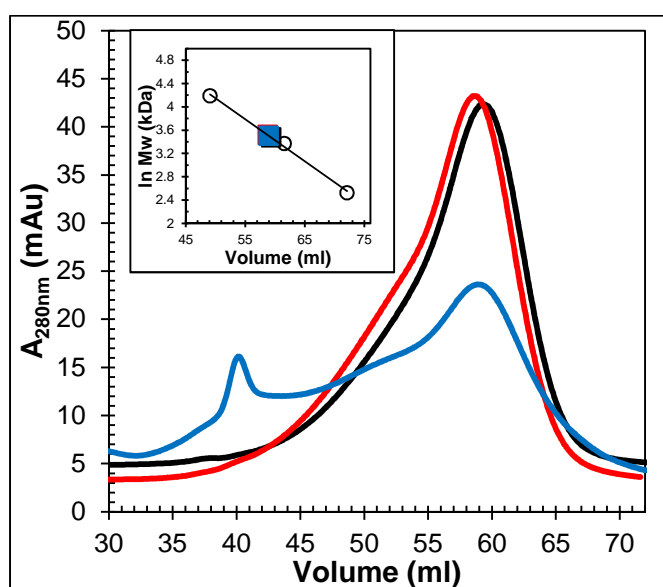

Figure 5.6. Gel filtration analysis of RsrR association state. Chromatograms for [2Fe-2S]$^{1+}$ (black line), [2Fe-2S]$^{2+}$ (red line) and apo-form (blue line) samples of RsrR (~220 µM protein) following elution from Sephacryl S-100 HR column. Inset, calibration curve for the Sephacryl 100HR column. Standard proteins (open circles) were BSA (66 kDa), apo-FNR (30 kDa), and cytochrome *c* (13 kDa). [2Fe-2S]$^{1+}$ RsrR, [2Fe-2S]$^{2+}$ RsrR and apo-RsrR are shown as a black, red and blue squares, respectively. Buffer F (50 mM TRIS, 2 M NaCl, 5% (v/v) glycerol, pH 8) was used for the holo RsrR and buffer G (50 mM Tris, 2 M NaCl, 5% (v/v) glycerol, 2 mM DTT, pH 8.0) for the apo-RsrR. mAu, milliabsorbance units.

5.2. Cluster- and oxidation state dependent binding of RsrR to RsrR-regulated promoter DNA.

To determine which form of RsrR is able to specifically bind DNA, EMSA experiments were performed with DNA fragments carrying the intergenic region between *sven1847* and *sven1848* of the *S. venezualae* chromosome which was shown by ChIP-seq experiments to be an *in vivo* binding site for RsrR. *Sven1847* encodes 3-oxoacyl-[acyl-carrier protein] reductase while *sven1848* is an unknown hypothetical protein. They were PCR amplified using *S. venezualae* genomic DNA with 5′ 6-FAM modified primers [12]. Increasing ratios of [2Fe-2S] RsrR to DNA resulted in a clear shift in the mobility of the promoter DNA from unbound to bound, see Figure 5.7.

Equivalent experiments with cluster-free RsrR did not result in a mobility shift, demonstrating that the cluster is required for the observed DNA-binding activity. These experiments were performed aerobically and so the [2Fe-2S] cofactor would have been in its oxidised state. To determine if oxidation state affects DNA binding activity, EMSA experiments were performed with $[2Fe-2S]^{2+}$ and $[2Fe-2S]^{1+}$ forms of RsrR. The oxidised cluster was generated by exposure to air and confirmed by UV-visible aborbance. The reduced cluster was obtained by reduction with sodium dithionite (confirmed by UV-visible absorbance) and the reduced state was maintained using EMSA running buffer containing an excess of dithionite. The concentration needed to maintain RsrR in a reduced state for the entire EMSA experiment was determined prior to beginning the EMSA analysis. The resulting EMSAs, Figure 5.7B and C, show that, in both cases, DNA-binding occurred but the oxidised form bound significantly more tightly. Tight binding could be restored to the reduced RsrR samples by allowing it to re-oxidise in air. It cannot be ruled out that the apparent low affinity DNA binding observed for the reduced sample results from partial re-oxidation of the cluster during the electrophoretic experiment.

104

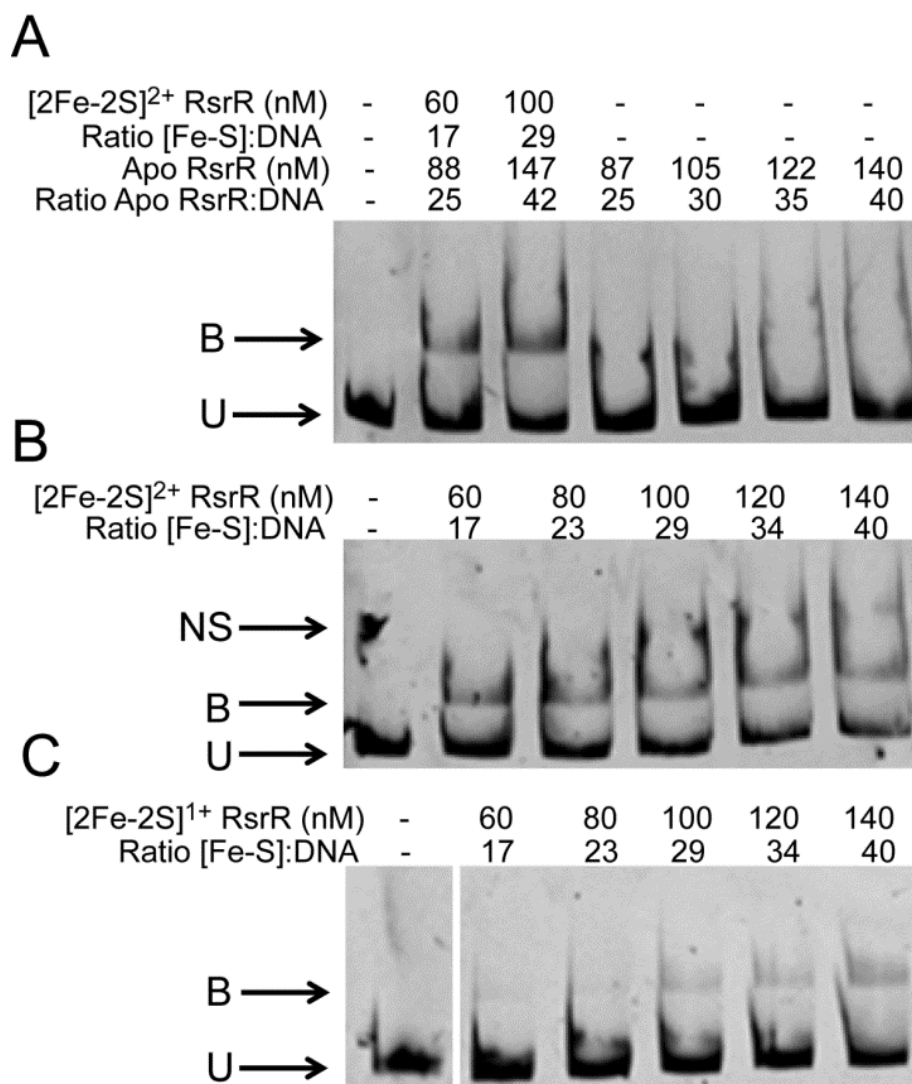Nevertheless, the conclusion is unaffected: oxidised $[2Fe-2S]^{2+}$ RsrR is the high affinity DNA-binding form.

Figure 5.7. Cluster and oxidation state-dependent DNA binding by [2Fe-2S] RsrR. EMSAs showing DNA probes unbound (U), bound (B), and non-specifically bound (NS) by **(A)** $[2Fe2S]^{2+}$ and apo-RsrR, **(B)** $[2Fe-2S]^{2+}$ RsrR and **(C)** $[2Fe-2S]^{1+}$ RsrR. Ratios of [2Fe-2S] RsrR and [RsrR] to DNA are indicated. DNA concentration was 3.5 nM for the $[2Fe-2S]^{2+/1+}$ and apo RsrR experiments. For (A) and (B) the reaction mixtures were separated at 30 mA for 50 min and the polyacrylamide gels were pre-run at 30 mA for 2 min prior to use. For (C) the reaction mixtures were separated at 30 mA for 1hr 45 min and the polyacrylamide gel was pre-run at 30 mA for 50 min prior to use using the de-gassed running buffer containing 5 mM sodium dithionite.

5.3. Identification of the ligands of the cluster.

5.3.1. Mössbauer studies.

Mössbauer spectroscopy provides definitive and quantitative determination of the type of iron-sulfur clusters present in a sample and in some cases can provide clues to the

nature of the ligands coordinated to the cluster [8]. Through a collaboration with Dr Saeed Kamali at the University of Tennessee Space Institute (Tullahoma, USA), Mössbauer spectra of RsrR were recorded. ^{57}Fe labelled [2Fe-2S] was generated as described in Chapter 2 (section 2.1). The spectrum of the ^{57}Fe-enriched RsrR was measured following exposure to air to generate the oxidized state (Figure 5.8). The Mössbauer spectrum for [2Fe-2S]$^{2+}$ RsrR consists of an unresolved asymmetric doublet. The spectrum was hence fitted with two subspectra, with close lying hyperfine parameters. The first component, Q_1, has an isomer shift (δ) value of 0.285 mm/s and quadrupole splitting (ΔE_Q) of 0.545 mm/s, while the second component, Q_2, has a δ value of 0.289 mm/s and a ΔE_Q of 0.761 mm/s. The isomer shifts and quadrupole splittings of both subspectra are characteristic of [2Fe-2S]$^{2+}$ clusters and are very similar to those reported for IscR [13] and Biotin synthase [14]. The hyperfine parameters for the oxidized sample are summarized in Table 5.2.

Mössbauer is a technique that can also help to differentiate the ligands of the clusters. When the cluster is coordinated to 4 cysteines, the doublet is symmetric because the irons are in essentially the same environment. Therefore the data indicate that the [2Fe-2S] cluster of RsrR is not coordinated to 4 cysteines [15]. The Rieske proteins contain two cysteines and two histidines as ligands. The Mossbauer spectrum of these types of proteins consists of a superposition of two quadrupole doublets [16, 17] where the two doublets are more distinct than observed here for RsrR. Accordingly, the RsrR cluster is not of the Rieske-type. However, the spectrum is characteristic of a [2Fe-2S] coordinated by 3 cysteines and 1 histidine [13, 15, 18], but because Mössbauer is not sufficiently discriminating, other possible combinations of ligands cannot be ruled out. Thus, other techniques were used to try to establish the ligands environment of the [2Fe-2S] cluster.
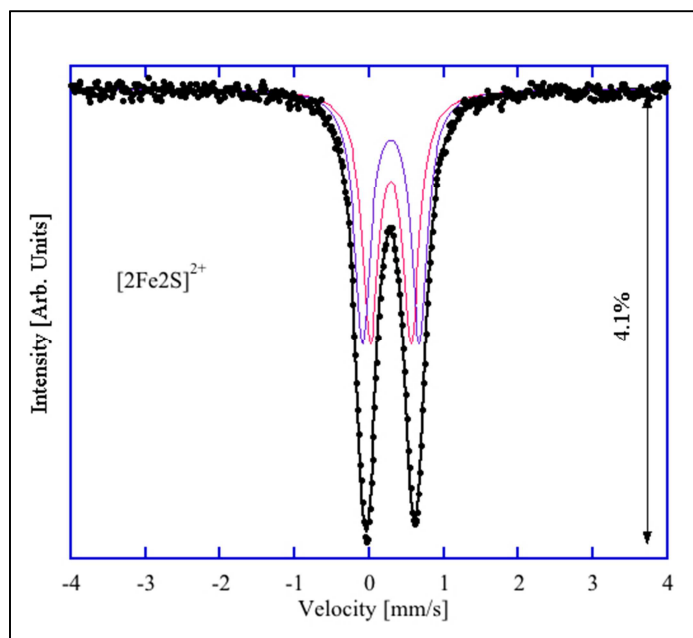
Figure 5.8. Mössbauer spectrum of ^{57}Fe- enriched [2Fe-2S]$^{2+}$ RsrR at 6 K. Mössbauer spectrum recorded of anaerobically isolated RsrR (1 mM [2Fe-2S] cluster in buffer F (50 mM TRIS, 2 M NaCl, 5% (v/v) glycerol, pH 8)) that had been exposed to air for 1 hr.

Table 5.2. Summary of refined Mössbauer parameters. Centroid shift, δ, quadrupole splitting, ΔE_Q, Lorentzian linewidth, Γ, and intensities, I, of the different components. Estimated errors are in I ±3%, in δ and ΔE_Q ±0.005 mm/s, and in Γ ±0.01 mm/s.

Components	Oxidized
δ_1 (mm/s)	0.285
ΔE_{Q1} (mm/s)	0.545
Γ_1 (mm/s)	0.27
I_1 (%)	50
δ_2 (mm/s)	0.289
ΔE_{Q2} (mm/s)	0.761
Γ_2 (mm/s)	0.26
I_2 (%)	50

5.3.2. Resonance Raman studies.

Through a collaboration with Prof. Michael Johnson at the University of Georgia (Athens, USA), resonance Raman spectra of RsrR were recorded. Resonance Raman facilitates identification of cluster type, and the spectra of air-oxidized and dithionite-reduced RsrR in the Fe-S stretching region shown Figure 5.9 and Figure 5.10 are uniquely characteristic of [2Fe-2S]$^{2+}$ and [2Fe-2S]$^{1+}$ clusters, respectively. Resonance Raman also

provides a useful indicator of [2Fe-2S]$^{2+}$ cluster ligation through detection of ligand- Fe vibrational bands [19] and is particularly helpful when used in conjunction with EPR of the reduced cluster and Mössbauer of the oxidized cluster.

The resonance Raman spectra of oxidized RsrR with laser excitation at different wavelengths are indicative of a [2Fe-2S]$^{2+}$ center with one His ligand and three Cys ligands based on published spectra for several [2Fe-2S] cluster containing proteins: the His-to-Cys variant of a Rieske-type protein (1 His and 3 Cys ligands) [20]; the structurally characterized mitoNEET protein (1 His and 3 Cys ligands) [21], IscR (1 His and 3 Cys ligands) [13], and the Grx3/Fra2 homodimer (1 His, 2 Cys, and one unknown ligand) [15]. Histidine ligation is evident in the low-frequency region due to the presence of two bands, one between 258-275 cm^{-1} and one between 292-304 cm^{-1}, in place of one broad band between 282-302 cm^{-1} that is attributed to the out-of-phase symmetric breathing modes of the two tetrahedral FeS$_4$ units in [2Fe-2S]$^{2+}$ centers with complete Cys ligation or with one Ser, Asp, or Arg in place of a Cys ligand [14, 22-25]. The available pH-dependence and N-isotope shift data for the Rieske-type and mitoNEET proteins argues against the assignment of the bands in the 258-275 cm^{-1} region to pure Fe-N(His) stretching modes [20, 21]. Instead the Fe-N(His) stretching is distributed over low-energy Fe-S stretching modes and internal modes of coordinated cysteine ligands and enhanced via the visible S-to-Fe(III) charge transfer transitions, see Figure 5.9.
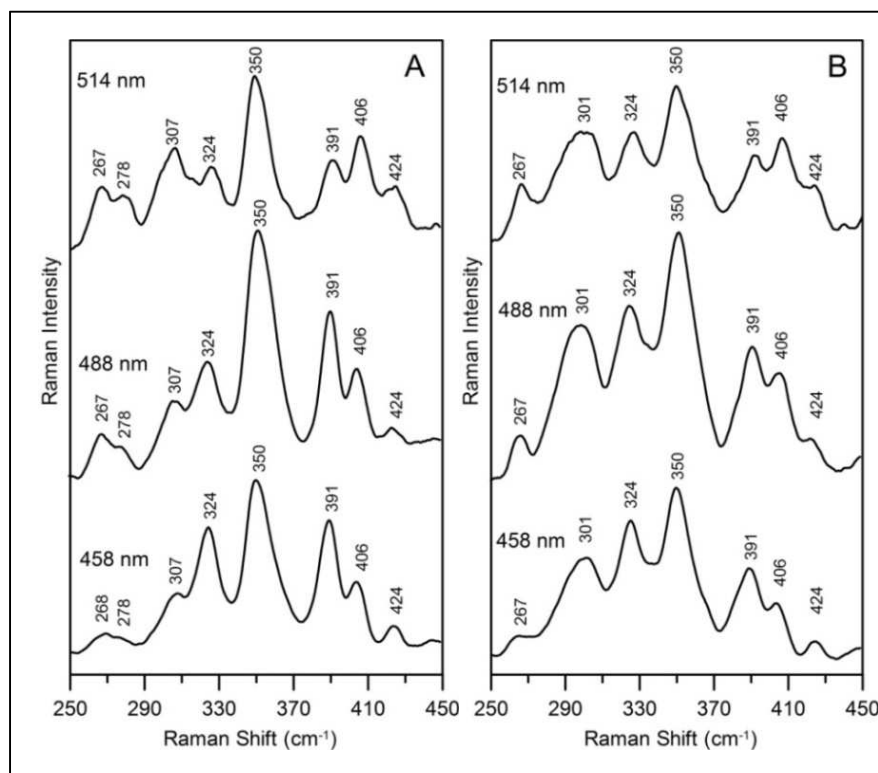
Figure 5.9. Resonance Raman spectra for oxidized RsrR at pH 7.0 and 8.0 using 514 nm, 488 nm and 458 nm excitation. A) Air-oxidized RsrR (4.8 mM in [2Fe-2S] clusters) in buffer F (50 mM TRIS, 2 M NaCl, 5% (v/v) glycerol, pH 8). **B)** Air-oxidized RsrR (4.0 mM in [2Fe-2S] clusters) in buffer F. The band at 424 cm^{-1} arises in whole or in part from glycerol.

Resonance Raman spectra of the valence-localized reduced [2Fe-2S]$^{1+}$ cluster in RsrR are shown in Figure 5.10. The spectra comprise only four Fe-S stretching modes and are very similar to the spectra reported with analogous visible excitation wavelengths for all-cysteinyl-ligated [2Fe-2S]$^{1+}$ ferredoxins [24, 25]. This is a consequence of only the stretching modes involving the four Fe-S bonds on the valence-localized Fe(III) site being significantly resonantly enhanced using 488- and 514-nm excitation. This indicates that in its reduced form RsrR has two cysteine ligands on the non-reducible Fe site of the [2Fe-2S]$^{2+}$ cluster.
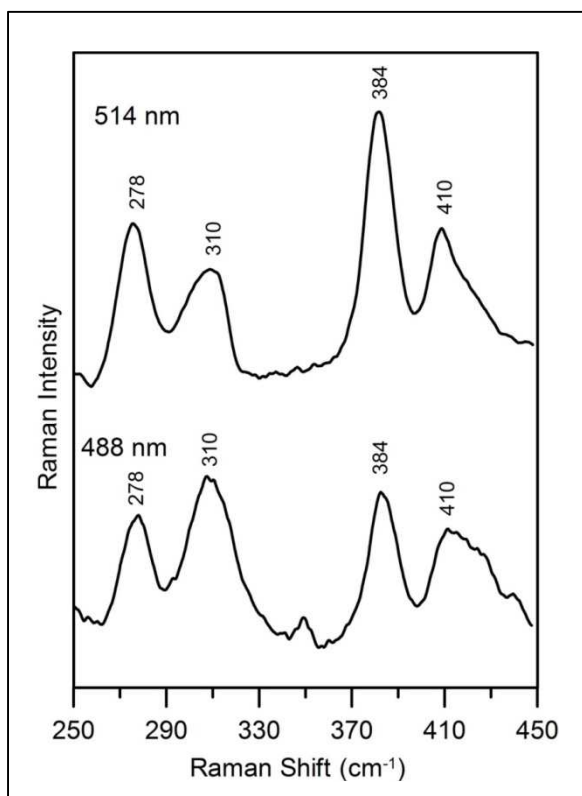
Figure 5.10. Resonance Raman spectra for reduced RsrR using 514 nm and 488 nm excitation. The RsrR sample (4.8 mM in [2Fe-2S] clusters), in buffer F (50 mM TRIS, 2 M NaCl, 5% (v/v) glycerol, pH 8), was reduced anaerobically with 1 equivalent of sodium dithionite.

5.4. Substitution of potential cluster ligands of RsrR.

5.4.1. Spectroscopic analysis of site-directed variants.

A series of site-directed substituted variants of RsrR were generated (constructs purchased from GenScript) and proteins purified. The Mössbauer and resonance Raman data described above confirm the presence of histidine as a cluster ligand. Therefore, the two histidines present in the RsrR sequence were substituted to alanine and cysteine (for His12) and to alanine (for His33). Recently, the crystal structure of holo-*Sc*NsrR has been obtained and it reveals coordination of the cluster by the three invariant Cys residues from one monomer and, unexpectedly, Asp8 from the other [26]. As RsrR and NsrR belong to the same Rrf2 family, the amino acid in the position 8 of RsrR, which is also a carboxylic acid residue (Glu8), was substituted with alanine and cysteine (E8A, E8C). An RsrR variant, E8C/H12C, was also generated in which two of the possible ligands were substituted to cysteine.

Upon purification, wild type RsrR contains a [2Fe-2S] cluster in the +1 state whereas in all of the Glu8 and His12 variants, the cluster was in the oxidised form after anaerobic purification. Figure 5.11 and Figure 5.12 show the UV-Vis and CD spectra for as isolated E8A and H12C respectively with the oxidized and reduced wild type RsrR presented for comparison. Although the shape of variant spectra do not exactly match that of oxidized wild type RsrR, it can conclude that after purification Glu8 and His12 variants are mostly oxidized (data for the E8C, H12A and E8C/H12C shown in the Appendix (Figure A-C)). On the contrary, for H33A, after purification the stable form is the reduced [2Fe-2S] (Appendix (Figure D)). RsrR variants were oxidized and then reduced to see if the [2Fe-2S] cluster that they contain is redox active. To confirm the [2Fe-2S]$^{2+}$ form of the cluster after purification, Glu8 and His12 variants were exposed to oxygen for 30 min. This did not cause a change in the shape of the spectrum, confirming the presence of a [2Fe-2S]$^{2+}$ cluster (Figure 5.13 and Figure 5.14, Appendix (Figure E-G)). Then, 30 µM sodium dithionite was added and the signal for the cluster dramatically diminished in both UV-Vis and CD spectra. This sample was then exposed to oxygen to determine if the sample could be re-oxidized. The spectra did not recover to that of the as isolated proteins. The same experiment was performed using H33A RsrR. In this case, the cluster was found to be redox active; the same redox cycling behavior as observed for wild type RsrR was apparent (Appendix (Figure H)).
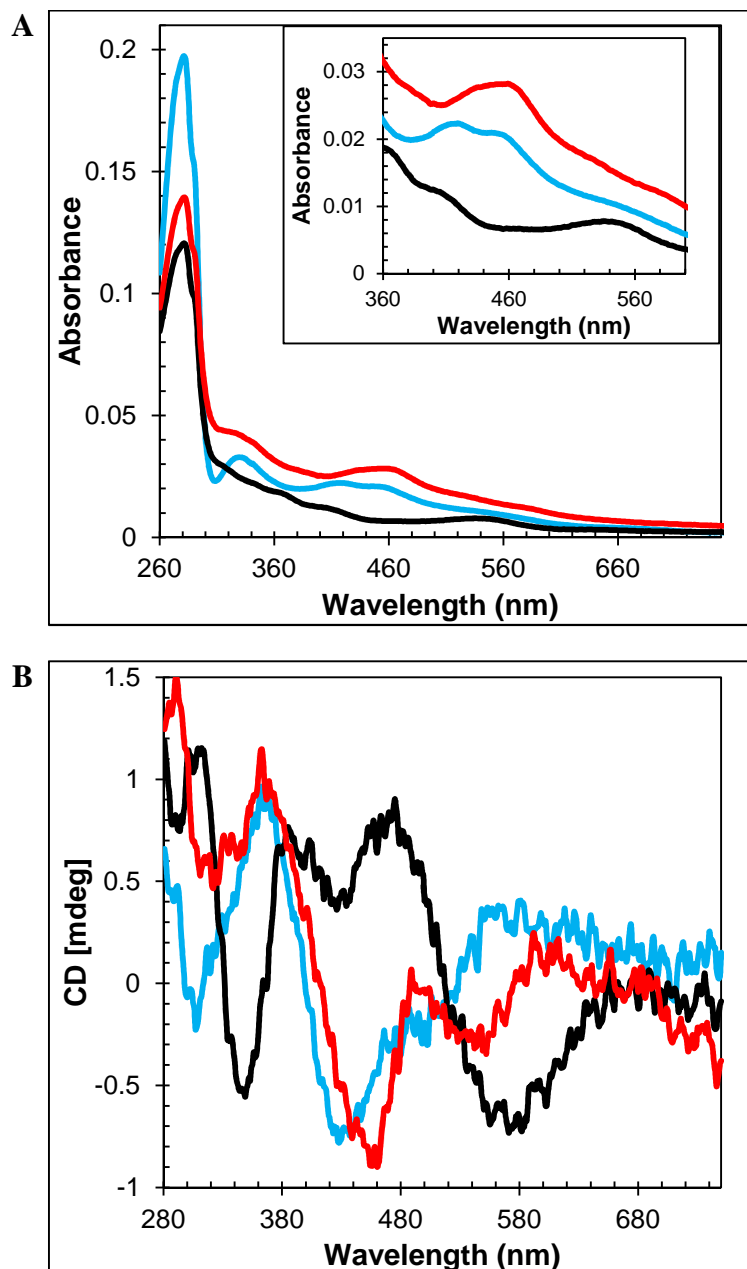
Figure 5.11. Spectroscopic characterization of E8A RsrR. UV-visible absorption (**A**) and CD (**B**) spectra of as isolated/oxidised E8A RsrR (blue line), wild type RsrR as isolated (black line) and wild type oxidised RsrR (red line). 30 µM [2Fe-2S] E8A RsrR and wild type RsrR were in buffer F (50 mM TRIS, 2 M NaCl, 5% (v/v) glycerol, pH 8). In A, inset is the iron-sulfur cluster absorbance in the 360 – 600 nm region in more detail. The measurements were obtained using a 1 mm sealed anaerobic cuvette and buffer B for the baseline.

Figure 5.12. Spectroscopic characterization of H12C RsrR. UV-visible absorption **(A)** and CD **(B)** spectra of as isolated/oxidised H12C RsrR (blue line), wild type RsrR as isolated (black line) and wild type oxidised RsrR (red line). 30 µM [2Fe-2S] H12C RsrR and wild type RsrR were in buffer F (50 mM TRIS, 2 M NaCl, 5% (v/v) glycerol, pH 8). In A, inset is the iron-sulfur cluster absorbance in the 360 – 600 nm region in more detail. The measurements were obtained using a 1 mm sealed anaerobic cuvette and buffer B for the baseline.
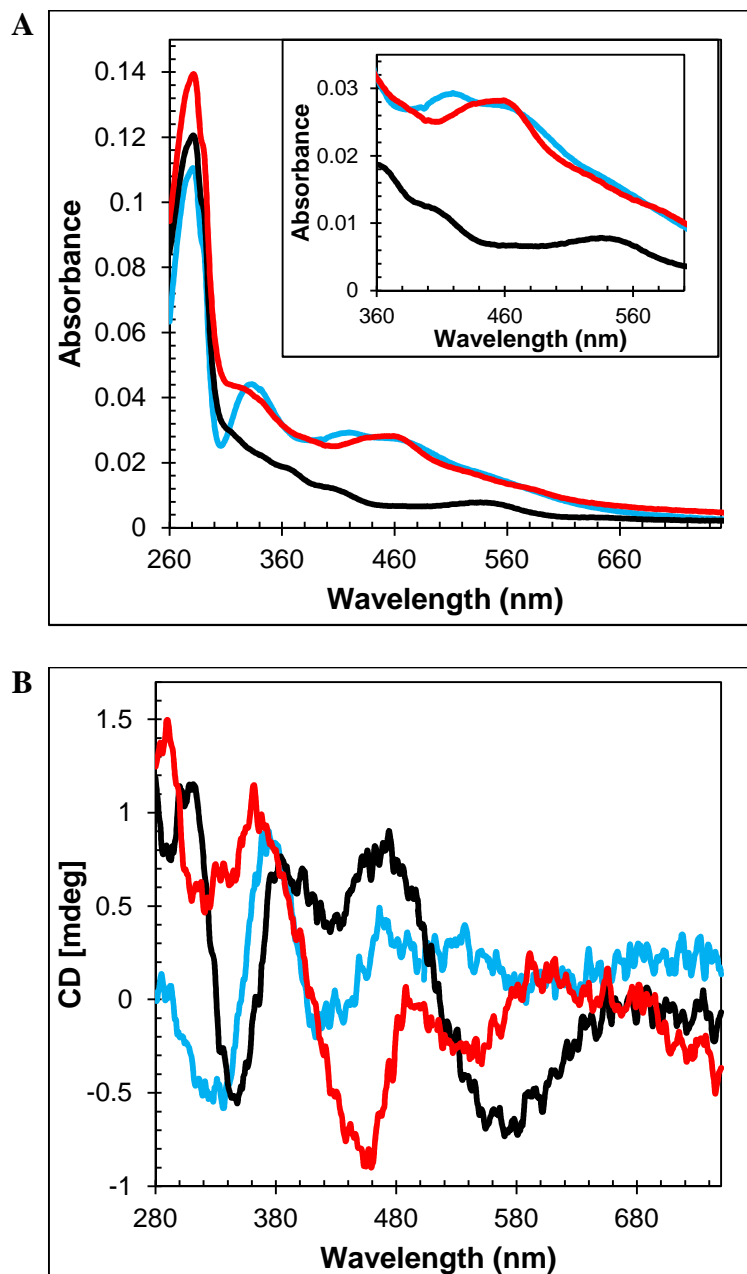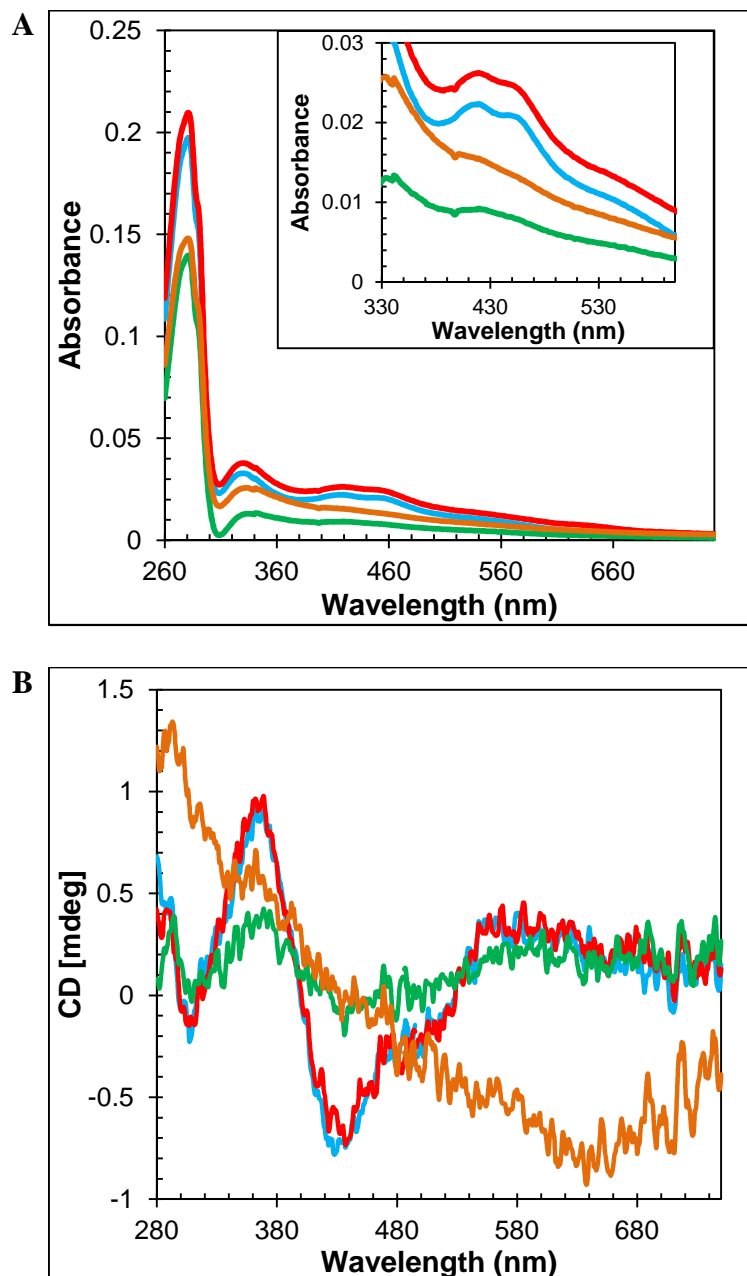
Figure 5.13. Redox cycling of E8A RsrR. UV-visible absorption (**A**) and CD (**B**) spectra of 30 µM [2Fe-2S] E8A in buffer F (50 mM TRIS, 2 M NaCl, 5% (v/v) glycerol, pH 8). E8A RsrR as isolated are shown in blue. Spectra following exposure to air for 30 min are shown in red. Spectra for samples subsequently treated with 30 µM of sodium dithionite for 1 hr 41 min are shown in green. Spectra of the same samples following re-exposure to air for 1 hr 33 min are shown in orange. The measurements were obtained using a 1 mm sealed anaerobic cuvette and buffer F for the baseline correction.
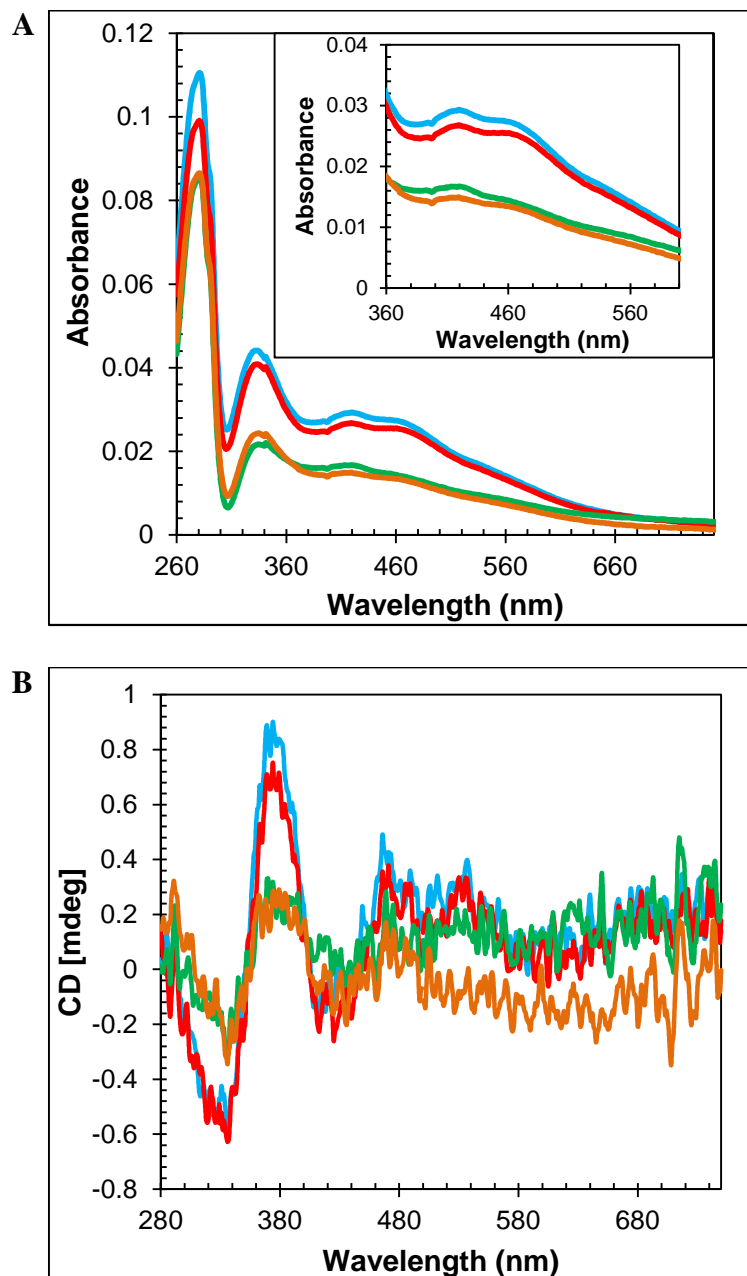
Figure 5.14. Redox cycling of H12C RsrR. UV-visible absorption (**A**) and CD (**B**) spectra of 30 µM [2Fe-2S] H12C in buffer F (50 mM TRIS, 2 M NaCl, 5% (v/v) glycerol, pH 8). H12C RsrR as isolated are shown in blue. Spectra following exposure to air for 30 min are shown in red. Spectra for samples subsequently treated with 30 µM of sodium dithionite for 1 hr 46 min are shown in green. Spectra of the same samples following re-exposure to air for 52 min are shown in orange. The measurements were obtained using a 1 mm sealed anaerobic cuvette and buffer F for the baseline correction.

5.4.2. Mass spectrometry analysis of site-directed variants.

Native-MS was used to investigate how the substitution of potential cluster ligands affects cluster incorporation. In the monomer region, apo-RsrR was the most abundant peak for all the variants with the exception of E8C/H12C where the most abundant peak was the [2Fe-2S], see Figure 5.15A-Figure 5.20A. In the dimer region, when the replacement residue was cysteine (E8C, H12C and E8C/H12C), the most abundant peak was the [2Fe-2S][2Fe-2S]. In the E8C and H12C spectra it is also possible to observe the peak due to the [2Fe-2S], see Figure 5.16B and Figure 5.18B. For E8A, peaks corresponding to apo and [2Fe-2S] RsrR have the same intensity. Also, sulfide adducts for the apo and the [2Fe-2S] forms are observed, see Figure 5.15B. Apo-RsrR is the most abundant peak for H12A, and sulphide adducts for the apo and [2Fe-2S] are observed as well (Figure 5.17B). For H33A, the most abundant peak was [2Fe-2S] although the peaks for the apo and the [2Fe-2S] [2Fe-2S] have similar intensity (Figure 5.20). An important observation from the MS data related to the E8C/H12C variant. The most abundant peaks in the monomer and dimer area corresponded to the [2Fe-2S] and the [2Fe-2S] [2Fe-2S] forms, respectively. Therefore, the cluster remained intact in this variant to a greater extent than the wild type or other variants. This suggests that these two substitutions in combination have an important effect on the cluster environment.

Figure 5.15. Native mass spectrometry of E8A RsrR. Positive ion mode ESI-TOF native deconvoluted mass spectrum of ~21 µM [2Fe-2S] E8A RsrR in 250 mM ammonium acetate pH 8.0, in the RsrR monomer (**A**) and dimer (**B**) regions.

117

Figure 5.16. Native mass spectrometry of E8C RsrR. Positive ion mode ESI-TOF native deconvoluted mass spectrum of ~21 μM [2Fe-2S] E8C RsrR in 250 mM ammonium acetate pH 8.0, in the RsrR monomer (**A**) and dimer (**B**) regions.
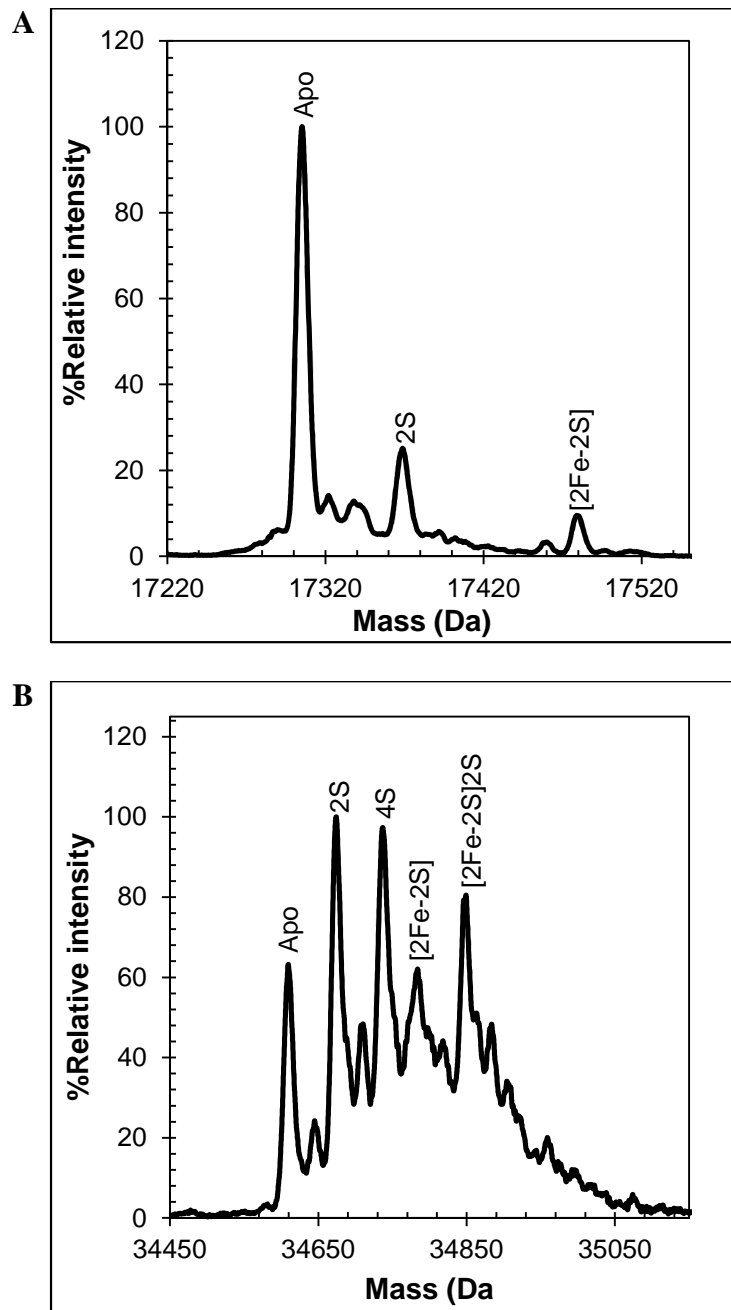
118

Figure 5.17. Native mass spectrometry of H12A RsrR. Positive ion mode ESI-TOF native deconvoluted mass spectrum of ~21 µM [2Fe-2S] H12A RsrR in 250 mM ammonium acetate pH 8.0, in the RsrR monomer (**A**) and dimer (**B**) regions.
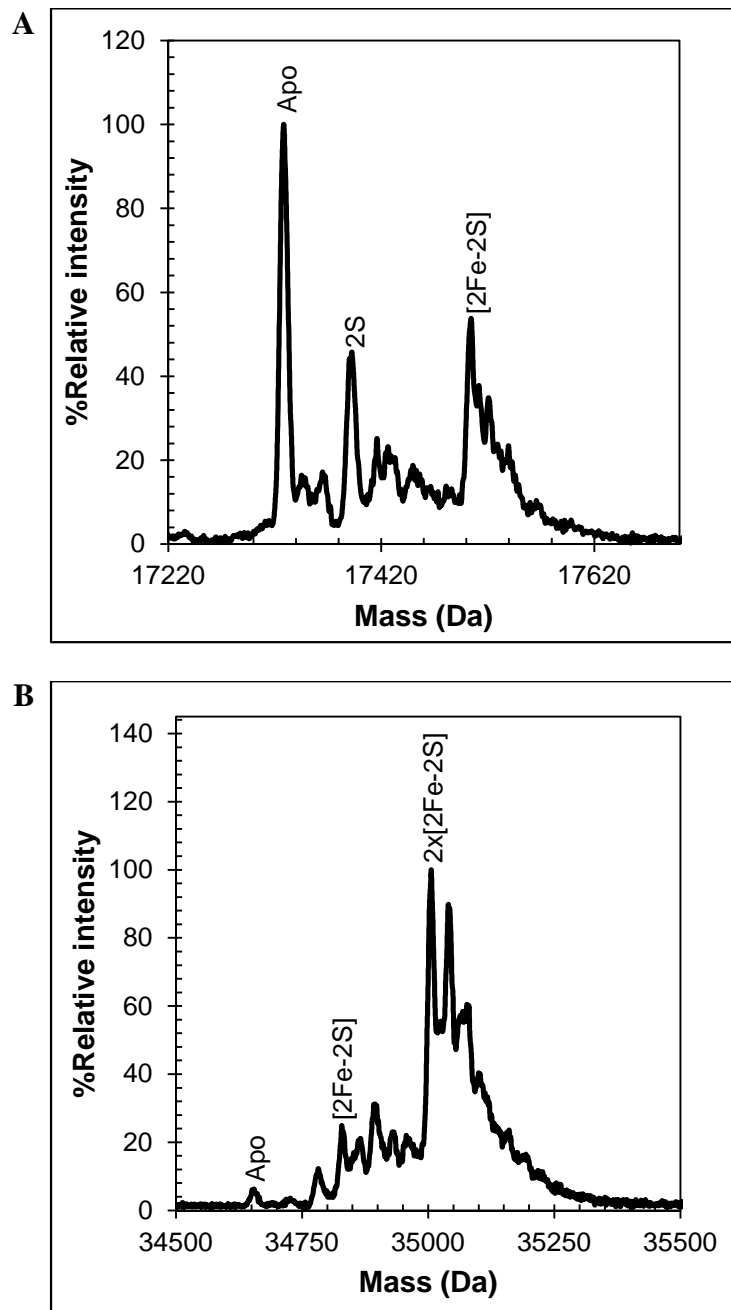
Figure 5.18. Native mass spectrometry of H12C RsrR. Positive ion mode ESI-TOF native deconvoluted mass spectrum of ~21 µM [2Fe-2S] H12C RsrR in 250 mM ammonium acetate pH 8.0, in the RsrR monomer (**A**) and dimer (**B**) regions.

120
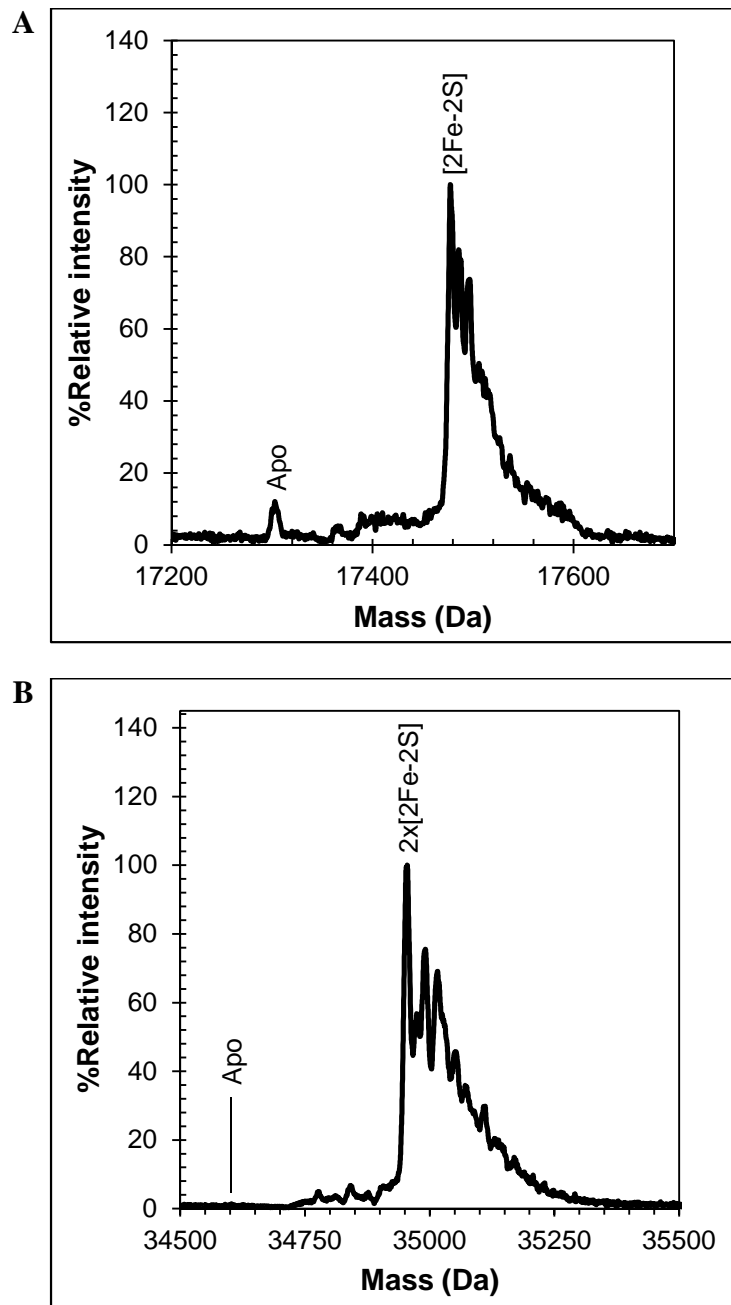
Figure 5.19. Native mass spectrometry of E8C/H12C RsrR. Positive ion mode ESI-TOF native deconvoluted mass spectrum of ~21 μM [2Fe-2S] E8C/H12C RsrR in 250 mM ammonium acetate pH 8.0, in the RsrR monomer (**A**) and dimer (**B**) regions.
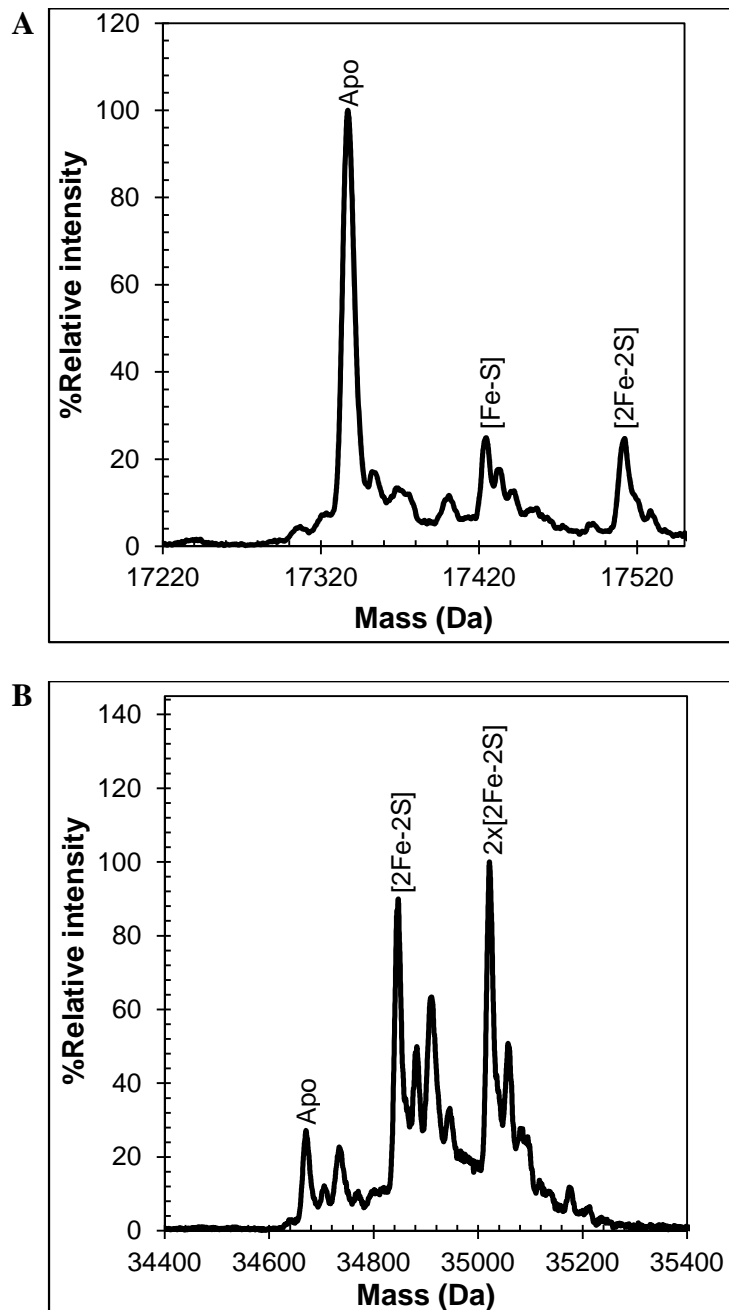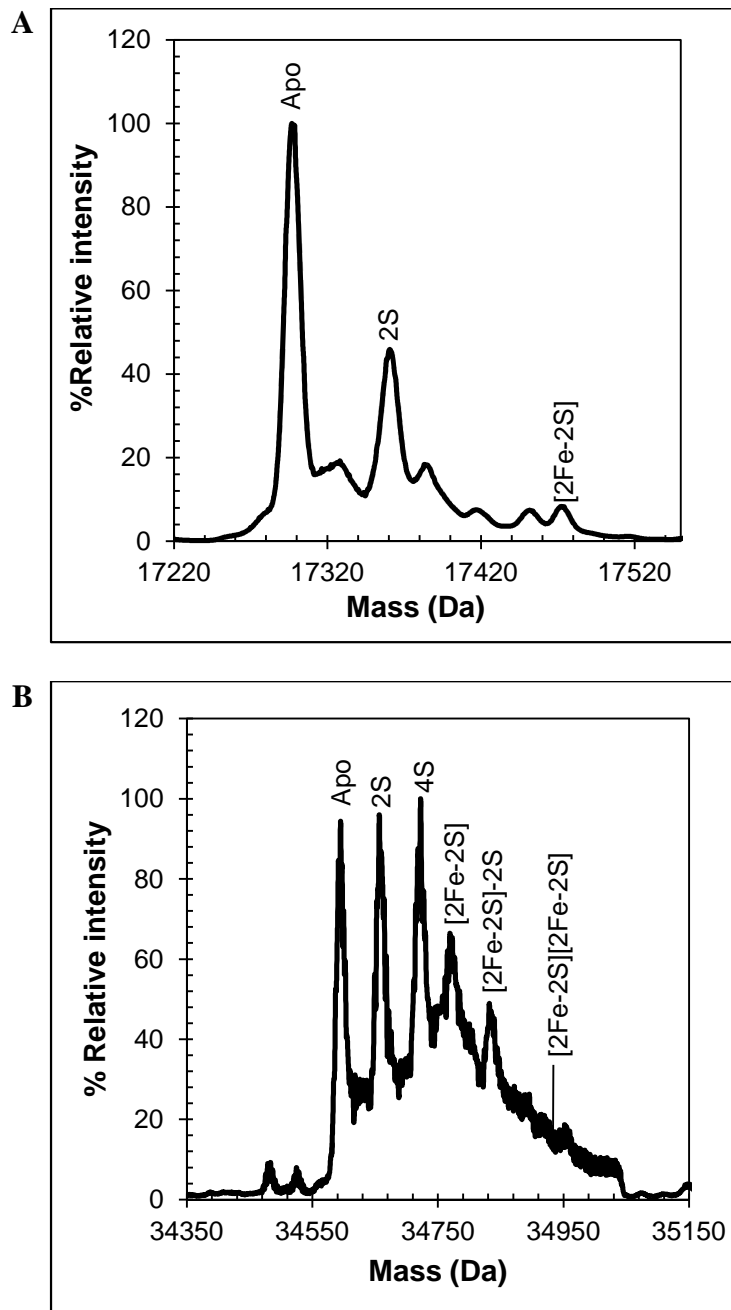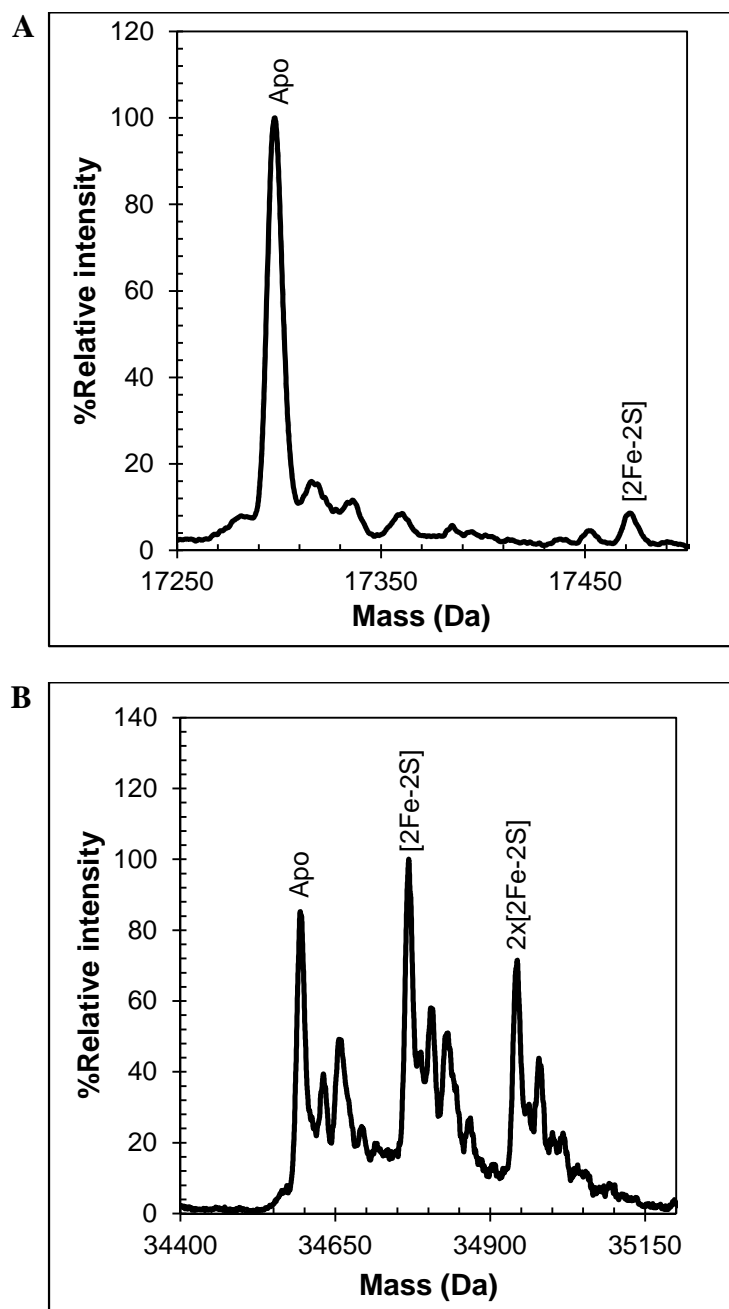
Figure 5.20. Native mass spectrometry of H33A RsrR. Positive ion mode ESI-TOF native deconvoluted mass spectrum of ~21 µM [2Fe-2S] H33A RsrR in 250 mM ammonium acetate pH 8.0, in the RsrR monomer **(A)** and dimer **(B)** regions.

5.4.3. EMSAs of site-directed variants.

EMSAs were performed using the RsrR variants. The presence of E8A, E8C, H12A, H12C and E8C/H12C variants did not result in significant specific DNA-binding (Figure 5.21 -Figure 5.23). E8A shows a very small amount of DNA-binding although the affinity remains the same when the concentration of cluster increases, therefore it is not possible conclude that E8A binds DNA. Non-specific bands appear for all the variants

with the exception of H12C. In the case of the variant H33A, the DNA-binding is weaker in comparison with that observed for wild type RsrR, but specific binding is clearly still present, see Figure 5.24. These results indicate that Glu8 and His12 are involved in cluster binding, and are required for the cluster bound protein to adopt the correct conformation for specific DNA binding.
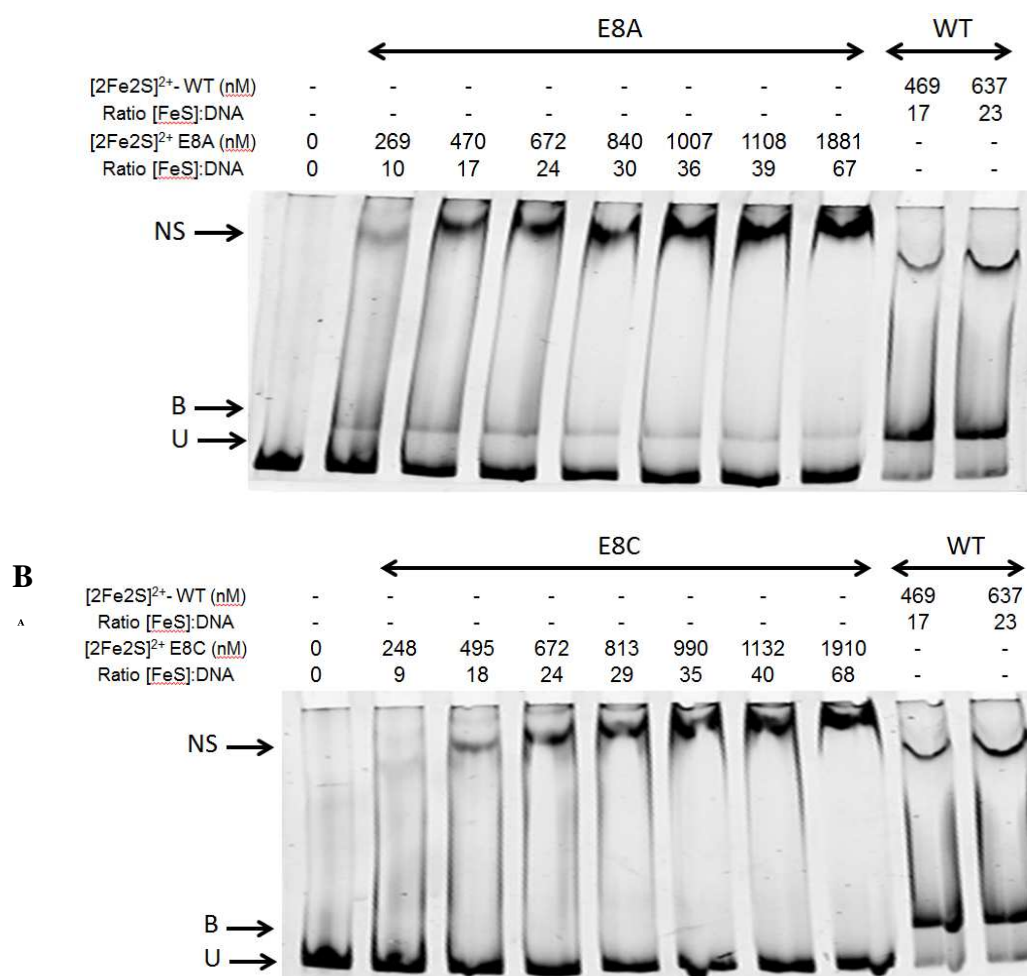
Figure 5.21. Cluster dependent DNA binding by Glu8 RsrR variants. EMSAs showing DNA probes unbound (U), bound (B), and non-specifically bound (NS) by **(A)** E8A RsrR and **(B)** E8C RsrR. Ratios of [2Fe-2S] RsrR and [RsrR] to DNA are indicated. DNA concentration was 2.5 nM. The reaction mixtures were separated at 30 mA for 50 min and the polyacrylamide gels were pre-run at 30 mA for 2 min prior to use.

123
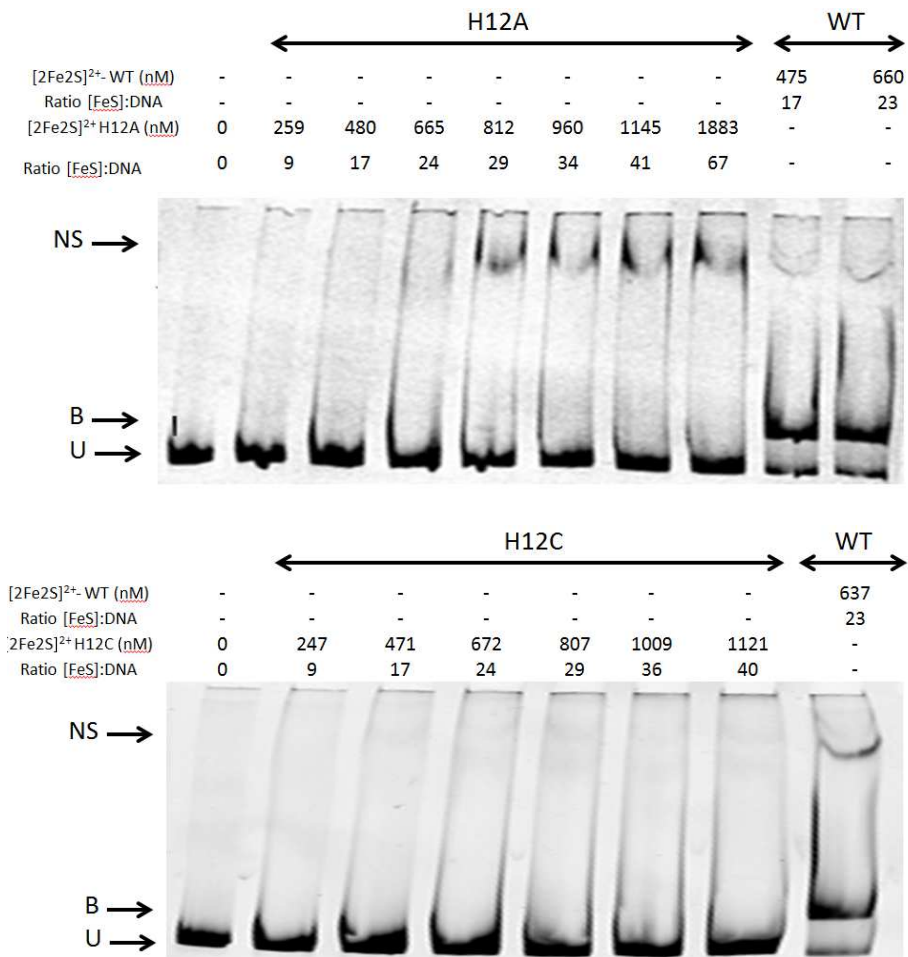
Figure 5.22. Cluster dependent DNA binding by His12 RsrR variants. EMSAs showing DNA probes unbound (U), bound (B), and non-specifically bound (NS) by **(A)** H12A RsrR and **(B)** H12C RsrR. Ratios of [2Fe-2S] RsrR and [RsrR] to DNA are indicated. DNA concentration was 2.5 nM. The reaction mixtures were separated at 30 mA for 50 min and the polyacrylamide gels were pre-run at 30 mA for 2 min prior to use.
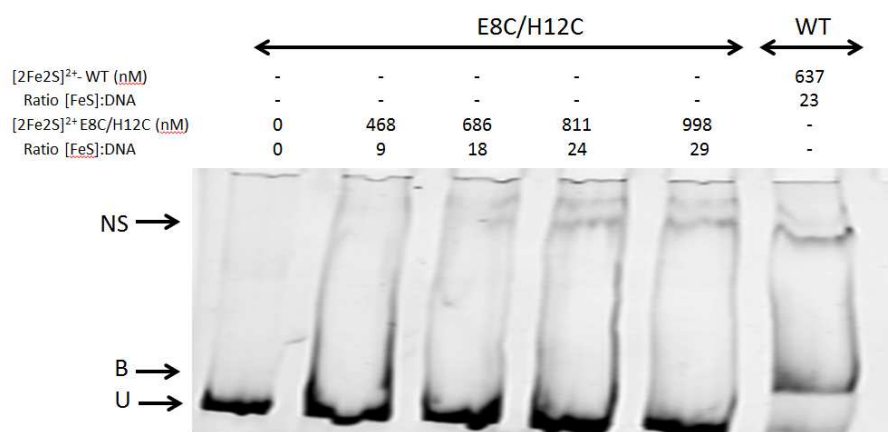
Figure 5.23. Cluster dependent DNA binding by E8C/H12C RsrR variant. EMSAs showing DNA probes unbound (U), bound (B), and non-specifically bound (NS) by E8C/H12C RsrR. Ratios of [2Fe-2S] RsrR and [RsrR] to DNA are indicated. DNA concentration was 2.5 nM. The reaction mixtures were separated at 30 mA for 50 min and the polyacrylamide gels were pre-run at 30 mA for 2 min prior to use.

|					H33A					WT	
[2Fe2S]²⁺- WT (nM)	-	-	-	-	-	-	-	-	-	475	660
Ratio [FeS]:DNA	-	-	-	-	-	-	-	-	-	17	23
[2Fe2S]²⁺ H33A (nM)	0	265	487	663	818	973	1128	1880	-	-	-
Ratio [FeS]:DNA	0	9	17	24	29	35	40	67	-	-	-

Figure 5.24. Cluster dependent DNA binding by H33A RsrR variant. EMSAs showing DNA probes unbound (U), bound (B), and non-specifically bound (NS) by H33A RsrR. Ratios of [2Fe-2S] RsrR and [RsrR] to DNA are indicated. DNA concentration was 2.5 nM. The reaction mixtures were separated at 30 mA for 50 min and the polyacrylamide gels were pre-run at 30 mA for 2 min prior to use.
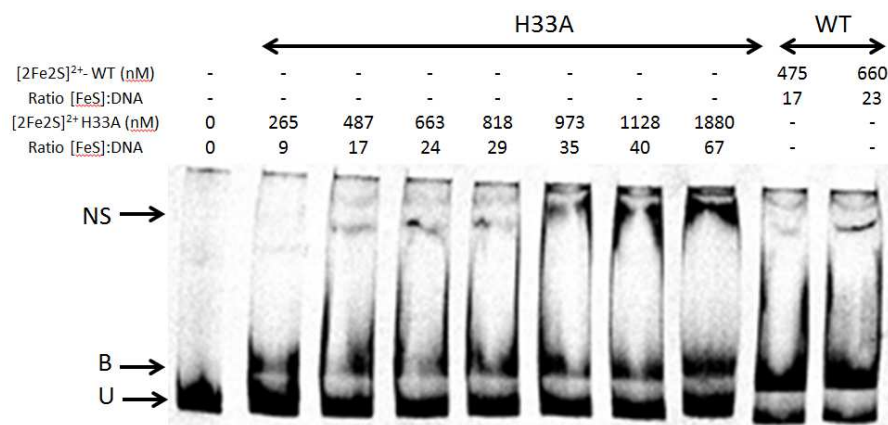
5.5. Discussion.

Filamentous *Streptomyces* bacteria produce bioactive secondary metabolites that account more than half of all known antibiotics as well as numerous other natural products that form the basis of anticancer, anti-helminthic and immunosuppressant drugs [27, 28]. *Streptomyces* bacteria are well adapted for life in the complex soil environment and more than a quarter of their ~9 Mbp genomes encode one and two-component signalling pathways that allow them to rapidly sense and respond to changes in their environment. They are obligate aerobes and have multiple systems for dealing with redox, oxidative and nitrosative stress [29]. NsrR which is the major bacterial NO stress sensor in *Streptomyces coelicolor* (ScNsrR) has been characterised recently. NsrR is a dimeric Rrf2 family protein with one [4Fe-4S] cluster per monomer that reacts rapidly with up to eight molecules of NO [8, 30]. Nitrosylation of the Fe-S cluster results in derepression of the *nsrR*, *hmpA1* and *hmpA2* genes [8], which results in transient expression of HmpA NO dioxygenase enzymes that convert NO to nitrate [31, 32].

In this work, RsrR, a new member of the Rrf2 protein family has been characterised. The purified protein contains a [2Fe-2S]$^{1+}$ cluster, which is stable in the presence of O_2 and can be reversibly cycled between reduced (+1) and oxidized (+2)

states. ChIP analyses show that RsrR binds to 630 sites on the *S. venezuelae* genome [12]. Approximately 2.7% of the RsrR targets contain class 1 binding sites which consist of a MEME identified 11-3-11 bp inverted repeat. Class 1 target genes include *sven6562* which encodes a LysR family regulator with an N terminal NmrA-type NAD(P)+ binding domain. NmrA proteins are thought to control redox poise in fungi by sensing the levels of NAD(P), which they can bind, and NAD(P)H, which they cannot. A model was proposed in which reduction of holo-RsrR induces expression of *Sven6562* which in turn senses redox poise via the ratio of NAD(P)+/NAD(P)H and then modulates expression of its own regulon which likely overlaps with that of RsrR. The >600 class 2 target genes contain only half sites with a single repeat but exhibit strong binding by RsrR in vitro. EMSA experiments showed that RsrR binds weakly to artificial half sites and this suggests additional sequence information is present at class 2 binding sites that increases the strength of DNA binding by RsrR. Six of the class 2 targets are involved in glutamate and glutamine metabolism [12]. The $[2Fe-2S]^{2+}$ form binds strongly to both class 1 and class 2 binding sequences *in vitro*, whereas the $[2Fe-2S]^{1+}$ form exhibited, at best, significantly weaker binding and the apo form does not bind to DNA at all [12]. Given these observations and the stability of the Fe-S cluster to aerobic conditions, it has been proposed that the activity of RsrR is modulated by the oxidation state of its cluster, becoming activated for DNA binding through oxidation and inactivated through reduction or cluster loss. Exposure to O_2 is sufficient to cause oxidation, but other oxidants may also be important *in vivo*. The properties of RsrR described here are reminiscent of an *E. coli* [2Fe-2S] cluster containing transcription factor called SoxR, which controls the expression of the gene encoding another regulator, SoxS, through the oxidation state of its cluster. However, SoxR is a transcriptional activator that switches on *soxS* transcription upon oxidation of the cluster to its $[2Fe-2S]^{2+}$ state [33].

Mössbauer and resonance Raman data confirm that RsrR binds a [2Fe-2S] cluster and demonstrate that it is bound by one histidine. Site-directed substitution of the two His

residues in the RsrR primary sequence (His12 and His33) indicated that His33 is not a cluster ligand (H33A behaved similarly to wild type protein). Data for H12A and H12C, on the other hand, are entirely consistent with His12 being a cluster ligand. The recent structure of NsrR revealed that Asp8 is a cluster ligand [26]. Because RsrR also features a carboxylate ligand, Glu8, at this position, the possibility that it serves as a ligand to the RsrR cluster was also investigated by site-directed substitution. Again, the data are consistent with Glu8 being a cluster ligand. Replacement of RsrR Glu8 and His12 with either Ala or Cys resulted in the loss of DNA binding affinity. When His33 was mutated, although it presented a weaker DNA binding the properties are similar to the wild type RsrR. Therefore, taking together the data obtained, it can be concluded that the histidine is bound to the [2Fe-2S] cluster of RsrR is His12. Despite the fact that resonance Raman data are indicative of a $[2Fe-2S]^{2+}$ center with one His ligand and three Cys ligands based on published spectra for several [2Fe-2S] cluster containing proteins, other possibilities in cluster ligation can not be ruled out. Glu8 is a strong candidate as a cluster ligand. If this was the case, it would be the first time that a [Fe-S] cluster with three different type of ligands has been characterised. Therefore, there are no resonance Raman data available in the published literature to compare with the data obtained in RsrR. The crystal structure of RsrR would help to clarify the [2Fe-2S] cluster ligands of RsrR.

The midpoint potential for the SoxR and OxyR were estimated to be -285 mV and -185 mV, respectively [34, 35]. For [2Fe-2S] RsrR the midpoint potential was estimated to be -165 mV very similar to OxyR (collaboration with John Wright and Dr. Maxie Roessler at the Queen Mary University of London (London, UK)), (data not published). Figure 5.25 shows the range of reduction potentials that have been reported for a variety of iron–sulfur cluster types. At neutral pH, clusters with His-ligands have a higher reduction potential than those with only Cys-ligands, due to the neutral charge of the ligating imidazole compared to the negative thiolate ligand. Unlike Cys-ligands, which are incapable of protonation (due to their depressed pK_a values), the distal nitrogen of a ligating His can

exist in either a neutral protonated form or a de-protonated imidazolate form, where the negatively charged state of the His-ligand results in a significant depression in the reduction potential at higher pH values. Replacement of these [2Fe–2S] cluster His-ligands with a Cys residue results in an approximately 300 mV decrease in reduction potential, suggesting that the charge on the cluster ligand strongly affects reduction potential in these systems [36]. The [2Fe-2S] cluster of SoxR is coordinated by four cysteines (Cys-119, 122, 124, and 130) [37] and has a reduction potential of -285 mV, while the [2Fe-2S] cluster of RsrR is ligated by a histidine and the reduction potential for this protein is -165 mV. This is consistent with the above discussion (Figure 5.25).
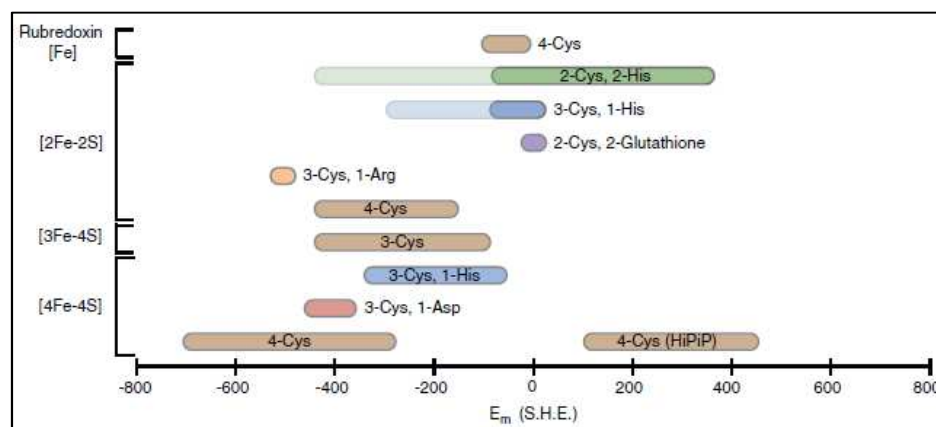

Figure 5.25. Fe–S cluster midpoint potential ranges for all known native cluster nuclearities and ligand arrangements. Common coloring denotes a similarity in the ligand environments for those cluster types. The more lightly shaded regions of 2-Cys, 2-His, and 3-Cys, 1-His clusters, represent potential ranges accessed by pH dependence [36].

Therefore SoxR is a stronger reducing agent than RsrR and OxyR. It has been proposed that whereas the activity of OxyR is responsive to the thiol-disulfide redox status of the cell, the activity of SoxR is responsive to reduced and oxidized nicotinamide adenine dinucleotide phosphate (NADP$^+$/NADPH, respectively) levels in the cell. In general, the difference in the redox potential of the two major intracellular redox buffers (GSSG /GSH and NADP$^+$/NADPH) should allow for the regulation of proteins with chemically diverse redox centers [35]. The function of RsrR in the cell has not been

established yet but its properties are consistent with those of a regulator that senses oxidative stress.

5.6. References.

1. Kimura, S., et al., *Tolerance of the Rieske-type [2Fe-2S] cluster in recombinant ferredoxin BphA3 from Pseudomonas sp. KKS102 to histidine ligand mutations.* Biochem J, 2005. **388**(Pt 3): p. 869-78.
2. Lin, J., et al., *Crystal structure of human mitoNEET reveals distinct groups of iron sulfur proteins.* Proc Natl Acad Sci U S A, 2007. **104**(37): p. 14640-5.
3. Stephens, P.J., et al., *Circular dichroism and magnetic circular dichroism of iron-sulfur proteins.* Biochemistry, 1978. **17**(22): p. 4770-8.
4. Link, T.A., et al., *Comparison of the "Rieske" [2Fe-2S] center in the bc1 complex and in bacterial dioxygenases by circular dichroism spectroscopy and cyclic voltammetry.* Biochemistry, 1996. **35**(23): p. 7546-52.
5. Couture, M.M., et al., *Characterization of BphF, a Rieske-type ferredoxin with a low reduction potential.* Biochemistry, 2001. **40**(1): p. 84-92.
6. Yukl, E.T., et al., *Transcription Factor NsrR from Bacillus subtilis Senses Nitric Oxide with a 4Fe-4S Cluster (dagger).* Biochemistry, 2008. **47**(49): p. 13084-92.
7. Santos, J.A., et al., *The unique regulation of iron-sulfur cluster biogenesis in a Gram-positive bacterium.* Proc Natl Acad Sci U S A, 2014. **111**(22): p. E2251-60.
8. Crack, J.C., et al., *NsrR from Streptomyces coelicolor is a nitric oxide-sensing [4Fe-4S] cluster protein with a specialized regulatory function.* J Biol Chem, 2015. **290**(20): p. 12689-704.
9. Zhang, B., et al., *Reversible cycling between cysteine persulfide-ligated [2Fe-2S] and cysteine-ligated [4Fe-4S] clusters in the FNR regulatory protein.* Proc Natl Acad Sci U S A, 2012. **109**(39): p. 15734-9.
10. Johnson, K.A., et al., *Probing the stoichiometry and oxidation states of metal centers in iron-sulfur proteins using electrospray FTICR mass spectrometry.* Anal Chem, 2000. **72**(7): p. 1410-8.
11. Kay, K.L., C.J. Hamilton, and N.E. Le Brun, *Mass spectrometry of B. subtilis CopZ: Cu(i)-binding and interactions with bacillithiol.* Metallomics, 2016. **8**(7): p. 709-19.
12. Munnoch, J.T., et al., *Characterization of a putative NsrR homologue in Streptomyces venezuelae reveals a new member of the Rrf2 superfamily.* Sci Rep, 2016. **6**: p. 31597.
13. Fleischhacker, A.S., et al., *Characterization of the [2Fe-2S] cluster of Escherichia coli transcription factor IscR.* Biochemistry, 2012. **51**(22): p. 4453-62.
14. Cosper, M.M., et al., *Characterization of the cofactor composition of Escherichia coli biotin synthase.* Biochemistry, 2004. **43**(7): p. 2007-21.
15. Li, H., et al., *The yeast iron regulatory proteins Grx3/4 and Fra2 form heterodimeric complexes containing a [2Fe-2S] cluster with cysteinyl and histidyl ligation.* Biochemistry, 2009. **48**(40): p. 9569-81.
16. Fee, J.A., et al., *Purification and characterization of the Rieske iron-sulfur protein from Thermus thermophilus. Evidence for a [2Fe-2S] cluster having non-cysteine ligands.* J Biol Chem, 1984. **259**(1): p. 124-33.
17. Kuila, D. and J.A. Fee, *Evidence for a redox-linked ionizable group associated with the [2Fe-2S] cluster of Thermus Rieske protein.* J Biol Chem, 1986. **261**(6): p. 2768-71.
18. Schmidt, C.L., et al., *Purification and characterization of the Rieske iron-sulfur protein from the thermoacidophilic crenarchaeon Sulfolobus acidocaldarius.* FEBS Lett, 1995. **359**(2-3): p. 239-43.
19. Iwasaki, T., et al., *Novel [2Fe-2S]-type redox center C in SdhC of archaeal respiratory complex II from Sulfolobus tokodaii strain 7.* J Biol Chem, 2002. **277**(42): p. 39642-8.
20. Kounosu, A., et al., *Engineering a three-cysteine, one-histidine ligand environment into a new hyperthermophilic archaeal Rieske-type [2Fe-2S] ferredoxin from Sulfolobus solfataricus.* J Biol Chem, 2004. **279**(13): p. 12519-28.

21. Tirrell, T.F., et al., *Resonance Raman studies of the (His)(Cys)3 2Fe-2S cluster of MitoNEET: comparison to the (Cys)4 mutant and implications of the effects of pH on the labile metal center.* Biochemistry, 2009. **48**(22): p. 4747-52.

22. Meyer, J., et al., *Mutated forms of the [2Fe-2S] ferredoxin from Clostridium pasteurianum with noncysteinyl ligands to the iron-sulfur cluster.* Biochemistry, 1994. **33**(46): p. 13642-50.

23. Moulis, J.-M., et al., *The coordination sphere of iron-sulfur clusters: lessons from site-directed mutagenesis experiments.* JBIC Journal of Biological Inorganic Chemistry, 1996. **1**(1): p. 2-14.

24. Fu, W., et al., *The role of the iron-sulfur cluster in Escherichia coli endonuclease III. A resonance Raman study.* J Biol Chem, 1992. **267**(23): p. 16135-7.

25. Han, S.H., et al., *Resonance Raman studies of Escherichia coli sulfite reductase hemoprotein. 3. Bound ligand vibrational modes.* Biochemistry, 1989. **28**(13): p. 5477-85.

26. Volbeda, A., et al., *Crystal structures of the NO sensor NsrR reveal how its iron-sulfur cluster modulates DNA binding.* Nat Commun, 2017. **8**: p. 15052.

27. Newman, D.J. and G.M. Cragg, *Natural products as sources of new drugs over the 30 years from 1981 to 2010.* J Nat Prod, 2012. **75**(3): p. 311-35.

28. Challis, G.L. and D.A. Hopwood, *Synergy and contingency as driving forces for the evolution of multiple secondary metabolite production by Streptomyces species.* Proc Natl Acad Sci U S A, 2003. **100 Suppl 2**: p. 14555-61.

29. Flardh, K. and M.J. Buttner, *Streptomyces morphogenetics: dissecting differentiation in a filamentous bacterium.* Nat Rev Microbiol, 2009. **7**(1): p. 36-49.

30. Crack, J.C., et al., *Differentiated, Promoter-specific Response of [4Fe-4S] NsrR DNA Binding to Reaction with Nitric Oxide.* J Biol Chem, 2016. **291**(16): p. 8663-72.

31. Gardner, P.R., et al., *Hemoglobins dioxygenate nitric oxide with high fidelity.* J Inorg Biochem, 2006. **100**(4): p. 542-50.

32. Forrester, M.T. and M.W. Foster, *Protection from nitrosative stress: a central role for microbial flavohemoglobin.* Free Radic Biol Med, 2012. **52**(9): p. 1620-33.

33. Lee, K.L., et al., *Factors affecting redox potential and differential sensitivity of SoxR to redox-active compounds.* Mol Microbiol, 2015. **97**(5): p. 808-21.

34. Ding, H., E. Hidalgo, and B. Demple, *The redox state of the [2Fe-2S] clusters in SoxR protein regulates its activity as a transcription factor.* J Biol Chem, 1996. **271**(52): p. 33173-5.

35. Zheng, M., F. Aslund, and G. Storz, *Activation of the OxyR transcription factor by reversible disulfide bond formation.* Science, 1998. **279**(5357): p. 1718-21.

36. Bak, D.W. and S.J. Elliott, *Alternative FeS cluster ligands: tuning redox potentials and chemistry.* Curr Opin Chem Biol, 2014. **19**: p. 50-8.

37. Watanabe, S., et al., *Crystal structure of the [2Fe-2S] oxidative-stress sensor SoxR bound to DNA.* Proc Natl Acad Sci U S A, 2008. **105**(11): p. 4121-6.

Chapter 6. General discussion.

This thesis presents studies of two proteins that have diverse functions in microorganisms. The first is RirA, a transcriptional repressor in conditions of iron sufficiency. While many bacteria maintain iron homeostasis primarily through the regulatory action of the Fe^{2+}-sensing protein Fur, some members of the Gram-negative alpha-proteobacteria *Rhizobia* utilize the transcription factors Irr and RirA. In *Rhizobium leguminosarum*, *Sinorhizobium meliloti*, and *Agrobacterium tumefaciens*, RirA has a global role in regulating the expression of genes involved in iron metabolism, including iron/heme uptake and siderophore synthesis [1, 2]. It belongs to the widespread Rrf2 super-family of transcriptional regulators, many members of which feature three conserved Cys residues that characterise the binding of an iron-sulfur cluster in Rrf2 family regulators that have been characterised [3]. The aims of this part of the project were to purify and characterise the RirA protein from *R. leguminosarum*, investigating the proposal that RirA is an iron-sulfur protein and identifying the nature of the cluster and how the regulation of iron is achieved.

A range of biophysical studies, including UV-visible absorbance, CD and EPR spectroscopies, mass spectrometry, and DNA-binding experiments, have been carried out that demonstrate RirA contains a [4Fe-4S] cluster, and that this form of the protein binds RirA-regulated promoter DNA, consistent with its function as a repressor of expression of many genes involved in iron uptake. Under conditions that simulate low iron availability, [4Fe-4S] RirA undergoes a cluster conversion reaction resulting in a [2Fe-2S] form, which exhibits much lower affinity for DNA. Under prolonged low iron conditions, the [2Fe-2S] cluster is unstable, resulting in apo-RirA, which does not bind DNA and can no longer function as a repressor of the cell's iron-uptake machinery. These properties lead to the proposal of a novel regulatory model for iron homeostasis. The three states ([4Fe-4S], [2Fe-2S] and apo) represent three distinct physiological responses within the cell, which

are accessed through the lability of iron in the cluster and which have different outcomes in terms of expression of RirA-controlled genes.

Recently developed methodologies for native ESI-MS studies of iron-sulfur cluster proteins [4] were applied to RirA, illustrating further how this technique can be used to study cluster reactions, in this case the disassembly of the cluster. This provided remarkably high resolution information about the reaction through detection of cluster conversion intermediates and products, including a novel [3Fe-3S] cluster, leading to a comprehensive understanding of the mechanism of RirA cluster conversion in the presence of EDTA. Analysis of the kinetic mass spectrometry data revealed a branched mechanism in which loss of a single iron (to form $[3Fe-4S]^0$) or sulfide (to form $[4Fe-3S]^{4+}$) appears to be the first step in the cluster conversion process with loss of sulfide or iron following. The resulting [3Fe-3S] cluster reported here was also detected as an important intermediate in [4Fe-4S] to [2Fe-2S] cluster conversion in the O_2 sensor regulator FNR from *E. coli* [4]. An inorganic model $[3Fe-3S]^{3+}$ cluster was recently reported for the first time, in which the iron and sulfide ions lie in the same plane generating a hexagonal arrangement [5]. In the case of RirA, the charge on the [3Fe-3S] cluster is not established. Loss of one sulfide ion from a $[3Fe-4S]^0$ cluster would be expected to generate a $[3Fe-3S]^{2+}$ cluster. The mass spectrometry data cannot provide unambiguous cluster charge state information, though the observed mass is consistent with a +3 or +2 charge. The $[3Fe-3S]^{3+}$ form would be expected to be EPR active, while the $[3Fe-3S]^{2+}$ form would not. Thus, future time-resolved EPR studies should provide further insight into this. This technique also detected the presence of [4Fe-4S], [2Fe-2S] and apo RirA consistent with their proposed importance in the regulation of iron by RirA. Another important observation from the mass spectrometry data was that persulfide-coordinated [2Fe-2S] was not observed. Such species were readily detected in the case of FNR, in which cluster repair was observed *in vitro* upon addition of iron and reductant [6]. This suggests that facile conversion of the RirA [2Fe-2S] cluster back to [4Fe-4S] does not

occur. This is consistent with a model for regulation in which RirA senses the iron status of the cell via iron-sulfur cluster 'availability'. The [2Fe-2S] form most likely represents an intermediate on the pathway between [4Fe-4S] and apo-RirA. Under some circumstances, the [2Fe-2S] form could be stabilised, but it appears to be for the most part an intermediate.

The combination of low iron and O_2 rapidly lead to cluster conversion/loss. Whether apo-RirA can be recycled to incorporate a second iron-sulfur cluster or becomes degraded is not known. This could be investigated using the same strategy that showed that FNR could be recycled, i.e. by monitoring regulation as iron levels are varied and protein synthesis is inhibited [7].

The second protein studied in this thesis is RsrR, a new member of the Rrf2 family of transcriptional regulators. The aims of this part of the project were to identify the cofactor that RsrR binds and to investigate its functional properties. Biophysical experiments showed that RsrR has a [2Fe-2S] cluster and that the switch between oxidized and reduced cluster controls its DNA binding activity *in vitro*, such that it binds RsrR-regulated promoter DNA tightly in its oxidised state but not in its reduced state. Site-directed replacement of Glu8 and His12 with either Ala or Cys had a clear impact on DNA binding affinity and on the redox cycling behaviour of the [2Fe-2S] cluster. Therefore Glu8 and His12 are potential ligands of the [2Fe-2S] cluster. The crystal structure of RsrR is necessary to provide definitive proof. Attempts to determine the structure are currently underway in the laboratory of Prof. Juan Fontecilla-Camps in Grenoble, France. ChIP-seq analysis in RsrR revealed that rather than regulating the nitrosative stress response like *Streptomyces coelicolor* NsrR, RsrR binds to a conserved motif at a different, much larger set of genes with a diverse range of functions, including a number of regulators, genes required for glutamine synthesis, NADH/NAD(P)H metabolism, as well as general DNA/RNA and amino acid/protein turn over [8]. Thus, while RsrR appears to be a sensor

of redox balance in the cytoplasm of *S. venezuelae*, the precise nature of the signal it senses remains unclear. Further studies will be required to establish this.

As has been mentioned above, RirA and RsrR bind [4Fe-4S] and [2Fe-2S] clusters, respectively. Comparisons can now be made with data reported for other members of the Rrf2 family and there are strong similarities to the well-studied family members [4Fe-4S] NsrR and [2Fe-2S] IscR. These proteins have three conserved cysteine residues to which iron-sulfur cluster are proposed to bind and have been demonstrated to do so in NsrR [11], see blue arrows in Figure 6.1. A major question arising from this is why these proteins coordinated different types of cluster if they share three conserved ligands. This might be answered by considering the nature of their effectors, which are quite distinct and so most likely require different cluster properties and environments. IscR binds the cluster with a ligation scheme of three cysteines and one histidine (Cys92, Cys98, and Cys104 and His107) [9]. His107 (green arrow in Figure 6.1) is not conserved in RsrR, NsrR and RirA; therefore this histidine can be considered as an atypical ligand and this feature is likely to be highly relevant for the function of IscR as a sensor of cellular Fe–S cluster status [10]. Recently studies of NsrR revealed coordination of the cluster by the three invariant Cys (blue arrows in Figure 6.1) residues from one monomer and, unexpectedly, Asp8 from the other (red arrow in Figure 6.1) [11]. Asp8 is not conserved in the other proteins either. Therefore this amino acid could be a key for the function of NsrR as a sensor of NO and the regulation of expression of genes responsible for NO metabolism [12]. RsrR data reported in this thesis have established spectroscopic characteristics that point to a His-coordinated [2Fe-2S] cluster and that His12 is an important amino acid residue for cluster redox cycling and DNA binding. Therefore His12 is very likely to be a ligand of the cluster (red arrow in Figure 6.1). Glu8 in RsrR aligns with Asp8 in NsrR and data presented here also show that this residue is important for cluster redox-cycling and DNA-binding. If both His12 AND Glu8 are ligands, then only two of the three conserved Cys residues would be ligands. This may be unlikely and it should be recognised that structural

changes that affect cluster properties and DNA-binding can occur when residues that do not coordinate the cluster are substituted. An example of this is Glu85 in NsrR [3]. A E85A variant of NsrR was severely affected in DNA-binding but Glu85 is is not a ligand. The recently determined structure of NsrR showed why this substitution had such an important effect; the side chain of this residue plays a key role in stabilising the N-terminal region of the protein. Thus, it remains a possibility that Glu8 has a similar function in RsrR. The structure is needed to resolve this.
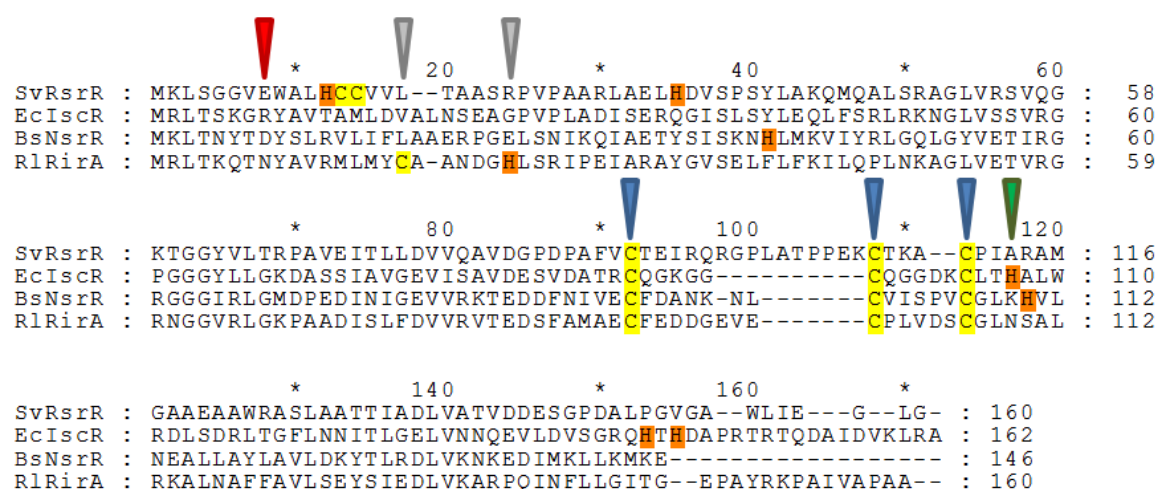
Figure 6.1. Alignment of *Streptomyces venezuelae* RsrR with other Rrf2 family regulators. Alignment of *S. venezuelae* RsrR (SvRsrR) with IscR sequence from *E. coli* (EcIscR), NsrR sequence from *Bacillus subtilis* (BsNsrR) and RirA sequence from *R. leguminosarum* (RlRirA). The alignment was carried out using Clustal Omega [13] and presented using Genedoc [14].

For RirA, a recent study demonstrated that the three conserved cysteines are essential for RirA mediated repression of the *sufS2BCDS1XA* operon, encoding the Fe-S cluster biogenesis pathway of *A. tumefaciens* [2]. The fourth ligand in RirA is still unknown but on the basis of sequence comparisons with NsrR and IscR it could be predicted that Asn8 or Asn109 (red and green arrows in Figure 6.1) might serve as the fourth ligand in RirA. Another two possible ligands are Cys17 and His23 (grey arrow in Figure 6.1) based on the fact that these residues are commonly found as ligands to Fe-S clusters. A model of the RirA structure was generated using the structure of holo-ScNsrR and the RirA sequence using the Swiss PDB program [15], see Figure 6.3. The three

conserved cysteines residues appear to be in the right positions to be cluster ligands (red sticks in Figure 6.3) and they are conserved among different RirA species (blue arrows in Figure 6.2). Cys17 is also conserved but His23 is not (grey arrows in Figure 6.2). In the model structure, Cys17 and His23 (magenta and blue sticks in Figure 6.3) are not located close to the cluster, and on this basis it seems unlikely that these amino acids are cluster ligands. Asn8 and Asn109 (black and orange sticks in Figure 6.3) are in a position close to the cluster, and so they are strong candidates as cluster ligands. Also, Asn8 and Asn109 are conserved in other RirA proteins from other species (orange arrows in Figure 6.2). Site-directed replacement of Asn8 and Asn109 would be an interesting experiment to perform in the future. Resonance Raman and the crystal structure of RirA would help to clarify the identity of the fourth ligand.
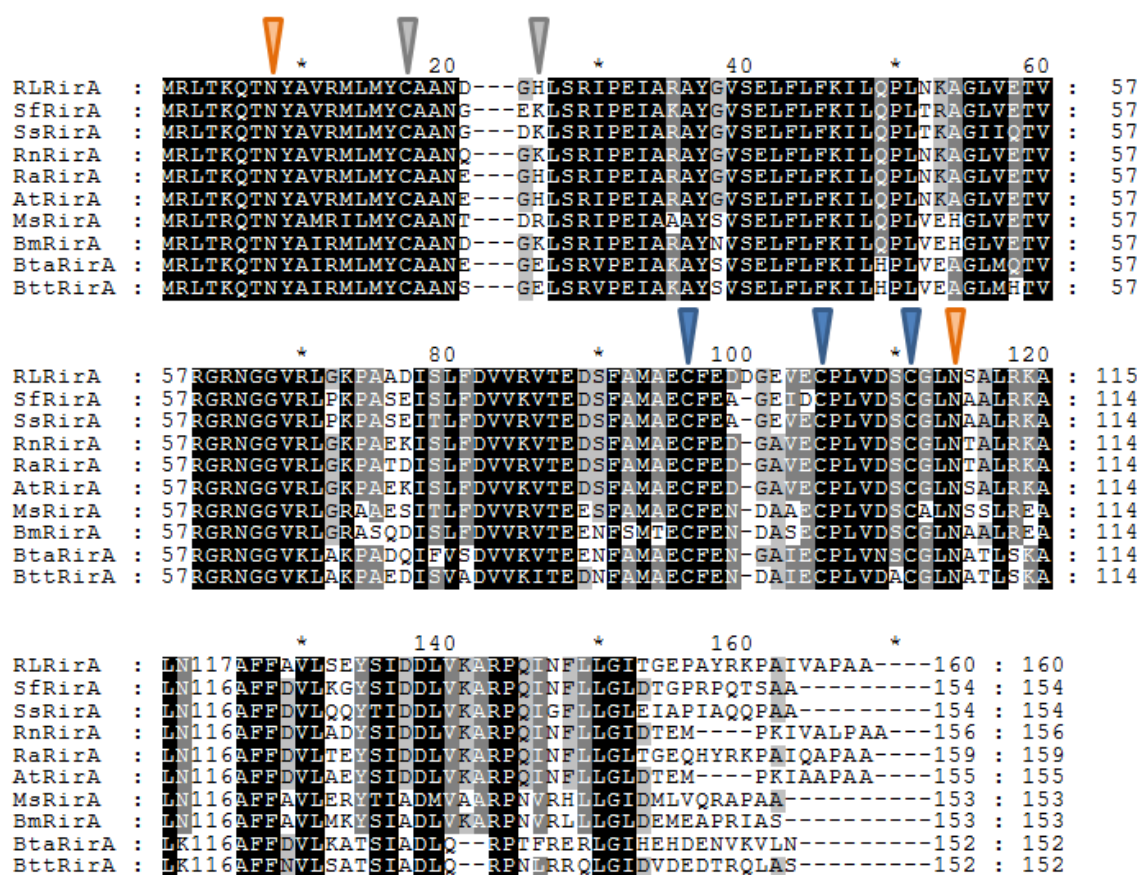

Figure 6.2. Alignment of *R. leguminosarum* RirA with other RirA species. Alignment of RirA sequence from *R. leguminosarum* (RlRirA) with RirA sequence from *Sinorhizobium fredii* (SfRirA), *Sinorhizobium sp. RAC02* (SsRirA), *Rhizobium nepotum* (RnRirA), *Rhizobium alamii* (RaRirA), *Agrobacterium tumefaciens* (AtRirA), *Mesorhizobium sp. L48C026A00* (MsRirA), B*rucella microti* (BmRirA), *Bartonella apis* (BtaRirA) and *Bartonella tamiae* (BttRirA). The alignment was carried out using Clustal Omega [13] and presented using Genedoc [14].
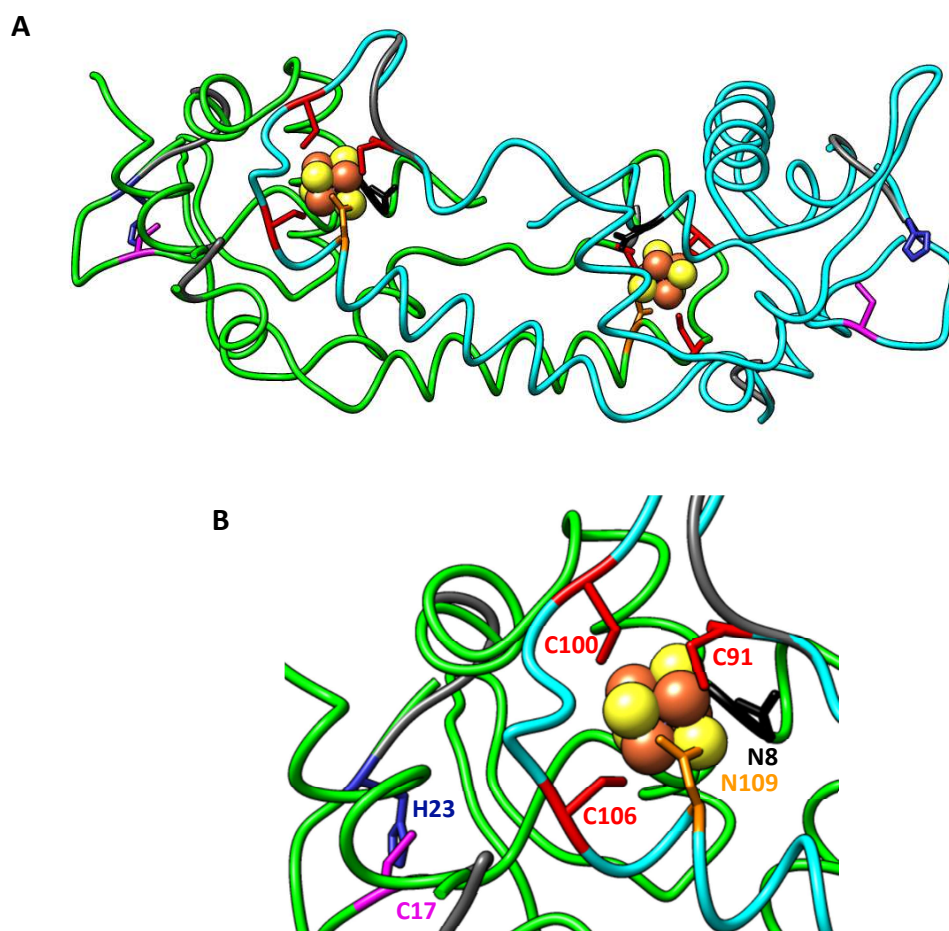
Figure 6.3. Superposition of holo-ScNsrR complex with RirA sequence. A) The RirA dimer is shown as a ribbon representation, with the subunits coloured green and cyan. The grey parts of the structure corresponds to the amino acids in the NsrR structure that do not fit the RirA sequence. The [4Fe-4S] clusters are represented as spheres. Iron and sulfur atoms are coloured orange and yellow, respectively. The positions of the conserved cysteines residues are shown in red (Cys91, Cys 100 and Cys106). The position of the candidates for the fourth cluster ligand are shown in black (Asn8), magenta (Cys17), blue (His23) and orange (Asn109). B) A close-up view showing the [4Fe-4S] cluster and the ligand candidates.

The studies reported in this thesis provide important new insight into two thus far poorly characterised members of the Rrf2 family of transcriptional regulators. The data confirm the variability of cluster type, as already illustrated by IscR and NsrR and significantly extend understanding of the functional importance of the family and the variable signals to which they respond.

The proteins involved in the biogenesis of Fe-S clusters are evolutionarily conserved from bacteria to humans, and many insights into the process of Fe-S cluster

biogenesis have come from studies of model organisms, including bacteria, fungi and plants [16]. The importance of iron-sulfur proteins for life is documented by an increasing number of human diseases attributable to defects in the basic process of Fe-S cluster biogenesis. Some of the diseases related to these proteins are colon cancer, different types of anaemias, Friedreich's ataxia (progressive damage to the nervous system), mutations in the tumour suppressor gene contribute to the development of a cancerous tumour, etc. [17]. It is clear that thorough molecular insights into the mechanisms of Fe–S-protein are prerequisite for the future development of therapeutic strategies in the treatment of iron-sulfur diseases.

6.1. References.

1.   Johnston, A.W., et al., *Living without Fur: the subtlety and complexity of iron-responsive gene regulation in the symbiotic bacterium Rhizobium and other alpha-proteobacteria.* Biometals, 2007. **20**(3-4): p. 501-11.
2.   Mettert, E.L. and P.J. Kiley, *Fe-S proteins that regulate gene expression.* Biochim Biophys Acta, 2015. **1853**(6): p. 1284-93.
3.   Crack, J.C., et al., *NsrR from Streptomyces coelicolor is a nitric oxide-sensing [4Fe-4S] cluster protein with a specialized regulatory function.* J Biol Chem, 2015. **290**(20): p. 12689-704.
4.   Crack, J.C., A.J. Thomson, and N.E. Le Brun, *Mass spectrometric identification of intermediates in the O2-driven [4Fe-4S] to [2Fe-2S] cluster conversion in FNR.* Proc Natl Acad Sci U S A, 2017. **114**(16): p. E3215-e3223.
5.   Lee, Y., et al., *A [3Fe-3S](3+) cluster with exclusively mu-sulfide donors.* Chem Commun (Camb), 2016. **52**(6): p. 1174-7.
6.   Crack, J.C., et al., *Iron-sulfur clusters as biological sensors: the chemistry of reactions with molecular oxygen and nitric oxide.* Acc Chem Res, 2014. **47**(10): p. 3196-205.
7.   Dibden, D.P. and J. Green, *In vivo cycling of the Escherichia coli transcription factor FNR between active and inactive states.* Microbiology, 2005. **151**(Pt 12): p. 4063-70.
8.   Munnoch, J.T., et al., *Characterization of a putative NsrR homologue in Streptomyces venezuelae reveals a new member of the Rrf2 superfamily.* Sci Rep, 2016. **6**: p. 31597.
9.   Fleischhacker, A.S., et al., *Characterization of the [2Fe-2S] cluster of Escherichia coli transcription factor IscR.* Biochemistry, 2012. **51**(22): p. 4453-62.
10. Romsang, A., et al., *The iron-sulphur cluster biosynthesis regulator IscR contributes to iron homeostasis and resistance to oxidants in Pseudomonas aeruginosa.* PLoS One, 2014. **9**(1): p. e86763.
11. Volbeda, A., et al., *Crystal structures of the NO sensor NsrR reveal how its iron-sulfur cluster modulates DNA binding.* Nat Commun, 2017. **8**: p. 15052.
12. Crack, J.C., et al., *Differentiated, Promoter-specific Response of [4Fe-4S] NsrR DNA Binding to Reaction with Nitric Oxide.* J Biol Chem, 2016. **291**(16): p. 8663-72.
13. Sievers, F., et al., *Fast, scalable generation of high-quality protein multiple sequence alignments using Clustal Omega.* Mol Syst Biol, 2011. **7**: p. 539.
14. Nicholas, K.B., *GeneDoc: analysis and visualization of genetic variation.*
15. Guex, N. and M.C. Peitsch, *SWISS-MODEL and the Swiss-PdbViewer: an environment for comparative protein modeling.* Electrophoresis, 1997. **18**(15): p. 2714-23.
16. Rouault, T.A. and W.H. Tong, *Iron-sulphur cluster biogenesis and mitochondrial iron homeostasis.* Nat Rev Mol Cell Biol, 2005. **6**(4): p. 345-51.

17. Rouault, T.A., *Biogenesis of iron-sulfur clusters in mammalian cells: new insights and relevance to human disease.* Dis Model Mech, 2012. **5**(2): p. 155-64.
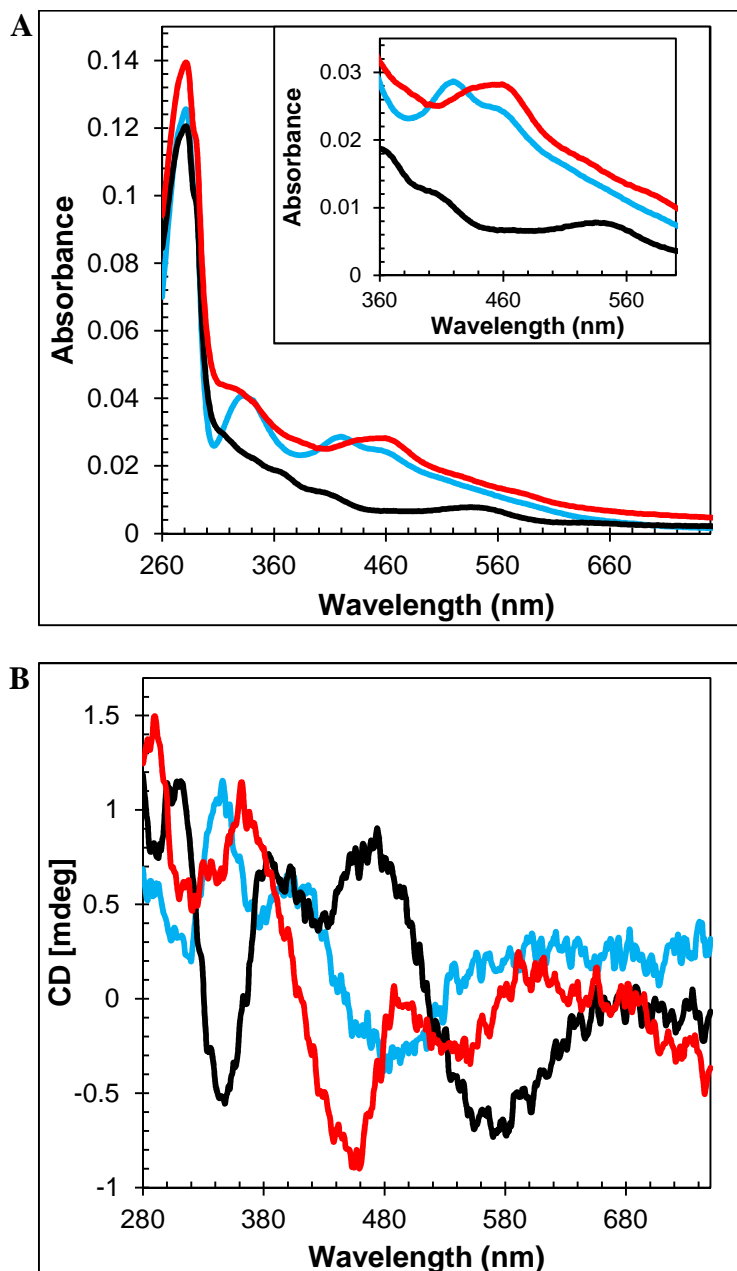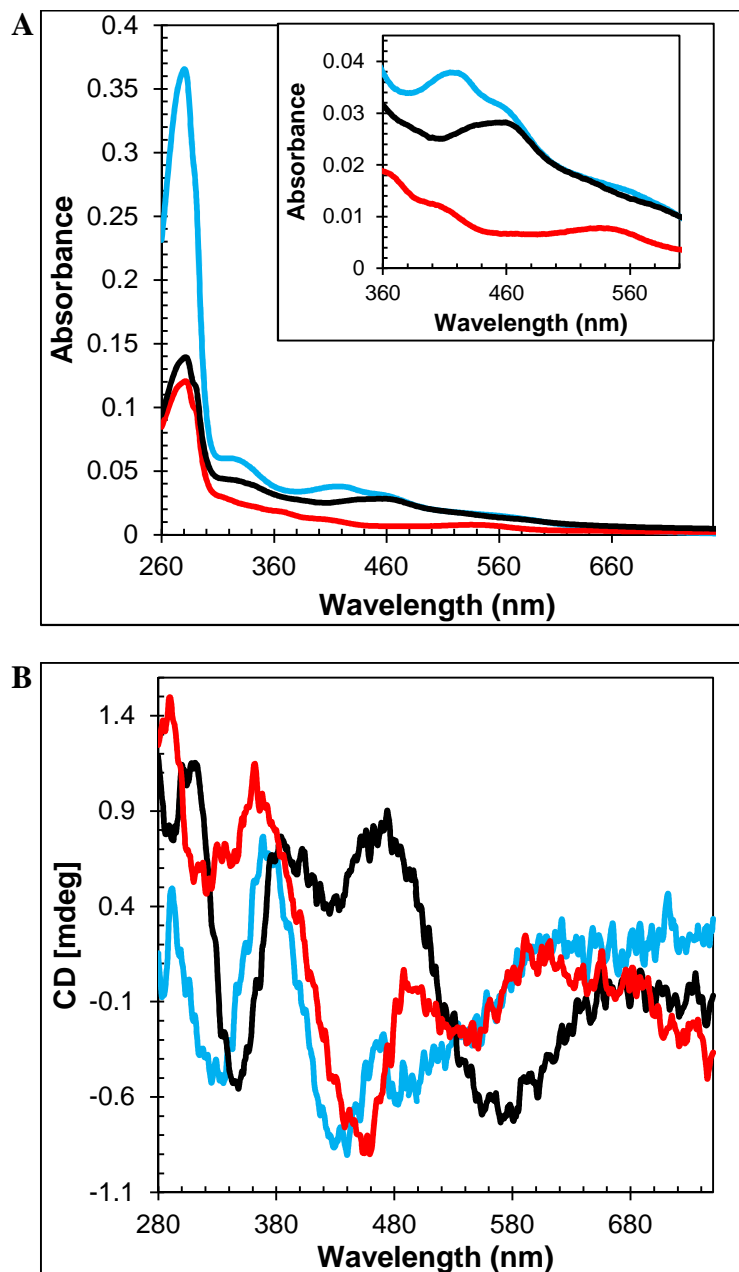
Appendix

Figure A. Spectroscopic characterization of E8C RsrR. UV-visible absorption **(A)** and CD **(B)** spectra of as isolated/oxidized E8C RsrR (blue line), wild type RsrR as isolated (black line) and wild type oxidized RsrR (red line). 30 µM [2Fe-2S] E8C RsrR and wild type RsrR were in buffer F (50 mM TRIS, 2 M NaCl, 5% (v/v) glycerol, pH 8). In A, inset is the iron-sulfur cluster absorbance in the 360 – 600 nm region in more detail. The measurements were obtained using a 1 mm sealed anaerobic cuvette and buffer F for the baseline.
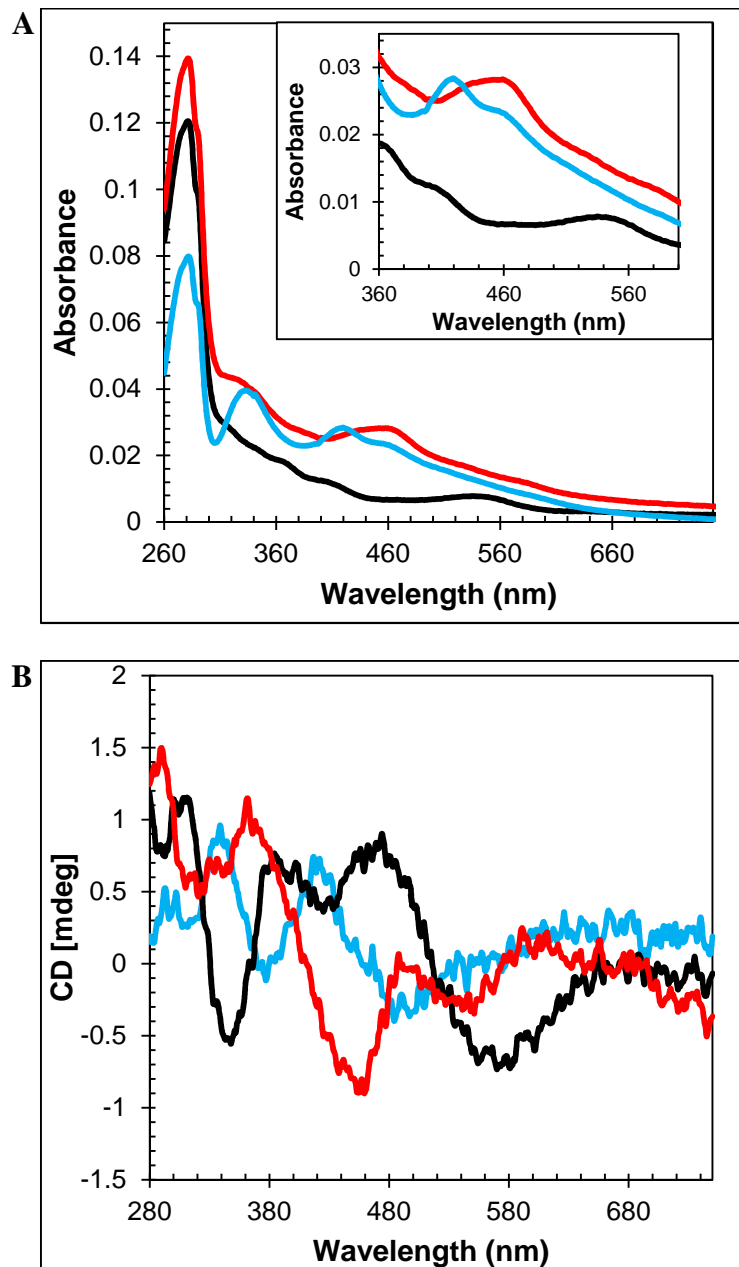
Figure B. Spectroscopic characterization of H12A RsrR. UV-visible absorption (**A**) and CD (**B**) spectra of as isolated/oxidized H12A RsrR (blue line), wild type RsrR as isolated (black line) and wild type oxidized RsrR (red line). 30 µM [2Fe-2S] H12A RsrR and wild type RsrR were in buffer F (50 mM TRIS, 2 M NaCl, 5% (v/v) glycerol, pH 8). In A, inset is the iron-sulfur cluster absorbance in the 360 – 600 nm region in more detail. The measurements were obtained using a 1 mm sealed anaerobic cuvette and buffer F for the baseline.
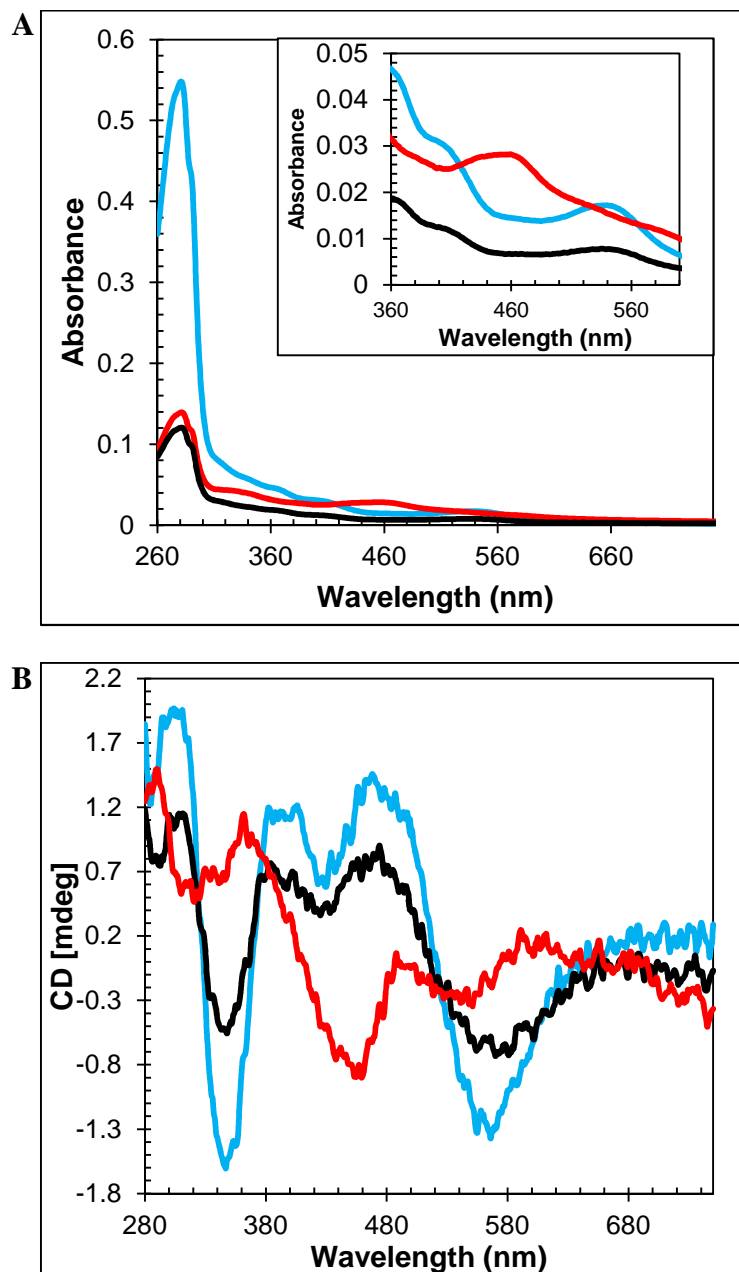
Figure C. Spectroscopic characterization of E8C/H12A RsrR. UV-visible absorption **(A)** and CD **(B)** spectra of as isolated/oxidized E8C/H12A RsrR (blue line), wild type RsrR as isolated (black line) and wild type oxidized RsrR (red line). 30 µM [2Fe-2S] E8C/H12A RsrR and wild type RsrR were in buffer F (50 mM TRIS, 2 M NaCl, 5% (v/v) glycerol, pH 8). In A, inset is the iron-sulfur cluster absorbance in the 360 – 600 nm region in more detail. The measurements were obtained using a 1 mm sealed anaerobic cuvette and buffer F for the baseline.

Figure D. Spectroscopic characterization of H33A RsrR. UV-visible absorption **(A)** and CD **(B)** spectra of as isolated/reduced H33A RsrR (blue line), wild type RsrR as isolated (black line) and wild type oxidized RsrR (red line). 30 µM [2Fe-2S] H33A RsrR and wild type RsrR were in buffer F (50 mM TRIS, 2 M NaCl, 5% (v/v) glycerol, pH 8). In A, inset is the iron-sulfur cluster absorbance in the 360 – 600 nm region in more detail. The measurements were obtained using a 1 mm sealed anaerobic cuvette and buffer F for the baseline.
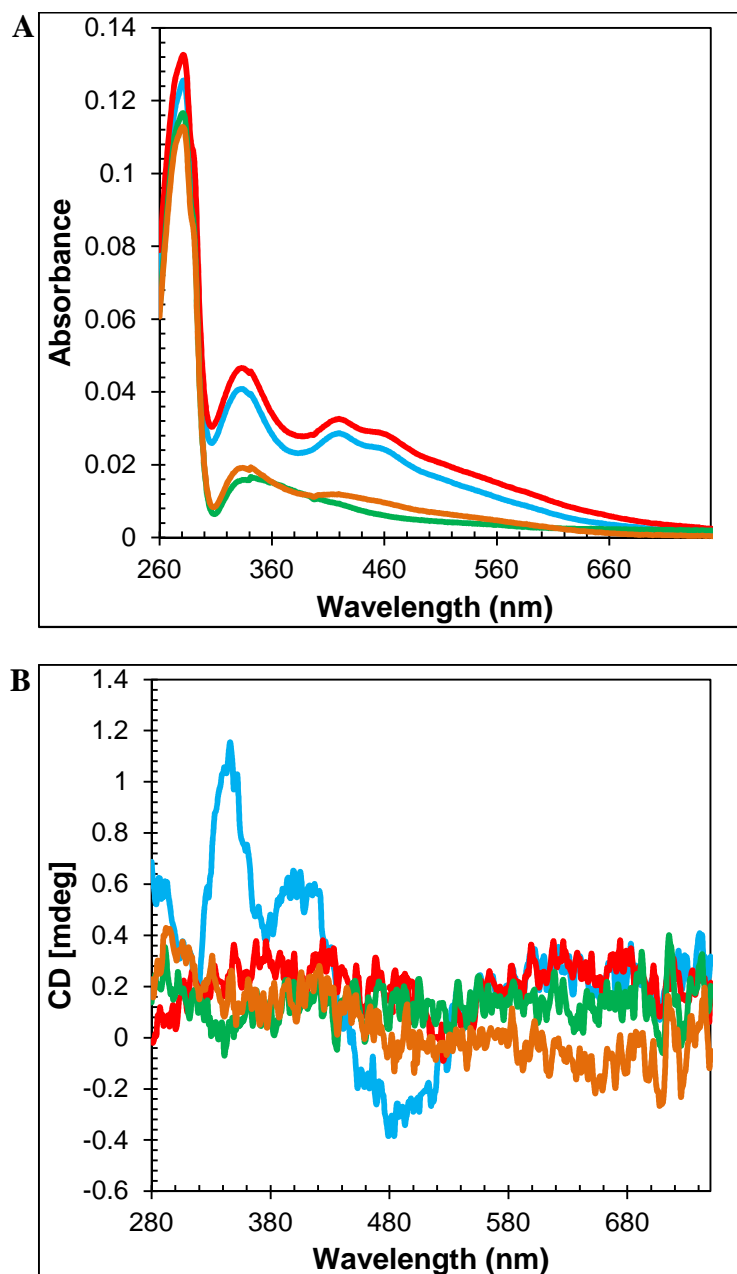
Figure E. Redox cycling of E8C RsrR. UV-visible absorption (**A**) and CD (**B**) spectra of 30 µM [2Fe-2S] in buffer F (50 mM TRIS, 2 M NaCl, 5% (v/v) glycerol, pH 8). E8C RsrR as isolated are shown in blue. Spectra following exposure to air for 30 min are shown in red. Spectra for samples subsequently treated with 30 µM of sodium dithionite for 1 hr 38 min are shown in green. Spectra of the same samples following re-exposure to air for 1 hr are shown in orange. The measurements were obtained using a 1 mm sealed anaerobic cuvette and buffer F for the baseline correction.
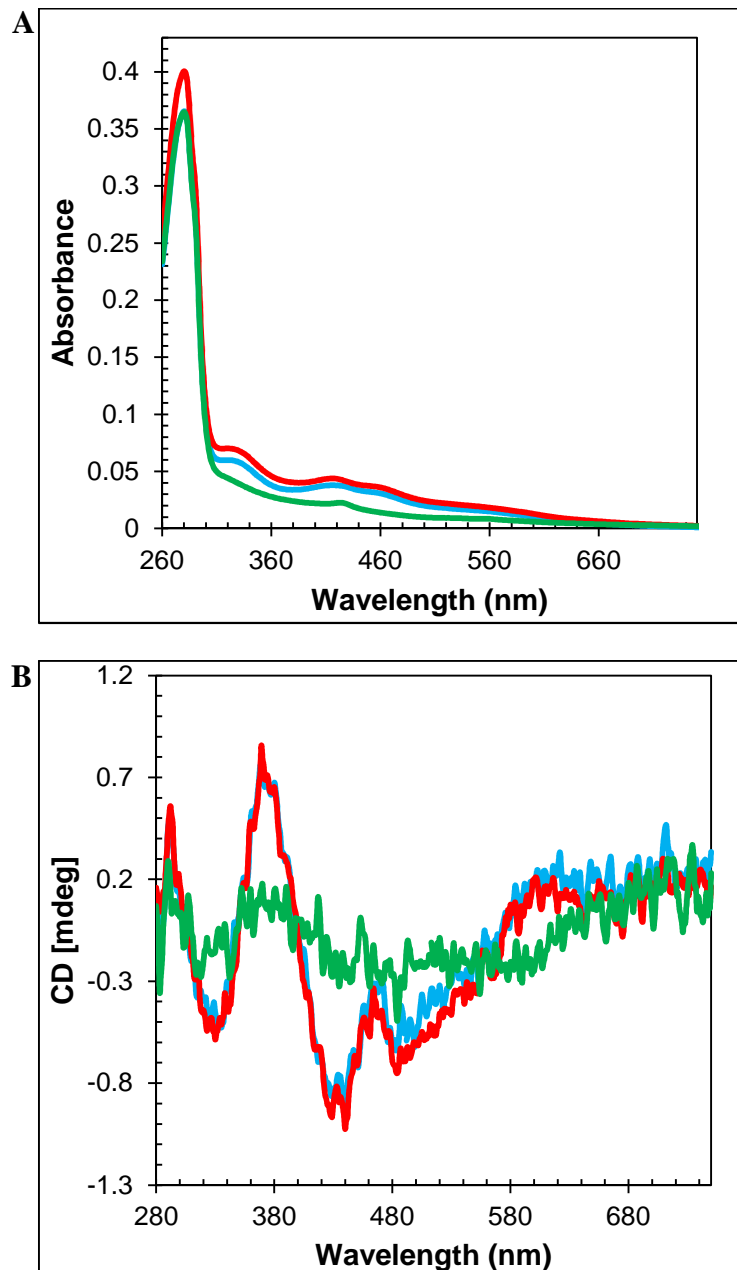
Figure F. Redox cycling of H12A RsrR. UV-visible absorption (**A**) and CD (**B**) spectra of 30 µM [2Fe-2S] in buffer F (50 mM TRIS, 2 M NaCl, 5% (v/v) glycerol, pH 8). H12A RsrR as isolated are shown in blue. Spectra following exposure to air for 30 min are shown in red. Spectra for samples subsequently treated with 30 µM of sodium dithionite for 146 min are shown in green. The measurements were obtained using a 1 mm sealed anaerobic cuvette and buffer F for the baseline correction.
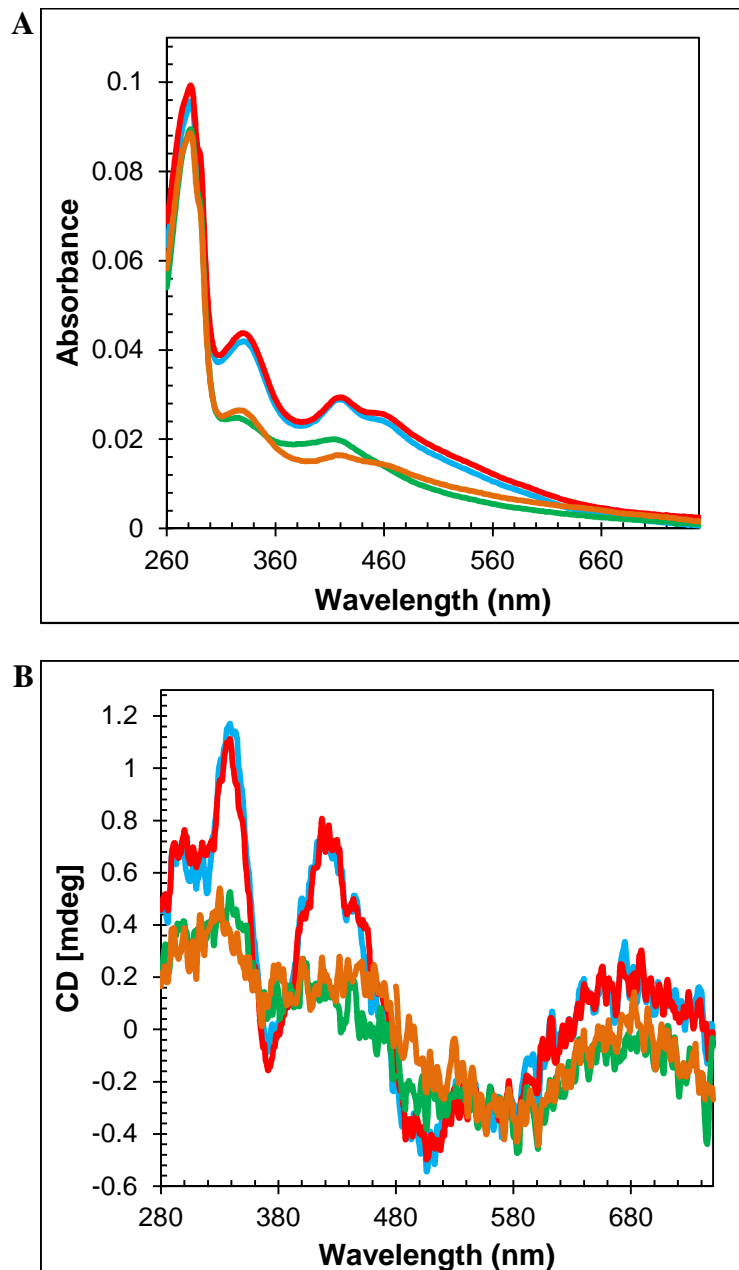
145

Figure G. Redox cycling of E8C/H12A RsrR. UV-visible absorption (**A**) and CD (**B**) spectra of 30 μM [2Fe-2S] in buffer F (50 mM TRIS, 2 M NaCl, 5% (v/v) glycerol, pH 8). E8C/H12C RsrR as isolated are shown in blue. Spectra following exposure to air for 30 min are shown in red. Spectra for samples subsequently treated with 30 μM of sodium dithionite for 189 min are shown in green. Spectra of the same samples following re-exposure to air for 30 min are shown in orange. The measurements were obtained using a 1 mm sealed anaerobic cuvette and buffer F for the baseline correction.
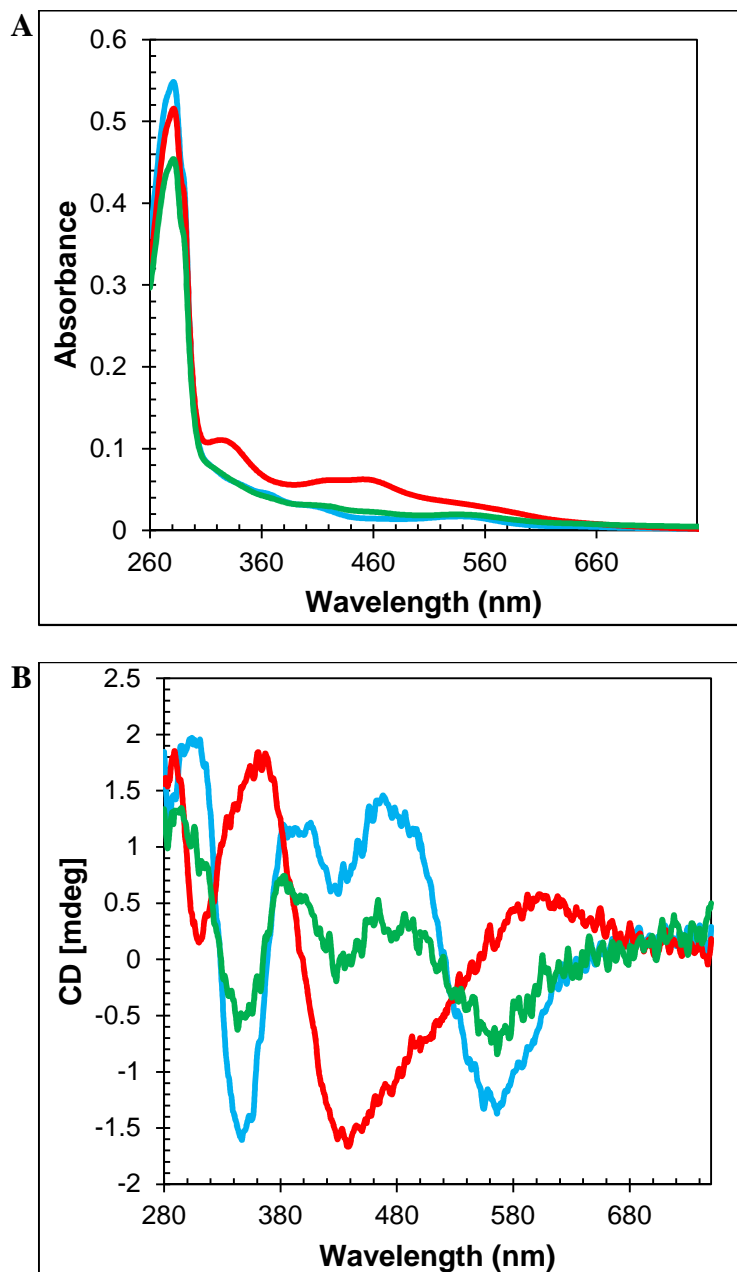
Figure H. Redox cycling of H33A RsrR. UV-visible absorption (**A**) and CD (**B**) spectra of 30 µM [2Fe-2S] in buffer F (50 mM TRIS, 2 M NaCl, 5% (v/v) glycerol, pH 8). H33A RsrR as isolated are shown in blue. Spectra following exposure to air for 30 min are shown in red. Spectra for samples subsequently treated with 30 µM of sodium dithionite for 144 min are shown in green. The measurements were obtained using a 1 mm sealed anaerobic cuvette and buffer F for the baseline correction.